Robust Control Design with Real Parameter Uncertainty using Absolute Stability Theory

Jonathan P. How
Steven R. Hall

January 1993 SERC #1-93

(Under the sponsorship of NASA and SERC)

NAGW-1335
NAGW-2014

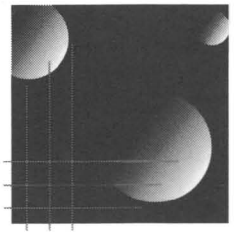

MIT Space Engineering Research Center

Massachusetts Institute of Technology
Cambridge Massachusetts 02139

DISPLAY 95N12782/2

95N12782*# ISSUE 2 CATEGORY 63

RPT#: NASA-CR-196971 NAS 1.26:196971 SERC-1-93 CNT#: NAGW-2014 NAGW-1335

93/01/00 194 PAGES UNCLASSIFIED DOCUMENT

UTTL: Robust control design with real parameter uncertainty using absolute stability theory TLSP: Ph.D. Thesis

AUTH: A/HOW, JONATHAN P.; B/HALL, STEVEN R.

CORP: Massachusetts Inst. of Tech., Cambridge. CSS: (Space Engineering Research Center.)

SAP: Avail: CASI HC A09/MF A03

CIO: UNITED STATES

MAJS: /*CONTROL STABILITY/*CONTROL SYSTEMS DESIGN/*CONTROL THEORY/*NONLINEAR SYSTEMS/*OPTIMAL CONTROL/*ROBUSTNESS (MATHEMATICS)/*SYSTEMS STABILITY

MINS: / ACTIVE CONTROL/ ALGORITHMS/ FEEDBACK CONTROL/ LIAPUNOV FUNCTIONS/ RICCATI EQUATION

ABA: Author

ABS: The purpose of this thesis is to investigate an extension of mu theory for robust control design by considering systems with linear and nonlinear real parameter uncertainties. In the process, explicit connections are made between mixed mu and absolute stability theory. In particular, it is shown that the upper bounds for mixed mu are a generalization of results from absolute stability theory. Both state space and frequency domain criteria are developed for several nonlinearities and stability

ENTER: MORE

DISPLAY 95N12782/2

multipliers using the wealth of literature on absolute stability theory and the concepts of supply rates and storage functions. The state space conditions are expressed in terms of Riccati equations and parameter-dependent Lyapunov functions. For controller synthesis, these stability conditions are used to form an overbound of the H2 performance objective. A geometric interpretation of the equivalent frequency domain criteria in terms of off-axis circles clarifies the important role of the multiplier and shows that both the magnitude and phase of the uncertainty are considered. A numerical algorithm is developed to design robust controllers that minimize the bound on an H2 cost functional and satisfy an analysis test based on the Popov stability multiplier. The controller and multiplier coefficients are optimized simultaneously, which avoids the iteration and curve-fitting procedures required by the D-K procedure of mu synthesis. Several benchmark problems and experiments on the Middeck Active Control Experiment at M.I.T. demonstrate that these controllers achieve good robust performance and guaranteed stability bounds.

ENTER:

Robust Control Design with Real Parameter Uncertainty using Absolute Stability Theory

Jonathan P. How
Steven R. Hall

January 1993 SERC #1-93

(Under the sponsorship of NASA and SERC)

This report is based on the thesis of Jonathan P. How submitted to the Department of Aeronautics and Astronautics in partial fulfillment of the requirements for the degree of Doctor of Philosophy at the Massachusetts Institute of Technology.

Abstract

The purpose of this thesis is to investigate an extension of μ theory for robust control design by considering systems with linear and nonlinear real parameter uncertainties. In the process, explicit connections are made between mixed μ and absolute stability theory. In particular, it is shown that the upper bounds for mixed μ are a generalization of results from absolute stability theory. Both state space and frequency domain criteria are developed for several nonlinearities and stability multipliers using the wealth of literature on absolute stability theory and the concepts of supply rates and storage functions. The state space conditions are expressed in terms of Riccati equations and parameter-dependent Lyapunov functions. For controller synthesis, these stability conditions are used to form an overbound of the $\mathcal{H}_2$ performance objective. A geometric interpretation of the equivalent frequency domain criteria in terms of off-axis circles clarifies the important role of the multiplier and shows that both the magnitude and phase of the uncertainty are considered.

A numerical algorithm is developed to design robust controllers that minimize the bound on an $\mathcal{H}_2$ cost functional and satisfy an analysis test based on the Popov stability multiplier. The controller and multiplier coefficients are optimized simultaneously, which avoids the iteration and curve-fitting procedures required by the D–K procedure of μ synthesis. Several benchmark problems and experiments on the Middeck Active Control Experiment at M.I.T. demonstrate that these controllers achieve good robust performance and guaranteed stability bounds.

Acknowledgements

This work was sponsored by the NASA Headquarters grant NAGW–2014 with Dr. Robert Hayduk as technical monitor, and by the M.I.T. Space Engineering Research Center under NASA grant NAGW-1335.

Contents

List of Figures

List of Tables

Nomenclature

$G(s)$	=	system transfer function
$\tilde{G}(s)$	=	transformed system transfer function
A, B, C, B_0, C_0	=	state space matrices for $G(s)$
$f(\cdot)$	=	nonlinear function
$\tilde{f}(\cdot)$	=	transformed nonlinear function
F_2, F_1, M_2, M_1	=	upper and lower sector (and slope) bounds for $f(\cdot)$
I_m, or I	=	$m \times m$ identity matrix
J, $\mathcal{J}$	=	performance cost functional and overbound
P	=	Lyapunov function matrix
$r(\cdot,\cdot)$, $R(\cdot,\cdot)$	=	supply rates
$V_G(\cdot)$, $V_{si}(\cdot)$	=	system and nonlinearity storage functions
$V(\cdot)$	=	Lyapunov function
$W(s)$	=	stability multiplier
u, x, y	=	system inputs, states, and outputs
z_{ij}	=	filtered outputs of $G(s)$
u_i, u_{ij}	=	$\tilde{f}_i(\tilde{y}_i)$, $\tilde{f}_i(z_{ij})$
H_j, N_j, S_j	=	matrices of multiplier coefficients
$\alpha, \beta, \gamma, \eta$	=	multiplier coefficients
Δ	=	uncertainty block
$\triangle A$	=	uncertainty in the matrix A
$\mathcal{K}$	=	uncertainty block structure for μ analysis
$\mathcal{D}_\mathcal{K}$, $\mathcal{N}_\mathcal{K}$	=	classes of scaling matrices for mixed μ analysis
D, N	=	scaling matrices for mixed μ
$\mathcal{U}$	=	set of admissible uncertainties
$\mathbb{N}^r$, $\mathbb{D}^r$, $\mathbb{S}^r$	=	$r \times r$ nonnegative definite, diagonal, and symmetric matrices.
$(\cdot)_i$, $(\cdot)_{ii}$	=	i^{th} row of $(\cdot)$, $(i,i)^{\text{th}}$ element of $(\cdot)$
E	=	expected value
$\mathbb{R}$, $\mathbb{C}$	=	sets of real and complex numbers
$(\cdot)^T$, $(\cdot)^*$	=	transpose and complex conjugate transpose
$\|\cdot\|_2$	=	Euclidean norm
$\|\cdot\|_F$	=	Frobenius matrix norm

$\sigma_{\max}(\cdot)$	=	maximum singular value
$\rho(\cdot)$, $\lambda(\cdot)$	=	spectral radius, eigenvalues
tr $(\cdot)$	=	trace operator
vec(A)	=	Kronecker "vec" operator. The vector obtained by vertically stacking the columns of the matrix A
$\mathcal{H}_2$	=	Hardy space of square-integrable functions on the imaginary axis, with analytic continuation into the right half-plane
$\mathcal{H}_\infty$	=	Hardy space of essentially bounded functions on the imaginary axis, with analytic continuation into the right half-plane

Chapter 1

Introduction

The implementation of high authority controllers on a system with uncertain parameters presents many difficult challenges. Stringent performance objectives often require that the controller be optimized with respect to a mathematical model of the system. Unfortunately, these models typically do not accurately represent the real plant, with the result that the controllers often destabilize the closed-loop system. This problem is particularly evident in the field of *Controlled Structures Technology* [42], which deals with the control of lightly damped structures. These structures are frequently difficult to model well. Furthermore, small changes in some parameters, such as modal frequencies, can result in large changes in the frequency response of the system. In addition, data recent from Shuttle flight experiments illustrate the changes due to gravity that can occur in flexible space structures [43]. These changes will result in large parameter uncertainties in the system models. Unfortunately, many standard control formulations, such as Linear Quadratic Gaussian (LQG or $\mathcal{H}_2$), may yield extremely sensitive controllers that are not robust to these parameter perturbations [7, 46, 59].

Consequently, the goal of much recent research has been to develop design techniques that yield controllers that are suboptimal in terms of performance, but robust to system parameter uncertainties. The elements of the standard synthesis problem are shown in Fig. 1.1 with the system G, a controller G_c, a performance loop $w_d \rightarrow z_p$, and an uncertainty block Δ. For a particular description (or class) of this uncertainty

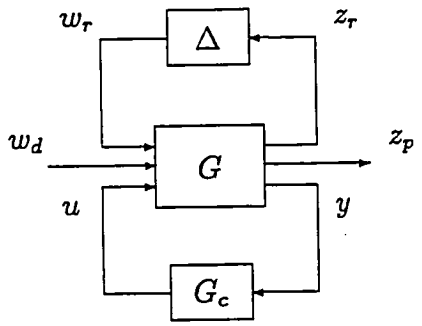

Fig. 1.1: Elements of the robust performance problem.

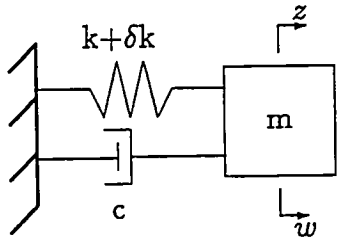

Fig. 1.2: Spring mass system with stiffness uncertainty.

block, a modified design problem is usually specified in terms of the *robust stability* and *robust performance* problems. The robust stability problem requires that a controller guarantee asymptotic stability of the closed-loop system for all perturbations in the class of uncertainties. The more difficult robust performance problem requires that the controllers also achieve a specified level of performance for the entire class of uncertainties. The central difficulty in solving these two problems is obtaining a model that adequately represents the system uncertainty, yet is not overly conservative.

A good stability analysis tool forms the foundation for many of the best approaches to robust control synthesis. Developing an effective analysis tool requires balancing the accuracy of the uncertainty description against the computational feasibility of the analysis test. It is clear that a good description of the uncertainty is not much use if the resulting stability criteria cannot be computed or easily approximated. Conversely, simple uncertainty descriptions can result in synthesis techniques that are too conservative for practical use. For example, an *unstructured* representation of the uncertainty with a single block Δ is useful for system uncertainties such as unmodelled high frequency modes. However, it is far too conservative an approach for a system with multiple uncorrelated uncertainties, which is called a *structured* uncertainty problem.

A similar problem exists with *complex* models of *real* uncertainties. Complex models result in simpler analysis tools, but they ignore the phase (0° or 180°) in the real uncertainty. The conservatism of these complex models can be clearly demonstrated using the simple example of a spring mass system in Fig. 1.2. The stiffness uncer-

tainty, which is real and constant, results in the changes shown in Fig. 1.3a. The results with a complex model are illustrated in part (b), where the uncertainty is represented by a disk in parameter space. The corresponding region in the s-plane lies on both sides of the Imaginary-axis. The conservatism of the complex model is evident by the fact that it erroneously predicts a potential instability for this uncertainty. The degree of this conservatism can be quantified by analyzing the roots of the characteristic equation for the system. These are the given by the zeroes of the equation $ms^2 + cs + k(1+\delta) = 0$, with $k/m = \omega^2$ and $c/m = 2\zeta\omega$. If δ is complex, the stability limit is $|\delta| < 2\zeta$. If δ is real, the only restriction is that $\delta > -1$. Since complex values of δ result in changes of the system damping, they place very tight restrictions on the uncertainty bounds. These restrictions are particularly severe for structures, which typically have modal damping values on the order of 0.5% or less [92]. The conservatism of these complex models has been one of the key motivations for developing accurate but computationally feasible analysis tests for systems with constant real parameter uncertainties.

One of the overall objectives of this thesis is to develop less conservative analysis tools for systems with constant real parameter uncertainties. These tests are developed as state space stability criteria written in terms of Riccati equations and Lyapunov functions. Clarifying frequency domain interpretations of these stability tests are also presented. While much of the recent literature on parameter uncertainty has focused on systems with linear perturbations, we draw on the recent work by Haddad and Bernstein [66,67,70,71] and the wealth of literature on *absolute stability theory* [2,100,119,121,123,131,132,140,172] to consider both linear and nonlinear uncertainties.

The research in this thesis addresses several important issues for robust control. First, the analysis directly addresses the issue of real time-invariant nonlinear parameter uncertainties, and thus is considered to be an extension of μ theory discussed in Ref. [47]. As will be discussed, the robustness problem with real time-invariant linear uncertainties is extremely difficult to address directly. As a result, many techniques, such as mixed μ analysis [53], use approximations or upper bounds to develop com-

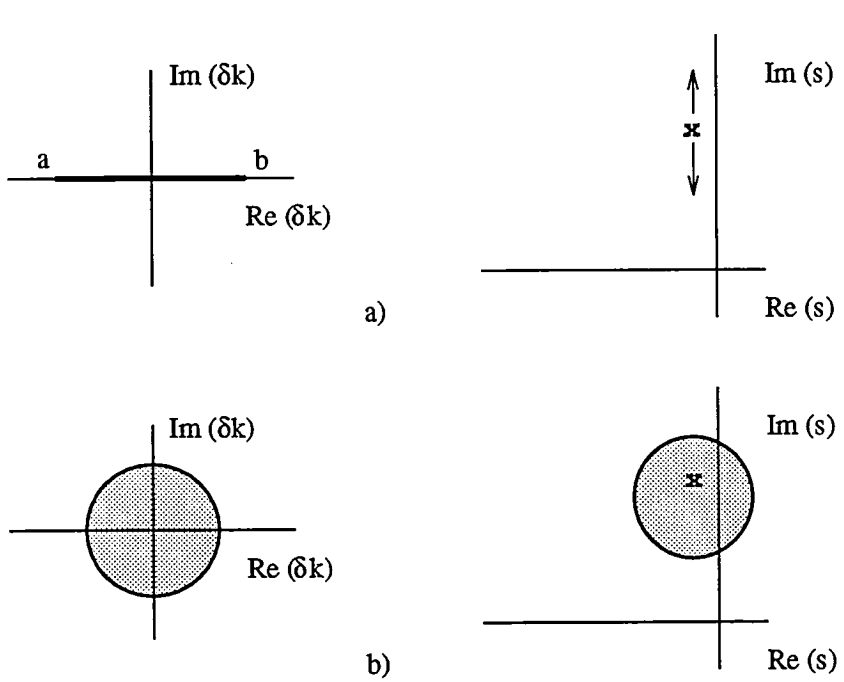

Figure 1.3: Real and complex models of parameter uncertainty in the pole location $\times$. Uncertainty in the spring stiffness is represented by the uncertainty in the damped modal frequency. (a) Real parameter variations. (b) Complex parameter variations.

putationally feasible analysis tools. However, it is shown in this thesis that the upper bounds for mixed μ are essentially equivalent to the results from absolute stability theory. Furthermore, by explicitly considering these nonlinear uncertainties, it is possible to develop physical interpretations of these robustness tests. Finally, because the state space stability criteria can be included in an $\mathcal{H}_2$ design problem, the results in this thesis provide a powerful tool for robust controller synthesis for systems with constant real parameter uncertainties.

1.1 Background and Previous Research

As outlined by Bhattacharyya [25], several approaches have been developed to improve the modelling techniques for the robust stabilization problem with parameter uncertainty. Many of these approaches fall within one of six categories: polynomial, state space, multiple model, μ, stochastic, and de-sensitization techniques. The following section provides a brief overview of these approaches, focusing on the classes

of uncertainties that they address and the resulting analysis and synthesis tools.

Polynomial approaches directly analyze the characteristic equation to determine the stability of an uncertain system. Included in this category, are the Routh-Hurwitz criterion [125], Kharitonov's theorem [96] with the recent extensions to multiple input multiple output systems (MIMO) [25], and the Edge Theorem [15]. These tests deal with the zeroes of a family of interval polynomials $p(s) = \sum_{i=0}^{n} p_i s^i$, where $0 < p_{il} \leq p_i \leq p_{ih}$, $i = 1, \ldots, n$. Kharitonov's theorem states that the entire family is asymptotically stable if and only if four extreme polynomials are asymptotically stable. These extreme polynomials are constructed using the coefficients p_{il} and p_{ih} in a specified pattern. For complicated plants, it is often difficult to correlate the parameter uncertainty to an uncertainty in the coefficients of the characteristic equation of the system. Even if this correlation can be made, there are still further difficulties because the polynomial coefficients will be related to each other by the set of uncertain parameters. These relationships can be ignored, but this will lead to a conservative result.

The parameter space method has been developed as an alternative to the standard Routh-Hurwitz or Nyquist tests for stability [1, 32, 150]. As discussed in Šiljak's overview [150], the approach also deals directly with the roots of the characteristic equation. A correlation between the parameter uncertainties and the pole locations is used to provide a graphical representation of the system stability in parameter space. With several uncertainties, the resulting analysis tools are much simpler than the standard Nyquist or Nichols plots [150]. Unfortunately, as with other polynomial approaches, it is typically quite difficult to develop and interpret the relationships between the uncertain parameters and the roots of the characteristic equation. This is particularly true for large order systems with multiple uncertainties. A further problem is that these techniques deal only with the problem of robust stability.

The $\mathcal{H}_\infty$ theory provides a framework for designing controllers that guarantee robust stability with an unstructured, complex uncertainty [50,54]. This uncertainty can be interpreted as a plant uncertainty, an $\mathcal{H}_\infty$ performance specification, or an approximate combination of both [49]. Several authors have investigated a mixed

$\mathcal{H}_2/\mathcal{H}_\infty$ problem specification to add robustness to the LQG controllers [51, 65, 116, 137, 168, 175]. Writing the performance specification as an additional uncertainty block in the robust stability problem results in a structured uncertainty problem, for which Doyle [47] introduced μ-analysis techniques. The difficulty of computing the structured singular value μ has led to the development of upper and lower bounds. These upper bounds can be refined using the scaling matrices [47]. These refinements can then be combined with $\mathcal{H}_\infty$ control synthesis to form the so-called D–K iteration, where D refers to the scaling matrices and K to the controller design.

The μ synthesis approach has proven to be an effective technique for designing robust controllers for low order systems with a small number of complex uncertainties [11, 117]. The upper bounds for this structured analysis test are not exact for a large number of uncertainties [169]. Furthermore, the iterative D–K algorithm is non-convex and may result in solutions corresponding to local minima. Since these $\mathcal{H}_\infty$, $\mathcal{H}_2/\mathcal{H}_\infty$, and complex μ tests are based on a complex model of the uncertainty, they are effective for system errors such as unmodelled high frequency dynamics. However, these approaches can be very conservative for systems with constant real parameter uncertainties.

Recent research has focused on the extensions of this complex μ approach to develop less conservative analysis tools for systems with real parameter uncertainties [48, 53, 113, 170]. Again, the difficulty of computing the actual bound requires that upper and lower bounds be developed. Research has focused on the continuity of these robustness indicators [14,99,127] and the computational aspects of the upper and lower bounds for mixed μ [10,53,171]. In both the real and complex μ problems, the upper bound can be solved using convex minimization. However, a remaining difficulty in the case of real μ is how to combine these scaling matrices with the original plant model to continue the synthesis iteration.

Recent work by Safonov *et al.* [34, 140–143, 155] has focused on the multivariable stability margin K_m, which is related to $1/\mu$. They develop a technique for linear uncertainties using Generalized Popov Multipliers. Scaling matrices, which are related to the ones in the μ framework, are parameterized in terms of this multiplier. The

advantage of this approach over real μ lies in the way that these multipliers are evaluated. Each iteration step of the current μ synthesis algorithm in Ref. [117] requires that the optimal multipliers D be evaluated at each frequency point using a convex program and then approximated by curve-fitting. Recently, K_m synthesis has been introduced to eliminate this curve-fitting by formulating a second convex problem that directly yields the multiplier coefficients. The rest of the synthesis approach is similar to the D–K iteration. As will be seen in later developments, the K_m approach is related to the analysis techniques developed in this thesis. However, these two approaches differ in their interpretation of the analysis techniques and their algorithms for robust control synthesis.

As the name suggests, the goal of the multiple model approach is to design a single controller for several models of the uncertain system [8, 59, 95, 103, 106, 107, 112]. These models are used to represent the nominal system and the expected perturbations. However, it is often difficult to represent all of the expected perturbations because the number of models required increases combinatorially with the number of uncertainties. Consequently, a smaller number of models, which correspond to particular combinations of the uncertainties, are usually selected. The overall objective is typically specified as a weighted sum of the closed-loop $\mathcal{H}_2$ performance of each system model. Minimizing this objective yields a controller that guarantees stability for each of the models. However, there are no such guarantees for other combinations of the uncertainties.

Hagood [74, 75] has recently investigated cost averaging techniques for robust control. In his approach, the $\mathcal{H}_2$ cost is averaged over a set of systems that vary as a continuous function of a set of bounded real parameters. However, because numerical approximations of the exact average are computationally intensive, several analytical approximations are presented. Hall *et al.* [77] have recently demonstrated that one of these, the Bourret approximation, can be directly related to multiple model approaches.

As discussed by Weinmann [162], several techniques have been developed to directly address the sensitivity problems associated with LQG controllers. One ap-

proach is to penalize the variations of the optimal cost with respect to changes in the plant parameters. The approach by Blelloch and Mingori [26] modifies the LQG problem statement to account for structured parameter uncertainty. Terms are added to the state and noise weighting matrices to reduce the optimality of the LQG controller. Mukhopadhyay [114, 115] describes a similar technique for developing robust LQG controllers using frequency dependent weighting matrices and constraints on the singular values of the return difference matrix. Skelton *et al.* [126, 161, 167] suggests an approach that directly penalizes the sensitivity of the performance objective to parameter variations. The key difficulty is that the plant must be augmented with the sensitivity states, so that, with m uncertainties, the closed-loop system order increases to $(m+1)(n+n_c)$. Sesak [145] modified this approach by eliminating the sensitivity states using a singular perturbation reduction. The state and control weighting matrices are also modified to account for the reduction, and the result is very similar to the one in Ref. [26]. While these approaches are computationally effective tools for robust control design, they are *ad hoc* and offer no *a priori* robust stability or performance guarantees. This is especially true for large parameter variations, where the first derivative is insufficient to predict the actual changes in the cost.

Several approaches to robust control design have been developed based on the Linear Quadratic Gaussian/Loop Transfer Recovery (LQG/LTR) methodology [152]. As originally developed, the technique provided an effective loop shaping tool for unstructured model errors. Although the LQG/LTR controller recovers the guaranteed stability margins of a Linear Quadratic Regulator, the approach can be very sensitive to parameter uncertainties, as demonstrated by Shaked and Soroka [146]. Tahk and Speyer [153, 154] present a similar approach for structured uncertainty called asymptotic LQG synthesis. In this approach, the weighting matrices of the target loop are modified to reflect the structure of the plant uncertainty. The improvement of this technique over standard LQG designs is discussed in Ref. [33]. Calise and Byrns [30] present an approximate LTR procedure based on the sensitivity methods discussed previously. However, a difficulty with this approximate method is that the structure of the state weighting matrix restricts the parameter uncertainties that can

be considered.

Several stochastic approaches for parameter robust controllers have been developed [87,90,108]. In particular, we consider the so-called Maximum Entropy approach developed by Hyland [90] that uses a multiplicative white noise model to capture the effects of the parameter uncertainty on the system. In Ref. [21], Bernstein *et al.* develop a Lyapunov function for the Maximum Entropy approach to provide a rigorous foundation for a technique that has had several interpretations [22,91]. Bernstein and Hyland [24] discuss the "left-shift" phenomenon and how it results in robust compensators for structures with uncertain frequencies. Recent work has demonstrated the approach on the Active Control Technique Evaluation Spacecraft (ACES) [38] and the two mass benchmark problem [40]. Unfortunately, it is often difficult to correlate the uncertainty represented by the stochastic model of the system to the robustness levels achieved by the controller. The applicability of the technique is also restricted by the required assumptions on the structure of the plant uncertainty [77].

The direct method of Lyapunov [100] is an appealing analysis technique because it tests for system stability without dealing with the characteristic equation. However, the main difficulty with this approach is developing non-conservative Lyapunov functions for systems with parameter uncertainty [17, 94, 101, 128, 129]. As noted by Haddad and Bernstein [66], many quadratic Lyapunov functions do not restrict the time variation of the uncertainty and can result in conservative tests for constant model errors. A further problem with many state space approaches is imposing the structure of the analysis problem with multiple uncertainties [67].

Using convex optimization techniques, Boyd and Yang [27] address this conservatism for their simultaneous stability problem. They consider mixed uncertainties and incorporate information about the errors into the structure of the P matrix in the Lyapunov function $x^T P x$. In a similar approach, Šiljak uses vector Lyapunov functions to develop tests for connective stability [149]. These criteria were developed for the design of decentralized controllers, but have applications to the problem of determining system stability with respect to norm-bounded parameter variations. Majorant Lyapunov functions have also been developed for the problem of robust sta-

bility for large-scale systems [89]. Haddad and Bernstein have recently developed a series of Lyapunov functions that include more information about the uncertainty [69]. Recent results in Ref. [20, 67] demonstrate the advantage of tests based on positive real models of the uncertainty over those based on bounded gain models.

Barmish [13] introduced the concept of an adaptive Lyapunov function to reduce the conservatism in requiring that a single Lyapunov function guarantee stability for the entire class of uncertainties. To achieve a similar goal, Leal and Gibson [98] use a first order expansion of a Lyapunov function in terms of the uncertain parameters. For certain examples, they demonstrate that the tests provide significantly tighter bounds on the actual regions of stability.

An important recent extension of these two approaches by Haddad and Bernstein [66, 69] forms the background for this thesis. The approach is to use *parameter-dependent Lyapunov functions* that explicitly contain the uncertain parameters. Much of this work is based on the development of Lyapunov functions of the Lur'e–Postnikov form from *absolute stability theory* [2, 123, 131]. In this case, for a system with states x, output $y = cx$, and a sector-bounded nonlinear function $f(y)$ in the block Δ, the Lyapunov function is of the form

$$V(x, f) = x^T P x + 2 \int_0^{cx} f(\sigma)\, d\sigma. \tag{1.1}$$

The structure of this Lyapunov function will be developed in detail in this thesis. Haddad and Bernstein [66] have shown that, in the linear case with $f(\sigma) = F\sigma$, Eq. 1.1 can be rewritten as $V(x, F) = x^T P(F) x$. It is the dependence of V on the uncertainty F that places beneficial restrictions on the types of functions that can be considered.

As discussed by Haddad and Bernstein [67], the principal limitation of norm-based $\mathcal{H}_\infty$ theory and many quadratic Lyapunov functions is that they employ a complex model of the uncertainty which ignores phase information. The result is that the constant real parameter plant uncertainties are captured as a non-parametric frequency-dependent uncertainty. In the time domain, this non-parametric uncertainty can be interpreted as including arbitrarily time-varying, sector-bounded nonlinear un-

certainties. One technique for considering the constant real parameter robustness problem is to restrict the allowable time-variation of these uncertainties. This restriction can be imposed with parameter-dependent Lyapunov functions similar to the one in Eq. 1.1. Since $V(x, F)$ explicitly contains the uncertain parameter F, the allowable time-variation of this parameter is severely restricted. If the parameter can vary as an arbitrary function of time, then the nonnegative definiteness of $\dot{V}(x, F)$ could be subverted [69]. The approach used in this thesis and Ref. [69] is to generalize the nonlinearity-dependent Lur'e-Postnikov Lyapunov function of the classical Popov criterion to a parameter-dependent Lyapunov function for linear real parameter uncertainty. One of the key contributions of this thesis is to present these results in a unifying framework and then extend them to consider slope restricted monotonic and odd monotonic nonlinear uncertainties.

1.2 Thesis Objectives and Overview

The primary goal of this thesis is to develop analysis and synthesis tools that are less conservative for real parameter uncertainties [72,81–85]. Much of the recent literature on parameter uncertainty has focused on linear perturbations. In this thesis, we investigate nonlinear uncertainty models and consider linear uncertainty as a special case of this much broader class. In this way, it is possible to develop less conservative analysis tools for systems that exhibit nonlinear phenomena, such as spring hardening, sensor or actuator saturations, backlash, integrator windup, and certain types of friction. To consider these nonlinear uncertainties, this thesis builds on the wealth of literature on absolute stability theory [2,100,123,131,132,140,172].

The focus of this research is on developing both frequency domain and state space analysis tests. A graphical interpretation of the frequency domain criteria provides insight into the role of the free parameters in the tests. These graphical tests will also provide a connection between current analysis tools, such as those in Ref. [53,171], and the results from absolute stability theory.

Stability criteria are developed in this thesis using the concepts of *dissipation*, *supply rates*, and *storage functions* [79,80,165,166]. The approach is demonstrated

to be an effective technique for developing state space tests for system stability. The resulting Riccati equation tests for stability can be directly integrated into an $\mathcal{H}_2$ design problem using the Ω-bound fixed architecture framework [24]. The question addressed in this thesis is, given that the state space tests can be incorporated into an $\mathcal{H}_2$ synthesis problem, can analysis criteria be developed that are less conservative for systems with constant real parameter uncertainty?

The results in this thesis address several different issues to answer this question. First, frequency domain and state space tests for system stability with various classes of plant uncertainty are developed. These tests are demonstrated to represent a significant improvement over previous state space criteria for robust control. Furthermore, these results are used to show the direct connection between absolute stability theory from the 1960's and current μ approaches to robust control. These state space tests are then combined with optimal $\mathcal{H}_2$ synthesis to develop controllers that achieve robust stability and performance. Finally, several examples and experiments are used to show the effectiveness of the design approach for systems with real parameter uncertainty.

Chapter 2 of the thesis outlines some of the mathematical preliminaries for this work. In particular, an overview of the storage function and Ω-bound frameworks are presented because of the essential roles that they play in later developments. The state space stability tests are developed in Chapter 3 using supply rates, storage functions, and stability multipliers from absolute stability theory. As mentioned, both linear and nonlinear functions are used to represent the parameter uncertainties. The results for sector-bounded nonlinear functions are presented first. These are then extended to include the more specific classes of monotonic and odd monotonic nonlinear functions. The nonlinear functions can either be used for nonlinear parameter uncertainties or to approximate linear ones.

Frequency domain tests are also presented to give insight into the role of the free parameters in the stability criteria. These tests provide a direct connection with current μ analysis and synthesis techniques. A geometric interpretation of the frequency domain criteria also provides an understanding of the role of the scaling

functions in these techniques and how they differ from more conservative approaches.

Chapter 4 builds on the overview of Ω-bound techniques outlined in the preliminaries to give the results for specific classes of multipliers. Both the robust stability and robust performance problems are considered. Auxiliary $\mathcal{H}_2$ minimization problems are presented. The optimality conditions for the optimal static and (reduced-order) dynamic output feedback controllers are also given. The focus in this work is on parameter uncertainty, and not on unstructured errors such as high frequency unmodelled dynamics. It is assumed that, if necessary, techniques, such as frequency weighted cost functionals in the LQG performance specification, have been used to address this issue of unstructured model errors [62].

Chapter 4 presents the full control design problem for the case with the extended stability multipliers. The design process is further clarified in Chapter 5, which considers the simpler Popov multiplier. A numerical algorithm is presented to solve the optimality conditions. Several of the key numerical issues in the design of the robust controllers are also discussed. The relative advantages of the algorithm over other synthesis techniques are presented at the end of the chapter.

Chapters 6 and 7 demonstrate the effectiveness of Popov controller synthesis for several systems with real parameter uncertainty. In particular, full and reduced-order controllers are designed for several systems with single and multiple uncertainties. Three benchmark problems are used to demonstrate the changes in the controllers that are required to achieve guaranteed robustness. Several experiments are used to demonstrate that the approach is feasible for more realistic systems. In Chapter 7, the robust performance achieved with Popov controllers is experimentally demonstrated on the Middeck Active Control Experiment (MACE).

Chapter 2

Mathematical Preliminaries

This chapter provides the background material necessary to develop the stability criteria in Chapter 3 and the synthesis approach in Chapters 4 and 5.

2.1 Matrix Transfer Functions

The basic terminology is presented in the nomenclature. The following provides some further key definitions for matrix transfer functions. Let $M \geq 0$ ($M > 0$) denote the fact that the Hermitian matrix M is nonnegative (positive) definite. In this thesis, a *real-rational matrix function* is a matrix whose elements are rational functions with real coefficients. Furthermore, it is assumed that a *transfer function* is a real-rational matrix function each of whose elements is *proper*, *i.e.*, finite at $s = \infty$. A *strictly proper transfer function* is a transfer function that is zero at infinity. Finally, an *asymptotically stable transfer function* is a transfer function with all of its poles in the open left half plane. The space of asymptotically stable transfer functions is denoted by $\mathcal{RH}_\infty$, *i.e.*, the real-rational subset of $\mathcal{H}_\infty$. Let

$$G(s) \sim \left[\begin{array}{c|c} A & B \\ \hline C & D \end{array}\right] \tag{2.1}$$

denote a state space realization of a transfer function $G(s) = C(sI - A)^{-1}B + D$. The notation "$\overset{\text{min}}{\sim}$" is used to denote a minimal realization.

The $\mathcal{H}_2$ and $\mathcal{H}_\infty$ norms of an asymptotically stable transfer function $G(s)$ are

defined as

$$\|G(s)\|_2^2 \triangleq \frac{1}{2\pi}\int_{-\infty}^{\infty} \|G(\jmath\omega)\|_{\mathrm{F}}^2 \,\mathrm{d}\omega, \tag{2.2}$$

$$\|G(s)\|_\infty \triangleq \sup_{\omega\in\mathbb{R}} \sigma_{\max}\left[G(\jmath\omega)\right]. \tag{2.3}$$

From Ref. [5], a square transfer function $G(s)$ is *positive real* if: (1) all poles of $G(s)$ are in the closed left half plane, and (2) $G(s)+G^*(s)$ is nonnegative definite for $\mathrm{Re}[s] > 0$. Also, from Ref. [102,163], a square transfer function $G(s)$ is *strictly positive real* if (1) $G(s)$ is asymptotically stable, and (2) $G(\jmath\omega)+G^*(\jmath\omega)$ is positive definite for all real ω. A square transfer function $G(s)$ is *strongly positive real* if it is strictly positive real and $D+D^T > 0$, where $D \triangleq G(\infty)$. Finally, from Ref. [3], a minimal realization of a positive real transfer function is stable in the sense of Lyapunov, and from Ref. [102] a strictly positive real transfer function is asymptotically stable. With these definitions, we can proceed with an outline of an approach for modelling system parameter uncertainty.

2.2 System Parameter Uncertainty

The first step in the analysis of an uncertain system is to develop a technique for modelling the parameter uncertainties. It is assumed that the uncertain system $\hat{G}(s)$ can be written as

$$\hat{G}(s) \sim \left[\begin{array}{c|c} \hat{A} & \hat{B} \\ \hline \hat{C} & 0 \end{array}\right] = \left[\begin{array}{c|c} A & B \\ \hline C & 0 \end{array}\right] + \left[\begin{array}{c|c} \Delta A & \Delta B \\ \hline \Delta C & 0 \end{array}\right]. \tag{2.4}$$

As illustrated in Fig. 1.1, the plant uncertainty is usually expressed using an internal feedback model. The parameter uncertainties are written in terms of new system inputs and outputs that are added to the system [113]. These correspond to w_r and z_r in Fig. 1.1. An assumption in this approach is that the system uncertainty can be written as an outer product of two matrices

$$\left[\begin{array}{c|c} \Delta A & \Delta B \\ \hline \Delta C & 0 \end{array}\right] = B_0 \Delta C_0. \tag{2.5}$$

The matrices B_0 and C_0 are partitioned to be compatible with the structure of the uncertainty, and Δ is a partitioned to be compatible with the repetition of the uncertainties. Note the distinction between ΔA, the uncertainty in the matrix A, and

Δ, the uncertainty block. The columns of B_0 and the rows of C_0 correspond to the B and C matrices of these extra inputs and outputs.

There is a limitation to this decomposition approach when it is applied to the closed-loop system. In this case, with a compensator triple (A_c, B_c, C_c), the closed-loop dynamics of the system are

$$A_{cl} = \begin{bmatrix} \hat{A} & \hat{B}C_c \\ B_c\hat{C} & A_c \end{bmatrix} \tag{2.6}$$

$$= \begin{bmatrix} A & BC_c \\ B_cC & A_c \end{bmatrix} + \begin{bmatrix} \triangle A & \triangle BC_c \\ B_c\triangle C & 0 \end{bmatrix}. \tag{2.7}$$

The difficulty arises in the case with nonzero uncertainty in the B or C matrices of the plant. Consider the example of a system with uncertainty in the matrix C ($\triangle A$ and $\triangle B$ are both zero). Then, as in Eq. 2.5, we can decompose the uncertainty as $\triangle C = B_{0c}\Delta_c C_{0c}$. The uncertainty in the closed-loop system can then be written as

$$\triangle A_{cl} = \begin{bmatrix} 0 & 0 \\ B_c\triangle C & 0 \end{bmatrix} = \begin{bmatrix} 0 \\ B_cB_{0c} \end{bmatrix} \Delta_c \begin{bmatrix} C_{0c} & 0 \end{bmatrix}. \tag{2.8}$$

The result is that the matrices used to decompose the uncertainty depend on the B_c compensator matrix, which complicates the derivation of the optimality conditions. Note, however, that in this case

$$\begin{bmatrix} C_{0c} & 0 \end{bmatrix} \begin{bmatrix} 0 \\ B_cB_{0c} \end{bmatrix} = 0, \tag{2.9}$$

which results in several major simplifications. To simplify the developments in later chapters, only uncertainties in the matrix A will be considered.

As discussed in the Introduction, much of this thesis work has been motivated by the problem of parameter uncertainties in the control of lightly damped structures. The roll-off region of a high authority compensator plays a critical role in determining the importance of various modelling errors. If the cross-over frequencies are where the loop gain is unity, then the roll-off region consists of the frequency range between the first and last of these points. Pole uncertainties are especially important in this roll-off region, because high performance controllers typically include notches at these frequencies [7]. Uncertainty in the zero frequencies is particularly important within

the compensator bandwidth, because the zeros are often canceled by compensator poles.

One approach to modelling frequency uncertainty in the plant zeroes is to reflect them as an error in the residues of the structural modes. However, this is difficult for SISO systems and virtually impossible for MIMO ones. As will be demonstrated in Chapter 7, changing the frequencies of poles in a given frequency range also has a large effect on the system zeroes in that range. Consequently, a good approximation to the problem with uncertainty in both the poles and the zeroes is just to consider the uncertainty in the poles.

For other uncertainties in the B and C matrices, the approach by Tahk and Speyer [153] can be used to incorporate the uncertainty into the matrix A. If the i^{th} column of B (b_i) is uncertain, we can add an extra state x_b that tracks u_i fast enough that the filter dynamics ($\eta > 0$) are negligible with respect to the modes that u_i controls. The resulting system is

$$\begin{bmatrix} \dot{x} \\ \dot{x}_b \end{bmatrix} = \begin{bmatrix} A & b_i \\ 0 & -\eta \end{bmatrix} \begin{bmatrix} x \\ x_b \end{bmatrix} + \begin{bmatrix} B_t \\ b_0 \end{bmatrix} u \tag{2.10}$$

where $B_t = B - [0, \ldots, b_i, \ldots, 0]$ and $b_0 = [0, \ldots, \eta, \ldots, 0]$. A similar approach can be used for uncertainty in the C matrix. The plant order must be increased to model this uncertainty, but the approach provides a technique for approximating all other parameter uncertainties as errors in the dynamics matrix A.

Two possible state space representations of the open-loop system are

$$A_1 = \begin{bmatrix} 0 & 1 \\ -\omega^2 & -2\zeta\omega \end{bmatrix} \text{ and } A_2 = \begin{bmatrix} -\zeta\omega & -\omega\sqrt{1-\zeta^2} \\ \omega\sqrt{1-\zeta^2} & -\zeta\omega \end{bmatrix}. \tag{2.11}$$

The choice as to which representation is appropriate depends on several factors. Of the two, the A_2 representation is better numerically conditioned because it avoids quadratic terms in ω. Conditioning is a particularly important problem for lightly damped structures because $\zeta \approx 0.01 \ll 1$. In terms of frequency uncertainty, a standard approach with both representations is to focus on the imaginary part of the pole. This approach essentially ignores the second order effect of the uncertainty on the real part of the pole. With the A_1 representation, a real constant uncertainty

is considered in the frequency squared term, $\omega_{act}^2 = \omega^2(1 + \delta_1)$. Then the actual dynamics can be written as

$$\hat{A}_1 = A_1 + \begin{bmatrix} 0 \\ -\omega \end{bmatrix} \delta_1 \begin{bmatrix} \omega & 0 \end{bmatrix}. \tag{2.12}$$

With the A_2 representation, the frequency is considered to be uncertain, so that $\omega_{act} = \omega(1 + \delta_2)$. Then, we can write

$$\hat{A}_2 = A_2 + \begin{bmatrix} 0 & -\omega\sqrt{1-\zeta^2} \\ \omega\sqrt{1-\zeta^2} & 0 \end{bmatrix} \begin{bmatrix} \delta_2 & 0 \\ 0 & \delta_2 \end{bmatrix} \begin{bmatrix} 1 & 0 \\ 0 & 1 \end{bmatrix}. \tag{2.13}$$

Note that in this case, the uncertainty δ_2 is repeated. The repetition significantly complicates the problem formulation, and treating the two frequency uncertainties as independent leads to a conservative result. Consequently, the A_1 representation and scalar, frequency squared uncertainties are typically used in this thesis. Since δ_1 is an uncertainty on ω^2, its effective uncertainty on ω is approximately $\delta_1/2$.

As discussed, the results in this thesis are developed for parameter errors in the system matrix A. As before, it is assumed that appropriate B_0 and C_0 matrices exist to specify the structure of these uncertain parameters. The form of the block Δ then determines the uncertainties that are to be considered.

To develop a better understanding of the robustness problem, it is important to consider several Δ blocks and the equivalent classes of uncertain functions that they represent. Frequency dependent complex Δ blocks contain no phase information about the parameter uncertainty. These complex robustness tests can be interpreted as including the class of sector-bounded arbitrarily time-varying nonlinear functions [64]. For many problems with real parameter uncertainties, the Δ block can be represented by real time-invariant linear functions. There also exist many cases for which real time-invariant nonlinear parameter uncertainties are important. As discussed in the Introduction, one approach to the stability problem with real uncertainties is to develop robustness tests for these time-invariant nonlinear uncertainties. In this approach, the aim is to constrain the class of complex uncertainties to develop robustness tests that are less conservative for problems with real uncertainties.

Absolute stability theory provides a technique for developing stability tests with nonlinear uncertainties. The theory provides tests to determine stability of a system

coupled to an entire class of nonlinear functions. In particular, using the Popov stability criteria, it is possible to determine stability for the class of time-invariant sector-bounded nonlinear functions [131, 132]. Thus, in this thesis, the linear block $\Delta(y) = Fy$ of the μ framework is replaced with a nonlinear function $\tilde{\Delta}(y) = f(y)$. By specifying various characteristics of these nonlinear functions, stability tests are developed in this thesis for three main classes of nonlinear parameter uncertainties. Equivalent frequency domain criteria are used to illustrate that the robustness tests include phase information, and are thus less conservative than complex models for problems with real uncertainties.

The arbitrarily time-varying nonlinear function interpretation follows from the complex models of the uncertainty. The effort here is aimed at two main goals. The first is to use tests that restrict the time-variation of the uncertainty. The second goal is to consider more specific classes of nonlinear functions to develop potentially less conservative tests. As will be shown in later developments, a key advantage of this nonlinear approach to the robustness problem is the physical insight that it provides to the stability conditions. Furthermore, the state space stability criteria can be used to develop a combined $\mathcal{H}_2$/real μ synthesis algorithm. These points will be discussed once the connections to μ analysis are developed in Chapter 3 and the synthesis algorithm is presented in Chapters 4 and 5.

2.3 Supply Rates, Storage Functions, and System Stability

As discussed by Grujić *et al.* [60], one of the difficulties with Lyapunov's direct method is developing a framework in which Lyapunov functions can be constructed for systems with parameter uncertainty. However, Willems [165,166] and Hill and Moylan [78,80] provide such a framework based on the concepts of supply rates, storage functions, and system dissipation. This approach plays a vital role in the developments of Chapter 3. The purpose of this section is to provide the key definitions necessary to develop the framework.

Consider a dynamic system $\mathcal{G}$ of the form

$$\dot{x}(t) = Ax(t) + Bu(t), \tag{2.14}$$

$$y(t) = g(x(t)) + Du(t), \tag{2.15}$$

where $u(t) \in \mathbb{R}^m$, $y(t) \in \mathbb{R}^l$, and $x(t) \in \mathbb{R}^n$. In the special case where the output function is linear ($g(x) = Cx$) $\mathcal{G} = G(s)$ is a linear time-invariant (LTI) system with realization of the form in Eq. 2.1.

For the dynamic system $\mathcal{G}$ of Eqs. 2.14 and 2.15, a function $r : \mathbb{R}^l \times \mathbb{R}^m \to \mathbb{R}$, is called a *supply rate* if it is locally integrable, so that $\int_{t_1}^{t_2} |r(y(\xi), u(\xi))| \, d\xi < \infty$ for all $t_1, t_2 > 0$, and if $\oint r(y(\xi), u(\xi)) \, d\xi \geq 0$ for every path that takes the dynamic system from some initial state to the same final state. A more general form for the supply rate presented in by Pinzoni and Willems [130] will be used in this thesis. Under the new definition, the supply rate can be a function of the signals (u, y) and, if they exist, their time derivatives.

Definition 2.1. (Willems [165]). *A system $\mathcal{G}$ of the form in Eqs. 2.14 and 2.15, with states $x \in \mathbb{R}^n$ is said to be* dissipative with respect to the supply rate $r(\cdot, \cdot)$ *if there exists a nonnegative definite function $V_s : \mathbb{R}^n \to \mathbb{R}$, called a* storage function, *that satisfies the dissipation inequality*

$$V_s(x(t_2)) \leq V_s(x(t_1)) + \int_{t_1}^{t_2} r(y(\xi), u(\xi)) \, d\xi, \tag{2.16}$$

for all t_1, t_2 and for all $x(\cdot), y(\cdot)$, and $u(\cdot)$ satisfying Eqs. 2.14 and 2.15.

If $V_s(x)$ is a differentiable function, then an equivalent statement of dissipativeness [165] of the system $\mathcal{G}$ with respect to the supply rate r:

$$\dot{V}_s(x(t)) \leq r(y(t), u(t)), \qquad t \geq 0, \tag{2.17}$$

where $\dot{V}$ denotes the total derivative of $V(x)$ along the state trajectory $x(t)$. For a *strongly dissipative system,* Eq. 2.17 is replaced by the condition $\dot{V}_s(x(t)) < r(y(t), u(t))$ $(x \neq 0)$ with a similar modification to Eq. 2.16. It is assumed in the following that the storage functions are differentiable so that the condition in Eq. 2.17 can be used.

For the particular example of a mechanical system with force inputs and velocity outputs, we can associate the storage function with the stored or available energy in the system, and the supply rate with the net flow of energy into the system.

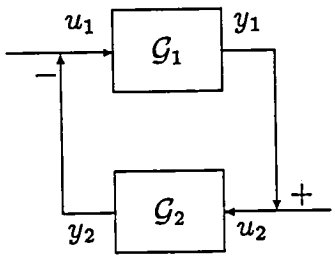

Fig. 2.1: Two interconnected systems.

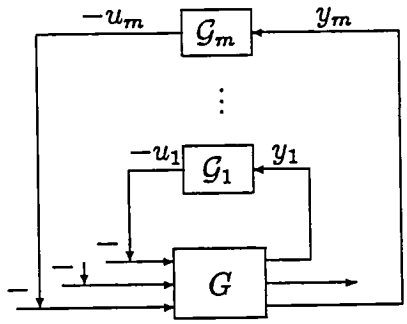

Fig. 2.2: Interconnection of multiple systems for mixed robustness tests.

However, the concepts of the supply rates and storage functions also apply to more general systems for which this energy interpretation is not valid.

A variety of supply rates have been considered by Willems [165,166] and Hill and Moylan [78, 80]. An appropriate supply rate for testing the passivity of a system $y = G(s)u$ is $r(y,u) = u^T y$. This choice can be motivated by the same example of a mechanical system with a force input and velocity output, so that the product $u^T y$ is the power input to the system. For bounded gain tests, the appropriate supply rate is $r(y,u) = u^T u - \gamma^2 y^T y$. A motivation for this choice follows from the identity:

$$\int_0^T r(y,u)\ \mathrm{d}t = \int_0^T u^T u\ \mathrm{d}t - \gamma^2 \int_0^T y^T y\ \mathrm{d}t. \tag{2.18}$$

Eq. 2.18 consists of two parts: the first associated with the energy at the system input, and the second with the weighted energy at the system output. If the integral on the left hand side of Eq. 2.18 is positive, indicating that the weighted output energy is less than the input energy at any time T. Then the system is gain bounded, or, equivalently, $\|G\|_\infty < \gamma^{-1}$.

As will now be shown, storage functions and supply rates provide a means for developing Lyapunov functions for determining the stability of coupled feedback systems. In particular, if there exists a storage function for each system that is dissipative with respect to an appropriate supply rate, then these functions can be combined to form a Lyapunov function for the interconnected system. A more precise statement of this result for two systems interconnected as in Fig. 2.1 is provided by the following lemma.

Lemma 2.1. (Willems [165]) *Consider two dynamic systems $\mathcal{G}_1$ and $\mathcal{G}_2$ with state space representation as in Eqs. 2.14 and 2.15, and input-output pairs (u_1, y_1) and (u_2, y_2) respectively. Assume that the two systems are connected as illustrated in Fig. 2.1, so that $u_1 = -y_2$ and $u_2 = y_1$. Furthermore, associated with these systems are states x_1, x_2, supply rates $r_1(y_1, u_1)$, $r_2(y_2, u_2)$ and storage functions $V_{s1}(x_1)$, $V_{s2}(x_2)$ respectively. Suppose that both $V_{s1}(x_1)$ and $V_{s2}(x_2)$ positive definite, and that the supply rates satisfy $r_1(y_1, u_1) + r_2(y_2, u_2) = 0$, for all $u_1 = -y_2$ and $u_2 = y_1$. Then the solution $(x_1, x_2) = 0$ of the feedback interconnection of $\mathcal{G}_1$ and $\mathcal{G}_2$ is Lyapunov stable with Lyapunov function $V = V_{s1} + V_{s2}$.*

Proof. Since $V = V_{s1} + V_{s2}$ is the sum of two positive definite functions, it is positive definite. Furthermore, $\dot{V}(x_1, x_2) = \dot{V}_{s1}(x_1) + \dot{V}_{s2}(x_2) \leq r_1(y_1, u_1) + r_2(y_2, u_2) = 0$. From the positive definiteness of V and the negative semidefiniteness of $\dot{V}$, it follows that V is a Lyapunov function that guarantees the Lyapunov stability of the solution $(x_1, x_2) = 0$. □

In the special case that the states $x_2(t)$ can be written in terms of the states $x_1(t)$ for all $t \geq 0$, then it is possible to relax the assumptions on V_{s2} in Lemma 2.1. In this case, if the storage function V_{s1} is positive definite and the storage function V_{s2} is nonnegative definite, then V is positive definite [165].

Next, we extend the results of Lemma 2.1 to the case of interest in this thesis, where a single LTI system $G(s)$ is interconnected to m independent systems, as illustrated in Fig. 2.2. In this case, we consider a system G with m scalar inputs and outputs such that each u_i is only influenced by y_i. The systems in this example are special cases of those in Lemma 2.1, because one is LTI and the other is block diagonal.

Corollary 2.1. *Consider an LTI system $G(s)$ with inputs u_i, outputs y_i, $i = 1, \ldots, m$, and states x. Introduce the dynamic systems $\mathcal{G}_i$*

$$\dot{x}_i(t) = A_i x_i(t) + B_i y_i(t), \tag{2.19}$$

$$-u_i(t) = g_i(x_i(t)), \tag{2.20}$$

with supply rates $r_i(-u_i(t), y_i(t))$ *and positive definite storage functions* $V_{si}(x_i(t))$. *Define an* overall supply rate

$$R(y_1(t), \ldots, y_m(t), u_1(t), \ldots, u_m(t)) = \sum_{i=1}^{m} \gamma_i r_i(-u_i(t), y_i(t)),$$

with $\gamma_i > 0$, $i = 1, \ldots, m$. *If there exists a positive definite storage function* $V_G(x)$ *for the system* $G(s)$ *that is dissipative with respect to the negative of the overall supply rate, then the interconnected system is Lyapunov stable.*

Proof. Consider the positive definite function

$$V(x, x_1, \ldots, x_m) = V_G(x) + \sum_{i=1}^{m} \gamma_i V_{si}(x_i).$$

From the definition of storage functions, it follows that $\dot{V}_{si}(x_i(t)) \leq r_i(-u_i(t), y_i(t))$, $i = 1, \ldots, m$, and $\dot{V}_G(x) \leq -R(y_1(t), \ldots, y_m(t), u_1(t), \ldots, u_m(t))$. Then

$$\begin{aligned} \dot{V}(x(t), x_1(t), \ldots, x_m(t)) &= \dot{V}_G(x(t)) + \sum_{i=1}^{m} \gamma_i \dot{V}_{si}(x_i(t)) \\ &\leq -R(\cdot, \cdot) + \sum_{i=1}^{m} \gamma_i r_i(\cdot, \cdot) = 0. \end{aligned}$$

where the arguments of the supply rates are dropped for clarity. □

As before, if the states $x_1, \ldots, x_m$ of the dynamic systems can be written in terms of x, then V is positive definite if V_G is positive definite and V_{si}, $i = 1, \ldots, m$ are nonnegative definite. Furthermore, if the positive definite storage function V_G is strongly dissipative with respect to the corresponding supply rate $-R(\cdot, \cdot)$, then the Lyapunov function V is positive definite and $\dot{V}$ is negative definite. It then follows that the interconnected system is asymptotically stable.

The results of Corollary 2.1 convert the problem of determining the stability of interconnected systems to that of determining appropriate supply rates and storage functions, and then testing for dissipativeness of the independent systems. For the problem addressed here, where insights into determining the supply rates are available from the characteristics of the nonlinearities, this approach greatly facilitates the construction of the Lyapunov functions. Both complex and real uncertainties can be incorporated into these tests by mixing the supply rates for the different dynamic systems.

In the following chapters, a framework is developed that uses the results of this section to derive stability criteria with several classes of nonlinear functions. Using equivalent frequency domain tests, these absolute stability criteria are related to the robust stability problems addressed by real μ. The next section presents the Ω-bound framework required to incorporate these stability criteria into an $\mathcal{H}_2$ control design.

2.4 The Ω-Bound Framework

The robust stability and robust performance problems were discussed in the Introduction. This section presents formal definitions of these problems, and shows how they can be solved by means of parameter-dependent bounding functions. The result is a framework that plays an important role in the later developments of the synthesis problem. The following is an overview of the results by Haddad and Bernstein [66,69]. Let $\mathcal{U} \subset \mathbb{R}^{n\times n}$ denote a set of perturbations ΔA of a nominal matrix $A \in \mathbb{R}^{n\times n}$. The robust stability problem is to determine if $A + \Delta A$ is asymptotically stable for all $\Delta A \in \mathcal{U}$.

Robust Stability Problem. Determine whether the linear system

$$\dot{x}(t) = (A + \Delta A)x(t), \quad \forall\, t \geq 0, \tag{2.21}$$

is asymptotically stable for all $\Delta A \in \mathcal{U}$.

To consider robust performance, introduce an external disturbance model involving white noise signals as in standard $\mathcal{H}_2$ theory. The robust performance problem focuses on the worst-case $\mathcal{H}_2$ norm over $\mathcal{U}$ of the expected value of a quadratic in $z(t) = Ex(t)$, when the system is subjected to a standard white noise disturbance $w(t) \in \mathbb{R}^d$ with weighting $D \in \mathbb{R}^{n\times d}$.

Robust Performance Problem. Consider the linear system

$$\dot{x}(t) = (A + \Delta A)x(t) + Dw(t), \quad \forall\, t \geq 0, \tag{2.22}$$

$$z(t) = Ex(t), \tag{2.23}$$

where $w(\cdot)$ is a zero-mean $d-$dimensional white noise signal with intensity I_d and $E \in \mathbb{R}^{q\times n}$. The aim is then to determine a performance bound β satisfying

$$J(\mathcal{U}) \triangleq \sup_{\Delta A \in \mathcal{U}} \limsup_{t\to\infty} \mathsf{E}\{\|z(t)\|_2^2\} \leq \beta. \tag{2.24}$$

The $\mathcal{H}_2$ performance measure in Eq. 2.24 can be expressed in terms of the observability Gramian for the pair $(A + \Delta A, E)$. Since D and E may be rank deficient, a finite performance bound β satisfying Eq. 2.24 may exist even though Eq. 2.21 is not asymptotically stable for all perturbations in $\mathcal{U}$. However, in practice, robust performance is mainly of interest when Eq. 2.21 is robustly stable. The approach here is to obtain robust stability as a consequence of the sufficient conditions for robust performance. In the following, define the nonnegative definite matrices $R \triangleq E^T E$ and $V \triangleq DD^T$.

Lemma 2.2. (Haddad and Bernstein [66]). *Suppose $A + \Delta A$ is asymptotically stable for all $\Delta A \in \mathcal{U}$. Then*

$$J(\mathcal{U}) = \sup_{\Delta A \in \mathcal{U}} \operatorname{tr} Q_{\Delta A} R, \tag{2.25}$$

where the $n \times n$ matrix $Q_{\Delta A} \triangleq \lim_{t \to \infty} \mathbb{E}[x(t)x^T(t)]$ is given by

$$Q_{\Delta A} = \int_0^\infty e^{(A+\Delta A)t} V \, e^{(A+\Delta A)^T t} \, dt, \tag{2.26}$$

that is the unique, nonnegative definite solution to

$$0 = (A + \Delta A)Q_{\Delta A} + Q_{\Delta A}(A + \Delta A)^T + V. \tag{2.27}$$

The connections with traditional Lyapunov function theory are clearer if the $\mathcal{H}_2$ performance measure is written in terms of a dual variable $P_{\Delta A}$. This matrix solves a Lyapunov equation in which the roles of $A + \Delta A$ and $(A + \Delta A)^T$ are reversed.

Proposition 2.1. *Suppose $A + \Delta A$ is asymptotically stable for all $\Delta A \in \mathcal{U}$. Then*

$$J(\mathcal{U}) = \sup_{\Delta A \in \mathcal{U}} \operatorname{tr} P_{\Delta A} V, \tag{2.28}$$

where $P_{\Delta A} \in \mathbb{R}^{n \times n}$ is the unique, nonnegative definite solution to

$$0 = (A + \Delta A)^T P_{\Delta A} + P_{\Delta A}(A + \Delta A) + R. \tag{2.29}$$

Proof. Note that

$$\operatorname{tr} Q_{\Delta A} R = \operatorname{tr} \int_0^\infty e^{(A+\Delta A)t} V \, e^{(A+\Delta A)^T t} \, \mathrm{d}t \, R = \operatorname{tr} P_{\Delta A} V, \tag{2.30}$$

where

$$P_{\Delta A} \triangleq \int_0^\infty e^{(A+\Delta A)^T t} R \, e^{(A+\Delta A)t} \, \mathrm{d}t \tag{2.31}$$

satisfies Eq. 2.29. □

Remark 2.1. In Lemma 2.2, $Q_{\Delta A}$ can also be viewed as the controllability Gramian for the pair $(A + \Delta A, D)$. Similarly, $P_{\Delta A}$ in Proposition 2.1 can be viewed as the observability Gramian for the pair $(E, A + \Delta A)$. □

Remark 2.2. The stochastic performance measure $J(\mathcal{U})$ given by Eq. 2.24 can also be written as

$$J(\mathcal{U}) = \sup_{\Delta A \in \mathcal{U}} \int_0^\infty \| E \, e^{(A+\Delta A)t} D \|_{\mathrm{F}}^2 \, \mathrm{d}t = \sup_{\Delta A \in \mathcal{U}} \| G_{\Delta A}(s) \|_2^2, \tag{2.32}$$

where

$$G_{\Delta A}(s) \triangleq E[sI - (A + \Delta A)]^{-1} D, \tag{2.33}$$

which involves the $\mathcal{H}_2$ norm of the impulse response of Eqs. 2.22 and 2.23. This stochastic performance measure can also be given a deterministic interpretation by letting $w(t)$ denote an impulse at $t = 0$. □

The key step in obtaining robust stability and performance is to bound the uncertain terms $\Delta A^T P_{\Delta A} + P_{\Delta A} \Delta A$ in the Lyapunov Eq. 2.29. These bounds can be achieved by using a parameter-dependent bounding function $\Omega(P, \Delta A)$ that guarantees robust stability by means of a family of Lyapunov functions. As shown in Ref. [66], this framework corresponds to the construction of a parameter-dependent Lyapunov function (PDLF) that guarantees robust stability. A key feature of these PDLF's is the fact that they constrain the class of allowable time-varying uncertainties. These constraints are very important for reducing the conservatism of the tests for systems with constant real parameter uncertainty.

Let $\mathbb{S}^r$ and $\mathbb{N}^r$ denote the sets of $r \times r$ symmetric and nonnegative definite matrices respectively. The following result is fundamental and forms the basis for all later developments:

Theorem 2.1. (Haddad and Bernstein [66]). *Let* $\Omega_0 : \mathbb{N}^n \to \mathbb{S}^n$ *and* $P_0 : \mathcal{U} \to \mathbb{S}^n$ *be such that*

$$\Delta A^T P + P\Delta A \leq \Omega(P, \Delta A) \triangleq \Omega_0(P) - [(A + \Delta A)^T P_0(\Delta A) + P_0(\Delta A)(A + \Delta A)], \quad (2.34)$$

for all $\Delta A \in \mathcal{U}$ *and* $P \in \mathbb{N}^n$. *Suppose there exists* $P \in \mathbb{N}^n$ *satisfying*

$$0 = A^T P + PA + \Omega_0(P) + R, \quad (2.35)$$

such that $P + P_0(\Delta A)$ *is nonnegative definite for all* $\Delta A \in \mathcal{U}$. *Then*

$$(A + \Delta A, E) \text{ is detectable, } \forall\, \Delta A \in \mathcal{U}, \quad (2.36)$$

if and only if

$$A + \Delta A \text{ is asymptotically stable, } \forall\, \Delta A \in \mathcal{U}. \quad (2.37)$$

In this case,

$$P_{\Delta A} \leq P + P_0(\Delta A), \quad \forall\, \Delta A \in \mathcal{U}, \quad (2.38)$$

where $P_{\Delta A}$ *is the solution of Eq. 2.29. Therefore,*

$$J(\mathcal{U}) \leq \operatorname{tr} PV + \sup_{\Delta A \in \mathcal{U}} \operatorname{tr} P_0(\Delta A)V. \quad (2.39)$$

Also, if there exists $\bar{P}_0 \in \mathbb{S}^n$ *such that*

$$P_0(\Delta A) \leq \bar{P}_0, \quad \forall\, \Delta A \in \mathcal{U}, \quad (2.40)$$

then $J(\mathcal{U}) \leq \beta$, *where* $\beta \triangleq \operatorname{tr}[(P + \bar{P}_0)V]$.

Proof. The details of the proof are presented in Ref. [66]. A key feature in the proof is demonstrating the inequality in Eq. 2.38. Rewrite Eq. 2.35 as

$$0 = (A + \Delta A)^T P + P(A + \Delta A) + \Omega_0(P) - (\Delta A^T P + P\Delta A) + R, \quad (2.41)$$

for any $\Delta A \in \mathbb{R}^{n \times n}$. Then, by adding and subtracting the term $[(A + \Delta A)^T P_0(\Delta A) + P_0(\Delta A)(A + \Delta A)]$, Eq. 2.41 becomes

$$\begin{aligned} 0 &= (A + \Delta A)^T (P + P_0(\Delta A)) + (P + P_0(\Delta A))(A + \Delta A) + \Omega_0(P) + R \\ &\quad -(\Delta A^T P + P\Delta A) - (A + \Delta A)^T P_0(\Delta A) - P_0(\Delta A)(A + \Delta A), \quad (2.42) \\ &= (A + \Delta A)^T (P + P_0(\Delta A)) + (P + P_0(\Delta A))(A + \Delta A) + \Omega_0(P) + R \\ &\quad +\Omega(P, \Delta A) - (\Delta A^T P + P\Delta A). \quad (2.43) \end{aligned}$$

Then, by the assumption in Eq. 2.34, there exists a solution $P \in \mathbb{N}^{n\times n}$ for all $\Delta A \in \mathcal{U}$. Next, subtract Eq. 2.29 from Eq. 2.43 to obtain

$$\begin{aligned} 0 = (A+\Delta A)^T[P + P_0(\Delta A) - P_{\Delta A}] + [P + P_0(\Delta A) - P_{\Delta A}](A+\Delta A) \\ +\Omega(P, \Delta A) - (\Delta A^T P + P\Delta A). \end{aligned} \tag{2.44}$$

From the detectability conditions, it follows that $A + \Delta A$ is asymptotically stable for all $\Delta A \in \mathcal{U}$, which in turn implies that $P + P_0(\Delta A) - P_{\Delta A} > 0$, yielding Eq. 2.38. □

Remark 2.3. If R is positive definite, then the detectability hypothesis of Theorem 2.1 is automatically satisfied. □

Remark 2.4. Theorem 2.1 can be strengthened by noting that the detectability assumption is, in a sense, superfluous. Robust stability concerns only the undisturbed system in Eq. 2.21, while R involves the $\mathcal{H}_2$ performance weighting. Hence, robust stability is guaranteed by the existence of a solution $P \in \mathbb{N}^n$ satisfying Eq. 2.35 with R replaced by αI_n, for some $\alpha > 0$. From Remark 2.3, detectability is automatic with this replacement. However, for robust performance, P in Eq. 2.39 must be obtained from Eq. 2.35. □

The last step is to establish connections between Theorem 2.1 and Lyapunov function theory. Specifically, it is shown that a parameter-dependent Ω-bound establishing robust stability is equivalent to the existence of a parameter-dependent Lyapunov function that establishes robust stability. To show this, assume there exists a positive definite solution to Eq. 2.35, let $P_0 : \mathcal{U} \to \mathbb{N}^n$, and define the parameter-dependent Lyapunov function

$$V(x, \Delta A) \triangleq x^T(P + P_0(\Delta A))x. \tag{2.45}$$

Note that, since P is positive definite and $P_0(\Delta A)$ is nonnegative definite, $V(x)$ is positive definite. Thus, the corresponding Lyapunov derivative is given by

$$\begin{aligned} \dot{V}(x) &= x^T[(A+\Delta A)^T(P + P_0(\Delta A)) + (P + P_0(\Delta A))(A+\Delta A)]x \\ &= x^T[A^TP + PA + \Delta A^TP + P\Delta A + A^TP_0(\Delta A) + P_0(\Delta A)A \\ &\qquad +\Delta A^TP_0(\Delta A) + P_0(\Delta A)\Delta A]x. \end{aligned} \tag{2.46}$$

Equivalently, using Eq. 2.35

$$\dot{V}(x) = -x^T[\Omega_0(P) - \{\Delta A^T P + P\Delta A + (A+\Delta A)^T P_0(\Delta A) + P_0(\Delta A)(A+\Delta A)\} + R]x. \qquad (2.47)$$

Thus, using Eq. 2.34, it follows that $\dot{V}(x) \leq 0$, so that $A+\Delta A$ is stable in the sense of Lyapunov. Asymptotic stability can be shown using La Salle's Theorem in Ref. [97] if $\dot{V}(x) = 0$ implies $x = 0$. Note that $\dot{V}(x) = 0$ implies $Rx = 0$, or equivalently, $Ex = 0$. With $\dot{x}(t) = (A + \Delta A)x(t)$, $Ex = 0$, and the detectability assumption in Eq. 2.36, it follows from the Popov-Belevitch-Hautus (PBH) test [104] that $x = 0$, which establishes asymptotic stability.

To apply Theorem 2.1, a function $\Omega_0(\cdot)$ must be specified and an uncertainty set $\mathcal{U}$ defined such that Eq. 2.34 holds. If the existence of a nonnegative definite solution P to Eq. 2.35 can be determined analytically or numerically and the detectability condition Eq. 2.36 is satisfied, then robust stability is guaranteed and the performance bound Eq. 2.39 can be computed. The $\Omega(\cdot)$-bounds for the examples in this thesis are developed in Chapters 4 and 5.

2.5 Summary

This chapter outlines some of the key definitions and preliminaries necessary to develop the analysis and synthesis tools in this thesis. The concepts of supply rates, storage functions, and system dissipation are used in the next chapter to provide a unifying framework in which Lyapunov functions can easily be constructed. State space criteria in terms of Riccati equations and parameter-dependent Lyapunov functions are developed for systems with several classes of nonlinear parameter uncertainties. Frequency domain tests from these supply rates are then used to demonstrate how these criteria are related to other current approaches to robust control. The Ω-bound framework is then used to develop synthesis techniques that enforce these stability criteria while minimizing an overbound of an $\mathcal{H}_2$ performance objective for the closed-loop system.

Chapter 3

Robust Stability Analysis

In this chapter, we use the powerful tool of system dissipativity to develop a framework for deriving stability criteria for interconnected systems. The concepts of supply rates and storage functions from Section 2.3 play a critical role in this development. In this unified framework, several classes of memoryless nonlinear functions are considered in the state space and frequency domain stability conditions. Furthermore, these stability criteria are derived in a way that can easily be incorporated into robust stability and performance problems, as will be shown in Chapters 4 and 5.

The robust stability analysis problem is considered in this chapter for the case of nonlinear parameter uncertainties. In this approach, the linear uncertainties used in μ analysis are considered to be a special case of this much broader nonlinear class. To illustrate the relationship between the two approaches, the discussion in this chapter emphasizes the differences in the formulation of the analysis problems with linear and nonlinear uncertainties.

The first three sections of this chapter investigate the stability tests for sector-bounded nonlinear functions using the Popov stability multiplier. These sections serve to illustrate the storage function and supply rate framework on a simple problem. The analysis is then extended to consider the more complex cases of monotonic and odd monotonic nonlinearities. The chapter concludes by demonstrating the importance of these stability criteria for robust control design. Some important connections between the approach in this thesis and concurrent work on mixed μ and K_m synthesis are

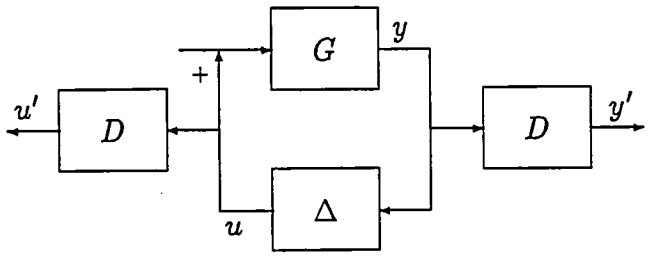

Figure 3.1: Standard framework for stability tests with linear systems and complex uncertainty blocks.

also presented.

3.1 Development of the Stability Criteria

We begin with a discussion of the analysis problem with both linear and nonlinear uncertainties. Fig. 3.1 illustrates the framework for linear uncertainties in the block Δ. In this thesis, we consider the case of diagonal uncorrelated uncertainties, and thus write $\Delta = \text{diag}(\delta_1, \ldots, \delta_m)$.

In this linear case, the stability of the interconnected system is typically determined using the small gain theorem [44]. State space tests for stability can be developed using the bounded gain supply rate in Section 2.3 with the system inputs and outputs $u(t)$, $y(t) \in \mathbb{R}^m$. As discussed by Doyle [47], these stability tests can be refined using the diagonal scaling functions $D(s)$ ($D = D^* > 0$), as shown in the figure. Note that in this linear case, $u' = D \circ \Delta \circ D^{-1} \circ y' = \Delta \circ y'$, where $A \circ B$ denotes the convolution of A and B. The result is that the uncertainty block is not influenced by the scaling functions, which implies that the properties of the uncertainty block Δ, such as magnitude bounds, are unchanged. This, in turn, implies that the same form of the supply rate can be used to develop stability criteria with the new input-output pair (u', y') instead of (u, y). Of course, the system matrix is now $G'(s) = D(s)G(s)D^{-1}(s)$. The scaling functions $D(s)$ are used to include information about the characteristics of the linear uncertainty block in the representation of the modified system $G'(s)$.

A different framework is required for a system $G(s)$ with nonlinear uncertainties, as illustrated in Fig. 3.2. The stability tests in this case will be developed using

the concepts of passivity. There are several key differences between this nonlinear case and the linear approach considered previously. For instance, consider the scaling functions. If the uncertainty block Δ is linear, then it was shown that, because they do not directly influence the block Δ, the scaling functions D are essentially arbitrary. However, the same approach cannot be used with nonlinear uncertainties. Consider Fig. 3.2 with the linear block Δ replaced with a class of nonlinear functions $f(\cdot)$. It is assumed that this class of functions has a well defined set of characteristics, such as sector or slope bounds. As before, we can consider the function from y' to u'. However, the resulting function in this case is $f'(\cdot) = D \circ f(D^{-1} \circ (\cdot))$. This change in $f'(\cdot)$ indicates that the scaling functions can adversely modify the characteristics of the nonlinearities, with the result that the properties of the new class are either not known or well defined. In this case, the same form of the supply rate based on (u', y') cannot be used, and the advantages of the scaling functions demonstrated in the linear case are essentially eliminated.

Consequently, in this nonlinear case, only a single scaling block, $W(s)$ is used, and it is selected based on the known slope or gain properties of the nonlinearity $f(\cdot)$ [172]. In the absolute stability literature, $W(s)$ is commonly called a *stability multiplier*. As in the linear case, these multipliers include additional information about the nonlinear functions in the stability tests. Note that in this figure, there is a forward path from $-u$ to $\hat{y}$ through $G(s)$ and $W(s)$, and a return path from $\hat{y}$ to u through $W(s)^{-1}$ and $f(\cdot)$. These paths correspond to the two systems that are considered in the tests for passivity.

The work in this thesis considers the case illustrated in Fig. 2.2 with m independent scalar nonlinear functions in the Δ block. In this case, $f(\cdot)$ is a component decoupled nonlinearity $f(y) = [f_1(y_1), \ldots, f_m(y_m)]^T$ and $W(s) = \text{diag}(W_1(s), \ldots, W_m(s))$. Using a different approach, Haddad and Bernstein [66, 69] have considered a full uncertainty block for the case of sector-bounded nonlinearities.

It was demonstrated in Section 2.3 that the process for determining the absolute stability of a system coupled to a nonlinear function can be broken down into several steps. For each input/output pair of the system $G(s)$, we consider the system $\mathcal{G}_i$ with

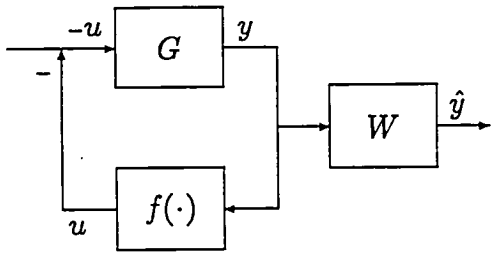

Fig. 3.2: Standard framework for stability tests with linear systems coupled to nonlinearities.

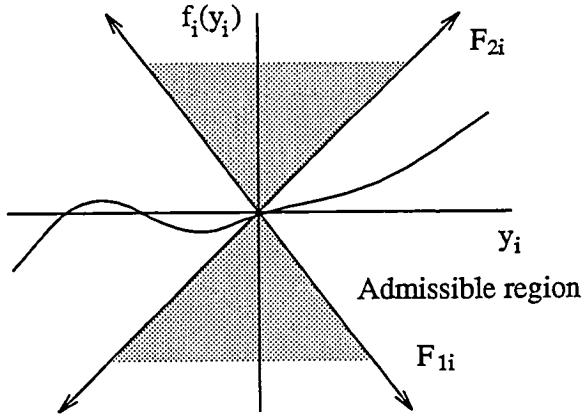

Fig. 3.3: Sector bounds for nonlinear functions in $\mathcal{F}(F_1, F_2)$.

state space representation given by Eqs. 2.19 and 2.20 that is formed by combining $f_i(\cdot)$ and $W_i(s)^{-1}$. Provided the states of the systems $\mathcal{G}_i$ are initialized correctly, they can be written in terms of the states x of the LTI system $G(s)$ [165]. A storage function is given to demonstrate that each system $\mathcal{G}_i$ is dissipative with respect to a supply rate $r(\hat{y}_i, u_i)$. These supply rates are combined into $r(\hat{y}, u)$ to test the dissipativity of the LTI system. We proceed using Corollary 2.1 to demonstrate the asymptotic stability of the interconnected system.

We first consider the case of time-invariant, sector-bounded nonlinear functions. An example of the sector bounds for these nonlinear functions is shown in Fig. 3.3. The constraint can be written as

$$F_{1i}\, y_i^2 \leq f_i(y_i)\, y_i \leq F_{2i}\, y_i^2, \text{ and } f_i(0) = 0. \tag{3.1}$$

In vector form, with $y = [y_1, \ldots, y_m]^T$, define $F_2 = \text{diag}\,(F_{21}, \ldots, F_{2m})$, $F_{2i} \in \mathbb{R}$ and a corresponding diagonal matrix for F_1. The constraints on the nonlinearities $f(\cdot)$ can then be combined as

$$(f(y) - F_1 y)^T\, (F_2 - F_1)^{-1}\, (F_2 y - f(y)) \geq 0, \text{ and } f(0) = 0, \tag{3.2}$$

which originates from work by Zames [173]. The continuous, memoryless nonlinearities $f(y)$ that satisfy the restrictions in Eq. 3.2 defines the class $\mathcal{F}(F_1, F_2)$. Other classes of nonlinear functions will be considered in Sections 3.5.2 and 3.5.3.

Equation 3.2 contains two important special cases that are crucial in the development of the stability criteria. The first case is the infinite sector Popov test ($F_{1i} = 0$, $F_{2i} = \infty$), which only restricts the elements of $f(y)$ to lie in the first and third quadrants of Fig. 3.3. The second is the principal Popov case ($F_{1i} = 0$, $0 < F_{2i} < \infty$), which restricts each gain bounded element of $f(y)$ to lie in the first and third quadrants. These two cases are important because they form the building blocks for problems with more general sector constraints.

3.2 Criteria for Absolute Stability

Many stability criteria ignore the phase information about the uncertainties and, as a result, do not restrict the allowable time variation of the uncertain parameters [64]. This failure to restrict the time-variation results in an important degree of freedom in the stability analysis of many systems. However, if it is expected that the system uncertainties are constant or slowly time-varying, this extra freedom can result in added conservatism in the stability test [98]. This research is primarily concerned with parameter errors that are assumed to be unknown but constant. As discussed in the Introduction, we can explicitly include the nonlinear functions in the Lyapunov function to restrict the time-variation of the uncertainty. The following presents a systematic development of these so-called parameter-dependent Lyapunov functions for sector-bounded nonlinearities.

The Popov criterion [131] was introduced in 1961 in response to the absolute stability problem stated by Lur'e and Postnikov [123]. The appeal of the criterion is the simplicity of the test, which is based on the frequency response of the linear part of the system. However, the main difficulty with stability tests of this nature is determining the appropriate multiplier $W(s)$ in Fig. 3.2. Using a variety of techniques, Popov [131], Zames [173], and Brockett and Willems [28, 29] have shown that the appropriate multiplier is

$$W(s) = (I_m + Ns), \tag{3.3}$$

where $N \in \mathcal{N} = \{\mathbb{R}^{m\times m}; n_{ij} = 0, i \neq j; n_{ii} \geq 0\}$.

Only the form of the multiplier in Eq. 3.3 is considered here. Brockett and

Willems [28, 29] point out that the multiplier $(I_m + \hat{N}s)^{-1}$ corresponds to the case $N \leq 0$ in Eq 3.3, which has a simple frequency domain interpretation. However, the state space tests are invalid in this case, because they can result in a sign indefinite parameter-dependent Lyapunov function. The state space tests can be validated *a posteriori* by confirming that the Lyapunov function is positive definite with a negative value of N.

With this multiplier, we address the derivation of the state space tests with single sector $\mathcal{F}(0_m, F_2)$ nonlinear functions using the combined supply rate

$$r_2(\hat{y}, u) = -u^T \left[(y + N\dot{y}) - F_2^{-1} u \right]. \tag{3.4}$$

This supply rate is related to the one in Section 2.3 for tests of system passivity. Section 3.5 will discuss the derivation of more complicated versions of this supply rate.

The key point in the following development is the framework of supply rates and storage functions in the generation of the Lyapunov functions and Riccati equations to test system stability. Similar results have been developed by Narendra [123] and Haddad and Bernstein [66] via the Positive Real Lemma or, equivalently, the Kalman–Yakubovich Lemma. The goal here is to demonstrate the relative simplicity of the storage function framework before it is applied to more complex problems in subsequent sections. We proceed by developing the time domain conditions for asymptotic stability of the interconnected systems in Fig. 3.2, dealing with m independent sector-bounded nonlinear parameter uncertainties:

Theorem 3.1. ([66,83,123]). *Consider an LTI system $G(s)$ coupled to m independent nonlinear functions that satisfy the sector constraint $0 \leq f_i(y_i)\, y_i \leq F_{2i}\, y_i^2$. If there exists a multiplier $W(s) = (I_m + Ns)$ with $N \in \mathcal{N}$ and a matrix $R = R^T > 0$ $\in \mathbb{R}^{n \times n}$ such that*

(i) $\hat{R}_0 \triangleq \left[(F_2^{-1} + NC_0B_0) + (F_2^{-1} + NC_0B_0)^T \right] > 0$, *and*

(ii) *there exists a symmetric $P > 0$ that satisfies*

$$0 = A^T P + PA + R + (C_0 + NC_0A - B_0^T P)^T \hat{R}_0^{-1}(C_0 + NC_0A - B_0^T P), \qquad (3.5)$$

then the negative feedback interconnection of the system $G(s)$ and the nonlinearities $f_i(\cdot)$, $i = 1, \ldots, m$ is asymptotically stable. In this case, a Lyapunov function for the combined system is given by

$$V = x^T P x + 2\sum_{i=1}^{m} n_{ii} \int_0^{C_{0i}x} f_i(\sigma)\, \mathrm{d}\sigma \qquad (3.6)$$

where C_{0i} corresponds to the i^{th} row of C_0.

Proof: The proof of this theorem follows from the results of Corollary 2.1. Consider a dynamic system $\mathcal{G}_i$ with state space representation given by Eqs. 2.19 and 2.20 that is formed by combining $f_i(\cdot)$ and W_i^{-1}. A storage function can be constructed in terms of the states of $\mathcal{G}_i$. These states can in turn be related to the states (x) of the LTI system $G(s)$ [165]. From Corollary 2.1, we can combine these m storage functions and demonstrate that they satisfy Eq. 2.17 using the supply rate $-r_2(\hat{y}, u)$. We proceed to show that the interconnection is asymptotically stable by demonstrating that the system $G(s)$ is strongly dissipative with respect to the supply rate $r_2(\hat{y}, u)$.

For the combination of $f(\cdot)$, $W(s)$ in Eq. 3.3, and the supply rate in Eq. 3.4, introduce the storage function

$$\begin{aligned} V_{NL} &= \int_0^t u^T N \dot{y}\, \mathrm{d}t = \sum_{i=1}^{m} n_{ii} \int_0^t u_i \dot{y}_i\, \mathrm{d}t, \\ &= \sum_{i=1}^{m} n_{ii} \int_0^{y_i} f_i(\sigma)\, \mathrm{d}\sigma. \end{aligned} \qquad (3.7)$$

The functions $u_i = f_i(y_i)$ satisfying the constraint $0 \leq f_i(y_i)\, y_i \leq F_{2i}\, y_i^2$ lie in the first and third quadrants in Fig. 3.3. Then V_{NL} in Eq. 3.7 represents a sum of the areas under each $f_i(\cdot)$ curve in Fig. 3.3 and is thus nonnegative. Also, from Eq. 3.2, with $u = f(y)$ and $F_1 = 0$, we have that

$$\dot{V}_{NL} = u^T N \dot{y}, \qquad (3.8)$$

$$\leq u^T N \dot{y} + u^T (y - F_2^{-1} u), \qquad (3.9)$$

$$= u^T (y + N\dot{y} - F_2^{-1} u) = -r_2(\hat{y}, u). \qquad (3.10)$$

For the LTI system, introduce a candidate quadratic storage function

$$V_G(x) = \frac{1}{2}x^T P x, \tag{3.11}$$

Clearly, $V_G(x)$ is a positive definite function if P is a positive definite matrix. Then, Eq. 2.17 requires that, for $x \neq 0$

$$\dot{V}_G(x) = \frac{1}{2}\frac{d}{dt}x^T P x < r_2(\hat{y}, u). \tag{3.12}$$

Next, define $\Gamma(x,u) \triangleq \dot{V}_G(x) - r_2(\hat{y},u)$. The condition for dissipation is that

$$\Gamma(x,u) = x^T P \dot{x} + u^T \left[(y - F_2^{-1}u) + N\dot{y}\right] < 0. \tag{3.13}$$

Since $\dot{x} = Ax - B_0 u$, $y = C_0 x$, and $\dot{y} = C_0 \dot{x}$, Eq. 3.13 can be written as

$$\Gamma(x,u) = x^T P A x + u^T(C_0 + NC_0A - B_0^T P)x - u^T(NC_0B_0 + F_2^{-1})u < 0. \tag{3.14}$$

Taking the derivative of $\Gamma(x,u)$ with respect to u yields

$$\frac{\partial \Gamma}{\partial u} = (C_0 + NC_0A - B_0^T P)x - \left[(F_2^{-1} + NC_0B_0) + (F_2^{-1} + NC_0B_0)^T\right]u. \tag{3.15}$$

Solving the equation $\frac{\partial \Gamma}{\partial u} = 0$ gives the sequence of inputs $u_w(t)$ that correspond to a stationary point in the dissipation function of the system. This solution exists if N is selected so that condition (i) of the theorem is satisfied. Furthermore, this condition guarantees that the second derivative $\frac{\partial^2 \Gamma}{\partial u^2} = -\hat{R}_0 < 0$. Then the solution, which corresponds to a maximum stationary point in the function Γ, is given by

$$u_w(t) = \hat{R}_0^{-1}(C_0 + NC_0A - B_0^T P)x(t). \tag{3.16}$$

Substitution of $u_w(t)$ into the expression for $\Gamma(x,u)$ provides a simple way to complete the square, and gives the condition that P satisfy

$$A^T P + PA + (C_0 + NC_0A - B_0^T P)^T \hat{R}_0^{-1}(C_0 + NC_0A - B_0^T P) < 0. \tag{3.17}$$

The selection of any other $u(t) = u_w(t) + \delta u(t)x(t)$, which includes those possibly generated by the nonlinear function $f(y)$, results in a more dissipative system. This follows because substitution of $u_w(t)$ yields

$$\Gamma(x, u_w) - x^T \delta u^T \hat{R}_0^{-1} \delta u \, x < 0. \tag{3.18}$$

where the last term is nonpositive, independent of the form of $\delta u(t)$. Consequently, $u_w(t)$ represents the worst case input in the sense that it minimizes the dissipation of the system. To guarantee that the system be dissipative, it is sufficient to require that this worst case input result in a negative maximum of $\Gamma(x, u_w)$. Thus, select $R = R^T > 0$, and require that $\max_u \Gamma(x, u) = -\frac{1}{2}x^T R x < 0$. Applying this constraint to Eq. 3.17 gives Eq. 3.5. Then, because $P = P^T > 0$, the quadratic function $V_G(x)$ is a positive definite storage function for the system.

Since $y = C_0 x$, we can write $y_i = C_{0i} x$ in the storage functions. From Corollary 2.1, adding the two storage functions in Eqs. 3.7 and 3.11 yields the Lyapunov function

$$\begin{aligned} V &= 2V_G + 2V_{NL} \\ &= x^T P x + 2\sum_{i=1}^{m} n_{ii} \int_0^{C_{0i}x} f_i(\sigma)\, \mathrm{d}\sigma. \end{aligned} \tag{3.19}$$

which shows the explicit dependence on the nonlinear functions. □

3.3 General Sector Bounds

The approach of the preceding section can easily be extended to the general sector problem, where the diagonal elements of both F_2 and F_1 are nonzero. The advantage of this form of the sector constraints is that it does not place limitations on the sign of the uncertainty. As might be expected, the symmetric case $-F_1 = F = F_2$ is of particular importance.

The pole-shift technique of Rekasius and Gibson [133] is shown in Fig. 3.4. This transformation is closely related to the Linear Fractional Transformations (LFT's) that play a key role in μ analysis [171]. The system transformation relates the problems with general sector bounds to the single sector problems considered previously. It is assumed in this analysis that $F_2 > 0$ and $F_2 > F_1$, so that the admissible regions in Fig. 3.3 exist. The shifted system $\tilde{G}$ has inputs $-\tilde{u}$, outputs y, and a state space representation

$$\begin{aligned} \dot{x} &= Ax + B_0(-\tilde{u} - F_1 y), \\ &= (A - B_0 F_1 C_0)x - B_0 \tilde{u}, \end{aligned} \tag{3.20}$$

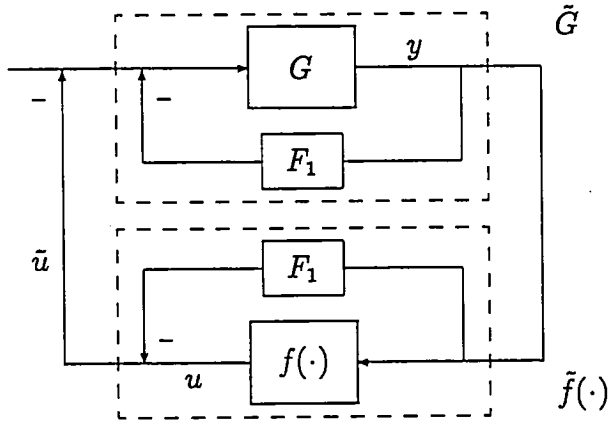

Figure 3.4: The general sector to finite sector transformation, with corresponding definitions of $\tilde{G}$, $\tilde{u}$, and $\tilde{f}(\cdot)$.

$$y = C_0 x, \tag{3.21}$$

where, as defined in the figure, $\tilde{u} = \tilde{f}(y) = u - F_1 y$. The pole-shift procedure transforms f in $\mathcal{F}(F_1, F_2)$ to the nonlinear function $\tilde{f}(\cdot)$ in the class $\mathcal{F}(0_m, F_2 - F_1)$.

To proceed, use the inputs and outputs of this transformed system to redefine the supply rate in Eq. 3.4 as

$$r_3(\hat{y}, \tilde{u}) = -\tilde{u}^T \left[(y + N\dot{y}) - F_d \tilde{u}\right], \tag{3.22}$$

$$= -(u - F_1 y)^T ((y + N\dot{y}) + F_d F_1 y - F_d u), \tag{3.23}$$

$$= -(u - F_1 y)^T F_d (F_2 y - u) - (u - F_1 y)^T N\dot{y}, \tag{3.24}$$

where $F_d = (F_2 - F_1)^{-1}$. Eq. 3.23 follows from Eq. 3.22 using the definition of $\tilde{u}$. Finally, Eq. 3.24 is a consequence of the fact that $(I_m + F_d F_1)y = F_d F_2 y$.

Similarly, the storage function for this case can be developed using Eq. 3.7 with $\tilde{f}(\cdot)$ to obtain

$$V_{NL} = \int_0^t \tilde{f}^T(y) N\dot{y}\, dt = \int_0^t (u - F_1 y)^T N\dot{y}\, dt. \tag{3.25}$$

Again, the function V_{NL} is nonnegative because it can be interpreted as the appropriately signed area between each function $f_i(y_i)$ and $F_{1i}\, y_i$. Also,

$$\begin{aligned} \dot{V}_{NL} &= (u - F_1 y)^T N\dot{y} \\ &\leq (u - F_1 y)^T N\dot{y} + (u - F_1 y)^T (F_2 - F_1)^{-1} (F_2 y - u), \\ &= -r_3(\hat{y}, \tilde{u}). \end{aligned} \tag{3.26}$$

With these results, we present the following:

Theorem 3.2. *Consider an LTI system $G(s)$ coupled to m independent nonlinear functions that satisfy the sector constraint $F_{1i}\, y_i^2 \leq f_i(y_i)\, y_i \leq F_{2i}\, y_i^2$. If there exists a multiplier $W(s) = (I_m + Ns)$ with $N \in \mathcal{N}$ and a matrix $R = R^T > 0 \in \mathbb{R}^{n\times n}$ such that*

(i) $\hat{R}_0 \triangleq \left[(F_d + NC_0B_0) + (F_d + NC_0B_0)^T\right] > 0$, *and*

(ii) *there exists a symmetric $P > 0$ that satisfies*

$$0 = (A - B_0F_1C_0)^TP + P(A - B_0F_1C_0) + R + \left[C_0 + NC_0(A - B_0F_1C_0) - B_0^TP\right]^T \hat{R}_0^{-1}\left[C_0 + NC_0(A - B_0F_1C_0) - B_0^TP\right], \tag{3.27}$$

then the negative feedback interconnection of system $G(s)$ and the nonlinearities $f_i(\cdot)$, $i = 1,\ldots,m$ is asymptotically stable. In this case, a Lyapunov function for the combined system is given by

$$V = x^TPx + 2\sum_{i=1}^{m} n_{ii}\int_0^{C_{0i}x}(f_i(\sigma) - F_{1i}\sigma)\,\mathrm{d}\sigma \tag{3.28}$$

where C_{0i} corresponds to the i^{th} row of C_0.

Proof: The proof of this theorem is exactly analogous to the one developed for Theorem 3.1. The difference in this case is that we must use the modified state space representation of $\tilde{G}$ and the supply rate in Eq. 3.22. □

As expected, the results of Theorem 3.1 are recovered for the case $F_1 = 0$. Since the symmetric case is of particular importance in later developments, we present the following corollary:

Corollary 3.1. *If the nonlinear functions in Theorem 3.2 satisfy the constraint $-F_iy_i^2 \leq f_i(y_i)y_i \leq F_iy_i^2$, and there exists a multiplier $W(s) = (I_m + Ns)$ with $N \in \mathcal{N}$ and a matrix $R = R^T > 0 \in \mathbb{R}^{n\times n}$ such that*

(i) $\hat{R}_{0a} \triangleq \left[F^{-1} + NC_0B_0 + (NC_0B_0)^T\right] > 0$, *and*

(ii) *there exists a symmetric $P > 0$ that satisfies*

$$0 = (A + B_0 F C_0)^T P + P(A + B_0 F C_0) + R + \left[C_0 + N C_0 (A + B_0 F C_0) - B_0^T P\right]^T \hat{R}_{0a}^{-1} \left[C_0 + N C_0 (A + B_0 F C_0) - B_0^T P\right], \quad (3.29)$$

then the negative feedback interconnection of system $G(s)$ and the nonlinearities $f_i(\cdot)$, $i = 1, \ldots, m$ is asymptotically stable.

Section 3.6 considers sufficient conditions in the frequency domain for the existence of positive definite solutions to the equations in Corollary 3.1 and Theorems 3.1 and 3.2. The results of Theorem 3.2 and Corollary 3.1 demonstrate the unified framework of Riccati equation and Lyapunov function tests for system stability. The free parameters in these tests are the sector bounds F_1 and F_2 and the multiplier values N. It is difficult to gain insight into their roles in these state space tests, but the following section demonstrates their function in a frequency domain test.

3.4 Frequency Domain Stability Conditions

The utility of absolute stability criteria such as the one from Popov [131] is the simplicity of their graphical interpretation in the frequency domain. The previous section developed state space conditions for the stability of an LTI system $G(s)$ coupled with two main classes of nonlinear functions. While recent trends in control theory are towards time domain or state space Riccati-based tests, one advantage of these frequency domain criteria is the insight that they provide into the role of the frequency domain multipliers. Lemma 3.1 provides a powerful tool for converting from state space to frequency domain stability conditions within the storage function framework.

Lemma 3.1. (Trentelman and Willems [159]). *Consider an LTI system $y = -Gu$ with supply rate $r(y,u)$. Define a system $z = -Hu$, $z \in \mathbb{R}^{m+l}$ with state space representation $H(s) \overset{\min}{\sim} \left[\begin{array}{c|c} A_h & B_h \\ \hline C_h & D_h \end{array}\right]$ and supply rate $\hat{r}(z,u) = z^T L z$, where $L = L^T \in \mathbb{R}^{(m+l)\times(m+l)}$ and $\hat{r}(z,u) \triangleq r(y,u)$. If A_h has no poles on the $j\omega$-axis, then the following statements are equivalent:*

(i) *the system $H(s)$ is dissipative with respect to the quadratic supply rate $\hat{r}(z,u)$;*

(ii) $H^*(j\omega) L H(j\omega) \geq 0$, $\omega \in \mathbb{R}$.

Proof. See Ref. [159]. □

The system $H(s)$ represents a modification of the system $G(s)$ to provide functions of both the inputs $-u$ and outputs $y = -Gu$ in the output vector z. Consider the simple example of the supply rate $\hat{r}(z,u) = -u^T y$, where

$$z = \begin{bmatrix} y \\ -u \end{bmatrix}, \; H(s) = \begin{bmatrix} G(s) \\ I_m \end{bmatrix}, \text{ and } L = \begin{bmatrix} 0 & I_m \\ I_m & 0 \end{bmatrix}. \tag{3.30}$$

The frequency domain test for dissipativity is then

$$H^*(\jmath\omega)LH(\jmath\omega) = G^*(\jmath\omega) + G(\jmath\omega) \geq 0, \qquad \omega \in \mathbb{R}, \tag{3.31}$$

which, along with the condition that $G(s)$ be asymptotically stable, is the standard matrix positive real test for the system $G(s)$. Note that similar statements can also be developed for the strongly dissipative conditions.

Thus Lemma 3.1 provides a tool for transforming the state space stability criteria given in the previous sections into equivalent frequency domain stability criteria. Furthermore, while these tests are interesting in terms of the extra interpretation that they provide for the multipliers, they also provide conditions for the existence of the positive definite matrices P in Theorems 3.1 and 3.2.

As with the standard Popov test, it is generally possible to interpret the frequency domain criteria as modified Nyquist tests that describe admissible regions of the complex s-plane for the plant transfer function. The goal here is to interpret these tests to develop insights, such as those in Fig. 1.3, towards the aim of modelling real parameter uncertainties.

For the sector-bounded constraints on the nonlinearity, the supply rate of Eq. 3.24 can be written as a function of the inputs $-u$ and outputs y of the system G. For complicated forms of the supply rate, it is useful to introduce the following notation. Let

$$z = T(s) \begin{bmatrix} y \\ -u \end{bmatrix} = T(s) \begin{bmatrix} G(s) \\ I_m \end{bmatrix} (-u) \tag{3.32}$$

where $T(s)$ is a $2m \times 2m$ matrix relating the inputs and outputs to the terms in the supply rate. For simple forms of the supply rate, such as $r = -u^T y$, we have $T = I_{2m}$. However, this more general form also allows us to incorporate the multiplier $W(s)$

and other input–output scaling terms. In particular, using $r_3(\hat{y}, \tilde{u})$ in Eq. 3.23, we define $T_{\text{gen}}(s)$ for the general sector problem as

$$T_{\text{gen}}(s) = \begin{bmatrix} W(s) + F_d F_1 & F_d \\ F_1 & I_m \end{bmatrix}. \tag{3.33}$$

With L fixed and of the form given in Eq. 3.30, the test for dissipativity of the system with respect to this supply rate is

$$0 \leq \begin{bmatrix} G^* & I_m \end{bmatrix} T^*_{gen} \begin{bmatrix} 0 & I_m \\ I_m & 0 \end{bmatrix} T_{gen} \begin{bmatrix} G \\ I_m \end{bmatrix} \quad \forall\, s = \jmath\omega \neq \lambda(A - BF_1C) \tag{3.34}$$

or,

$$0 \leq \begin{bmatrix} G^* & I_m \end{bmatrix} \begin{bmatrix} F_1(W + W^*) + 2F_1F_dF_1 & W^* + 2F_dF_1 \\ W + 2F_dF_1 & 2F_d \end{bmatrix} \begin{bmatrix} G \\ I_m \end{bmatrix} \tag{3.35}$$

As before, we concentrate on the symmetric sector case where $-F_1 = F = F_2$. Since $W(\jmath\omega) = I_m + N\jmath\omega$ and $2F_dF_1 = -I_m$, then $W + 2F_dF_1 = N\jmath\omega$. Furthermore, we have $W + W^* = 2I_m$ and $2F_1F_dF_1 = F$, which imply that $F_1(W + W^*) + 2F_1F_dF_1 = -F$. With these simplifications, the condition in Eq. 3.35 can be rewritten as

$$\begin{aligned} 0 &\leq -G^*FG - G^*(N\jmath\omega) + (N\jmath\omega)G + F^{-1} \\ &= -G^*FG + (\jmath\omega)(NG - G^*N) + F^{-1} \qquad (3.36) \\ &= -\left\{(G + \jmath\omega NF^{-1})^*F(G + \jmath\omega NF^{-1}) - \omega^2N^2F^{-1} - F^{-1}\right\} \qquad (3.37) \end{aligned}$$

Rearranging for ease of interpretation, the stability condition is whether there exists an $N \geq 0$ such that

$$(G + \jmath\omega NF^{-1})^*F(G + \jmath\omega NF^{-1}) \leq F^{-1}(I_m + \omega^2N^2) \tag{3.38}$$

for all ω.

To continue with the geometric interpretation of these extended tests, we consider the original formulation of Popov [131]. Consider a single nonlinear function with sector bounds $(0, h)$. The elements of the stability criterion with the multiplier $W(s) = (1 + \beta s)$ are shown in Fig. 3.5. The test is performed in a modified Nyquist domain $(\text{Re}(G), \omega\text{Im}(G))$, commonly referred to as the *Popov plane*. In the figure, the stability bound is a single straight line with slope governed by $1/\beta$ and real-axis intercept at

$-1/h$. The system is stable if there exist β and h such that the plot of the system transfer function in the Popov plane lies to the right of this line [123]. For a given multiplier coefficient β, there is an optimal value of h where the stability bound just touches the plot of $G(s)$. Collins *et al.* [39] have developed numerical techniques for this optimal analysis problem. Further discussions of this issue are presented in Section 3.7.

In the scalar case, the condition in Eq. 3.38 can be rewritten as

$$\|G(\jmath\omega) + \jmath\omega NF^{-1}\|_2^2 \leq F^{-2}(1 + N^2\omega^2). \tag{3.39}$$

With $G = x + \jmath y$, we obtain

$$\begin{aligned} x^2 + (y + \omega NF^{-1})^2 &\leq F^{-2}(1 + N^2\omega^2) \\ &= (NF^{-1}\omega)^2 + (F^{-1})^2 \end{aligned} \tag{3.40}$$

which leads directly to an interpretation in terms of frequency dependent off-axis circles. As illustrated in Fig. 3.6, the test is equivalent to requiring that, at each frequency ω_a, the transfer function for the system $G(\jmath\omega_a)$ lie within a circle centered on the $\jmath\omega$-axis at $-NF^{-1}\omega_a$. As will be seen, an important feature of these circles is that each one intersects the real axis at $\pm F^{-1}$.

The stability condition in Eq. 3.40 is similar to the ones considered by several authors. Hsu and Meyer [86] develop a similar result in their analysis of *exact frequency domain criteria* with a single, sector-bounded nonlinearity. A frequency dependent "circle" condition is also developed by Zames and Falb [174] using operator theory techniques. They did not consider the same case presented here, so the geometric interpretation is not as clear. Cho and Narendra [35] consider an over bounding off-axis circle test, but the key difference is that the test in Eq. 3.40 is frequency dependent. Bergen, Narendra, and Taylor [16, 123] simplify the problem by specializing to the case in which the elements of F_1 and F_2 have the same sign. The advantage of this assumption is that quadratic terms can be deleted from the stability constraint, which leads to a much simpler geometric interpretation of the condition. The result is that the straight line stability bound in the Popov test is replaced with a parabola. Then,

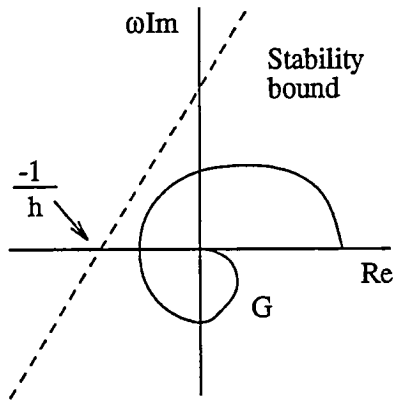

Figure 3.5: Standard Popov test in the modified frequency plane.

as before, only one fixed stability bound is used in the Popov plane. Unfortunately, in the symmetric sector case considered here, F_1 and F_2 have opposite signs, so this simplification is not applicable.

For a given sector bound, the remaining free parameter in the test is N. This value governs the multiplier phase, and from Eq. 3.40, determines the location of the circle centers as a function of frequency. It is the bound in Eq. 3.39 and the geometric interpretation that lead to some important conclusions in Section 3.7 about the upper bounds for real μ . With this new insight into the role of the matrix N, we make the following observation:

Remark 3.1. If $N = 0$, the center of the circle is at the origin for all frequencies. In this case, the frequency domain test is equivalent to the small gain theorem [44]. In the state space tests we can substitute $N = 0$ into condition (i) of Corollary 3.1 to obtain $\hat{R}_{0a}^{-1} = F$. A similar substitution into Eq. 3.29 yields

$$0 = (A + B_0 F C_0)^T P + P(A + B_0 F C_0) + R + \left[C_0 - B_0^T P\right]^T F \left[C_0 - B_0^T P\right]. \quad (3.41)$$

On expanding, Eq. 3.41 becomes

$$\begin{aligned} 0 = A^T P + PA + R + C_0^T F C_0 + P B_0 F B_0^T P + \\ C_0^T F B_0^T P + P B_0 F C_0 - P B_0 F C_0 - C_0^T F B_0^T P, \end{aligned} \quad (3.42)$$

which, after canceling the last four terms, yields

$$0 = A^T P + PA + R + C_0^T F C_0 + P B_0 F B_0^T P. \quad (3.43)$$

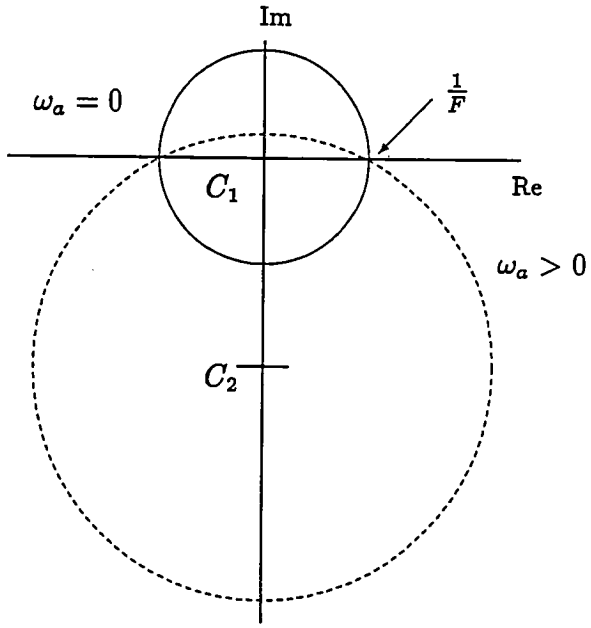

Figure 3.6: Examples of off-axis circle constraints for the symmetric sector Popov test at two frequencies with centers at C_i governed by ω_a. Each circle intersects the real axis at $\pm\frac{1}{F}$.

Since the elements of F just scale the system inputs and outputs, Eq. 3.43 is identical to the standard Riccati equation for the small gain test. □

We can now discuss these stability criteria in terms of the goal of performing stability analysis for a system with real parameter errors. It was shown in the Introduction that the linearized form of the Lyapunov functions in Eqs. 3.6 and 3.28 are parameter-dependent. These restrict the allowable time-variation of the uncertainty, thus incorporating more phase information about the system parameter errors. The geometric interpretation of frequency dependent off-axis circles can be related to other approaches for the system uncertainty. Consider the real parameter uncertainties in Fig. 1.3a scaled to lie between ± 1. With $F = 1$, all of the off-axis circles include this region of the real-axis. A further property of the test is that the center of the constraint circle is near the origin at low frequencies. However, at higher frequencies, when the circle center is far from the origin, the constraint circle is very large. In the limit, they fill the entire semi-plane. Consequently, the off-axis circle test is similar to a frequency blended combination of the small gain and positive real stability criteria.

The off-axis circle test in Fig. 3.6 corresponds to the bounds on the system $G(s)$, but a similar set exists for the uncertainty block. As suggested by the previous

discussion, a key feature of these circles is that, because the location of the circle center changes as a function of frequency, the phase of the uncertainty is restricted. As a result, the difference between real and complex numbers can be distinguished in the robustness test. As discussed in the Introduction, this distinction is crucial for developing less conservative robustness tests for problems with real parameter uncertainties.

In this section, it was demonstrated that the phase of the stability multiplier plays a crucial role in determining the location of the circle center in the frequency domain tests. The phase of the Popov multiplier increases monotonically from 0° to 90° and thus provides few degrees of freedom in the stability tests. The next three sections consider stability tests with more general representations of the stability multipliers. These results will allow us to extend the observations in this section and conclude the discussion on the applicability of this approach to the stability problem with constant real parameter uncertainties.

3.5 Stability Robustness for Extended Nonlinear Functions

The previous sections considered the state space and frequency domain stability tests with sector-bounded nonlinear functions. These analysis results can be extended by including the more specific classes of monotonic and odd monotonic nonlinear functions. These additional tests can be used to provide less conservative stability criteria for certain types of nonlinear parameter uncertainties. Furthermore, with these additional developments, the robustness tests developed in the following sections will cover the continuum of real parameter uncertainties from time-invariant sector-bounded nonlinear functions to constant bounded linear functions.

The results in the following sections will build on the simpler problem developed in the earlier sections of this chapter. The key difference in this case is that the multiplier has additional dynamics that must be augmented to the model of the system.

It is much simpler in this case to consider the supply rates and storage functions for each input-output pair (u_i, y_i) of the system $G(s)$ separately. Then, as in Corollary 2.1, the condition that the storage function for the linear system be dissipative

with respect to the combined supply rates for the nonlinear systems yields the stability criterion for the interconnected system. This criterion can be interpreted as requiring the existence of a positive definite solution of an algebraic Riccati equation. Furthermore, combining the storage functions for the linear and nonlinear systems provides a parameter-dependent Lyapunov function for the interconnected system.

Popov [131] introduced a multiplier for sector-bounded time-invariant nonlinear functions. Several authors have discussed the appropriate multipliers for monotonic and odd monotonic restrictions on the nonlinear functions. Specifically, Narendra and Taylor [123], Brockett and Willems [28,29], Narendra and Cho [120], Zames and Falb [174], and Thathachar and Srinath [158, 156] have developed suitable stability multipliers $W(s)$ for monotonic and odd monotonic nonlinear functions. These multipliers are given by the functions in the sets $\mathcal{W}_{RL}$ and $\mathcal{W}_{RC}$, which exhibit an interlacing pole-zero pattern on the negative real axis. The two sets are distinguished by which is closest to the origin, a pole ($\mathcal{W}_{RC}$) or a zero ($\mathcal{W}_{RL}$) [61]. The standard form of the multiplier for each $i = 1, \ldots, m$ is

$$W_i(s) = \alpha_{i0} + \beta_{i0} s + \sum_{j=1}^{m_{i1}} \alpha_{ij} \left(1 - \frac{\alpha_{ij}}{\beta_{ij}(s + \eta_{ij})} \right) + \sum_{j=m_{i1}+1}^{m_{i2}} \alpha_{ij} \left(1 + \frac{\alpha_{ij}}{\beta_{ij}(s + \eta_{ij})} \right), \quad (3.44)$$

where the coefficients α_{ij}, β_{ij}, and η_{ij} are nonnegative and satisfy $\eta_{ij}\beta_{ij} - \alpha_{ij} \geq 0$. To consider just monotonic nonlinearities, take $m_{i2} = m_{i1}$ in Eq. 3.44 (*i.e.*, eliminate the last summation). For odd monotonic nonlinearities, it is also possible to include multipliers with terms that explicitly contain complex poles and zeroes. While the extra freedom associated with this extension will be discussed later, one can develop very general forms of the multiplier $W_i(s)$ with the three main components of Eq. 3.44.

The frequency domain criteria in the previous sections demonstrate that the multiplier phase plays a crucial role in determining the conservativeness of the analysis test. The first two terms of Eq. 3.44 correspond to the standard Popov multiplier whose phase angle increases monotonically from 0° and 90°. The first sum in Eq. 3.44 is a partial fraction expansion of the driving point impedance of a resistor-inductor (RL) network. While the phase for this class also lies between 0° to 90°, it is not a

monotonically increasing function of frequency. The last summation in Eq. 3.44 is of the form of a driving point impedance of a resistor-capacitor (RC) network, with a pole closest to the origin, and phase between $0°$ and $-90°$.

As illustrated in Fig. 3.2, proving stability of the coupled system requires handling signals of the form $W(s)y$. While obtaining filtered outputs of this form is simple for the Popov multiplier, it is quite complicated for the multipliers in Eq. 3.44. In particular, with these extended multipliers, it is necessary to augment the multiplier dynamics to the original system so that the filtered outputs can be obtained directly from the augmented state vector. The resulting augmented matrix A_a then contains the poles of both the system $G(s)$ and the multipliers $W_i(s)$, $i = 1, \ldots, m$.

While much of absolute stability theory has been developed for infinite sector or slope restrictions on the nonlinearity, the shifting approach discussed in Section 3.2 has been used to handle finite bounds [44, 133]. Define M_1, $M_2 \in \mathbb{R}^{m \times m}$ as diagonal matrices whose nonzero elements represent the upper and lower sector bounds for each input-output loop. The transformations illustrated in Fig. 3.7 convert the general slope restrictions (M_1, M_2) to a one-sided condition $(0, M_2 - M_1)$, and then finally to an infinite one $(0, \infty)$. For now, we consider only the bounds $(0, M_2)$, and a later remark will consider the more general case. The following section outlines the process for shifting these sectors and augmenting the multiplier dynamics. Sections 3.5.2 and 3.5.3 contain the stability tests for systems coupled with monotonic and odd monotonic nonlinearities.

3.5.1 Multiplier augmentation

We begin with a discussion of the transformations illustrated in Fig. 3.7. In the following, take $M_1 = 0$ and $M_2 = M = \text{diag}(M_{11}, \ldots, M_{mm})$, and consider differentiable monotonic and odd monotonic nonlinear functions that satisfy the constraint $\frac{df_i(\sigma)}{d\sigma} < M_{ii}$ for all values of σ. Note that this constraint implies that $f_i(\sigma)$ satisfies the sector constraint $0 \leq \sigma f_i(\sigma) < M_{ii}\sigma^2$. From the figure, observe that $f(y) = \tilde{f}(\tilde{y})$, $\tilde{f}(0) = 0$, and

$$\tilde{y} = y - M^{-1}\tilde{f}(\tilde{y}). \tag{3.45}$$

Desoer and Vidyasagar [44] present a discussion of the existence and uniqueness of the solution of this equation. While these issues dominate the discussion for arbitrary nonlinearities, it is known from [156] that these properties are automatically satisfied for sector-bounded *monotonic* nonlinearities. Furthermore, for each nonlinearity $f_i(y_i)$, with $y_i \neq 0$, define

$$\frac{\tilde{f}_i(\tilde{y}_i)}{\tilde{y}_i} = \frac{f_i(y_i)/y_i}{1 - M_{ii}^{-1} f_i(y_i)/y_i} \quad . \tag{3.46}$$

If $f_i(\cdot)$ is sector-bounded by M_{ii}, then the equivalent condition for the shifted nonlinearity is $\tilde{y}_i \tilde{f}_i(\tilde{y}_i) \geq 0$. Also, by the chain rule,

$$\frac{\mathrm{d}\tilde{f}_i(\tilde{y}_i)}{\mathrm{d}\tilde{y}_i} = \frac{\mathrm{d}f_i(y_i)/\mathrm{d}y_i}{1 - M_{ii}^{-1}\mathrm{d}f_i(y_i)/\mathrm{d}y_i} \quad , \tag{3.47}$$

so that if $f_i(\cdot)$ is differentiable and satisfies the slope restrictions $0 \leq \frac{\mathrm{d}f_i(\sigma)}{\mathrm{d}\sigma} < M_{ii}$, then $\tilde{f}_i(\cdot)$ is also differentiable and satisfies $0 \leq \frac{\mathrm{d}\tilde{f}_i(\sigma)}{\mathrm{d}\sigma}$, and thus is monotonic. The same transformation can be used for slope restricted odd monotonic nonlinearities.

The corresponding changes to the LTI system are also illustrated in Fig. 3.7. In particular, for $M_1 = 0$, the shifted system is given by

$$\tilde{G}(s) = G(s) + M^{-1}, \tag{3.48}$$

with inputs $-u$, and outputs $\tilde{y}$. Each transformed nonlinearity $\tilde{f}_i(\cdot)$ is restricted to lie in the first and third quadrants, so that

$$\sigma\, \tilde{f}_i(\sigma) \geq 0, \qquad \forall\, \sigma \in \mathbf{R}. \tag{3.49}$$

Furthermore, because the transformed nonlinearities are monotonic, they satisfy

$$0 \leq (\tilde{f}_i(\sigma_1) - \tilde{f}_i(\sigma_2))(\sigma_1 - \sigma_2), \;\; \forall\, \sigma_1, \sigma_2 \in \mathbf{R}. \tag{3.50}$$

With these transformations, we can now proceed with the multiplier augmentation. An approach similar to the one in Fig. 3.2 (with $G(s)$, $f(\cdot)$ replaced by $\tilde{G}(s)$, $\tilde{f}(\cdot)$) is used to develop the stability tests. The supply rate in this case is a function of the new output (equivalent to $\hat{y}$ in Fig. 3.2), which is obtained by applying the appropriate multiplier to each element of the output of $\tilde{G}(s)$. Observing the form of

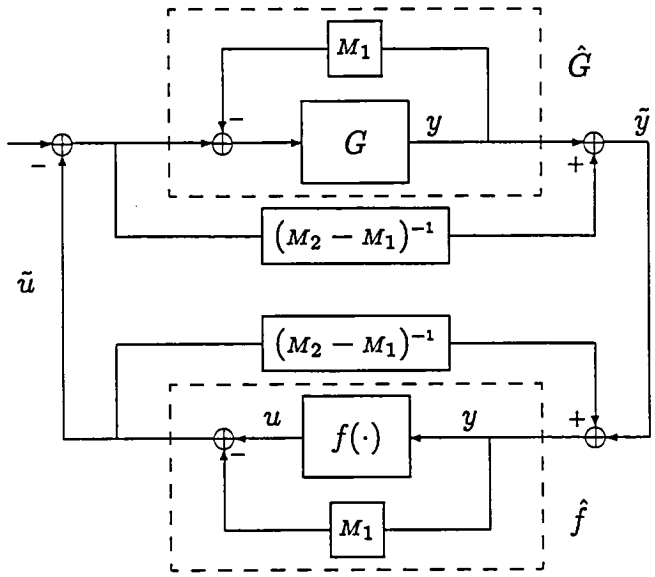

Figure 3.7: System transformations and the definitions of $\hat{G}$, $\hat{f}(\cdot)$, $\tilde{u}$, and $\tilde{y}$. If the lower slope bound $M_1 = 0$, then $\hat{f}(\cdot) = f(\cdot)$, $\hat{G}(s) = G(s)$, and $\tilde{u} = u$.

the multiplier in Eq. 3.44, it can be seen that in the expression $W_i(s)\tilde{y}_i$, there are terms of the form

$$z_{ij} = \frac{\alpha_{ij}\tilde{y}_i}{\beta_{ij}(s + \eta_{ij})}. \tag{3.51}$$

Hence, the corresponding supply rate will involve real signals z_{ij} obtained by passing the system output $\tilde{y}_i$ through a parallel bank of decoupled low pass filters with time constants $1/\eta_{ij}$ and positive gains $\alpha_{ij}/\beta_{ij}\eta_{ij}$. For the system as in Eqs. 2.19 and 2.20, formed from $W_i^{-1}(s)$ and $\tilde{f}_i(\cdot)$, with z_{ij} as the system states, the dynamics of each term in the multiplier can be augmented to the system by rewriting Eq. 3.51 as

$$\dot{z}_{ij} + \eta_{ij} z_{ij} = \frac{\alpha_{ij}}{\beta_{ij}}\tilde{y}_i = \frac{\alpha_{ij}}{\beta_{ij}}\left(C_0 x - M^{-1}u\right)_i, \tag{3.52}$$

where $(\cdot)_i$ denotes to the i^{th} row of $(\cdot)$. Writing the states in a vector $z_i^T \triangleq [z_{i1}, \ldots, z_{im_{i2}}]$, the dynamics associated with each multiplier $W_i(s)$ can be written as

$$\dot{z}_i = \begin{bmatrix} \hat{C}_i & A_i \end{bmatrix} \begin{bmatrix} x \\ z_i \end{bmatrix} - \hat{M}_i u. \tag{3.53}$$

In Eq. 3.53, $A_i \triangleq \text{diag}(-\eta_{ij})$, $j = 1, \ldots, m_{i2}$, and

$$\hat{C}_i \triangleq \begin{bmatrix} \frac{\alpha_{i1}}{\beta_{i1}} \\ \frac{\alpha_{i2}}{\beta_{i2}} \\ \vdots \\ \frac{\alpha_{im_{i2}}}{\beta_{im_{i2}}} \end{bmatrix} (C_0)_i, \quad \hat{M}_i \triangleq \begin{bmatrix} \frac{\alpha_{i1}}{\beta_{i1}} \\ \frac{\alpha_{i2}}{\beta_{i2}} \\ \vdots \\ \frac{\alpha_{im_{i2}}}{\beta_{im_{i2}}} \end{bmatrix} (M^{-1})_i, \tag{3.54}$$

where $(C_0)_i$ and $(M^{-1})_i$ denote the i^{th} rows of the respective matrices.

With m input-output pairs to the system $G(s)$, the multiplier dynamics can be augmented to the shifted system $\tilde{G}(s)$ to obtain a state space representation of $\tilde{G}_a(s)$ given by

$$\dot{x}_a = A_a x_a - B_a u, \tag{3.55}$$

$$\tilde{y} = C_a x_a - M^{-1} u, \tag{3.56}$$

where $n_a \triangleq n + \sum_{i=1}^{m} m_{i2}$, and $x_a \in \mathbb{R}^{n_a}$, A_a, B_a, and C_a are defined as

$$x_a = \begin{bmatrix} x \\ z_1 \\ z_2 \\ \vdots \\ z_m \end{bmatrix}, \; A_a = \begin{bmatrix} A & 0 & 0 & \cdots & 0 \\ \hat{C}_1 & A_1 & 0 & & 0 \\ \hat{C}_2 & 0 & A_2 & & 0 \\ \vdots & & & \ddots & \\ \hat{C}_m & 0 & 0 & & A_m \end{bmatrix}, \; B_a = \begin{bmatrix} B_0 \\ \hat{M}_1 \\ \hat{M}_2 \\ \vdots \\ \hat{M}_m \end{bmatrix}, \tag{3.57}$$

$$C_a = \begin{bmatrix} C_0 & 0 & 0 & \ldots & 0 \end{bmatrix}.$$

Next, define R_{ij} as an output matrix for this augmented system, designed to access the j^{th} element of z_i, so that

$$z_{ij} = R_{ij} x_a. \tag{3.58}$$

Then the only nonzero element of R_{ij} is the $(\sum_{l=1}^{i-1} m_{l2} + j)^{\text{th}}$ term, which is unity.

Note that, although extra dynamics associated with the multipliers have been added to the system $\tilde{G}_a(s)$, it can easily be shown that

$$\tilde{G}_a(s) = C_a(sI - A_a)^{-1} B_a + M^{-1} = C_0(sI - A)^{-1} B_0 + M^{-1} = \tilde{G}(s). \tag{3.59}$$

Hence, by pole-zero cancellation in each input-output loop, the frequency domain representations of $\tilde{G}(s)$ and $\tilde{G}_a(s)$ are equivalent in terms of their input-output properties. The following simple example is used to clarify the preceding notational development.

Example 3.1. Consider a LTI system with realization

$$G(s) \sim \left[\begin{array}{cc|c} 0 & 1 & 0 \\ -1 & -2 & 1 \\ \hline c_1 & c_2 & 0 \end{array}\right], \tag{3.60}$$

where $M = 1$, and the multiplier given by

$$W(s) = \alpha_1(1 - \frac{\alpha_1}{s+\eta_1}) + \alpha_2(1 - \frac{\alpha_2}{s+\eta_2}). \tag{3.61}$$

Let z_1, z_2 be the states corresponding to the multiplier dynamics. Then the augmented system is given by

$$x_a = \begin{bmatrix} x_1 \\ x_2 \\ z_1 \\ z_2 \end{bmatrix}, \; A_a = \begin{bmatrix} 0 & 1 & 0 & 0 \\ -1 & -2 & 0 & 0 \\ \alpha_1 c_1 & \alpha_1 c_2 & -\eta_1 & 0 \\ \alpha_2 c_1 & \alpha_2 c_2 & 0 & -\eta_2 \end{bmatrix}, \; B_a = \begin{bmatrix} 0 \\ 1 \\ \alpha_1 \\ \alpha_2 \end{bmatrix}, \tag{3.62}$$

$$C_a = \begin{bmatrix} c_1 & c_2 & 0 & 0 \end{bmatrix}, \; R_{11} = \begin{bmatrix} 0 & 0 & 1 & 0 \end{bmatrix}, \; R_{12} = \begin{bmatrix} 0 & 0 & 0 & 1 \end{bmatrix}. \tag{3.63}$$

Since

$$(sI - A_a)^{-1} = \begin{bmatrix} (sI - A)^{-1} & 0 & 0 \\ c_1'(s) & (s+\eta_1)^{-1} & 0 \\ c_2'(s) & 0 & (s+\eta_2)^{-1} \end{bmatrix}, \tag{3.64}$$

where

$$c_i'(s) = \frac{\alpha_i}{s+\eta_i} \begin{bmatrix} c_1 & c_2 \end{bmatrix} (sI - A)^{-1}, \quad i = 1, 2, \tag{3.65}$$

it follows that $C_a(sI - A_a)^{-1}B_a = C_0(sI - A)^{-1}B_0$. Furthermore,

$$\begin{aligned} R_{11}(sI - A_a)^{-1}B_a &= \begin{bmatrix} 0 & 0 & 1 & 0 \end{bmatrix} \begin{bmatrix} (sI - A)^{-1} & 0 & 0 \\ c_1'(s) & (s+\eta_1)^{-1} & 0 \\ c_2'(s) & 0 & (s+\eta_2)^{-1} \end{bmatrix} \begin{bmatrix} B \\ \alpha_1 \\ \alpha_2 \end{bmatrix}, \\ &= \begin{bmatrix} c_1'(s) & (s+\eta_1)^{-1} & 0 \end{bmatrix} \begin{bmatrix} B \\ \alpha_1 \\ \alpha_2 \end{bmatrix}, \qquad (3.66) \\ &= \frac{\alpha_1}{s+n_1}\tilde{G}(s), \qquad (3.67) \end{aligned}$$

and similarly for R_{12}.

From Corollary 2.1, it is known that, in the development of the storage functions and supply rates, each input-output pair of $G(s)$ can be considered independently. Hence, without loss of generality, the following develops the supply rates and storage functions for the separate single-input single-output nonlinearities coupled with the appropriate multiplier. Since the goal is to demonstrate that the combination of the nonlinear function and the multiplier, as in Fig. 3.2, is passive, it follows from Section 2.3 that an appropriate supply rate is a product of the system inputs and outputs. A modification of this supply rate is required for the multipliers in Eq. 3.44 if $M \neq 0$. In this case, with s denoting the standard Laplace variable and $\hat{y}_i = W_i(s)\tilde{y}_i$, we consider signals of the form

$$\overline{y}_i = W_i(s)\tilde{y}_i + \beta_{i0} M_{ii}^{-1} s u_i. \tag{3.68}$$

It will be seen that this additional term is equivalent to the quadratic term in Ref. [123] that is added to the Lur'e-Postnikov Lyapunov function to account for a direct transmission in the plant dynamics. As will also be shown in the following development, the term su_i is used to cancel an equivalent term from the Popov multiplier in the expression $\hat{y}_i = W_i(s)\tilde{y}_i$. The assumed differentiability of the shifted nonlinearities guarantees that the expression in Eq. 3.68 exists.

3.5.2 Monotonic nonlinear functions

In this section we develop the supply rates and storage functions for monotonic nonlinearities ($m_{i2} = m_{i1}$), and present robust stability conditions for the full system via algebraic Riccati equations. Using the definitions of $W_i(s)$ in Eq. 3.44, $\tilde{y}$ in Eq. 3.45, and the filtered outputs in Eq. 3.51, the signal in Eq. 3.68 becomes

$$\begin{aligned}
\overline{y}_i &= \sum_{j=1}^{m_{i1}} \alpha_{ij} \left(1 - \frac{\alpha_{ij}}{\beta_{ij}(s+\eta_{ij})}\right) \tilde{y}_i + (\alpha_{i0} + \beta_{i0} s)(y - M^{-1}u)_i + \beta_{i0} M_{ii}^{-1} s u_i \\
&= \sum_{j=1}^{m_{i1}} \alpha_{ij}(\tilde{y}_i - z_{ij}) + (\alpha_{i0} + \beta_{i0} s) y_i - \alpha_{i0} M_{ii}^{-1} u_i \\
&= \sum_{j=1}^{m_{i1}} \alpha_{ij}(\tilde{y}_i - z_{ij}) + \beta_{i0} s y_i + \alpha_{i0} \tilde{y}_i.
\end{aligned} \tag{3.69}$$

We then construct the supply rate $r_i(\overline{y}_i, u_i)$ in terms of the time domain representation of $\overline{y}_i$ and u_i, to obtain

$$r_i(\overline{y}_i, u_i) = \left[\sum_{j=1}^{m_{i1}} \alpha_{ij}(\tilde{y}_i - z_{ij}) + \beta_{i0}\dot{y}_i + \alpha_{i0}\tilde{y}_i\right] u_i. \tag{3.70}$$

An appropriate storage function for this supply rate is given in the following lemma.

Lemma 3.2. *Consider a differentiable monotonic nonlinear function $f_i(\cdot)$ that satisfies the slope restrictions $0 \leq \frac{df_i(\sigma)}{d\sigma} < M_{ii}$. As in Eq. 3.46, define the differentiable monotonic nonlinearity $\tilde{f}_i(\cdot)$ that satisfies Eqs. 3.49 and 3.50. Consider the dynamic system $\mathcal{G}_i$ that is a combination of $\tilde{f}_i(\cdot)$ and $W_i^{-1}(s)$ from Eq. 3.44 ($m_{i2} = m_{i1}$), with corresponding state space representation given by Eqs. 2.19 and 2.20. Then the function V_{si} defined by*

$$V_{si}(\tilde{y}_i, z_{i1}, \ldots, z_{im_{i1}}) = \beta_{i0}\left(\int_0^{\tilde{y}_i} \tilde{f}_i(\sigma)\, d\sigma + \frac{1}{2}M_{ii}^{-1}u_i^2\right) + \sum_{j=1}^{m_{i1}} \beta_{ij}\int_0^{z_{ij}} \tilde{f}_i(\sigma)\, d\sigma, \tag{3.71}$$

is a storage function for the supply rate in Eq. 3.70.

Proof. Since $u_i = \tilde{f}_i(\tilde{y}_i)$, and the dynamics of $\mathcal{G}_i$ can be written in terms of $\tilde{y}_i$ and z_i, $V_{si}(\cdot)$ is a function of the states of the dynamic system. Also, because $\tilde{f}(0) = 0$, it follows that $V_{si}(0) = 0$. From Eq. 3.49, because β_{ij}, $j = 0, 1, \ldots, m_{i1}$ are nonnegative, then V_{si} is nonnegative definite. Finally, to show that Eq. 3.71 is a storage function, it must be demonstrated that it is dissipative with respect to the supply rate of Eq. 3.70.

For notational convenience, let $u_{ij} = \tilde{f}_i(z_{ij})$ and $u_i = \tilde{f}_i(\tilde{y}_i)$. Now, dropping the arguments for convenience,

$$\dot{V}_{si} = \sum_{j=1}^{m_{i1}} \beta_{ij}u_{ij}\dot{z}_{ij} + \beta_{i0}\left[\dot{\tilde{y}}_i + M_{ii}^{-1}\frac{du_i}{dt}\right] u_i. \tag{3.72}$$

From the definition of $\tilde{y}$ in Eq. 3.45, terms of the form $\frac{du_i}{dt}$ cancel. Next, note that Eqs. 3.49 and 3.50 yield

$$0 \leq \alpha_{i0}\tilde{y}_i u_i, \tag{3.73}$$

$$0 \leq \alpha_{ij}(\tilde{y}_i - z_{ij})(u_i - u_{ij}), \tag{3.74}$$

$$0 \leq (\eta_{ij}\beta_{ij} - \alpha_{ij})z_{ij}u_{ij}, \tag{3.75}$$

for $j = 1, \ldots, m_{i1}$. Adding Eqs. 3.73, 3.74, and 3.75 to Eq. 3.72 yields

$$\dot{V}_{si} \leq \sum_{j=1}^{m_{i1}} u_{ij}(\beta_{ij}\dot{z}_{ij}+(\eta_{ij}\beta_{ij}-\alpha_{ij})z_{ij})+\sum_{j=1}^{m_{i1}} \alpha_{ij}(\tilde{y}_i-z_{ij})(u_i-u_{ij})+(\beta_{i0}\dot{y}_i+\alpha_{i0}\tilde{y})u_i. \quad (3.76)$$

Collecting terms yields

$$\dot{V}_{si} \leq \sum_{j=1}^{m_{i1}} \left[\beta_{ij}\dot{z}_{ij} + (\eta_{ij}\beta_{ij} - \alpha_{ij})z_{ij} - \alpha_{ij}(\tilde{y}_i - z_{ij})\right] u_{ij} + \left[\sum_{j=1}^{m_{i1}} \alpha_{ij}(\tilde{y}_i - z_{ij}) + \beta_{i0}\dot{y}_i + \alpha_{i0}\tilde{y}_i\right] u_i. \quad (3.77)$$

Now, it follows from Eq. 3.51 that

$$\beta_{ij}\dot{z}_{ij} = \alpha_{ij}\tilde{y}_i - \beta_{ij}\eta_{ij}z_{ij}, \quad (3.78)$$

so that the first summation of Eq. 3.77 is zero, and using Eq. 3.70 yields

$$\dot{V}_{si} \leq \sum_{j=1}^{m_{i1}} \alpha_{ij}(\tilde{y}_i - z_{ij})u_i + (\beta_{i0}\dot{y}_i + \alpha_{i0}\tilde{y}_i)u_i = r_i, \quad (3.79)$$

which demonstrates that the storage function is dissipative with respect to the supply rate. □

Note that the state space representation for $\mathcal{G}_i$ is in terms of the states $\tilde{y}_i$ and z_i which, because of the augmentation process discussed in the previous section, can easily be written in terms of x_a. While it is convenient to consider the supply rates and storage functions for each nonlinear function, these must be combined to form the supply rate for the linear system $\tilde{G}(s)$ and the full multiplier $W(s)$. Vector notation will simplify this development, but we must first define the following matrices. These definitions are complicated by the fact that each $W_i(s)$ can have a different number of expansion terms in Eq. 3.44. This difficulty can be handled by defining extended values of α_{ij}, β_{ij}, and η_{ij}. Let $m_1 = \max_i(m_{i1})$. Then, for each $i = 1, \ldots, m$, and $j = 1, \ldots, m_1$, let $\alpha_{ij} = 0$, $\beta_{ij} = 0$, $\eta_{ij} = 0$, and $R_{ij} = 0$ if $j > m_{i1}$. Furthermore, define $H_j = \text{diag}(\alpha_{1j}, \ldots, \alpha_{mj})$, $N_j = \text{diag}(\beta_{j1}, \ldots, \beta_{jm})$, $S_j = \text{diag}(\eta_{j1}, \ldots, \eta_{jm})$, $j = 0, 1, \ldots, m_1$. Finally, let $R_j = \left[R_{1j}^T, R_{2j}^T, \ldots, R_{mj}^T\right]^T$. Then as in Corollary 2.1, using Eq. 3.70 to form the overall supply rate for the LTI system $G(s)$ yields

$$R(\overline{y}, u) = \sum_{i=1}^{m} r_i(\overline{y}_i, u_i) \quad (3.80)$$

$$= \begin{bmatrix} u_1 & \cdots & u_m \end{bmatrix} \begin{bmatrix} \sum_{j=1}^{m_{11}} \alpha_{1j}(\tilde{y}_1 - z_{1j}) + \beta_{10}\dot{y}_1 + \alpha_{10}\tilde{y}_1 \\ \vdots \\ \sum_{j=1}^{m_{m1}} \alpha_{mj}(\tilde{y}_m - z_{mj}) + \beta_{m0}\dot{y}_m + \alpha_{m0}\tilde{y}_m \end{bmatrix} \tag{3.81}$$

$$= u^T \left[\sum_{j=1}^{m_1} H_j(\tilde{y} - \hat{z}_j) + N_0\dot{y} + H_0\tilde{y} \right], \tag{3.82}$$

where $\hat{z}_j = [\, z_{1j} \;\cdots\; z_{mj} \,]^T$. This representation of $R(\cdot,\cdot)$ can be simplified further by using the definition of R_j to note that for each j, $\hat{z}_j \triangleq R_j x_a$.

Furthermore, using Eq. 3.45 for $\tilde{y}$, and noting that $\dot{y} = C_a\dot{x}_a = C_a(A_a x_a - B_a u)$, the overall supply rate can then be written as

$$R(\overline{y}, u) = u^T[H_0C_a + N_0C_aA_a + \sum_{j=1}^{m_1} H_j(C_a - R_j)]x_a - u^T(N_0C_aB_a + \sum_{j=0}^{m_1} H_jM^{-1})u. \tag{3.83}$$

The stability condition for the interconnected system can now be presented using the overall supply rate.

Theorem 3.3. *Consider an LTI system $G(s)$ coupled to m independent, differentiable monotonic nonlinearities that satisfy the slope restrictions $0 \leq \frac{df_i(\sigma)}{d\sigma} < M_{ii}$. If for each input-output pair (u_i, y_i), there exist multipliers $W_i(s)$ as in Eq. 3.44 and a matrix $R = R^T > 0 \in \mathbb{R}^{n_a \times n_a}$ such that with the preceding definitions of H_j, N_j, and R_j,*

(i) $\hat{R}_0 \triangleq \left[(N_0C_aB_a + \sum_{j=0}^{m_1} H_jM^{-1}) + (N_0C_aB_a + \sum_{j=0}^{m_1} H_jM^{-1})^T \right] > 0$, *and*

(ii) *there exists a symmetric matrix $P > 0$, satisfying*

$$0 = A_a^TP + PA_a + R + [H_0C_a + N_0C_aA_a + \sum_{j=1}^{m_1} H_j(C_a - R_j) - B_a^TP]^T\hat{R}_0^{-1} [H_0C_a + N_0C_aA_a + \sum_{j=1}^{m_1} H_j(C_a - R_j) - B_a^TP], \tag{3.84}$$

then the negative feedback interconnection of the system $G(s)$ and the nonlinearities $f_i(\cdot)$, $i = 1, \ldots, m$ is asymptotically stable. Furthermore, a Lyapunov function for the

combined system is given by

$$V(x_a) = x_a^T P x_a + 2\sum_{i=1}^{m}\left[\beta_{i0}\left(\int_0^{\tilde{y}_i}\tilde{f}_i(\sigma)\,d\sigma + \frac{1}{2}M_{ii}^{-1}u_i^2\right) + \sum_{j=1}^{m_{i1}}\beta_{ij}\int_0^{z_{ij}}\tilde{f}_i(\sigma)\,d\sigma\right]. \quad (3.85)$$

Proof. The proof of this theorem is very similar to the one for Theorem 3.1. In this case we use the storage function

$$V_G(x_a) = \frac{1}{2}x_a^T P x_a. \quad (3.86)$$

Note that Eq. 3.71 gives a storage function for each input-output pair (u_i, y_i) that is dissipative with respect to a given supply rate. For asymptotic stability of the interconnected system, it must be demonstrated that the positive definite function V_G is strongly dissipative with respect to the negative sum of these supply rates. Clearly, if P is a positive definite matrix, then V_G is a positive definite function. Next, from Eqs. 2.17 and 3.83, we require that

$$\dot{V}_G(x_a(t)) < -R(\overline{y}, u). \quad (3.87)$$

Following the procedure in the proof of Theorem 3.1, $\Gamma(x_a, u)$ is formed and $\frac{\partial\Gamma(x_a,u)}{\partial u} = 0$ is solved for u_w. To prove that the system is dissipative, it is sufficient to guarantee that the worst case input results in a negative maximum of $\Gamma(x_a, u_w)$. Thus, select $R = R^T > 0$, and require that $\max_u \Gamma(x_a, u) = -\frac{1}{2}x_a^T R x_a < 0$. Substituting for u_w into $\Gamma(x_a, u)$ yields the condition that P of Eq. 3.86 satisfy

$$A_a^T P + P A_a + [H_0 C_a + N_0 C_a A_a + \sum_{j=1}^{m_1} H_j(C_a - R_j) - B_a^T P]^T \hat{R}_0^{-1}$$
$$[H_0 C_a + N_0 C_a A_a + \sum_{j=1}^{m_1} H_j(C_a - R_j) - B_a^T P] = -R < 0, \quad (3.88)$$

which is equivalent to Eq. 3.84. Hence, it follows from Corollary 2.1 that the Lyapunov function for the combined system is

$$V = 2V_G + 2\sum_{i=1}^{m} V_{si}. \quad (3.89)$$

Substituting the definitions of these storage functions from Eqs. 3.71 and 3.86 yields Eq. 3.85. □

Remark 3.2. $V(x_a)$ in Eq. 3.85 is an extended Lur'e-Postnikov Lyapunov function because it depends explicitly on the nonlinearity $\tilde{f}_i(\cdot)$. Similarly, in the linear uncertainty case, where $\tilde{f}_i(\tilde{y}_i) = F_i\tilde{y}_i$, $V(x_a)$ becomes a parameter-dependent Lyapunov function because the uncertain parameters F_i explicitly appear in the Lyapunov function. In this case, as discussed in the Introduction, the uncertain parameters are not allowed to be arbitrarily time-varying, and the result is a refined framework for constant real parameter uncertainty. □

3.5.3 Odd monotonic nonlinear functions

We now consider odd monotonic nonlinear functions. The procedure is identical to the one discussed in the previous section, the main difference now being that the transformed nonlinear function $\tilde{f}(\cdot)$ satisfies Eqs. 3.49, 3.50, and an additional constraint, from Ref. [122,123,156,158]

$$0 \leq \sigma_1\tilde{f}(\sigma_1) + \sigma_2\tilde{f}(\sigma_2) + \sigma_1\tilde{f}(\sigma_2) - \sigma_2\tilde{f}(\sigma_1), \quad \forall\, \sigma_1, \sigma_2 \in \mathbb{R}. \tag{3.90}$$

The definition of the supply rate and multiplier augmentation process are as discussed in Sections 3.5.1 and 3.5.2. In this case, we consider $m_{i2} > m_{i1}$ in $W_i(s)$ of Eq. 3.44.

Using the simplification of $r_i(\overline{y}_i, u_i)$ in Eq. 3.70, the definition of z_{ij} in Eq. 3.51, and noting the form of the multiplier terms in $W_i(s)$ for $j = m_{i1}+1, \ldots, m_{i2}$, the supply rate can be rewritten as

$$r_i(\overline{y}_i, u_i) = \left[\sum_{j=1}^{m_{i1}} \alpha_{ij}(\tilde{y}_i - z_{ij}) + \sum_{j=m_{i1}+1}^{m_{i2}} \alpha_{ij}(\tilde{y}_i + z_{ij}) + \beta_{i0}\dot{y}_i + \alpha_{i0}\tilde{y}_i\right] u_i. \tag{3.91}$$

A storage function for this supply rate is given in the following lemma.

Lemma 3.3. *Consider a differentiable odd monotonic nonlinear function $f_i(\cdot)$ that satisfies the slope restrictions $0 \leq \frac{\mathrm{d}f_i(\sigma)}{\mathrm{d}\sigma} < M_{ii}$. As in Eq. 3.46, define the differentiable odd monotonic nonlinearity $\tilde{f}_i(\cdot)$ that satisfies Eqs. 3.49 and 3.90. Consider the dynamic system $\mathcal{G}_i$ that is a combination of $\tilde{f}_i(\cdot)$ and the multiplier $W_i^{-1}(s)$ from Eq. 3.44 ($m_{i2} > m_{i1}$), with corresponding state space representation given by Eqs. 2.19 and 2.20. Then the function V_{si} defined by*

$$V_{si}(\tilde{y}_i, z_{i1}, \ldots, z_{im_{i2}}) = \beta_{i0}\left(\int_0^{\tilde{y}_i} \tilde{f}_i(\sigma)\,d\sigma + \frac{1}{2}M_{ii}^{-1}u_i^2\right) + \sum_{j=1}^{m_{i2}} \beta_{ij}\int_0^{z_{ij}} \tilde{f}_i(\sigma)\,d\sigma, \tag{3.92}$$

is a storage function for the supply rate in Eq. 3.91.

Proof. As in the proof of Lemma 3.2, V_{si} is a nonnegative definite function of the states of the system formed by combining $W_i^{-1}(s)$ with the nonlinearity $\tilde{f}_i(\cdot)$ as in Fig. 3.2. Furthermore, using the results of Lemma 3.2, note that

$$\dot{V}_{si} \leq \left[\sum_{j=1}^{m_{i1}} \alpha_{ij}(\tilde{y}_i - z_{ij}) + \beta_{i0}\dot{y}_i + \alpha_{i0}\tilde{y}_i\right] u_i + \sum_{j=m_{i1}+1}^{m_{i2}} \beta_{ij} u_{ij} \dot{z}_{ij}. \tag{3.93}$$

Note that Eq. 3.90 yields

$$0 \leq \alpha_{ij}\left((z_{ij} + \tilde{y}_i)u_i + (z_{ij} - \tilde{y}_i)u_{ij}\right), \tag{3.94}$$

for $j = m_{i1} + 1, \ldots, m_{i2}$. Next, adding Eqs. 3.73, 3.75, and 3.94 to Eq. 3.93 yields

$$\begin{aligned}\dot{V}_{si} \leq & \left[\sum_{j=1}^{m_{i1}} \alpha_{ij}(\tilde{y}_i - z_{ij}) + \beta_{i0}\dot{y}_i + \alpha_{i0}\tilde{y}_i\right] u_i \\ & + \sum_{j=m_{i1}+1}^{m_{i2}} \left[\beta_{ij} u_{ij}\dot{z}_{ij} + (\beta_{ij}\eta_{ij} - \alpha_{ij}) z_{ij} u_{ij} + \alpha_{ij}\left((z_{ij} + \tilde{y}_i)u_i + (z_{ij} - \tilde{y}_i)u_{ij}\right)\right].\end{aligned} \tag{3.95}$$

Next, Eq. 3.78 can be used to replace $\dot{z}_{ij}$, and after canceling terms, Eq. 3.95 becomes

$$\dot{V}_{si} \leq \left[\sum_{j=1}^{m_{i1}} \alpha_{ij}(\tilde{y}_i - z_{ij}) + \sum_{j=m_{i1}+1}^{m_{i2}} \alpha_{ij}(\tilde{y}_i + z_{ij}) + \beta_{i0}\dot{y}_i + \alpha_{i0}\tilde{y}_i\right] u_i. \tag{3.96}$$

Hence, from the definition of $r_i(\cdot,\cdot)$ in Eq. 3.91, it follows that $\dot{V}_{si} \leq r_i(\cdot,\cdot)$, or equivalently, that the storage function is dissipative with respect to the supply rate. □

To prove overall system stability, we again form augmented matrices using m_1 and $m_2 = \max_i(m_{i2})$. Then, from Eqs. 3.83 and 3.91, the overall supply rate can be written as

$$\begin{aligned}R(\overline{y}, u) = & u^T[H_0 C_a + N_0 C_a A_a + \sum_{j=1}^{m_1} H_j(C_a - R_j) + \sum_{j=m_1+1}^{m_2} H_j(C_a + R_j)]x_a \\ & - u^T(N_0 C_a B_a + \sum_{j=0}^{m_2} H_j M^{-1})u.\end{aligned} \tag{3.97}$$

The following theorem governing the overall stability of the system can now be stated.

Theorem 3.4. *Consider an LTI system $G(s)$ coupled to m independent, differentiable odd monotonic nonlinearities that satisfy the slope restrictions $0 \leq \frac{df_i(\sigma)}{d\sigma} < M_{ii}$.*

If, for each input-output pair (u_i, y_i), there exist multipliers $W_i(s)$ as in Eq. 3.44 and a matrix $R = R^T > 0 \in \mathbb{R}^{n_a \times n_a}$ such that, with the preceding definitions of H_j, N_j, and R_j,

(i) $R_0 \triangleq \left[(N_0 C_a B_a + \sum_{j=0}^{m_2} H_j M^{-1}) + (N_0 C_a B_a + \sum_{j=0}^{m_2} H_j M^{-1})^T \right] > 0$, *and*

(ii) *there exists a symmetric matrix $P > 0$, satisfying*

$$\begin{aligned} 0 = {} & A_a^T P + P A_a + R \\ & + [\ H_0 C_a + N_0 C_a A_a + \sum_{j=1}^{m_1} H_j (C_a - R_j) + \sum_{j=m_1+1}^{m_2} H_j (C_a + R_j) - B_a^T P]^T R_0^{-1} \\ & [\ H_0 C_a + N_0 C_a A_a + \sum_{j=1}^{m_1} H_j (C_a - R_j) + \sum_{j=m_1+1}^{m_2} H_j (C_a + R_j) - B_a^T P], \end{aligned} \tag{3.98}$$

then the negative feedback interconnection of the system $G(s)$ and the nonlinearities $f_i(\cdot)$, $i = 1, \ldots, m$ is asymptotically stable. In this case, a Lyapunov function for the combined system is given by

$$\begin{aligned} V(x_a) = {} & x_a^T P x_a \\ & + 2 \sum_{i=1}^{m} \left[\beta_{i0} \left(\int_0^{\tilde{y}_i} \tilde{f}_i(\sigma)\, d\sigma + \frac{1}{2} M_{ii}^{-1} u_i^2 \right) + \sum_{j=1}^{m_{i2}} \beta_{ij} \int_0^{z_{ij}} \tilde{f}_i(\sigma)\, d\sigma \right]. \end{aligned} \tag{3.99}$$

Proof. The proof is similar to the one for Theorem 3.3 and is omitted. □

Remark 3.3. To consider nonlinearities with both upper and lower slope constraints, we employ both transformations in Fig. 3.7. In particular, define $\tilde{f}(\cdot)$ and $\tilde{G}(s)$ in Eqs. 3.46 and 3.48 in terms of $\hat{f}(\cdot)$ and $\hat{G}(s)$, where

$$\hat{f}(y) = f(y) - M_1 y, \qquad \forall y \in \mathbb{R}^m \tag{3.100}$$

$$\hat{G}(s) = (I + G(s) M_1)^{-1} G(s) \sim \left[\begin{array}{c|c} A - B_0 M_1 C_0 & B_0 \\ \hline C_0 & 0 \end{array} \right]. \tag{3.101}$$

The previous analysis can then be repeated, starting with a system $\hat{G}(s)$ and differentiable (odd) monotonic nonlinearities $\hat{f}(\cdot)$ with upper slope bounds $M_2 - M_1$. The appropriate Riccati equations can then be obtained from Theorems 3.3 and 3.4 by redefining A_a in Eq. 3.57, replacing u with $\tilde{u} = u - M_1 y$, and then substituting $M_2 - M_1$ for M. □

In the next section, we make explicit connections between the time and frequency domain stability conditions. The result provides sufficient conditions for the existence of positive definite solutions to Eqs. 3.84 and 3.98. These conditions also lead to explicit connections between absolute stability theory and mixed μ theory.

3.6 Extended Frequency Domain Stability Conditions

Following the approach in Section 3.4, we introduce a system $H(s)$ with outputs that combine to form the negative of the overall supply rate. The results from Remark 3.3 are used to consider nonlinearities with both upper and lower slope constraints. Let $W(s) = \mathrm{diag}(W_i(s))$, and define the output vector z

$$\begin{aligned} z = H(s)(-\tilde{u}) &= \begin{bmatrix} W(s) & -N_0(M_2 - M_1)^{-1}s \\ 0 & I \end{bmatrix} \begin{bmatrix} \tilde{y} \\ -\tilde{u} \end{bmatrix}, \\ &= \begin{bmatrix} W(s) & -N_0(M_2 - M_1)^{-1}s \\ 0 & I \end{bmatrix} \begin{bmatrix} \tilde{G}_a \\ I \end{bmatrix} (-\tilde{u}). \end{aligned} \tag{3.102}$$

With the matrix L as in Eq. 3.30, it follows that the supply rate is $-R(\overline{y}, u) = z^T L z$. From Lemma 3.1, the test for dissipativeness is then whether $H^*(\jmath\omega)LH(\jmath\omega) \geq 0 \ \forall\omega$. Substituting the definition of $H(s)$ into this condition (noting that N_0, M_1, and M_2 are diagonal) yields

$$\begin{aligned} H^*LH = \begin{bmatrix} \tilde{G}_a^* & I \end{bmatrix} &\begin{bmatrix} W^*(\jmath\omega) & 0 \\ N_0(M_2 - M_1)^{-1}\jmath\omega & I \end{bmatrix} \begin{bmatrix} 0 & I \\ I & 0 \end{bmatrix} \\ &\begin{bmatrix} W(\jmath\omega) & -N_0(M_2 - M_1)^{-1}\jmath\omega \\ 0 & I \end{bmatrix} \begin{bmatrix} \tilde{G}_a \\ I \end{bmatrix}, \\ = \begin{bmatrix} \tilde{G}_a^* & I \end{bmatrix} &\begin{bmatrix} W^*(\jmath\omega) & 0 \\ N_0(M_2 - M_1)^{-1}\jmath\omega & I \end{bmatrix} \begin{bmatrix} 0 & I \\ W(\jmath\omega) & -N_0(M_2 - M_1)^{-1}\jmath\omega \end{bmatrix} \begin{bmatrix} \tilde{G}_a \\ I \end{bmatrix}, \\ = \tilde{G}_a^* W^* + W\tilde{G}_a. \end{aligned} \tag{3.103}$$

Consequently, an equivalent test for stability is that $T_1(s) \triangleq W(s)\tilde{G}_a(s)$ be positive real. Furthermore, since it follows from Eq. 3.59 that $\tilde{G}(s)$ and $\tilde{G}_a(s)$ are equivalent in terms of their input-output properties, we need only consider the positive realness of $T(s) \triangleq W(s)\tilde{G}(s)$. Hence, it follows that if A_a is asymptotically stable and $T(s)$ is strongly positive real, then there exists an $n_a \times n_a$ symmetric matrix $P > 0$ that

satisfies Eq. 3.84 or Eq. 3.98, depending on the form of the multiplier $W(s)$. Conversely, for a given selection of $W(s)$, if there exists a $P > 0$ for all $R > 0$, then A_a is asymptotically stable, and $T(s)$ is strongly positive real.

In the following, we consider the case involving finite upper and lower bounds on the slope of the nonlinearity. In particular, it is assumed that the upper bound satisfies $M_2 > 0$ and the lower bound satisfies $M_1 < M_2$. In this case, because the double shift illustrated in Fig. 3.7 must be used, Eq. 3.48 must be replaced with

$$\tilde{G}(s) = (I + GM_1)^{-1}(I + GM_2)(M_2 - M_1)^{-1}, \tag{3.104}$$

where it is assumed that M_1 is selected so that $I + GM_1$ is invertible at all frequencies. To clarify the physical interpretation of the stability criterion and develop connections with the upper bounds for mixed μ, the symmetric bound $M_1 = -M_2$ will be used in the following development. Narendra and Taylor [123] develop similar frequency domain tests for the case where $M_1 \neq -M_2$.

Theorem 3.5. *Consider the LTI system $G(s)$ with m independent nonlinearities $f_i(\cdot)$ with appropriate sector bounds given by M_1 and M_2. Assume $M_1 = -M_2 < 0$, and that $I - G(\jmath\omega)M_2$ is invertible for all $\omega \in \mathbb{R}$. For each $i = 1, \ldots, m$, select the multiplier $W_i(s)$ as in Eq. 3.44 based on the characteristics of $f_i(\cdot)$. Furthermore, define $W(s) = W_{\mathrm{Re}}(s) + \jmath W_{\mathrm{Im}}(s) = \mathrm{diag}(W_i(s))$. If*

$$G^* W_{\mathrm{Re}} M_2 G - \jmath (W_{\mathrm{Im}} G - G^* W_{\mathrm{Im}}) - W_{\mathrm{Re}} M_2^{-1} \leq 0, \tag{3.105}$$

for all $\omega \in \mathbb{R}$, then the negative feedback interconnection of $G(s)$ and the m nonlinearities as illustrated in Fig. 2.2 is Lyapunov stable.

Proof. With $M_1 = -M_2$, it can easily be demonstrated that the first two factors of $\tilde{G}(s)$ commute. Then from Eqs. 3.103 and 3.104, the condition for stability is that

$$0 \leq T(\jmath\omega) + T^*(\jmath\omega), \qquad \forall \omega \in \mathbb{R}, \tag{3.106}$$

where

$$T(s) = W(s)(I + G(s)M_2)(I - G(s)M_2)^{-1}(2M_2)^{-1}. \tag{3.107}$$

Since $I - G(s)M_2$ is assumed to be invertible and M_2 is positive, an equivalent test can be developed by pre and post-multiplying Eq. 3.106 by $(I - G(\jmath\omega)M_2)^* M_2$ and $M_2(I - G(\jmath\omega)M_2)$ respectively. Performing this operation, and substituting for $T(s)$ from Eq. 3.107, the condition of Eq. 3.106 is equivalent to the requirement that for all $\omega \in \mathbb{R}$,

$$\begin{aligned}
0 &\leq (I - GM_2)^* M_2 W (I + GM_2) + (I + GM_2)^* W^* M_2 (I - GM_2) \\
&= M_2(W_{\mathrm{Re}} + \jmath W_{\mathrm{Im}}) + M_2(W_{\mathrm{Re}} + \jmath W_{\mathrm{Im}})GM_2 - M_2G^*M_2(W_{\mathrm{Re}} + \jmath W_{\mathrm{Im}}) \\
&+ M_2(W_{\mathrm{Re}} - \jmath W_{\mathrm{Im}}) - M_2(W_{\mathrm{Re}} - \jmath W_{\mathrm{Im}})GM_2 + M_2G^*M_2(W_{\mathrm{Re}} - \jmath W_{\mathrm{Im}}) \\
&- M_2G^*M_2(W_{\mathrm{Re}} + \jmath W_{\mathrm{Im}})GM_2 - M_2G^*M_2(W_{\mathrm{Re}} - \jmath W_{\mathrm{Im}})GM_2. \qquad (3.108)
\end{aligned}$$

Collecting terms and dividing through by $2M_2^2$ yields the condition in Eq. 3.105. □

Remark 3.4. The stability criterion in Eq. 3.105 of Theorem 3.5 is very general, because it may involve a mixture of the time-invariant sector-bounded nonlinearities as in a Popov test, the differentiable monotonic and odd monotonic nonlinearities discussed in Sections 3.5.2 and 3.5.3, and the time-varying nonlinearities considered in a bounded gain test. □

Remark 3.5. As discussed in Section 3.6, Eq. 3.105 has a graphical interpretation in the scalar case. Specifically, since $W_{\mathrm{Re}} > 0$, Eq. 3.105 can be rewritten as

$$(G + \jmath\frac{W_{\mathrm{Im}}}{W_{\mathrm{Re}}M_2})^*(G + \jmath\frac{W_{\mathrm{Im}}}{W_{\mathrm{Re}}M_2})W_{\mathrm{Re}}M_2 - W_{\mathrm{Re}}M_2(\frac{W_{\mathrm{Im}}}{W_{\mathrm{Re}}M_2})^2 - \frac{W_{\mathrm{Re}}}{M_2} \leq 0. \qquad (3.109)$$

Equivalently, with $G = x + \jmath y$, Eq. 3.109 can be written as

$$x^2 + (y + \frac{W_{\mathrm{Im}}}{W_{\mathrm{Re}}M_2})^2 \leq \frac{1}{M_2^2} + (\frac{W_{\mathrm{Im}}}{W_{\mathrm{Re}}M_2})^2. \qquad (3.110)$$

As in Section 3.4, this test can be interpreted in terms of circles with a frequency dependent center at $-\frac{W_{\mathrm{Im}}(\omega^2)}{W_{\mathrm{Re}}(\omega^2)M_2}$ and constant real-axis intercepts at $\pm M_2^{-1}$. □

The expression for the circle center in this case is significantly more complicated, but serves to illustrate the importance of the multiplier phase. The role of this phase and its relationship to the conservatism of the test are presented in the next section.

Remark 3.6. For odd monotonic nonlinearities, Narendra and Taylor [123] and Thathachar and Srinath [158,156] discuss multiplier terms that contain complex poles and zeroes of the form

$$\tilde{W}_i(s) = \text{RHS(Eq. 3.44)} + \sum_{j=m_{i2}+1}^{m_{i3}} \alpha_{ij} \frac{s^2 + a_{ij}s + b_{ij}}{s^2 + \lambda_{ij}s + \eta_{ij}}. \tag{3.111}$$

This case can be handled exactly as the other terms in the multiplier, but the proofs of stability are much more involved. The benefit of these additional terms is the rapid phase variations that they allow in the frequency domain test of Theorem 3.5. Of course, for linear time-invariant uncertainties, these results can be extended even further because the only restriction on the multiplier is that it be a positive real function. □

3.7 Connections to Mixed μ Analysis

In order to compare the upper bounds for real μ and the frequency domain stability tests developed in the previous section, a brief summary of the notation in Ref. [53] is presented. For the system matrix $G(s) \in \mathbb{C}^{m\times m}$, let m_r, m_c, and m_C ($m_t = m_r + m_c + m_C \leq m$) define the types and number of uncertainties expected in the system. The positive integers k_i ($\sum_{i=1}^{m_t} k_i = m$) then define the block structure and repetition of the uncertainties denoted by $\mathcal{K}(m_r, m_c, m_C) = (k_1, \ldots, k_{m_r}, \ldots, k_{m_r+m_c}, \ldots, k_{m_t})$. The set of allowable perturbations for the system G is then defined to be

$$\begin{aligned}\mathcal{X}_\mathcal{K} = \{\Delta = \text{block diag}(&\delta_1^r I_{k_1}, \ldots, \delta_{m_r}^r I_{k_{m_r}}, \delta_1^c I_{k_{m_r+1}}, \ldots, \delta_{m_c}^c I_{k_{m_r+m_c}}, \ldots, \\ &\Delta_1^C, \ldots, \Delta_{m_C}^C) : \delta_i^r \in \mathbb{R}, \delta_i^c \in \mathbb{C}, \Delta_i^C \in \mathbb{C}^{k_l \times k_l}, {}_{l=m_r+m_c+i}\}.\end{aligned} \tag{3.112}$$

Definition 3.1. (Doyle [47]). *For $G \in \mathbb{C}^{m\times m}$, $\mu_\mathcal{K}(G)$ is defined as*

$$\mu_\mathcal{K}(G) = \left(\min_{\Delta \in \mathcal{X}_\mathcal{K}} \{\sigma_{\max}(\Delta) : \det(I - \Delta G) = 0\} \right)^{-1}, \tag{3.113}$$

where $\mu_\mathcal{K}(G) = 0$ if no $\Delta \in \mathcal{X}_\mathcal{K}$ exists such that $\det(I - \Delta G) = 0$.

The complexity inherent in the definition and computation of $\mu_\mathcal{K}(G)$ has led to the use of approximations by both upper and lower bounds. For purely complex uncertainties, the bounds

$$\rho(G) \leq \mu_\mathcal{K}(G) \leq \sigma_{\max}(G) \tag{3.114}$$

involving the spectral radius and the maximum singular value are commonly employed. These bounds are usually refined scaling matrices. As shown in Fig. 3.1, the upper bound can be refined with the frequency dependent scaling matrices D.

As discussed in Ref. [47, 171], the scaled upper bounds are exact if $m_r = 0$ and $2m_c + m_C \leq 3$. However, for a larger number of complex uncertainties, results from these papers demonstrate that the upper bounds are in error by approximately 15%. Furthermore, with real parameter uncertainties, the bounds in Eq. 3.114 can be arbitrarily poor. Recent developments have led to new upper and lower bounds for mixed μ ($m_r \neq 0$) [48,53,171]. For the upper bound, define the Hermitian scaling matrices

$$\mathcal{D}_{\mathcal{K}} = \{\text{block diag}(D_1, \ldots, D_{m_r+m_c}, d_1 I_{k_{m_r+m_c+1}}, \ldots, d_{m_C} I_{k_{m_t}}) : \\ 0 < D_i = D_i^* \in \mathbb{C}^{k_i \times k_i}, 0 < d_i \in \mathbb{R}\}, \tag{3.115}$$

$$\mathcal{N}_{\mathcal{K}} = \{\text{block diag}(N_1, \ldots, N_{m_r}, 0_{k_{m_r+1}}, \ldots, 0_{k_{m_t}}) : N_i = N_i^* \in \mathbb{C}^{k_i \times k_i}\}, \tag{3.116}$$

that are partitioned to be compatible with the uncertainty structure $\mathcal{X}_{\mathcal{K}}$. The set of matrices $\mathcal{D}_{\mathcal{K}}$ includes elements for all three types of uncertainties, whereas $\mathcal{N}_{\mathcal{K}}$ has nonzero terms only in those parts corresponding to the real uncertainties. Members of both $\mathcal{D}_{\mathcal{K}}$ and $\mathcal{N}_{\mathcal{K}}$ are frequency dependent weighting functions and are constrained to be Hermitian. The elements of $\mathcal{D}_{\mathcal{K}}$ are further constrained to be positive. Note that within the block definition of Eq. 3.116, the elements of the scaling matrix N are essentially arbitrary.

An upper bound for mixed μ is developed by Fan *et al.* [53] using the generalized numerical range [52]. The approach develops constraints from the eigenvectors of the system ΔG ($\Delta \in \mathcal{X}_{\mathcal{K}}$ and $m_r \neq 0$) and combines them with standard μ upper bounds. The result is an improved analysis test that includes phase information about the real uncertainties. To compare with the analysis results in the previous section, it is sufficient to note the following definition.

Definition 3.2. (Young *et al.* [171]). *For $G(s) \in \mathbb{C}^{m \times m}$ and compatible uncertainty block structure $\mathcal{K}$, define*

$$\alpha_* = \inf_{D \in \mathcal{D}_{\mathcal{K}}, N \in \mathcal{N}_{\mathcal{K}}} \left[\min_{\alpha \in \mathbb{R}} \{\alpha : (G^* D G + \jmath(NG - G^* N) - \alpha D) \leq 0\} \right]. \tag{3.117}$$

It is shown in Refs. [53, 171] that α_* is an upper bound for the mixed μ problem in the sense that $\mu_{\mathcal{K}}(G) \leq \sqrt{\max(0, \alpha_*)}$.

Remark 3.7. Consider the diagonal case where $k_i = 1, i = 1, \ldots, m_t$ in $\mathcal{K}$. Then it follows from Theorem 3.5 with $W_{\mathrm{Re}} M_2$ replaced by D, W_{Im} replaced by $-N$, and M_2^{-2} bounded by α, that the conditions in Eq. 3.105 and Eq. 3.117 are identical. In the case of m_r linear time-invariant and $m_c + m_C$ nonlinear time-varying functions, then the bound in Eq. 3.117 is recovered. Finally, for sector-bounded nonlinear time-varying functions, take $W_{\mathrm{Re}} > 0$ and $W_{\mathrm{Im}} = 0$ in Eq. 3.105 to recover complex μ. This follows in the linear case since the only restriction on $W(s)$ is that it be a positive real function, and thus W_{Re} and W_{Im} can be any functions in the sets $\mathcal{D}_{\mathcal{K}}$ and $\mathcal{N}_{\mathcal{K}}$. □

The equivalence of these two stability criteria is even stronger if we recognize that the upper bound for mixed μ is related to M_2^{-1}. Then, as in Eq. 3.117, minimizing over α for a particular selection of D and N functions is equivalent to determining the largest bound M_2 that will destabilize the system for a given multiplier selection. As discussed by Narendra and Taylor [123], this analysis process is, of course, one of the key elements of absolute stability theory. The relationships between these results and concurrent work by Safonov *et al.* is discussed in Section 3.9.

From these observations, it is clear that there are very strong connections between the symmetric sector stability criteria and the upper bounds for real μ. In particular, the multiplier in Eq. 3.44 represents a particular parameterization of the D and N scaling functions. These results also imply that the same physical interpretation of off-axis circles can be applied to the upper bounds derived by Fan *et al.* [53]. For instance, it is now clear why, as in Theorem 7 in Ref. [171], we can set $N = 0$ if the system matrix $G(s)$ is real. In this case, the plot of $G(s)$ lies in a segment of the real axis that is contained in every circle. This observation indicates that the analysis tests are independent of N, and the stability bounds cannot be improved by changing N.

From these results, it is also evident that expanding the class of functions describing the real constant uncertainty from linear to sector-bounded nonlinear functions introduces conservatism to the stability tests. This follows because W_{Re} and W_{Im} can only be selected from a subset of $\mathcal{D}_{\mathcal{K}}$ and $\mathcal{N}_{\mathcal{K}}$ for any nonlinear function. The off-axis circle interpretation provides a qualitative measure of the conservatism of various restrictions on the parameterization of the multipliers.

Most importantly of all, these results also indicate that, as long as the multiplier phase is nonzero, the criteria should be much less conservative than tests developed with multipliers that have zero phase. Thus, by deriving tests based on these nonlinear functions, the results in this thesis provide a major extension in the development of state space stability criteria for systems with real parameter uncertainties.

Furthermore, a key advantage of this approach is that the state space tests, written as Riccati equations and Lyapunov functions, can easily be incorporated into an $\mathcal{H}_2$ synthesis problem. The result provides a powerful robust control design technique. Other particular advantages of the approach are given in Section 5.3 after the synthesis technique has been developed.

3.8 Summary

This chapter investigates the robust stability analysis problem with both linear and nonlinear parameter uncertainties. A unifying framework based on the supply rate and storage function concepts of Willems [165, 166] was used to derive state space stability criteria for linear systems coupled with these nonlinearities. The wealth of literature on absolute stability theory [123, 131, 172] was used to reformulate and extend recent work by Haddad and Bernstein [66,69]. The resulting storage functions were combined to form parameter-dependent Lyapunov functions that restrict both the allowable time-variation and the class of the nonlinear uncertainties. Equivalent frequency domain criteria provide physical insight into the role of the free parameters in these stability conditions. In contrast to the standard Popov test [131], these stability conditions are presented in terms of frequency dependent off-axis circles.

As shown, the frequency domain stability conditions are closely related to the

approach used in mixed μ theory. This observation leads to several conclusions: (1) The stability criteria and multipliers for the case of symmetric bounds on the nonlinear functions correspond to particular parameterizations of the upper bounds for real μ, (2) The physical interpretation of frequency dependent off-axis circles can be applied to the real μ upper bounds, yielding new insight to the conservatism of these tests, and (3) The restrictions on the center location for the circles provide a qualitative measure of the conservatism of the nonlinear models.

These analysis results in this chapter indicate that this approach represents a major extension in the development of state space stability criteria for robust control with real parameter uncertainties. Furthermore, the connections, which have largely been ignored, are important because they unify absolute stability theory and many of the recent developments in robust control theory. The following chapters demonstrate how these stability conditions can be used to develop a combined $\mathcal{H}_2$/real μ synthesis technique.

3.9 Relationship to Other Research

The close connections between the work in this thesis and research on mixed μ can be extended to concurrent work on the *Multivariable Stability Margin* K_m by Safonov *et al.* [34,141,142]. In these recent papers, the authors present the K_m synthesis approach as an alternative to μ synthesis for systems with both real and complex uncertainties. As discussed by Doyle and Safonov [47,142], $K_m = 1/\mu$, so much of the discussion in Section 3.7 can be used to develop close connections between K_m analysis and the results in this thesis. The work by Safonov*et al.* focuses on modifying two key features of μ theory. One goal is to extend μ theory to systems with real and complex uncertainties. A second goal of their work is to eliminate the curve-fitting step in the synthesis algorithm. These goals are very similar to the ones that motivated the work in this thesis, and thus it is important to understand the relationships between the two approaches.

We consider the framework in Fig. 3.1 because K_m analysis was explicitly developed for systems with linear uncertainties. In this approach, both real and complex

uncertainties are considered by relaxing the restrictions on the scaling functions in Fig. 3.1. In particular, they introduce new multipliers $M(s)$ that can be real or complex functions of frequency. The Popov multiplier in Eq. 3.3 is one particular $M(s)$ function, so the functions are called *Generalized Popov Multipliers* [34]. It is quite clear that these functions $M(s)$ are closely related to the multipliers in Eq. 3.44. Safonov and Lee [142] refer to the case of nonlinear uncertainties and the connections to frequency domain tests by Cho and Narendra [35]. However, they do not develop these interpretations to the same depth that is presented in this thesis. As shown in Sections 3.4 and 3.6, these frequency domain tests provide important geometric interpretations of the characteristics of the uncertainties considered by the stability tests. The off-axis circle criteria also illustrate the importance of the multiplier phase in these stability tests, and they demonstrate the role of the free parameters in the state space tests.

Since the approach in this thesis and K_m synthesis are both developed using concepts from absolute stability theory, the analysis tools are quite similar. However, the analysis techniques are developed using two different approaches that reflect the difference in the synthesis algorithms. As discussed in the Introduction, K_m synthesis uses the standard D–K iteration for controller synthesis. As a result, the controllers are designed using $\mathcal{H}_\infty$ or small gain theory [117]. The synthesis approach in this thesis is discussed in detail in Chapters 4 and 5. For now, it is sufficient to note that the technique involves an $\mathcal{H}_2$ synthesis approach that is modified by including the state space analysis tests from this chapter. As shown, the criteria were developed in this chapter using the concepts of supply rates and storage functions to test for system dissipation. Of course, it is well known that these small gain and passivity tests for stability are closely related [4].

One difficulty with μ synthesis is that, for each iteration, a series of convex optimization problems must be solved to obtain the scaling functions $D(j\omega)$. These functions must then be approximated by curve-fitting [117]. This difficulty is compounded in the real μ case because there are now two scaling functions. In K_m synthesis, these scaling functions are parameterized by the fixed-order polynomials

$M(s)$. A new convex optimization problem is then solved to obtain the multiplier coefficients. The result is a modified synthesis approach called an M–K iteration.

There are several advantages to the $\mathcal{H}_2$ synthesis approach that will be developed in the Chapters 4 and 5. First of all, the synthesis problem with an $\mathcal{H}_2$ performance objective can be solved with a single optimization algorithm. The solution then yields both the optimal robust controller and the optimal multipliers. Solving for these parameters simultaneously eliminates the need to explicitly iterate between multiplier evaluation and controller synthesis. Furthermore, the approach is presented for the case of reduced-order controllers, and can easily be extended to the case with architecture constraints on the compensator [109]. These two restrictions are essential for most realistic systems, but they cannot be directly addressed by either μ or K_m synthesis techniques. These points will be discussed in more detail at the end of Chapter 5.

Chapter 4

Robust Performance Synthesis

The discussion in Section 3.7 demonstrated that the stability analysis tests in Chapter 3 are very effective for systems with constant real parameter uncertainties. The next step is to develop techniques for designing robust controllers based on these criteria. This chapter uses the Ω-bound framework from Section 2.4 to include these stability criteria in a synthesis approach that minimizes an overbound of an $\mathcal{H}_2$ norm of the performance. In the following derivation, the analysis results of the previous chapter are specialized to the case of linear uncertainties. Many of the developments in this chapter follow Haddad, How, Hall, and Bernstein [72].

4.1 Introduction

As shown in Section 3.5.1, in order to account for the extra dynamics introduced by the stability multiplier, the resulting state space model is of increased dimension. Therefore, let $\mathcal{U} \subset \mathbb{R}^{n_a \times n_a}$ denote a set of perturbations ΔA_a of a given nominal augmented dynamics matrix $A_a \in \mathbb{R}^{n_a \times n_a}$. Within the context of robustness analysis, it is assumed that A_a is asymptotically stable and $0 \in \mathcal{U}$. The results in Section 2.4 can be applied to this augmented system to determine whether or not $A_a + \Delta A_a$ is asymptotically stable for all $\Delta A_a \in \mathcal{U}$. Note that, since A_a in Eq. 3.57 is lower block triangular, it follows that, if $A_a + \Delta A_a$ is asymptotically stable, then $A + \Delta A$ is asymptotically stable for all perturbations ΔA. With the development in Section 2.4, the next step, which is to determine the parameter-dependent Lyapunov functions.

4.2 Construction of Parameter-dependent Lyapunov Functions for Monotonic and Odd Monotonic Nonlinearities

From the theoretical basis of the approach in Section 2.4, the next step is to specify the structure of the set $\mathcal{U}$ and the parameter-dependent bounding function $\Omega(\cdot,\cdot)$. Specifically, the uncertainty set $\mathcal{U}$ is defined by

$$\mathcal{U} \triangleq \left\{ \Delta A_a \in \mathbb{R}^{n_a \times n_a} : \Delta A_a = -B_a F \left(I + M^{-1}F\right)^{-1} C_a,\ F \in \mathcal{F} \right\}, \tag{4.1}$$

where $\mathcal{F}$ satisfies

$$\mathcal{F} \triangleq \left\{ F \in \mathbb{R}^{m \times m} : F \geq 0 \right\}, \tag{4.2}$$

and where $B_a \in \mathbb{R}^{n_a \times m}$ and $C_a \in \mathbb{R}^{m \times n_a}$ are fixed matrices denoting the structure of the uncertainty, $M \in \mathbb{R}^{m \times m}$ is a given diagonal positive-definite matrix, and $F \in \mathbb{R}^{m \times m}$ is a diagonal uncertain matrix. An alternative characterization of the uncertainty set $\mathcal{U}$ can also be given. In order to state the next result, define the subset $\hat{\mathcal{F}}$ of $\mathcal{F}$ by

$$\hat{\mathcal{F}} \triangleq \left\{ \hat{F} :\ \hat{F} = F\left(I + M^{-1}F\right)^{-1},\ F \in \mathcal{F} \right\}, \tag{4.3}$$

where by Lemma 3.2 of Ref. [67], $\det(I + M^{-1}F) \neq 0$.

Proposition 4.1. *Let $M \in \mathbb{R}^{m \times m}$ be positive definite. Then*

$$\hat{\mathcal{F}} = \left\{ \hat{F} \in \mathbb{R}^{m \times m} : \det(I - \hat{F}M^{-1}) \neq 0 \text{ and } \hat{F}M^{-1}\hat{F} \leq \hat{F} \right\}. \tag{4.4}$$

Proof. (Haddad *et al.* [72]) "$\subset$:" Let $\hat{F} \in \hat{\mathcal{F}}$. Then there exists $F \in \mathcal{F}$ such that $\hat{F} = F(I + M^{-1}F)^{-1}$. Hence, $\hat{F}M^{-1} = F(I + M^{-1}F)^{-1}M^{-1}$ so that

$$\begin{aligned} \operatorname{spec}(\hat{F}M^{-1}) &= \operatorname{spec}[F(I + M^{-1}F)^{-1}M^{-1}] \\ &= \operatorname{spec}[M^{-1}F(I + M^{-1}F)^{-1}] \\ &= \left\{ \frac{\lambda}{1+\lambda} :\ \lambda \in \operatorname{spec}(M^{-1}F) \right\}, \end{aligned} \tag{4.5}$$

where "spec" denotes spectrum. Hence, $\operatorname{spec}(\hat{F}M^{-1})$ does not include 1, and $\det(I - \hat{F}M^{-1}) \neq 0$. Next, note that $F = (I - \hat{F}M^{-1})^{-1}\hat{F}$. Hence, it follows that

$$\begin{aligned} \hat{F} - \hat{F}M^{-1}\hat{F} &= \frac{1}{2}\hat{F}(I - M^{-1}\hat{F}) + \frac{1}{2}(I - \hat{F}M^{-1})\hat{F} \\ &= \frac{1}{2}(I - \hat{F}M^{-1})\left[(I - \hat{F}M^{-1})^{-1}\hat{F} + \hat{F}(I - M^{-1}\hat{F})\right](I - M^{-1}\hat{F}) \\ &= (I - \hat{F}M^{-1})F(I - \hat{F}M^{-1}) \geq 0, \end{aligned} \tag{4.6}$$

which proves "$\subset$".

"$\supset$:" Let $\hat{F}$ be such that $\det(I - \hat{F}M^{-1}) \neq 0$ and $\hat{F}M^{-1}\hat{F} \leq \hat{F}$. Since $\det(I - \hat{F}M^{-1}) \neq 0$, define $F \triangleq (I - \hat{F}M^{-1})^{-1}\hat{F}$. It then follows that

$$\begin{aligned} F &= \frac{1}{2}(I - \hat{F}M^{-1})^{-1}\hat{F} + \frac{1}{2}\hat{F}(I - \hat{F}M^{-1})^{-1} \\ &= \frac{1}{2}(I - \hat{F}M^{-1})^{-1}\left[\hat{F}(I - \hat{F}M^{-1}) + (I - \hat{F}M^{-1})\hat{F}\right](I - \hat{F}M^{-1})^{-1} \\ &= \frac{1}{2}(I - \hat{F}M^{-1})^{-1}\left[\hat{F} - \hat{F}M^{-1}\hat{F}\right](I - \hat{F}M^{-1})^{-1} \geq 0. \end{aligned} \tag{4.7}$$

Hence, $F \in \mathcal{F}$. Furthermore, because $F = (I - \hat{F}M^{-1})^{-1}\hat{F}$ is equivalent to $\hat{F} = F(I + M^{-1}F)^{-1}$, $\hat{F} \in \hat{\mathcal{F}}$, which proves "$\supset$". □

Finally, the following key Lemma shows the equivalence of $0 \leq \hat{F} \leq M$ and the structure presented in Proposition 4.1.

Lemma 4.1. *Let $F \in \mathbb{R}^{m\times m}$ be a nonnegative definite diagonal matrix and $M \in \mathbb{R}^{m\times m}$ a positive definite diagonal matrix. Then $\hat{F}M^{-1}\hat{F} \leq \hat{F}$ if and only if $0 \leq \hat{F} \leq M$.*

Proof. The proof is a direct consequence of Lemma 4.4 in Ref. [66]. □

Now, it follows from Proposition 4.1 and Lemma 4.1 that an equivalent representation for the uncertainty set $\mathcal{U}$ in Eq. 4.1 is

$$\mathcal{U} \triangleq \left\{\Delta A_a \in \mathbb{R}^{n_a\times n_a} : \Delta A_a = -B_a\hat{F}C_a,\ \hat{F} \in \hat{\mathcal{F}}\right\}. \tag{4.8}$$

For the structure of $\mathcal{U}$ satisfying Eq. 4.1, the parameter-dependent bound $\Omega(\cdot,\cdot)$ satisfying Eq. 2.34 can now be given a concrete form. Since the elements ΔA_a in $\mathcal{U}$ are parameterized by the elements F in $\mathcal{F}$, for convenience in the following results $P_0(\Delta A_a)$ will be replaced with $P_0(F)$.

Proposition 4.2. *Let N_0, N_j, H_j, $S_j \in \mathbb{R}^{m\times m}$ be nonnegative definite diagonal matrices and $H_0 \in \mathbb{R}^{m\times m}$ be a positive definite diagonal matrix. Assume that, as in Theorem 3.2, $R_0 > 0$, and that these matrices satisfy*

$$N_jS_j - H_j \geq 0, \qquad j = 1,\ldots,m_2. \tag{4.9}$$

Then the functions

$$\Omega_0(P) = [H_0C_a + N_0C_aA_a + \sum_{j=1}^{m_1} H_j(C_a - R_j) + \sum_{j=m_1+1}^{m_2} H_j(C_a + R_j) - B_a^TP]^TR_0^{-1}$$
$$[H_0C_a + N_0C_aA_a + \sum_{j=1}^{m_1} H_j(C_a - R_j) + \sum_{j=m_1+1}^{m_2} H_j(C_a + R_j) - B_a^TP], \quad (4.10)$$

$$P_0(F) = C_a^T(I + M^{-1}F)^{-1}\left[FN_0 + FM^{-1}N_0F\right](I + M^{-1}F)^{-1}C_a + \sum_{j=1}^{m_2} R_j^TFN_jR_j, \quad (4.11)$$

or, equivalently,

$$P_0(\hat{F}) = C_a^T\hat{F}N_0C_a + \sum_{j=1}^{m_2} R_j^T(I - \hat{F}M^{-1})^{-1}\hat{F}N_jR_j, \quad (4.12)$$

satisfy Eq. 2.34 with $\mathcal{U}$ given by Eq. 4.1.

Proof. The proof is a direct consequence of Theorem 3.2, with $\tilde{f}(\tilde{y}) = F\tilde{y} = F(I + M^{-1}F)^{-1}C_ax_a$. For further details on a similar proof, see Ref. [66]. □

The definitions in Proposition 4.2 can be combined with Theorem 2.1 (with an appropriate change in notation) to yield:

Theorem 4.1. *Let N_0, N_j, H_j, $S_j \in \mathbb{R}^{m\times m}$ be nonnegative definite diagonal matrices and $H_0 \in \mathbb{R}^{m\times m}$ be a positive definite diagonal matrix. As before, assume that $R_0 > 0$ and Eq. 4.9 is satisfied. Furthermore, suppose that there exists a nonnegative definite matrix P satisfying*

$$0 = A_a^TP + PA_a + R$$
$$+ [\ H_0C_a + N_0C_aA_a + \sum_{j=1}^{m_1} H_j(C_a - R_j) + \sum_{j=m_1+1}^{m_2} H_j(C_a + R_j) - B_a^TP)]^TR_0^{-1}$$
$$[\ H_0C_a + N_0C_aA_a + \sum_{j=1}^{m_1} H_j(C_a - R_j) + \sum_{j=m_1+1}^{m_2} H_j(C_a + R_j) - B_a^TP], \quad (4.13)$$

Then

$$(A_a + \triangle A_a, E) \textit{is detectable}, \quad \forall\ \triangle A_a \in \mathcal{U}, \quad (4.14)$$

if and only if

$$A_a + \triangle A_a \textit{ is asymptotically stable}, \quad \forall\ \triangle A_a \in \mathcal{U}. \quad (4.15)$$

In this case,

$$J(\mathcal{U}) \leq \text{tr}\ \ PV + \sup_{\hat{F} \in \hat{\mathcal{F}}} \text{tr}\ \left[(C_a^T \hat{F} N_0 C_a + \sum_{j=1}^{m_2} R_j^T (I - \hat{F}M^{-1})^{-1} \hat{F} N_j R_j) V \right]. \quad (4.16)$$

Proof. The result is a direct specialization of Theorem 2.1 using Proposition 4.2. Note that $P_0(\Delta A_a)$ now has the form $P_0(\hat{F}) = C_a^T \hat{F} N_0 C_a + \sum_{j=1}^{m_2} R_j^T (I - \hat{F}M^{-1})^{-1} \hat{F} N_j R_j$. Since $\hat{F}N_j \geq 0$, $j = 0, \ldots, m_2$, for all $\hat{F} \in \hat{\mathcal{F}}$ it follows that $P + P_0(\hat{F})$ is nonnegative definite for all $\hat{F} \in \hat{\mathcal{F}}$ as required by Theorem 2.1. □

Theorem 4.1 is directly applicable to dynamic systems with m-mixed uncertainties. Specifically, it follows from Theorem 3.2 that if the nonlinearity $f(y)$ is an m-vector composed of n_1 time-invariant first and third quadrant functions, $n_2 - n_1$ monotone increasing functions, and $m - n_2$ odd monotone increasing functions, then the nominal system is robustly stable for all such mixed uncertainty. Furthermore, in the linear uncertainty case, $f(y) = \hat{F}y$ it was recently shown by Haddad and Bernstein [66] that under certain compatibility assumptions between N_0 and $\hat{\mathcal{F}}$ (for the Popov case), the set $\mathcal{U}$ allows a richer class of multivariable uncertainties in that F may represent a fully populated uncertainty matrix.

It is the compatibility conditions between $\hat{\mathcal{F}}$ and the multiplier matrices (in this Popov case N_0) that enforce the structure of the uncertainty in the block Δ. As discussed by Haddad and Bernstein in Ref. [67], many tests are overly conservative for systems with multiple uncertainties because they do not account for the structure in the internal feedback model. As an example, consider the system from Ref. [45] with multiple uncertainties and a stability test based on the small gain theorem. The structure of these uncertainties can be specified in the problem statement, but the resulting stability test considers a completely unstructured block Δ [124]. There is no equivalent of the compatibility conditions to enforce the structure of the uncertainty, and, as a result, the unstructured analysis tests can be very conservative, even if the uncertainties are complex.

4.3 Static Output Feedback Controller Synthesis

This section introduces the robust stability and performance problem with static output feedback control. As mentioned in the previous section, due to the extra dynamics introduced by the multiplier, the resulting state space model is of increased dimension. Hence, this problem involves a set $\mathcal{U} \subset \mathbb{R}^{n_a \times n_a}$ of uncertain perturbations ΔA_a of the nominal augmented system matrix A_a.

Robust Stability and Performance Problem. Given the n_a^{th}-order stabilizable augmented plant with constant real-valued plant parameter variations

$$\dot{x}_a(t) = (A_a + \Delta A_a)x_a(t) + Bu(t) + Dw(t), \qquad t \in [0, \infty), \tag{4.17}$$

$$y(t) = Cx_a(t), \tag{4.18}$$

where $u(t) \in \mathbb{R}^{m_0}$ and $w(t) \in \mathbb{R}^d$, and $y(t) \in \mathbb{R}^l$, determine an output feedback control law

$$u(t) = Ky(t) \tag{4.19}$$

that satisfies the following design criteria:

(i) the closed-loop system Eqs. 4.17-4.19 is asymptotically stable for all $\Delta A_a \in \mathcal{U}$, that is, $A_a + BKC + \Delta A_a$ is asymptotically stable for all $\Delta A_a \in \mathcal{U}$; and

(ii) the performance functional

$$J(K) \triangleq \sup_{\Delta A_a \in \mathcal{U}} \limsup_{t \to \infty} \frac{1}{t} \mathrm{E}\{\int_0^t [x_a^T(s) R_{xx} x_a(s) + u^T(s) R_{uu} u(s)]\, ds\} \tag{4.20}$$

is minimized.

The aim is to control the actual system dynamics, *i.e.*, the non-augmented dynamics. So, in accordance with the partitioning in Eq. 3.57, the control, measurement, disturbance, and state weighting matrices B, C, D, and R_{xx}, have the structure:

$$B = \begin{bmatrix} \hat{B} \\ 0 \end{bmatrix}, \; C = \begin{bmatrix} \hat{C} & 0 \end{bmatrix}, \; D = \begin{bmatrix} \hat{D} \\ 0 \end{bmatrix}, \; R_{xx} = \begin{bmatrix} \hat{R}_{xx} & 0 \\ 0 & 0 \end{bmatrix}. \tag{4.21}$$

For each variation $\Delta A_a \in \mathcal{U}$, the closed-loop system in Eqs. 4.17-4.19 can be written as

$$\dot{x}_a(t) = (\hat{A} + \Delta A_a)x_a(t) + Dw(t), \; t \in [0, \infty), \tag{4.22}$$

where

$$\hat{A} \triangleq A_a + BKC, \tag{4.23}$$

and the white noise disturbance has intensity $V = DD^T$. Finally, note that if $\hat{A}_a + \Delta A_a$ is asymptotically stable for all $\Delta A_a \in \mathcal{U}$ for a given K, then Eq. 4.20 can be written as

$$J(K) = \sup_{\Delta A_a \in \mathcal{U}} \operatorname{tr} P_{\Delta A_a} V, \tag{4.24}$$

where $P_{\Delta A_a}$ satisfies Eq. 2.29 with A replaced by $\hat{A}$ and R replaced by

$$\hat{R} \triangleq R_{xx} + C^T K^T R_{uu} K C. \tag{4.25}$$

To consider controller synthesis, the performance bound Eq. 2.39 is used to replace the actual $\mathcal{H}_2$ performance as in Theorem 4.1, with A_a, R replaced by $\hat{A}$ and $\hat{R}$ to address the closed-loop control problem. This results in the following optimization problem:

Optimization Problem. Determine $K \in \mathbb{R}^{m_0 \times l}$ that minimizes

$$\mathcal{J}(K) \triangleq \operatorname{tr} PV + \sup_{\hat{F} \in \hat{\mathcal{F}}} \operatorname{tr}[(C_a^T \hat{F} N_0 C_a + \sum_{j=1}^{m_2} R_j^T (I - \hat{F} M^{-1})^{-1} \hat{F} N_j R_j) V] \tag{4.26}$$

subject to

$$\begin{aligned} 0 = {} & \hat{A}^T P + P\hat{A} + \hat{R} \\ & + [\ H_0 C_a + N_0 C_a \hat{A} + \sum_{j=1}^{m_1} H_j (C_a - R_j) + \sum_{j=m_1+1}^{m_2} H_j (C_a + R_j) - B_a^T P]^T R_0^{-1} \\ & [\ H_0 C_a + N_0 C_a \hat{A} + \sum_{j=1}^{m_1} H_j (C_a - R_j) + \sum_{j=m_1+1}^{m_2} H_j (C_a + R_j) - B_a^T P]. \end{aligned} \tag{4.27}$$

The following proposition provides the relationship between this optimization problem and the robust stability and performance problems:

Proposition 4.3. *If $P \in \mathbb{N}^{n_a}$, $K \in \mathbb{R}^{m_0 \times l}$ satisfies Eq. 4.26, and the detectability condition Eq. 2.36 holds, then $\hat{A} + \Delta A_a$ is asymptotically stable for all $\Delta A_a \in \mathcal{U}$, and*

$$J(K) \leq \mathcal{J}(K). \tag{4.28}$$

Proof. Since Eq. 4.27 has a solution $P \in \mathbb{N}^{n_a}$ and the detectability condition Eq. 2.36 holds, the hypotheses of Theorem 2.1 are satisfied, so that robust stability with a robust performance bound is guaranteed. The condition in Eq. 4.28 is merely a restatement of Eq. 2.39. □

Note that, since the last term in Eq. 4.26 is not a function of either the controller gain K or the constraint Eq. 4.27, it plays no role in the current optimization process. However, this last term does contain information about the multiplier, and will play a important part in the developments of the next chapter. The sufficient conditions for robust stability and performance with static output feedback are presented next. For arbitrary P, $Q \in \mathbb{R}^{n_a \times n_a}$ define the notation:

$$\tilde{C} \triangleq H_0 C_a + N_0 C_a A_a + \sum_{j=1}^{m_1} H_j (C_a - R_j) + \sum_{j=m_1+1}^{m_2} H_j (C_a + R_j), \tag{4.29}$$

$$R_{2a} \triangleq R_{uu} + B^T C_a^T N_0 R_0^{-1} N_0 C_a B, \tag{4.30}$$

$$P_a \triangleq B^T P + B^T C_a^T N_0 R_0^{-1} (\tilde{C} - B_a^T P), \tag{4.31}$$

$$A_P \triangleq A_a - B_a R_0^{-1} \tilde{C}, \tag{4.32}$$

$$\nu \triangleq Q C^T (C Q C^T)^{-1} C, \qquad \nu_\perp \triangleq I_{n_a} - \nu, \tag{4.33}$$

when the indicated inverses exist.

Theorem 4.2. *Assume $R_0 > 0$ and assume Eq. 4.9 holds. Furthermore, suppose there exist $n_a \times n_a$ nonnegative definite matrices P, Q such that $CQC^T > 0$ and*

$$\begin{aligned} 0 = {} & A_P^T P + P A_P + R_{xx} + \tilde{C}^T R_0^{-1} \tilde{C} + P B_a R_0^{-1} B_a^T P \\ & - P_a^T R_{2a}^{-1} P_a + \nu_\perp^T P_a^T R_{2a}^{-1} P_a \nu_\perp, \end{aligned} \tag{4.34}$$

$$\begin{aligned} 0 = {} & \left[A_P + (B_a R_0^{-1} N_0 C_a - I) B R_{2a}^{-1} P_a \nu + B_a R_0^{-1} B_a^T P \right] Q \\ & + Q \left[A_P + (B_a R_0^{-1} N_0 C_a - I) B R_{2a}^{-1} P_a \nu + B_a R_0^{-1} B_a^T P \right]^T + V, \end{aligned} \tag{4.35}$$

and let K be given by

$$K = -R_{2a}^{-1} P_a Q C^T (C Q C^T)^{-1}. \tag{4.36}$$

Then $(\hat{A} + \triangle A_a, \hat{R})$ is detectable for all $\triangle A_a \in \mathcal{U}$ if and only if $\hat{A} + \triangle A_a$ is asymptotically stable for all $\triangle A_a \in \mathcal{U}$. In this case the closed-loop system performance in Eq. 4.24

satisfies the parameter-dependent $\mathcal{H}_2$ bound

$$J(K) \leq \operatorname{tr} PV + \sup_{\hat{F} \in \hat{\mathcal{F}}} \operatorname{tr}[(C_a^T \hat{F} N_0 C_a + \sum_{j=1}^{m_2} R_j^T (I - \hat{F}M^{-1})^{-1} \hat{F} N_j R_j) V]. \quad (4.37)$$

Proof. The proof follows from a similar one by Haddad and Bernstein [66]. □

Remark 4.1. The definiteness condition $CQC^T > 0$ holds if C has full row rank and Q is positive-definite. Conversely, if $CQC^T > 0$, then C must have full row rank but Q need not necessarily be positive-definite. This condition implies the existence of the static gain projection ν. □

4.4 Dynamic Output Feedback Controller Synthesis

The next step is to consider the robust stability and performance problem with dynamic output-feedback control. Since the multiplier dynamics increase the plant order from n to n_a, to allow for greater design flexibility, it is assumed that the compensator dimension n_c can be less than the augmented plant order n_a. Hence, define $\tilde{n} = n_a + n_c$. Note that in this context, an n^{th}-order controller can be regarded as a reduced-order design. The constraint leads to an oblique projection that introduces extra equations and extra coupling [88]. The coupling shows that regulator/estimator separation breaks down in the reduced-order controller case.

Dynamic Robust Stability and Performance Problem. Given the n_a^{th}-order stabilizable and detectable plant with constant structured real-valued plant parameter variations

$$\dot{x}_a(t) = (A_a + \triangle A_a)x_a(t) + Bu(t) + D_1 w(t), \qquad t \geq 0, \quad (4.38)$$

$$y(t) = Cx_a(t) + D_2 w(t), \quad (4.39)$$

where $u(t) \in \mathbb{R}^{m_0}$, $w(t) \in \mathbb{R}^d$, and $y(t) \in \mathbb{R}^l$, determine an n_c^{th}-order dynamic compensator

$$\dot{x}_c(t) = A_c x_c(t) + B_c y(t), \quad (4.40)$$

$$u(t) = C_c x_c(t), \quad (4.41)$$

that satisfies the following design criteria:

(i) the closed-loop system in Eqs. 4.38-4.41 is asymptotically stable for all $\Delta A_a \in \mathcal{U}$; and

(ii) the performance functional in Eq. 4.20 with $J(K)$ replaced by $J(A_c, B_c, C_c)$ is minimized.

For each uncertain variation $\Delta A_a \in \mathcal{U}$, the closed-loop system in Eqs. 4.38-4.41 can be written as

$$\dot{\tilde{x}}(t) = (\tilde{A} + \Delta\tilde{A})\tilde{x}(t) + \tilde{D}w(t), \qquad t \geq 0, \tag{4.42}$$

where

$$\tilde{x}(t) \triangleq \begin{bmatrix} x_a(t) \\ x_c(t) \end{bmatrix}, \ \tilde{A} \triangleq \begin{bmatrix} A_a & BC_c \\ B_cC & A_c \end{bmatrix}, \text{ and } \Delta\tilde{A} \triangleq \begin{bmatrix} \Delta A_a & 0_{n_a \times n_c} \\ 0_{n_c \times n_a} & 0_{n_c \times n_c} \end{bmatrix}. \tag{4.43}$$

The closed-loop disturbance $\tilde{D}w(t)$ has intensity $\tilde{V} = \tilde{D}\tilde{D}^T$, where

$$\tilde{D} \triangleq \begin{bmatrix} D_1 \\ B_cD_2 \end{bmatrix}, \text{ so that } \tilde{V} \triangleq \begin{bmatrix} V_1 & 0 \\ 0 & B_cV_2B_c^T \end{bmatrix}, \tag{4.44}$$

where $V_1 = D_1D_1^T$ and $V_2 = D_2D_2^T$. The closed-loop system uncertainty $\Delta\tilde{A}$ has the form

$$\Delta\tilde{A} = -\tilde{B}_a\hat{F}\tilde{C}_a, \tag{4.45}$$

where

$$\tilde{B}_a \triangleq \begin{bmatrix} B_a \\ 0_{n_c \times m} \end{bmatrix}, \ \tilde{C}_a \triangleq \begin{bmatrix} C_a & 0_{m \times n_c} \end{bmatrix}. \tag{4.46}$$

Finally, if $\tilde{A} + \Delta\tilde{A}$ is asymptotically stable for all $\Delta A_a \in \mathcal{U}$ for a given compensator (A_c, B_c, C_c), then it follows from Proposition 2.1 that the performance measure in Eq. 4.19 is given by

$$J(A_c, B_c, C_c) = \sup_{\Delta A_a \in \mathcal{U}} \operatorname{tr} \tilde{P}_{\Delta\tilde{A}}\tilde{V}, \tag{4.47}$$

where $\tilde{P}_{\Delta\tilde{A}}$ satisfies the $\tilde{n} \times \tilde{n}$ Lyapunov equation

$$0 = (\tilde{A} + \Delta\tilde{A})^T\tilde{P}_{\Delta\tilde{A}} + \tilde{P}_{\Delta\tilde{A}}(\tilde{A} + \Delta\tilde{A}) + \tilde{R}. \tag{4.48}$$

For this equation, define

$$\tilde{E} = \begin{bmatrix} E_1 & E_2C_c \end{bmatrix}, \ \tilde{R} = \tilde{E}^T\tilde{E} = \begin{bmatrix} R_{xx} & 0 \\ 0 & C_c^TR_{uu}C_c \end{bmatrix}. \tag{4.49}$$

To proceed, the Lyapunov Eq. 4.48 is replaced with a Riccati equation that guarantees that the closed-loop system is robustly stable. Then, for the dynamic output feedback problem, Theorem 4.1 holds with A_a, R, V replaced by $\tilde{A}$, $\tilde{R}$, $\tilde{V}$. For clarity, the dynamic optimization problem can be stated as:

Dynamic Optimization Problem. Determine the controller (A_c, B_c, C_c) that minimizes

$$\mathcal{J}(A_c, B_c, C_c) \triangleq \operatorname{tr} \tilde{P}\tilde{V} + \sup_{\hat{F} \in \hat{\mathcal{F}}} \operatorname{tr} [(\tilde{C}_a^T \hat{F} N_0 \tilde{C}_a + \sum_{j=1}^{m_2} \tilde{R}_j^T (I - \hat{F}M^{-1})^{-1} \hat{F} N_j \tilde{R}_j) \tilde{V}], \quad (4.50)$$

where $\tilde{R}_j \triangleq [\, R_j \;\; 0_{m \times n_c} \,]$, and $\tilde{P} \in \mathbb{N}^{\tilde{n}}$ solves

$$\begin{aligned} 0 &= \tilde{A}^T \tilde{P} + \tilde{P}\tilde{A} + \tilde{R} \\ &\quad + [H_0 \tilde{C}_a + N_0 \tilde{C}_a \tilde{A} + \sum_{j=1}^{m_1} H_j (\tilde{C}_a - \tilde{R}_j) + \sum_{j=m_1+1}^{m_2} H_j (\tilde{C}_a + \tilde{R}_j) - \tilde{B}_a^T \tilde{P}]^T \tilde{R}_0^{-1} \\ &\qquad [H_0 \tilde{C}_a + N_0 \tilde{C}_a \tilde{A} + \sum_{j=1}^{m_1} H_j (\tilde{C}_a - \tilde{R}_j) + \sum_{j=m_1+1}^{m_2} H_j (\tilde{C}_a + \tilde{R}_j) - \tilde{B}_a^T \tilde{P}], \end{aligned} \quad (4.51)$$

with

$$\tilde{R}_0 \triangleq \left[(N_0 \tilde{C}_a \tilde{B}_a + \sum_{j=0}^{m_2} H_j M^{-1}) + (N_0 \tilde{C}_a \tilde{B}_a + \sum_{j=0}^{m_2} H_j M^{-1})^T \right] > 0, \quad (4.52)$$

such that (A_c, B_c, C_c) is minimal, and Eq. 4.9 holds.

Deriving the optimality conditions for the dynamic optimization problem yields equations that characterize the fixed-order dynamic output feedback controllers which guarantee robust stability and performance. The following lemma is required for the statement of the main theorem:

Lemma 4.2. (Bernstein and Haddad [19]) *Let $\hat{Q}, \hat{P}$ be $n_a \times n_a$ nonnegative definite matrices and suppose that rank $\hat{Q}\hat{P} = n_c$. Then there exist $n_c \times n_a$ G, Γ and $n_c \times n_c$ invertible M, unique except for a change of basis in $\mathbb{R}^{n_c}$, such that*

$$\hat{Q}\hat{P} = G^T M \Gamma, \;\; \Gamma G^T = I_{n_c}. \quad (4.53)$$

Furthermore, the $n_a \times n_a$ matrices

$$\tau \triangleq G^T \Gamma, \;\; \tau_\perp \triangleq I_{n_a} - \tau, \quad (4.54)$$

are idempotent and have rank n_c and $n_a - n_c$ respectively.

Proof. See Bernstein and Haddad [19]. □

The main results of this section concerning reduced-order controllers can now be stated. Recall the definitions of R_0, P_a, A_P, R_{2a}, $\tilde{C}$, and define

$$\overline{\Sigma} \triangleq C^T V_2^{-1} C, \tag{4.55}$$

$$A_{\hat{P}} \triangleq A_a - Q\overline{\Sigma} - B_a R_0^{-1}(\tilde{C} - B_a^T P), \tag{4.56}$$

$$A_{\hat{Q}} \triangleq A_a - BR_{2a}^{-1}P_a + B_a R_0^{-1} N_0 C_a B R_{2a}^{-1} P_a - B_a R_0^{-1}(\tilde{C} - B_a^T P), \tag{4.57}$$

for arbitrary Q, $P \in \mathbb{R}^{n_a \times n_a}$.

Theorem 4.3. *Let $n_c \leq n_a$, and assume $R_0 > 0$ and Eq. 4.9 holds. Furthermore, suppose there exist $n_a \times n_a$ nonnegative definite matrices $P, Q, \hat{P}, \hat{Q}$ satisfying*

$$0 = A_P^T P + P A_P + R_{xx} + \tilde{C}^T R_0^{-1} \tilde{C} + P B_a R_0^{-1} B_a^T P - P_a^T R_{2a}^{-1} P_a + \tau_\perp^T P_a^T R_{2a}^{-1} P_a \tau_\perp, \tag{4.58}$$

$$0 = (A_P + B_a R_0^{-1} B_a^T \left[P + \hat{P}\right])Q + Q(A_P + B_a R_0^{-1} B_a^T \left[P + \hat{P}\right])^T + V_1 - Q\overline{\Sigma}Q + \tau_\perp^T Q \overline{\Sigma} Q \tau_\perp, \tag{4.59}$$

$$0 = A_{\hat{P}}^T \hat{P} + \hat{P} A_{\hat{P}} + \hat{P} B_a R_0^{-1} B_a^T \hat{P} + P_a^T R_{2a}^{-1} P_a - \tau_\perp^T P_a^T R_{2a}^{-1} P_a \tau_\perp, \tag{4.60}$$

$$0 = A_{\hat{Q}} \hat{Q} + \hat{Q} A_{\hat{Q}}^T + Q\overline{\Sigma}Q - \tau_\perp Q \overline{\Sigma} Q \tau_\perp^T, \tag{4.61}$$

$$\operatorname{rank} \hat{Q} = \operatorname{rank} \hat{P} = \operatorname{rank} \hat{Q}\hat{P} = n_c, \tag{4.62}$$

with A_c, B_c, C_c given by

$$A_c = \Gamma \left[A_{\hat{Q}} - Q\overline{\Sigma}\right] G^T, \tag{4.63}$$

$$B_c = \Gamma Q C^T V_2^{-1}, \tag{4.64}$$

$$C_c = -R_{2a}^{-1} P_a G^T. \tag{4.65}$$

Then $(\tilde{A} + \Delta\tilde{A},\ \tilde{E})$ is detectable for all $\Delta A_a \in \mathcal{U}$ if and only if $\tilde{A} + \Delta\tilde{A}$ is asymptotically stable for all $\Delta A_a \in \mathcal{U}$. In this case, the performance of the closed-loop system Eq. 4.42 satisfies the parameter-dependent $\mathcal{H}_2$ bound

$$J(A_c, B_c, C_c) \leq \operatorname{tr}\left[(P + \hat{P})V_1 + \hat{P}Q\overline{\Sigma}Q\right] + \sup_{\hat{F} \in \hat{\mathcal{F}}} \operatorname{tr}\left[(C_a^T \hat{F} N_0 C_a + \sum_{j=1}^{m_2} R_j^T (I - \hat{F}M^{-1})^{-1} \hat{F} N_j R_j) V_1\right]. \tag{4.66}$$

Proof. The proof of Theorem 4.3 involves a complicated manipulation of algebraic equations. For simplicity, only the key points are presented. To optimize the overbounding cost $\mathcal{J}$ in Eq. 4.50 subject to the constraint in Eq. 4.51, form the Lagrangian

$$\mathcal{L}(A_c, B_c, C_c, \tilde{P}, \tilde{Q}, \lambda) \triangleq \text{tr}\,[(\text{RHS of 4.50})\lambda + \tilde{Q}(\text{RHS of 4.51})]. \tag{4.67}$$

The Lagrange multipliers $\lambda \geq 0$ and $\tilde{Q} \in \mathbb{R}^{\tilde{n}\times\tilde{n}}$ in this equation are not both zero. Setting $\partial\mathcal{L}/\partial\tilde{P} = 0$, $\lambda = 0$ implies that $\tilde{Q} = 0$. Hence, it can be assumed without loss of generality that $\lambda = 1$. Furthermore, $\tilde{Q}$ is the nonnegative definite solution of

$$\begin{aligned} 0 = &[\tilde{A} - \tilde{B}_a\tilde{R}_0^{-1}(H_0\tilde{C}_a + N_0\tilde{C}_a\tilde{A} + \sum_{j=1}^{m_1} H_j(\tilde{C}_a - \tilde{R}_j) + \sum_{j=m_1+1}^{m_2} H_j(\tilde{C}_a + \tilde{R}_j) - \tilde{B}_a^T\tilde{P})]\tilde{Q} \\ &+ \tilde{Q}[\tilde{A} - \tilde{B}_a\tilde{R}_0^{-1}(H_0\tilde{C}_a + N_0\tilde{C}_a\tilde{A} + \sum_{j=1}^{m_1} H_j(\tilde{C}_a - \tilde{R}_j) + \sum_{j=m_1+1}^{m_2} H_j(\tilde{C}_a + \tilde{R}_j) - \tilde{B}_a^T\tilde{P})]^T + \tilde{V} \end{aligned} \tag{4.68}$$

The remainder of the derivation parallels the technique in Ref. [18], with the principal steps being:

Step 1: Compute $\partial\mathcal{L}/\partial A_c$, $\partial\mathcal{L}/\partial B_c$, and $\partial\mathcal{L}/\partial C_c$.

Step 2: Partition Eqs. 4.51 and 4.68 into six equations (a)–(f) that correspond to the $n \times n$, $n \times n_c$, and $n_c \times n_c$ blocks of $\tilde{P}$ and $\tilde{Q}$. Since the compensator triple (A_c, B_c, C_c) is controllable and observable, the lower righthand $n_c \times n_c$ blocks of $\tilde{P}$ and $\tilde{Q}$ are positive definite.

Step 3: Multiply Eq. (b) by the $n \times n_c$ sub-block of $\tilde{Q}$ and add it to the $n_c \times n_c$ sub-block of $\tilde{Q}$ times Eq. (c). The result can be used to define the projection τ and the new variables P, Q, $\hat{P}$, $\hat{Q}$, G, and Γ.

Step 4: Use the results of step 1 and step 3 to solve for the compensator matrices in Eqs. 4.63–4.65.

Step 5: This is the key step in the process. With the results from the previous steps, Eqs. (a), (b), (d), and (e) can be manipulated to yield Eqs. 4.58–4.61.

Step 6: The results of step 3 can then be used to demonstrate that Eq. 4.66 is equivalent to Eq. 4.50.

□

Remark 4.2. Several special cases can immediately be discerned from Theorem 4.3. For example, in the full-order case, set $n_c = n_a$ so that $\tau = G = \Gamma = I_{n_a}$ and $\tau_\perp = 0$. In this case, the last term in each of Eqs. 4.58-4.60 is zero and Eq. 4.61 is superfluous. Alternatively, letting $B_a = 0$, $C_a = 0$ and retaining the reduced-order constraint $n_c < n_a$ yields the results of Ref. [88]. Finally, setting $m_2 = 0$ yields the results of Ref. [66] for the case in which F is diagonal. □

Theorem 4.3 provides constructive sufficient conditions that yield reduced-order dynamic feedback gains A_c, B_c, C_c for robust stability and performance. Note that when solving Eqs. 4.58-4.61 numerically, the matrices M, N_j, H_j, and S_j, $j = 0, \ldots, m_2$, and the structure of B_a and C_a appearing in the design equations can be adjusted to examine tradeoffs between performance and robustness. To reduce the conservatism even further, the multiplier matrices N_j, H_j, and S_j can also be viewed as free parameters in the optimization of the worst case $\mathcal{H}_2$ performance bound. The optimal compensators and multipliers can then be computed simultaneously, avoiding the need for an iterative solution algorithm. A numerical algorithm for a particular form of this problem is presented in the next chapter.

4.5 Summary

This chapter uses the Ω-bound framework to develop a synthesis approach for robust control design using the state space analysis tools presented in Chapter 3. For a specified LQG problem, the $\mathcal{H}_2$ cost functional is replaced with a parameter-dependent $\mathcal{H}_2$ bound. The overbound contains terms related to the extra constraints on the robustness of the controllers. The standard Lyapunov equation in the LQG synthesis is also replaced with a Riccati equation from Theorem 3.2. A nonnegative definite solution to this Riccati equation guarantees that the closed-loop system is robustly stable. The controllers then guarantee stability and minimize an $\mathcal{H}_2$ performance objective. The optimality conditions for a reduced-order robust controller are presented

C-2.

in Theorem 4.3. The discussion at the end of the chapter also indicates that conservatism can be reduced even further by optimizing this overbounding cost functional with respect to the multipliers. This step is explored in detail in the next chapter which deals with the Popov synthesis problem.

Chapter 5

Robust Controller Synthesis with Diagonal Popov Multipliers

In this chapter, we continue the controller synthesis algorithm by considering a special case of the robust performance problem in Chapter 4. In particular, the following sections consider the case of m independent, sector-bounded, scalar uncertainties with multipliers of the standard Popov form:

$$W_i(s) = \alpha_{i0} + \beta_{i0} s. \tag{5.1}$$

These restrictions simplify the notation of the previous chapter, so the following section restates the problem formulation to demonstrate the entire synthesis procedure as outlined at the end of Chapter 4. The Lagrangian formulation for the optimal robust controller is also presented. The potential conservatism of the approach is further reduced by optimizing the cost bound with respect to the multiplier matrices. A numerical algorithm for solving the necessary conditions is also presented. The chapter concludes with a discussion on the relative merits of the synthesis approach in this thesis and mixed μ (K_m) synthesis.

5.1 Parameter-dependent Lyapunov Functions for Popov Multipliers

For simplicity, the following development considers the case illustrated in Fig. 2.2, with m independent scalar uncertainties. The more general, fully populated uncer-

tainty matrix case is considered by Haddad and Bernstein [66]. The first step is to define the uncertainty set $\mathcal{U}$ and the parameter-dependent bounding function $\Omega(\cdot,\cdot)$. The diagonal matrices $M_1, M_2 \in \mathbb{D}^m$ are introduced for the problem with independent scalar uncertainties. It is assumed that $M_2 - M_1$ is positive definite and thus invertible. For this class of uncertainties, the set $\mathcal{U}$ is defined as

$$\mathcal{U} \triangleq \{\Delta A \in \mathbb{R}^{n\times n}:\ \Delta A = -B_0 F C_0,\ F \in \mathcal{F}\}, \tag{5.2}$$

where $\mathcal{F}$ is given by

$$\mathcal{F} \triangleq \{F \in \mathbb{D}^m :\ M_1 \le F \le M_2\}, \tag{5.3}$$

$B_0 \in \mathbb{R}^{n\times m}$ and $C_0 \in \mathbb{R}^{m\times n}$ are fixed matrices denoting the structure of the uncertainty, and $F \in \mathbb{D}^m$ is an uncertain matrix.

Since $F \in \mathcal{F}$ is constrained to have the diagonal structure $\mathrm{diag}[F_1, F_2, \ldots, F_m]$, define $M_1 \triangleq \mathrm{diag}[M_{11}, M_{12}, \ldots, M_{1m}]$, and similarly for M_2. In this case, M_2 and M_1 represent upper and lower bounds, respectively, on the uncertain diagonal matrix F because $M_{1i} \le F_i \le M_{2i},\ i = 1, \ldots, m$. As in Chapter 4, $P_0(\Delta A)$ is replaced with $P_0(F)$. These results are based on the notation in Section 2.4 and Chapter 4.

Proposition 5.1. *Let $M_1, M_2, H_0, N_0 \in \mathbb{D}^m$ be such that $M_2 - M_1$ is positive definite, H_0 and N_0 are positive and nonnegative definite respectively. Redefine*

$$R_0 \triangleq [H_0(M_2 - M_1)^{-1} + N_0 C_0 B_0] + [H_0(M_2 - M_1)^{-1} + N_0 C_0 B_0]^T > 0. \tag{5.4}$$

Then the functions

$$\begin{aligned}\Omega_0(P) \triangleq\ & [H_0 C_0 + N_0 C_0 (A - B_0 M_1 C_0) - B_0^T P]^T R_0^{-1} \\ & [H_0 C_0 + N_0 C_0 (A - B_0 M_1 C_0) - B_0^T P] \\ & - P B_0 M_1 C_0 - C_0^T M_1 B_0^T P, \end{aligned} \tag{5.5}$$

$$P_0(F) \triangleq C_0^T (F - M_1) N_0 C_0, \tag{5.6}$$

satisfy Eq. 2.34 with $\mathcal{U}$ given by Eq. 5.2.

Proof. See Haddad and Bernstein [70]. □

The results of Theorem 2.1 and Proposition 5.1 can now be used to present an upper bound for the $\mathcal{H}_2$ performance of a system that satisfies the conditions for robust stability for all perturbations $\mathcal{U}$ given by Eq. 5.2.

Theorem 5.1. *Let $M_1, M_2, H_0, N_0 \in \mathbf{D}^m$ be such that $M_2 - M_1$ is positive definite, $R_0 > 0$, H_0 is positive definite, and N_0 is nonnegative definite. Furthermore, suppose there exists a nonnegative definite matrix P satisfying*

$$0 = (A - B_0 M_1 C_0)^T P + P(A - B_0 M_1 C_0) + [H_0 C_0 + N_0 C_0 (A - B_0 M_1 C_0) - B_0^T P]^T R_0^{-1} [H_0 C_0 + N_0 C_0 (A - B_0 M_1 C_0) - B_0^T P] + R. \tag{5.7}$$

Then

$$(A + \triangle A, E) \text{ is detectable}, \qquad \forall\, \triangle A \in \mathcal{U}, \tag{5.8}$$

if and only if

$$A + \triangle A \text{ is asymptotically stable}, \qquad \forall\, \triangle A \in \mathcal{U}. \tag{5.9}$$

In this case,

$$J(\mathcal{U}) \leq \mathcal{J}(\mathcal{U}) \triangleq \operatorname{tr} [P + C_0^T (M_2 - M_1) N_0 C_0] V. \tag{5.10}$$

Proof. The result is a direct specialization of Theorem 2.1 using Proposition 5.1, where $P_0(F)$ now has the form in Eq. 5.6. Since F is lower bounded by M_1 and N is nonnegative definite and diagonal, then $(F - M_1)N \geq 0$ for all $F \in \mathcal{F}$. It then follows that $P + P_0(F)$ is nonnegative definite for all $F \in \mathcal{F}$, as required by Theorem 2.1. □

The results in Section 3.6 can be used to present a sufficient condition for the existence of a solution to Eq. 5.7 in Theorem 5.1.

Theorem 5.2. *Let*

$$\hat{G}(s) \overset{\min}{\sim} \left[\begin{array}{c|c} A - B_0 M_1 C_0 & B_0 \\ \hline H_0 C_0 + N_0 C_0 (A - B_0 M_1 C_0) & H_0 (M_2 - M_1)^{-1} + N_0 C_0 B_0 \end{array}\right]. \tag{5.11}$$

If A is asymptotically stable and $\hat{G}(s)$ is strongly positive real, then there exists an $n \times n$ matrix $P > 0$ satisfying Eq. 5.7. Conversely, if $R_0 > 0$ and there exists $P > 0$ satisfying Eq. 5.7 for all $R > 0$, then A is asymptotically stable and $\hat{G}(s)$ is strongly positive real.

Proof. This result is an immediate consequence of the discussion in Section 3.6. □

The results in Theorem 5.1 can now be used to complete the development of the control synthesis procedure.

5.2 Dynamic Output Feedback Controller Synthesis

To expand on the development in Section 4.4, this section restates the dynamic robust stability and performance problems with this particular multiplier. The problem involves the set $\mathcal{U} \subset \mathbb{R}^{n\times n}$ of the uncertain perturbations of the nominal system matrix A. As before, the optimization problem is specified and then replaced by an auxiliary minimization problem with an overbounding cost function. The optimality conditions for this auxiliary problem are presented in two forms – one more useful for numerical solution, and the other more enlightening in terms of the structure of the optimal compensator.

Dynamic Robust Stability and Performance Problem. Consider the n^{th}-order stabilizable and detectable plant with constant structured real-valued parameter variations

$$\dot{x}(t) = (A + \Delta A)x(t) + Bu(t) + D_1 w(t), \quad t \geq 0, \tag{5.12}$$

$$y(t) = Cx(t) + D_2 w(t), \tag{5.13}$$

where $u(t) \in \mathbb{R}^{m_0}$, $w(t) \in \mathbb{R}^d$, and $y(t) \in \mathbb{R}^l$. The problem is to determine an n_c^{th}-order dynamic compensator

$$\dot{x}_c(t) = A_c x_c(t) + B_c y(t), \tag{5.14}$$

$$u(t) = C_c x_c(t), \tag{5.15}$$

that satisfies the following design criteria:

(i) the closed-loop system in Eqs. 5.12-5.15 is asymptotically stable for all $\Delta A \in \mathcal{U}$; and

(ii) the performance functional

$$J(A_c, B_c, C_c) \triangleq \sup_{\Delta A \in \mathcal{U}} \limsup_{t\to\infty} \frac{1}{t} \mathrm{E}\{\int_0^t [x^T(s) R_{xx} x(s) + u(s)^T R_{uu} u(s)]\, ds\} \tag{5.16}$$

is minimized.

For the uncertainties $\Delta A \in \mathcal{U}$, the closed-loop system in Eqs. 5.12-5.15 can be written as

$$\dot{\tilde{x}}(t) = (\tilde{A} + \Delta\tilde{A})\tilde{x}(t) + \tilde{D}w(t), \quad t \geq 0, \tag{5.17}$$

where

$$\tilde{x}(t) \triangleq \begin{bmatrix} x(t) \\ x_c(t) \end{bmatrix}, \ \tilde{A} \triangleq \begin{bmatrix} A & BC_c \\ B_cC & A_c \end{bmatrix}, \text{ and } \Delta\tilde{A} \triangleq \begin{bmatrix} \Delta A & 0_{n\times n_c} \\ 0_{n_c\times n} & 0_{n_c\times n_c} \end{bmatrix}. \tag{5.18}$$

Furthermore, the closed-loop disturbance $\tilde{D}w(t)$ has intensity $\tilde{V} \triangleq \tilde{D}\tilde{D}^T$, where

$$\tilde{D} \triangleq \begin{bmatrix} D_1 \\ B_cD_2 \end{bmatrix}, \text{ so that } \tilde{V} \triangleq \begin{bmatrix} V_1 & 0 \\ 0 & B_cV_2B_c^T \end{bmatrix}, \tag{5.19}$$

where $V_1 \triangleq D_1D_1^T$ and $V_2 \triangleq D_2D_2^T$. The closed-loop system uncertainty $\Delta\tilde{A}$ has the form

$$\Delta\tilde{A} = -\tilde{B}_0F\tilde{C}_0, \quad \text{where } \tilde{B}_0 \triangleq \begin{bmatrix} B_0 \\ 0_{n_c\times m} \end{bmatrix}, \text{ and } \tilde{C}_0 \triangleq \begin{bmatrix} C_0 & 0_{m\times n_c} \end{bmatrix}. \tag{5.20}$$

In this case, note that $\tilde{C}_0\tilde{B}_0 = C_0B_0$ so that

$$\begin{aligned} \tilde{R}_0 &\triangleq H_0(M_2 - M_1)^{-1} + N_0\tilde{C}_0\tilde{B}_0 + [H_0(M_2 - M_1)^{-1} + N_0\tilde{C}_0\tilde{B}_0]^T, \\ &= H_0(M_2 - M_1)^{-1} + N_0C_0B_0 + [H_0(M_2 - M_1)^{-1} + N_0C_0B_0]^T, \\ &= R_0. \end{aligned} \tag{5.21}$$

Finally, if $\tilde{A} + \Delta\tilde{A}$ is asymptotically stable for all $\Delta A \in \mathcal{U}$ and a given compensator (A_c, B_c, C_c), then the performance measure in Eq. 5.16 is given by

$$J(A_c, B_c, C_c) = \sup_{\Delta A \in \mathcal{U}} \text{tr } \tilde{P}_{\Delta\tilde{A}}\tilde{V}, \tag{5.22}$$

where $\tilde{P}_{\Delta\tilde{A}}$ satisfies the $(n + n_c) \times (n + n_c)$ algebraic Lyapunov equation

$$0 = (\tilde{A} + \Delta\tilde{A})^T\tilde{P}_{\Delta\tilde{A}} + \tilde{P}_{\Delta\tilde{A}}(\tilde{A} + \Delta\tilde{A}) + \tilde{R}, \tag{5.23}$$

where

$$\tilde{E} = \begin{bmatrix} E_1 & E_2C_c \end{bmatrix}, \ \tilde{R} = \tilde{E}^T\tilde{E} = \begin{bmatrix} R_{xx} & 0 \\ 0 & C_c^TR_{uu}C_c \end{bmatrix}. \tag{5.24}$$

As before, the results of Theorem 5.1 (with A, R, V replaced by $\tilde{A}$, $\tilde{R}$, $\tilde{V}$) are used to replace the Lyapunov Eq. 5.23 with a Riccati equation that guarantees that the closed-loop system is robustly stable. This leads to the following design problem:

Dynamic Auxiliary Minimization Problem. Determine the compensator (A_c, B_c, C_c) that minimizes the overbounding $\mathcal{H}_2$ cost

$$\mathcal{J}(A_c, B_c, C_c) \triangleq \text{tr}\,[\tilde{P} + \tilde{C}_0^T(M_2 - M_1)N_0\tilde{C}_0]\tilde{V}, \tag{5.25}$$

where $\tilde{P} \in \mathbb{N}^{n+n_c}$ satisfies

$$\begin{aligned} 0 = (\tilde{A} - \tilde{B}_0 M_1 \tilde{C}_0)^T \tilde{P} + \tilde{P}(\tilde{A} - \tilde{B}_0 M_1 \tilde{C}_0) + [H_0\tilde{C}_0 + N_0\tilde{C}_0(\tilde{A} - \tilde{B}_0 M_1 \tilde{C}_0) - \tilde{B}_0^T\tilde{P}]^T \\ R_0^{-1}[H_0\tilde{C}_0 + N_0\tilde{C}_0(\tilde{A} - \tilde{B}_0 M_1 \tilde{C}_0) - \tilde{B}_0^T\tilde{P}] + \tilde{R}, \end{aligned} \tag{5.26}$$

such that (A_c, B_c, C_c) is minimal, H_0 and N_0 are positive and nonnegative definite respectively, and $R_0 > 0$.

The optimality conditions for the dynamic auxiliary minimization problem provide sufficient conditions to characterize the reduced-order dynamic output feedback controllers that guarantee robust stability and performance. The approach outlined in the proof of Theorem 4.3 is used to derive these conditions. The cost overbound $\mathcal{J}(A_c, B_c, C_c)$ is augmented with the constraint in Eq. 5.26 using the Lagrange multiplier $\tilde{Q} \in \mathbb{N}^{n+n_c}$. This leads to

$$\begin{aligned} \mathcal{L}(A_c, B_c, C_c, \tilde{P}, \tilde{Q}) = \text{tr}\,[(\tilde{P} + \tilde{C}_0^T(M_2 - M_1)N_0\tilde{C}_0)\tilde{V} \\ +\tilde{Q}\{(\tilde{A} - \tilde{B}_0 M_1 \tilde{C}_0)^T\tilde{P} + \tilde{P}(\tilde{A} - \tilde{B}_0 M_1 \tilde{C}_0) + [H_0\tilde{C}_0 + N_0\tilde{C}_0(\tilde{A} - \tilde{B}_0 M_1 \tilde{C}_0) - \tilde{B}_0^T\tilde{P}]^T \\ R_0^{-1}[H_0\tilde{C}_0 + N_0\tilde{C}_0(\tilde{A} - \tilde{B}_0 M_1 \tilde{C}_0) - \tilde{B}_0^T\tilde{P}] + \tilde{R}\}]. \end{aligned} \tag{5.27}$$

Since the results are necessary to implement the numerical solution for the optimal controllers, the following presents the gradients of the augmented cost in Eq. 5.27 with respect to the free parameters A_c, B_c, C_c, $\tilde{P}$, and $\tilde{Q}$. First, note that $\partial\mathcal{L}/\partial\tilde{Q}$ recovers Eq. 5.26. For convenience, partition the symmetric matrices $\tilde{P}$ and $\tilde{Q}$ as

$$\tilde{P} = \begin{bmatrix} P_{11} & P_{12} \\ P_{12}^T & P_{22} \end{bmatrix}, \quad \tilde{Q} = \begin{bmatrix} Q_{11} & Q_{12} \\ Q_{12}^T & Q_{22} \end{bmatrix}, \tag{5.28}$$

and similarly for their product $\tilde{P}\tilde{Q}$. In Eq. 5.28, $P_{11} \in \mathbb{R}n \times n$ and $P_{22} \in \mathbb{R}n_c \times n_c$. Then

$$0 = \frac{\partial \mathcal{L}}{\partial \tilde{P}} = [\tilde{A} - \tilde{B}_0 M_1 \tilde{C}_0 - \tilde{B}_0 R_0^{-1}(H_0\tilde{C}_0 + N_0\tilde{C}_0(\tilde{A} - \tilde{B}_0 M_1 \tilde{C}_0) - \tilde{B}_0^T \tilde{P})]\tilde{Q}$$
$$+\tilde{Q}[\tilde{A} - \tilde{B}_0 M_1 \tilde{C}_0 - \tilde{B}_0 R_0^{-1}(H_0\tilde{C}_0 + N_0\tilde{C}_0(\tilde{A} - \tilde{B}_0 M_1 \tilde{C}_0) - \tilde{B}_0^T \tilde{P})]^T + \tilde{V}, \quad (5.29)$$

$$0 = \frac{1}{2}\frac{\partial \mathcal{L}}{\partial A_c} = P_{12}^T Q_{12} + P_{22} Q_{22} = [\tilde{P}\tilde{Q}]_{22}, \quad (5.30)$$

$$0 = \frac{1}{2}\frac{\partial \mathcal{L}}{\partial B_c} = P_{22} B_c V_2 + [\tilde{P}\tilde{Q}]_{21} C^T, \quad (5.31)$$

$$0 = \frac{1}{2}\frac{\partial \mathcal{L}}{\partial C_c} = B^T(I - B_0 R_0^{-1} N_0 C_0)^T [\tilde{P}\tilde{Q}]_{12} + (R_{uu} + B^T C_0^T N_0 R_0^{-1} N_0 C_0 B)\, C_c Q_{22}$$
$$+B^T C_0^T N_0 R_0^{-1}[H_0 C_0 + N_0 C_0(A - B_0 M_1 C_0)] Q_{12}. \quad (5.32)$$

The above gradient expressions can be used to derive explicit expressions for the optimal controller in terms of the solutions of four coupled Riccati equations. For convenience in stating the main result, recall the definitions of R_0 and $\overline{\Sigma} \triangleq C^T V_2^{-1} C$, and redefine

$$\tilde{C} \triangleq H_0 C_0 + N_0 C_0(A - B_0 M_1 C_0), \quad (5.33)$$

$$R_{2a} \triangleq R_{uu} + B^T C_0^T N_0 R_0^{-1} N_0 C_0 B, \quad (5.34)$$

$$P_a \triangleq B^T P + B^T C_0^T N_0 R_0^{-1}(\tilde{C} - B_0^T P), \quad (5.35)$$

$$A_P \triangleq A - B_0 M_1 C_0 - B_0 R_0^{-1} \tilde{C}, \quad (5.36)$$

$$A_{\hat{P}} \triangleq A_P - Q\overline{\Sigma} + B_0 R_0^{-1} B_0^T P, \quad (5.37)$$

$$A_{\hat{Q}} \triangleq A_P + B_0 R_0^{-1} B_0^T P - (I_n - B_0 R_0^{-1} N_0 C_0) B R_{2a}^{-1} P_a, \quad (5.38)$$

for arbitrary Q, $P \in \mathbb{R}^{n \times n}$.

Theorem 5.3. *Let $n_c \leq n$, assume $R_0 > 0$, and let N_0 and H_0 be nonnegative and positive definite diagonal matrices, respectively. Furthermore, suppose there exist $n \times n$ nonnegative definite matrices $P, Q, \hat{P}$, and $\hat{Q}$ satisfying*

$$0 = A_P^T P + P A_P + R_{xx} + \tilde{C}^T R_0^{-1} \tilde{C} + P B_0 R_0^{-1} B_0^T P - P_a^T R_{2a}^{-1} P_a$$
$$+\tau_\perp^T P_a^T R_{2a}^{-1} P_a \tau_\perp, \quad (5.39)$$

$$0 = (A_P + B_0 R_0^{-1} B_0^T [P + \hat{P}])Q + Q(A_P + B_0 R_0^{-1} B_0^T [P + \hat{P}])^T$$

$$+V_1 - Q\overline{\Sigma}Q + \tau_\perp^T Q\overline{\Sigma}Q\tau_\perp, \tag{5.40}$$

$$0 = A_{\hat{P}}^T\hat{P} + \hat{P}A_{\hat{P}} + \hat{P}B_0R_0^{-1}B_0^T\hat{P} + P_a^TR_{2a}^{-1}P_a - \tau_\perp^T P_a^T R_{2a}^{-1}P_a\tau_\perp, \tag{5.41}$$

$$0 = A_{\hat{Q}}\hat{Q} + \hat{Q}A_{\hat{Q}}^T + Q\overline{\Sigma}Q - \tau_\perp Q\overline{\Sigma}Q\tau_\perp^T \tag{5.42}$$

$$\text{rank } \hat{Q} = \text{rank } \hat{P} = \text{rank } \hat{Q}\hat{P} = n_c \tag{5.43}$$

with A_c, B_c, C_c given by

$$A_c = \Gamma\left[A_{\hat{Q}} - Q\overline{\Sigma}\right]G^T, \tag{5.44}$$

$$B_c = \Gamma QC^TV_2^{-1}, \tag{5.45}$$

$$C_c = -R_{2a}^{-1}P_aG^T. \tag{5.46}$$

Then $(\tilde{A} + \triangle\tilde{A}, \tilde{E})$ is detectable for all $\triangle A \in \mathcal{U}$ if and only if $\tilde{A} + \triangle\tilde{A}$ is asymptotically stable for all $\triangle A \in \mathcal{U}$. In this case the performance of the closed-loop system Eq. 5.17 satisfies the $\mathcal{H}_2$ bound

$$J(A_c, B_c, C_c) \leq \text{tr}\,[(P + \hat{P} + C_0^T(M_2 - M_1)N_0C_0)V_1 + \hat{P}Q\overline{\Sigma}Q]. \tag{5.47}$$

Proof. The proof follows the same outline given for Theorem 4.3. □

As discussed in the previous chapter, the diagonal matrices M_1, M_2, H_0, and N_0 and the structure in B_0 and C_0 can be used to examine tradeoffs between performance and robustness. Also, conservatism can be further reduced by taking the multiplier matrices H_0 and N_0 as free parameters and optimizing the worst case $\mathcal{H}_2$ performance bound. The derivatives are

$$\frac{1}{2}\frac{\partial\mathcal{L}}{\partial N_0} = \frac{1}{2}(M_2 - M_1)\tilde{C}_0\tilde{V}\tilde{C}_0^T + R_0^{-1}[H_0\tilde{C}_0 + N_0\tilde{C}_0(\tilde{A} - \tilde{B}_0M_1\tilde{C}_0) - \tilde{B}_0^T\tilde{P}]\tilde{Q}$$
$$[(\tilde{A} - \tilde{B}_0M_1\tilde{C}_0) - \tilde{B}_0R_0^{-1}(H_0\tilde{C}_0 + N_0\tilde{C}_0(\tilde{A} - \tilde{B}_0M_1\tilde{C}_0) - \tilde{B}_0^T\tilde{P})]^T\tilde{C}_0^T, \tag{5.48}$$

$$\frac{1}{2}\frac{\partial\mathcal{L}}{\partial H_0} = R_0^{-1}[H_0\tilde{C}_0 + N_0\tilde{C}_0(\tilde{A} - \tilde{B}_0M_1\tilde{C}_0) - \tilde{B}_0^T\tilde{P}]\tilde{Q}$$
$$[\tilde{C}_0^T - (H_0\tilde{C}_0 + N_0\tilde{C}_0(\tilde{A} - \tilde{B}_0M_1\tilde{C}_0) - \tilde{B}_0^T\tilde{P})^TR_0^{-1}(M_2 - M_1)^{-1}]. \tag{5.49}$$

Since N_0, $H_0 \in \mathbf{D}^m$, only the diagonal elements of $\partial\mathcal{L}/\partial N_0$ and $\partial\mathcal{L}/\partial H_0$ can be set to zero in the optimization process.

Remark 5.1. In the full-order case, set $n_c = n$ in Theorem 5.3 so that $\tau = G = \Gamma = I_n$ and $\tau_\perp = 0$. Then the last term in each of Eqs. 5.39-5.41 is zero and Eq. 5.42 is superfluous. □

Remark 5.2. If the plant uncertainty ΔA is such that $C_0 B_0 = 0$, then R_0 and Eq. 5.48 are of a much simpler form. As will be seen in the next chapter, this condition holds for an important class of parameter uncertainties. □

5.3 Numerical Issues for Controller Synthesis

There are several important issues to be considered in the development of an technique to numerically solve the optimality conditions in the previous sections. This section addresses these issues while providing an outline of the algorithm used to compute the controllers for the examples in the next two chapters.

The robust compensators are developed using a BFGS (Broyden-Fletcher-Goldfarb-Shanno) quasi-Newton search algorithm to solve the optimality conditions in Eqs. 5.26, 5.29-5.32, 5.48, and 5.49. [144,147,148]. As discussed in the previous section, the optimal compensator and multiplier are obtained simultaneously. This avoids the need to explicitly iterate between controller design and optimal multiplier evaluation, as required in the current algorithms for μ synthesis [117] and K_m synthesis [142].

The free parameters in the compensator and multiplier matrices are accumulated in the vector

$$x = \begin{bmatrix} \mathrm{vec}(A_c) \\ \mathrm{vec}(B_c) \\ \mathrm{vec}(C_c) \\ \mathrm{diag}(N_0) \\ \mathrm{diag}(H_0) \end{bmatrix}. \tag{5.50}$$

There are two main steps in the solution algorithm for the optimal x value. An inner loop step optimizes the cost functional by solving the gradient Eqs. 5.26, 5.29-5.32, 5.48, and 5.49 for the current value of x. Each inner loop step is performed for fixed values of the stability bounds M_1 and M_2, which are changed in the outer loop.

The inner loop itself consists of two main parts. The first of these determines a search direction that reduces the cost functional. The second part performs a line

search to determine the step size to be taken in this search direction. The purpose of the line search is to minimize the cost function in the specified direction subject to various error constraints, which are discussed later. If, at a particular value of x, a normalization of the system gradients is below a given tolerance, then this inner loop optimization is said to have converged to a solution. Then the bounds M_1 and M_2 are increased in the outer loop, and the current value of x is used as an initial guess for the next inner loop iteration. If the inner loop optimization fails to converge, the last increments in M_1 and M_2 are reduced. This two step iterative process is continued until the desired stability bounds M_{1f} and M_{2f} are achieved, if possible. Consequently, the iteration in this design process is to develop a family of robust controllers which then facilitates an analysis of the trade-offs between guaranteed robustness and performance.

The robust control synthesis approach is closely related to the homotopy techniques discussed by Richter [136] for the design of reduced-order $\mathcal{H}_2$ controllers. In one formulation of these homotopy problems, the parameter to be varied is written in terms of the initial and final values, and a homotopy variable $\lambda \in [0,1]$. For example, in this problem we could write

$$M_1(\lambda) = M_{1i} + \lambda(M_{1f} - M_{1i}), \tag{5.51}$$

so that $M_1(0) = M_{1i}$ and $M_1(1) = M_{1f}$. The solution vector x can then be parameterized in terms of the variable λ. The solution algorithm employed here is a zeroth order homotopy algorithm, because the current optimal solution vector $x(\lambda)$ is not updated in the outer loop to account for changes in λ [37,38,109,136].

Several homotopic continuation algorithms have been developed for the related class of reduced-order $\mathcal{H}_2$ controllers [38,109]. These algorithms employ linear updating schemes for the current solution vector using the derivative of the solution with respect to λ to obtain

$$x(\lambda + \Delta\lambda) = x(\lambda) + \Delta\lambda \frac{\partial x}{\partial \lambda}. \tag{5.52}$$

This approach has proven to be an effective solution technique provided that suitable homotopy parameters can be isolated for the problem of interest. With several sim-

ple examples, Mercadal [109] demonstrates that choosing internal plant parameters (*e.g.* spring stiffnesses or subsystem coupling levels) can lead to poorly conditioned homotopy solution paths. However, Collins [37] has recently reported good success with a homotopy on the control authority and sensor noise.

A linear prediction homotopy algorithm has been applied to the optimal Popov analysis problem, but this level of sophistication was not found to be necessary for the examples in the next two chapters. Recent results by Collins *et al.* [38] compare various prediction techniques on a low order system ($n = 8$). Compared with an approach that uses no prediction, the linear prediction scheme improves the numerical conditioning of the homotopy path and reduces the overall computational time. However, a critical issue in implementing this update approach is the feasibility of computing and inverting the Hessian matrix to determine $\partial x/\partial\lambda$. With 300-500 degrees of freedom in the optimization for the SISO and MIMO examples discussed in Chapter 7, the computational effort for each outer loop step is enormous. Collins also reports that quasi-Newton approximations for this Hessian often result in poorly conditioned updates. Unfortunately, determining a good solution technique for this related problem of optimal reduced-order $\mathcal{H}_2$ controllers is an issue that extends well beyond the scope of this thesis.

There are several interesting features of the solution algorithm. For instance, each of the inner loop gradient steps requires the solution of two $(n+n_c)\times(n+n_c)^{\text{th}}$ order equations: a Riccati equation for $\tilde{P}$ and a Lyapunov equation for $\tilde{Q}$. The "A" matrices of these two equations are strongly related. If $A_{\tilde{P}}$, denotes the "A" matrix for the $\tilde{P}$ equation, then the "A" matrix for the $\tilde{Q}$ equation is $A_{\tilde{Q}} = A_{\tilde{P}} + \tilde{B}_0 R_0^{-1}\tilde{B}_0^T\tilde{P}$. From the structure of this coupling, if there exists a nonnegative definite matrix $\tilde{P}$ that solves the Riccati equation, then $A_{\tilde{Q}}$ is known to be stable. This can be seen from the Hamiltonian matrix used to determine $\tilde{P}$

$$H = \begin{bmatrix} A_{\tilde{P}} & \tilde{B}_0 R_0^{-1}\tilde{B}_0^T \\ -Q_{\tilde{P}} & -A_{\tilde{P}}^T \end{bmatrix}. \tag{5.53}$$

Following the approach in Francis [54], this Hamiltonian matrix is transformed using

$$T = \begin{bmatrix} I & 0 \\ \tilde{P} & I \end{bmatrix}, \tag{5.54}$$

to form $H_2 = T^{-1}HT$. Then, if $\tilde{P}$ solves the Riccati equation $A_{\tilde{P}}^T\tilde{P} + \tilde{P}A_{\tilde{P}} + Q_{\tilde{P}} + \tilde{P}\tilde{B}_0R_0^{-1}\tilde{B}_0^T\tilde{P} = 0$, H_2 can be rewritten as

$$H_2 = \begin{bmatrix} A_{\tilde{P}} + \tilde{B}_0R_0^{-1}\tilde{B}_0^T\tilde{P} & \tilde{B}_0R_0^{-1}\tilde{B}_0^T \\ 0 & -(A_{\tilde{P}} + \tilde{B}_0R_0^{-1}\tilde{B}_0^T\tilde{P})^T \end{bmatrix}, \tag{5.55}$$

$$= \begin{bmatrix} A_{\tilde{Q}} & \tilde{B}_0R_0^{-1}\tilde{B}_0^T \\ 0 & -A_{\tilde{Q}}^T \end{bmatrix}. \tag{5.56}$$

So, if there exists a nonnegative definite $\tilde{P}$ that solves this Riccati equation, then $A_{\tilde{Q}}$ is stable. Then, with the detectability assumption, this implies the existence of a nonnegative definite $\tilde{Q}$ that solves the corresponding Lyapunov equation. Consequently, only two main error flags need to be checked during the line search of the inner loop optimization. The first flag checks that the compensator stabilizes the nominal system. The second checks that a positive definite $\tilde{P}$ solution exists for Eq. 5.26, which indicates that the closed-loop system satisfies the criteria for robust stability. When both of these conditions are satisfied, the Lyapunov equation is solved for $\tilde{Q}$, and the overbounding cost function and gradients are computed.

Good initial guesses for this nonlinear, non-convex optimization problem are essential because of the presence of local minima. For small values of M_1 and M_2, an initial guess can be found from an iterative solution of Eqs. 5.39-5.42. Consider the full order case in which $\tau_\perp = 0$ and Eq. 5.42 is eliminated. The matrix P_a can be written in terms of P using Eq. 5.35, which implies that Eq. 5.39 can be written as a standard Riccati equation in P. However, the two remaining equations are strongly coupled by terms in the "A" matrices. In Eq. 5.40, there is a term of the form $[A_P + B_0R_0^{-1}B_0^TP] + B_0R_0^{-1}B_0^T\hat{P}$, and in Eq. 5.41, there is $A_{\hat{P}} = [A_P + B_0R_0^{-1}B_0^TP] - Q\overline{\Sigma}$. For given values of N_0, H_0, M_1, and M_2, we first solve for P. Combining this solution and a given Q_0, we then determine $\hat{P}_0$. The values for P and $\hat{P}_0$ are in turn used to solve for Q_1. The sequence is continued, and

the convergence is checked with the error $e_s = \max(\|Q_i - Q_{i-1}\|_2, \|\hat{P}_i - \hat{P}_{i-1}\|_2)$. If convergent, the iterations are terminated when e_s is sufficiently small.

The best selection of the initial Q_0 matrix is an open question. One approach is just to use the Q solution matrix from the LQG design. Since controllers are being developed for a whole range of control authority and robustness values, the $\hat{P}$ and Q matrices from previous designs can also be used as an initial guess. Unfortunately, as with many iterative solution techniques for nonlinear optimization problems, convergence of the sequence outlined above is not guaranteed. For higher order problems, more sophisticated approaches to the design of initial conditions were employed. These were based on the sensitivity weighted [30] and multiple model [59] controllers discussed in the Introduction. The overall design sequence then results in a unified approach to robust control design, with each step providing further guarantees in the robustness of the controller.

There are extra degrees of freedom in the solution algorithm that are associated with the N_0 and H_0 matrices. The elements of these matrices must be picked using the known values of M_2 and M_1. The numerical results from the examples in Chapters 6 and 7 indicate that it is quite simple to select these multiplier matrices to obtain controllers that stabilize the system with large initial guarantees.

An extremely important feature of this design process is that the synthesis approach is virtually insensitive to the number of uncertain parameters. Consider the multiple model approach to robust control [59]. The addition of each new uncertainty could potentially require that several new models of the system be included in the optimization of the controllers. Adding new models significantly increases the computational effort, but leaving them out results in even fewer guarantees of stability. For the algorithm in this thesis, each new uncertainty requires that additional multiplier states be included in the system matrices. However, this only increases the system size by the order of the multiplier. Of course, for the case in this chapter, where no augmentation is required, the only change is two extra degrees of freedom in x. In practice, it was found to be quite simple to add extra uncertainties to the system as the control designs evolved to the final M_1 and M_2 values.

Another important feature of the technique is the flexibility of both upper and lower stability bounds. The values of M_1 and M_2 can be changed independently to account for any known biases in the uncertainties. The examples in the next two chapters will show that many systems exhibit a "stiff" uncertainty direction that is more difficult than the rest. This additional flexibility in the selection of M_1 and M_2 can be used to tailor the uncertainty bounds to account for these directions.

For the experiments, a family of robust controllers is typically developed for several values of control weighting ρ. One successful technique for starting the optimization is to use an optimal design with $R_{uu} = \rho_1 > \rho_2$ as an initial guess for controllers with $R_{uu} = \rho_2$. A homotopy on the control (and possibly sensor noise) weighting R_{uu} is then performed to develop the optimal compensator with the desired values of M_1, M_2, and ρ. Although this optimization was found to be well conditioned, it typically takes 3-7 times more gradient steps than an inner loop optimization step requires. The approach was found to be particularly effective for the reduced-order designs because it is often quite difficult to determine high authority controllers that satisfy both the robustness and order constraints. It is typically much simpler to find low authority designs that satisfy both of these conditions.

A further consideration in the numerical solution for the optimal controller is the parameterization of the A_c matrix in Eq. 5.14 [38,109]. As is well known, a state space representation of the controller is only unique to within a similarity transformation. Furthermore, the selection of a canonical form for the compensator representation can significantly reduce the number of free parameters in the optimization. As a result, the computational effort required for each optimization step is also reduced. However, reducing the number of free parameters does not guarantee that the solution will converge more quickly, because constraining the parameterization of the compensator may introduce local minima into the problem and adversely affect the conditioning of the solution. Extra degrees of freedom in the compensator result in a solution hyperplane rather than a single point, and as a result, the problem is poorly conditioned near the minimum. MacMartin [105] suggests switching between different parameterizations of the controller depending on the progress of the solution

procedure. A canonical form with fewer degrees of freedom should be used near the optimal solution. Unfortunately, determining when to switch between the different representations of the controller is often quite difficult.

Mercadal [109] and Collins *et al.* [38] suggest a tridiagonal A_c with arbitrary B_c and C_c as a good compromise between reducing the computational effort and maintaining a well conditioned solution. To take advantage of the better conditioning of the solution, no controller parameterization is used in the low order designs in Chapter 6. The higher order compensator designs in Chapter 7 are tridiagonal.

In the development of the stability criteria in Chapter 3, the multiplier matrices H_0 and N_0 were constrained to be positive definite and nonnegative definite respectively. The solution of the optimization problem must be constrained to ensure that these conditions are satisfied. Scales [144] suggests the barrier function technique for nonlinear minimization problems with inequality constraints. Logarithmic barrier functions were selected for this work. The cost function is augmented with functions that penalize the constrained state values as they approach the boundary. The barrier functions are augmented to the cost $\mathcal{J}(x)$ to obtain

$$\Phi_k(x, \alpha_k, \beta_k) = \mathcal{J}(x) - \alpha_k \log(\det H_0) - \beta_k \log(\det N_0), \tag{5.57}$$

which is then used as the objective function in an unconstrained optimization problem. The gradients of the Lagrangian with respect to N_0 and H_0 in Eqs. 5.48 and 5.49 are modified to account for the extra terms in Eq. 5.57 using the derivatives from Athans [9]. As any of the elements of H_0 or N_0 approach the boundary at 0, $\Phi_k \to \infty$. The magnitude of α_k and β_k determine the relative importance of the inequality conditions on H_0 and N_0.

Further safeguards must be incorporated into the line search in this case to ensure that no inadmissible values of N_0 and H_0 are accepted. One element of H_0 is typically fixed, and the other values of H_0 and N_0 are scaled relative to this number. It is interesting to note that, in the examples considered in the next two chapters, the optimal solutions for H_0 and N_0 were found to be positive. Consequently, there was no need to enforce these constraints on their definiteness.

Most of the previous issues were concerned with numerical aspects of robust control design. There are also some very important experimental implementation issues. In particular, the stability of the compensator is important because the resulting closed-loop system is conditionally stable. Unstable controllers have been successfully implemented on hardware at the Space Engineering Research Center at MIT. However, if they are to be used reliably in future systems, several additional safety measures must be incorporated into the software of the computer that runs the control design, known as the real-time computer.

Several authors [55,73,76,93,151] discuss ways to avoid this problem of unstable compensators. One such technique is to penalize the $\mathcal{H}_2$ norm of the controller in the objective function. As with the barrier functions, the coefficient of this additional cost term determines the importance of the controller constraint, *i.e.* how close the compensator poles lie to the line of instability. Other tests can be used to constrain the placement of the compensator poles using more complicated geometric shapes [68].

An important issue in the numerical design of robust controllers is the convergence of the solution algorithm to a global minimum. The problems with the D–K iteration for μ synthesis were discussed in the Introduction. As the name suggests, the solution algorithm consists of an iteration between multiplier evaluation (D) and $\mathcal{H}_\infty$ controller design (K). Since the iteration sequence is non-convex, it may result in a suboptimal solution at a local minimum. The first part of this iteration requires that the scaling functions be found by solving a series of convex minimization problems. These functions are then approximated using a curve-fitting procedure [117]. As a result, the transfer function $D(s)$ can be written in state space form and augmented to the system to continue the synthesis process. However, as discussed by Safonov and Chiang [141], there is little indication of the sensitivity of the synthesis approach to errors in the approximate curve-fitting step. A further important point is that the curve-fitting is performed during each iteration step. The process is further complicated in mixed μ synthesis because there are now two scaling functions [170].

It was shown in Sections 3.4 and 3.6 that the multiplier $W(s)$ corresponds to a particular parameterization of these scaling functions. A key difference in the

combined $\mathcal{H}_2$/real μ approach in this thesis over μ synthesis is that the approximations on the order and representation of the scaling functions are made at the beginning of the synthesis process, not during each synthesis iteration. Moreover, the frequency domain tests in Section 3.4 and 3.6 provide qualitative measures of the conservatism in these approximations. The K_m synthesis discussed in Section 3.9 also avoids this curve-fitting step, but it still results in an iterative solution algorithm.

As with other state space optimization techniques, there are no guarantees that the optimal solution of the robust control algorithm outlined in this section is not at a local minimum. Furthermore, there are no guarantees that the homotopy to the desired stability bounds can be achieved. The only recourse for the designer is to try several initial conditions and select the best of the converged designs. In spite of these apparent difficulties, the results in this thesis clearly demonstrate that the algorithm can be used to design robust controllers for high order, complex systems with multiple parameter uncertainties.

The synthesis approach offers several distinct advantages over the μ and K_m synthesis techniques. The approach permits the designer to pre-specify the compensator order and architecture so that an optimal design with these extra conditions can be obtained. These design specifications cannot be incorporated into the standard $\mathcal{H}_\infty$ synthesis problem, but are critical for most realistic problems. Furthermore, the algorithm does not require an explicit iteration between the multiplier evaluation and control design because the optimal values of both are obtained simultaneously.

5.4 Summary

This chapter investigates the design of robust controllers using analysis tests based on the Popov stability multiplier. The resulting necessary conditions simultaneously yield the optimal controller and multiplier values. The optimal compensators guarantee robust stability for a given class of time-invariant sector-bounded uncertainties. By minimizing a worst case $\mathcal{H}_2$ performance bound, these designs also achieve robust performance. A numerical algorithm is presented to solve the optimality conditions in Theorem 5.3, Eq. 5.48, and Eq. 5.49. The analysis results in Chapter 3 also indi-

cate that this synthesis technique can be applied to the robust control problem with linear and nonlinear real parameter uncertainties. The following two chapters use this combined $\mathcal{H}_2$/real μ approach to design robust Popov controllers for low order benchmark problems and more complicated experiments.

Chapter 6

Numerical Synthesis Examples

6.1 Introduction

The goal of this chapter is to present examples of optimal $\mathcal{H}_2$ robust controllers developed using the Popov synthesis algorithm discussed in Chapter 5. Robust controllers are designed for two simple systems with constant real parameter uncertainties. The analysis in Chapter 3 and Refs. [39,69,143] indicates that, for systems with constant real parameter uncertainties, the approach in this thesis is less conservative than equivalent tests developed using bounded gain and positive real uncertainty models. The aim here is to extend these analysis results by considering optimal robust controller synthesis.

Two benchmark problems with constant real parameter uncertainty are considered in order to demonstrate the importance of analysis methods that restrict the time-variation of the system uncertainty. The first is the two mass spring system shown in Fig. 6.1. The second is the coupled four disk system from Ref. [31] shown in Fig. 6.2.

For the system in Fig. 6.1, the uncertainty enters the plant through errors in the spring connecting the two masses. For the system in Fig. 6.2, uncertainty in the inertia of disk 1 is considered first. The problem is then reformulated to capture multivariable uncertainty in the stiffness values of the springs k_1 and k_3. The inertia uncertainty in the second system is complicated because it influences all three flexible modes of the system and can result in the poles and zeroes exchanging order, as illustrated in Fig. 6.3. The sensitivity of the plant transfer function to parameter variations makes

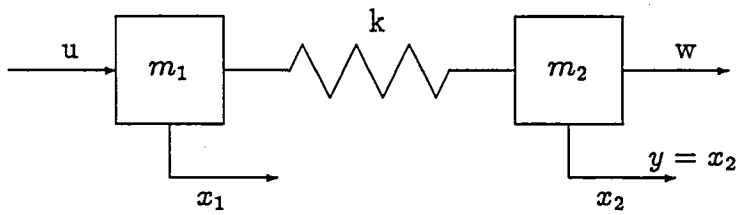

Figure 6.1: Two mass oscillator.

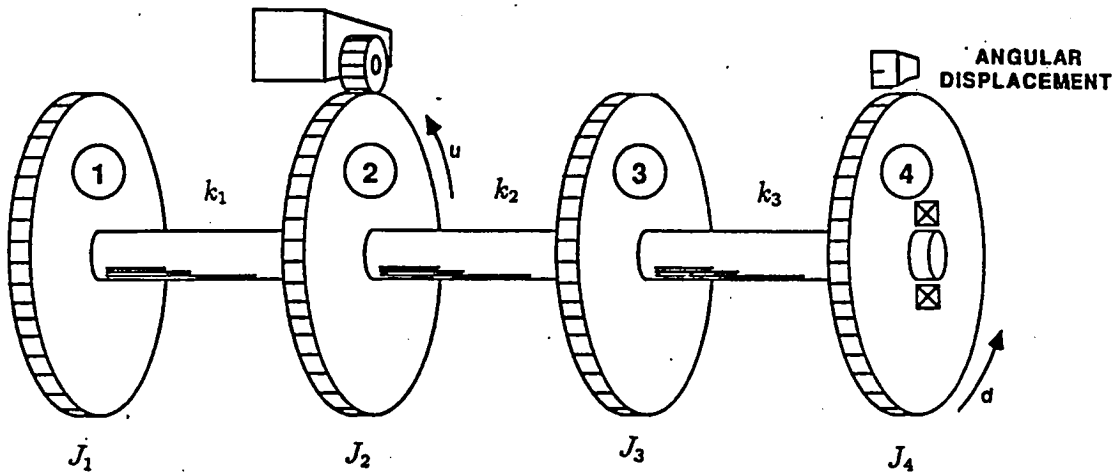

Figure 6.2: Four disk oscillator.

this four disk system a difficult challenge for robust control design [31,42].

Both full and reduced-order controllers are developed in this chapter, but no consideration is given to the potential problem of higher frequency unmodelled dynamics. Frequency weighted cost functionals in the specification of the $\mathcal{H}_2$ problem can be used to address this unstructured uncertainty. The results are presented in terms of performance robustness curves or "buckets" for several values of the stability bounds M_1 and M_2. Also, where possible, an interpretation of how this robustness is achieved is also presented. Recall from the previous developments that M_1 and M_2 represent the guaranteed robust stability bounds, which are lower bounds on the magnitude of the actual stability limits achieved.

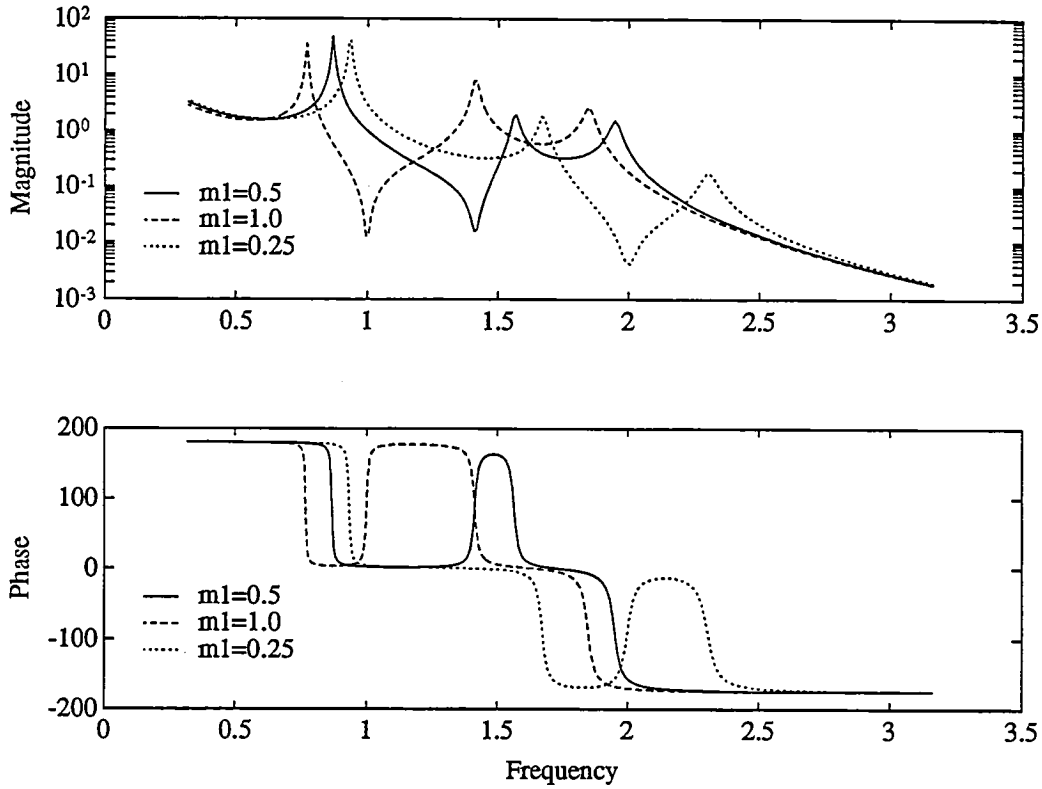

Figure 6.3: Transfer function from force actuator to angle sensor for the four disk oscillator, demonstrating the influence of inertia perturbations to disk 1 (m1) on the order of the poles and zeroes.

6.2 Two Mass Spring System

Consider the two mass spring system illustrated in Fig. 6.1 with $m_1 = m_2 = 1$ and an uncertain spring stiffness k. A control force acts on mass 1, and the position of mass 2 is measured, resulting in a noncollocated control problem. The nominal dynamics, with the states defined in the figure, are then governed by the matrices

$$A = \begin{bmatrix} 0 & 0 & 1 & 0 \\ 0 & 0 & 0 & 1 \\ -k_{\text{nom}} & k_{\text{nom}} & 0 & 0 \\ k_{\text{nom}} & -k_{\text{nom}} & 0 & 0 \end{bmatrix}, \; B = \begin{bmatrix} 0 \\ 0 \\ 1 \\ 0 \end{bmatrix}, \; D_1 = \begin{bmatrix} 0 & 0 \\ 0 & 0 \\ 0 & 0 \\ 1 & 0 \end{bmatrix}, \; C = \begin{bmatrix} 0 & 1 & 0 & 0 \end{bmatrix}, \quad (6.1)$$

and $D_2 = [0\ 1]$. The actual spring stiffness can be written as $k = k_{\text{nom}} + \Delta k$, where $k_{\text{nom}} = 1$. The actual dynamics of the system are given by the matrix $A_k = A - \Delta k B_0 C_0$, where $C_0 = [\,1\ -1\ 0\ 0\,]$ and $B_0^T = -[\,0\ 0\ -1\ 1\,]$. Note that with

this stiffness uncertainty, $C_0B_0 = 0$. The simplifications in the synthesis procedure resulting from this observation are discussed in Remark 5.2.

The benchmark problem is discussed in detail in Ref. [164]. The following example only considers design problem 1:

Design Problem 1 (Ref. [164]): Design a constant linear feedback compensator of the form

$$\dot{x}_c(t) = A_c x_c(t) + B_c y(t) \tag{6.2}$$

$$u(t) = C_c x_c(t) + D_c y(t) \tag{6.3}$$

with the following properties:

(i) The closed-loop system is stable for $m_1 = m_2 = 1$ and $0.5 < k < 2.0$.

(ii) For $w(t)$ = unit impulse response at t=0, the performance variable $z = x_2$ has a settling time of about 15 seconds for the nominal system $m_1 = m_2 = k = 1$.

(iii) The control system can tolerate reasonable measurement noise signals.

(iv) The control system achieves reasonable performance/stability robustness with reasonable bandwidth.

(v) The control system uses reasonable control effort and complexity. □

For this example, the displacement of mass 2 was penalized, so $R_{xx} = C^TC$, $V_2 = R_{uu} = \rho$, and $V_1 = D_1D_1^T$, where $\rho = 0.001$. The goals are to achieve good nominal performance and demonstrate robust stability and performance for perturbed spring stiffness values in the range $0.5 \leq k \leq 2$.

Using the algorithm in Section 5.2, several full-order ($n_c = n$) Popov compensators were designed for this uncertain system. The designs are distinguished by the labels "Popov(a)(b)", where (a) refers to the number of the example, and (b) refers to the different compensators for that example. Two robust designs are compared with the optimal LQG controller in Fig. 6.4. The stability robustness and performance levels achieved are presented in Table 6.1. As mentioned earlier, there are no guaranteed

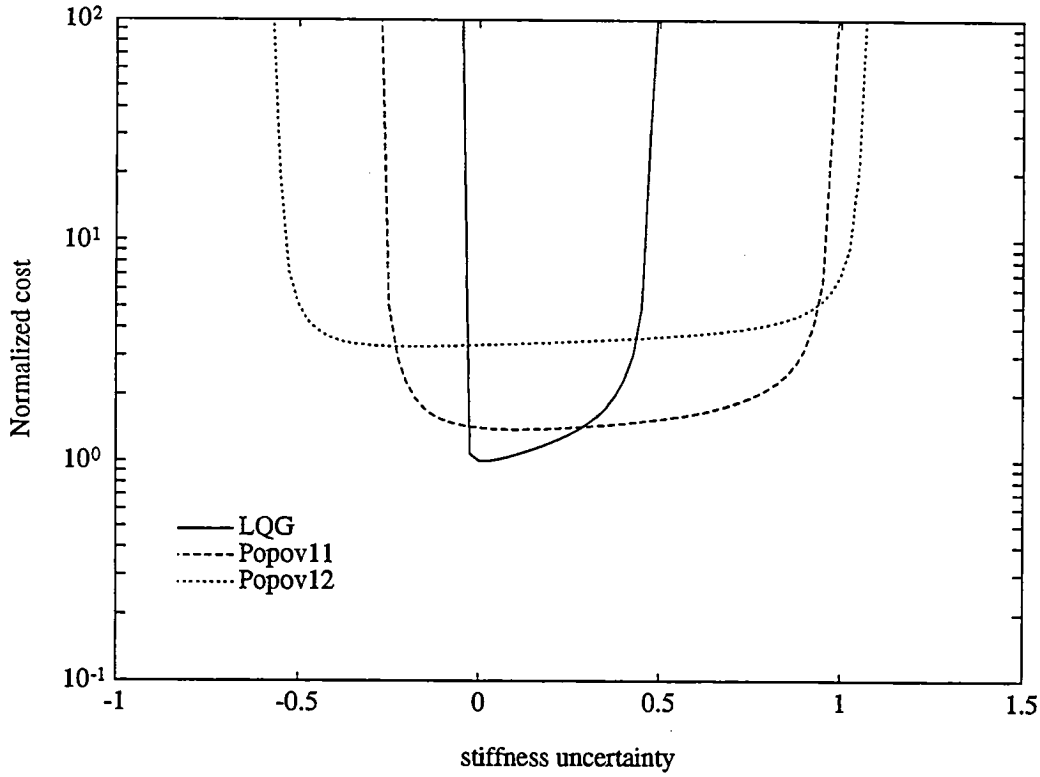

Figure 6.4: Performance cost curves illustrating the trade-off between guaranteed (and achieved) robust stability and nominal/robust performance. See Table 6.1 for stability bounds.

stability robustness bounds for the LQG design. The costs have been normalized with respect to the optimal LQG value to obtain J_{norm}.

As is apparent from Fig. 6.4, the lower stability limit is the more challenging goal to achieve. The Popov12 compensator guarantees stability for stiffness values in the range $(-0.4, 0.6)$, but achieves robust stability over the range of stiffness values specified in problem 1. The optimal multiplier for the Popov12 compensator is $W(s) = 1 + 0.33s$.

The optimal Popov12 and LQG controllers are compared in Fig. 6.5 and Table 6.2. While similar at high frequencies, the compensators are strikingly different for frequency values near the uncertain mode. The more lightly damped nonminimum phase zero in the Popov compensator at 0.9 rad/sec phase stabilizes the system

Table 6.1: Closed-loop robust performance for the two mass system with spring uncertainty.

Fig. 6.4 Label	J_{norm}	Lower stability bound achieved	Lower stability bound guaranteed	Upper stability bound guaranteed	Upper stability bound achieved
LQG	1.00	-0.03	0	0	0.45
Popov11	1.42	-0.25	-0.10	0.30	0.95
Popov12	3.34	-0.55	-0.40	0.60	1.05

Table 6.2: Comparison of LQG and Popov12 compensators for the two mass system.

Compensator	Gain	Poles	Zeroes
LQG	-1.28	$-1.76 \pm 4.26j$ $-4.98 \pm 3.42j$	-0.65 $0.15 \pm 1.23j$
Popov12	-0.36	$-7.16 \pm 0.88j$ $-3.63 \pm 6.23j$	-0.29 $0.04 \pm 0.93j$

for negative values of Δk. Similarly, the phase of the Popov compensator is higher at high frequencies, leading to a stable system for larger positive values of Δk. A comparison of the modifications required for the Popov compensator at high and low frequencies clearly illustrates why the lower stability limit presents the more difficult design challenge.

The robustness of the two compensator designs can be compared further in terms of the gain and phase margins of the loop transfer functions. With the LQG compensator, the phase margin at 0.98 rad/sec is only 4° and gain margin at 1.00 rad/sec is only 1.06. With the Popov compensator, the phase margin at 2.02 rad/sec is 37° and the gain margin at 3.53 rad/sec is 2.5.

The impulse responses in Fig. 6.6 are presented to address the robust performance and control effort issues in problem 1. These figures compare the responses for the closed-loop systems with nominal and perturbed stiffness values. The degradation of nominal performance to achieve a larger stability region is shown by the plots on the left. Note that the Popov12 compensator meets the performance specification of

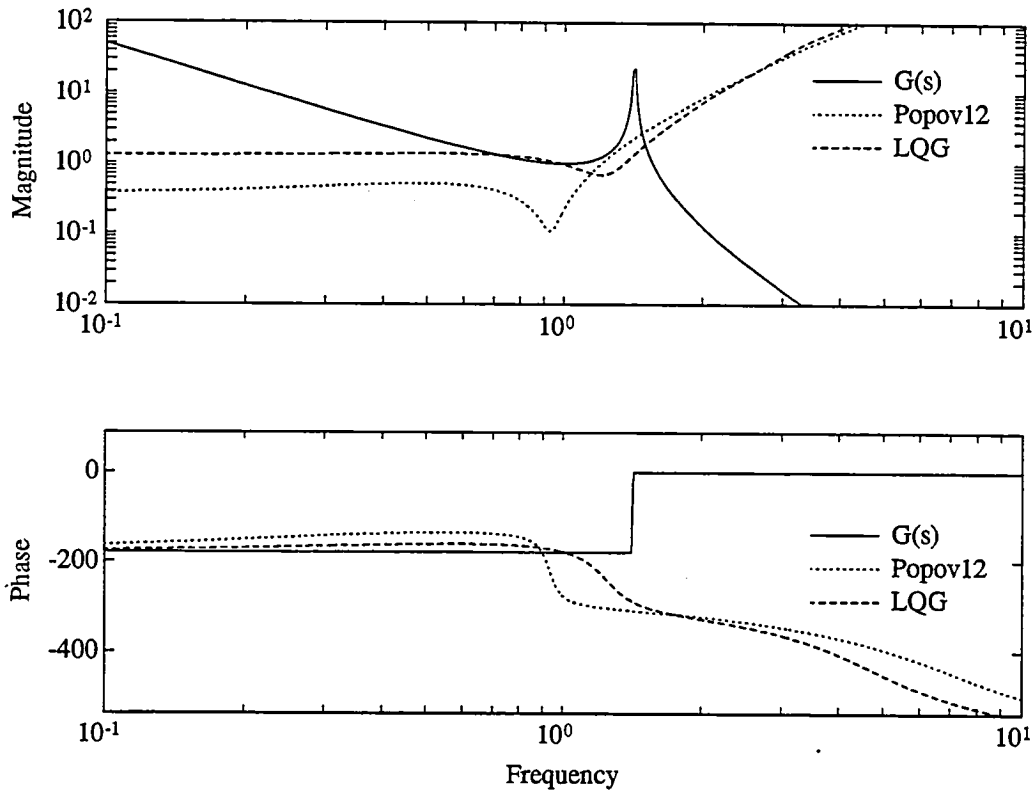

Figure 6.5: Comparison of LQG and Popov12 compensators for the two mass system, illustrating the phase stabilization of the Popov controller.

15 sec, but the transient response of mass 2 is worse than that achieved by the LQG design. However, the plots on the right illustrate that similar levels of performance are achieved by the Popov compensator, even at the limits of guaranteed stability. Fig. 6.4 clearly shows that the LQG controller destabilizes the system for these values of the parameter errors. The two lower plots demonstrate that the Popov compensator does not require significantly increased control authority over the LQG design.

The open and closed-loop pole locations for the two mass system with LQG and Popov compensators are presented in Fig. 6.7. These graphs show the nominal closed-loop poles and, for the Popov designs, the poles at the limits of guaranteed stability. The closed-loop poles are given for several values of Δk in the range $(-0.75, 1.5)$. The extreme sensitivity of the LQG design can be seen by the rapid movement of the lowest frequency closed-loop pole into the right half plane. With the Popov compensator,

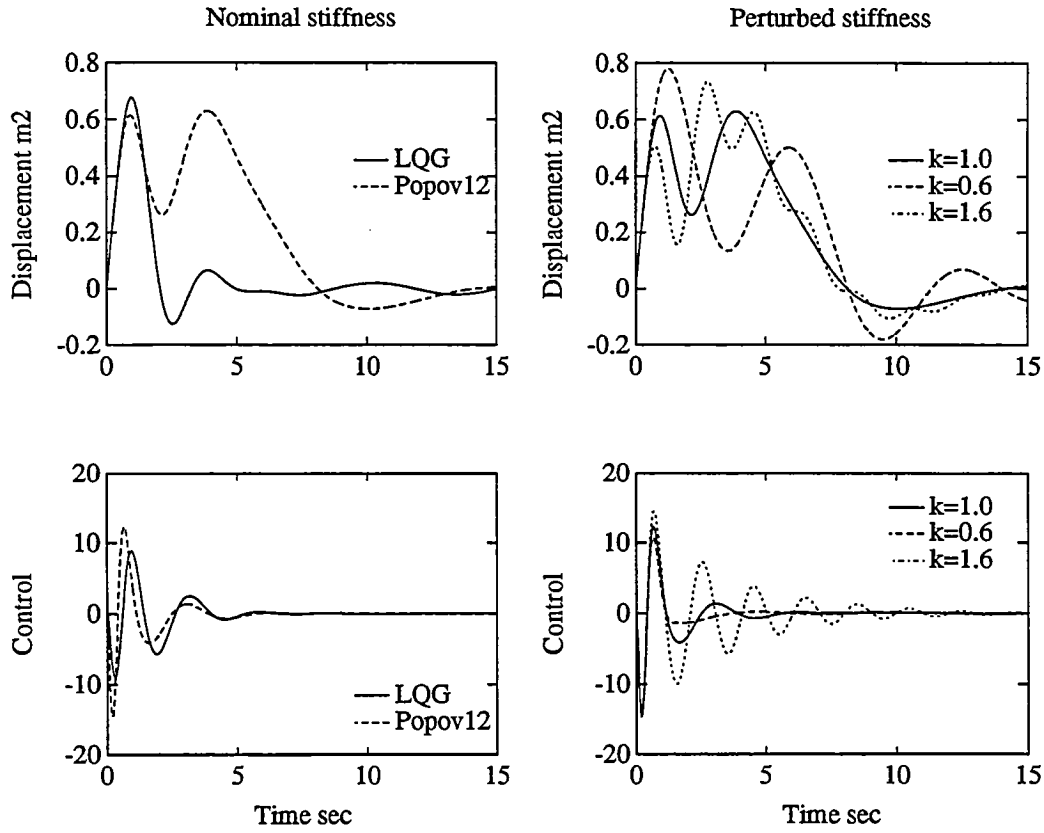

Figure 6.6: Impulse responses for the two mass system with nominal and perturbed stiffness values. The nominal performance with the Popov12 compensator meets the 15 sec settling time specification. Popov12 performance degrades with perturbed stiffness values, but remains stable.

the equivalent pole pair remain in the left half plane for much larger values of the parameter uncertainty. In fact, it is actually the higher frequency pole pair that is destabilized first.

The modifications to the optimal $\mathcal{H}_2$ compensator as the requested stability bounds are increased are shown in Fig. 6.8. These figures give the poles and zeroes for the LQG controller and several Popov designs. For this uncertainty set, as M_1 and M_2 are increased, the trend is towards more heavily damped compensator poles and more lightly damped compensator zeroes.

This simple example serves to illustrate that the Popov synthesis technique results in robust controllers that achieve good guaranteed robust performance. The following sections investigate the design approach for more complicated systems.

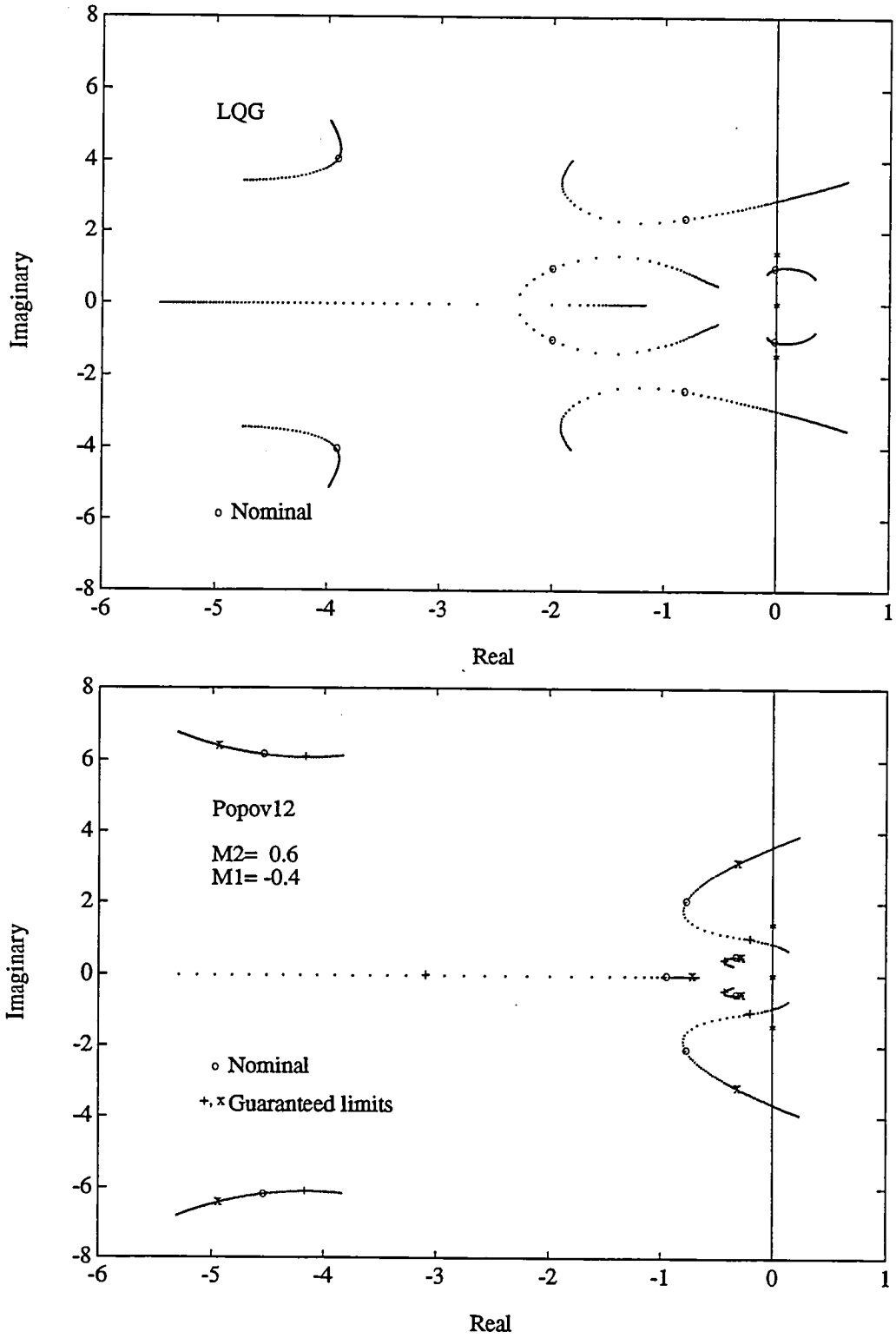

Figure 6.7: Closed-loop pole locations with the LQG and Popov12 compensators for $-0.75 \leq \Delta k \leq 1.5$.

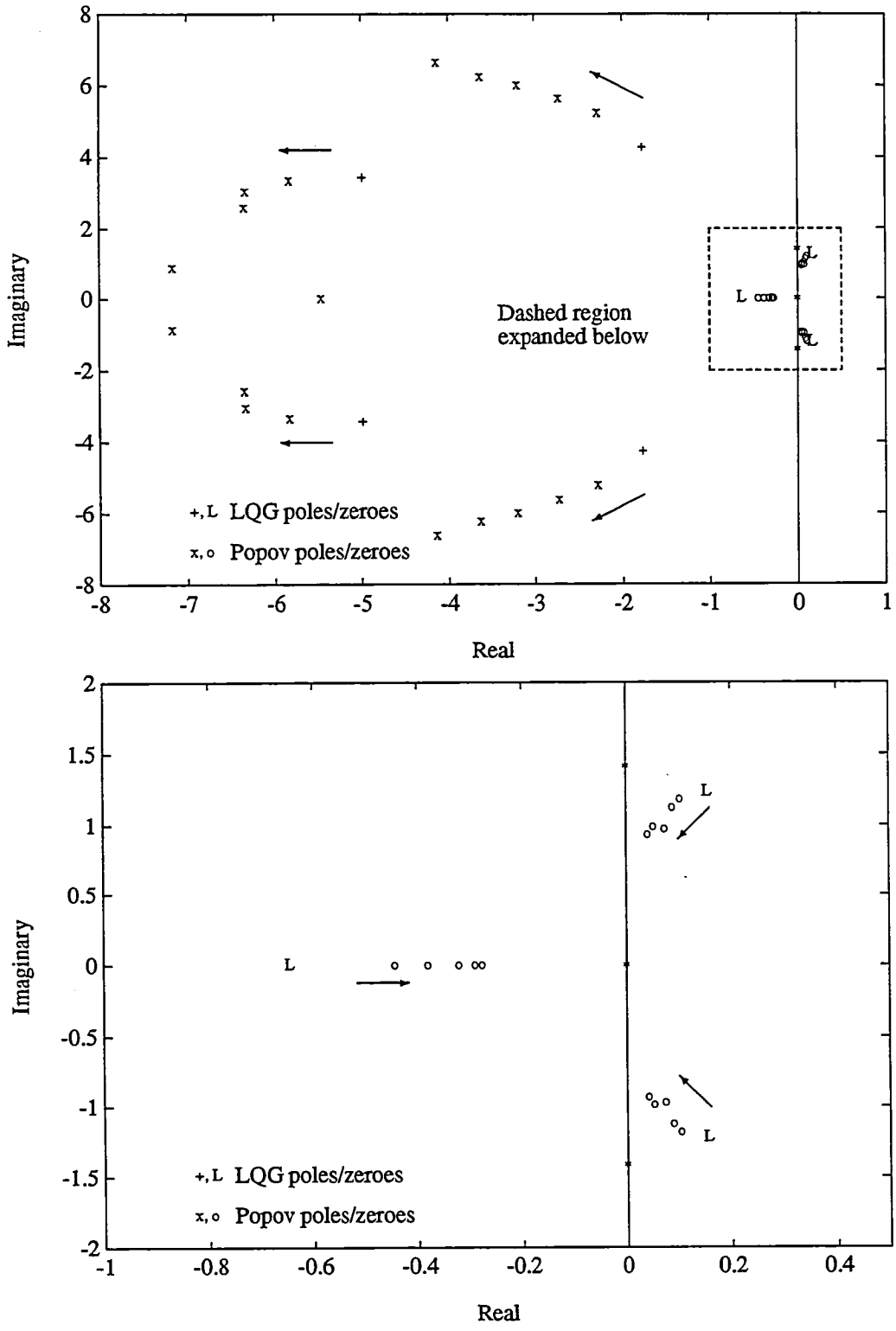

Figure 6.8: Compensator pole and zero locations as a function of increased robustness guarantees. The arrows indicate the trends with increasing M_2.

6.3 Coupled Rotating Disk System

We can extend these results and observations by considering two versions of the more complicated four disk problem. A state space model for the four disk system illustrated in Fig. 6.2, with states associated with the angular positions of each disk, is given by the matrices

$$A = \begin{bmatrix} 0 & I \\ -J^{-1}K & -J^{-1}D \end{bmatrix}, \; B = \begin{bmatrix} 0 \\ 0 \\ 0 \\ 0 \\ 0 \\ \frac{1}{m} \\ 0 \\ 0 \end{bmatrix}, \; C^T = \begin{bmatrix} 0 \\ 0 \\ 0 \\ 1 \\ 0 \\ 0 \\ 0 \\ 0 \end{bmatrix}, \; D_1 = \begin{bmatrix} 0 & 0 \\ 0 & 0 \\ 0 & 0 \\ 0 & 0 \\ 0 & 0 \\ 0 & 0 \\ 0 & 0 \\ \frac{1}{m} & 0 \end{bmatrix}, \tag{6.4}$$

and $D_2 = [0 \; 1]$, where

$$J = m \begin{bmatrix} 0.5 & 0 & 0 & 0 \\ 0 & 1 & 0 & 0 \\ 0 & 0 & 1 & 0 \\ 0 & 0 & 0 & 1 \end{bmatrix}, K = k \begin{bmatrix} 1 & -1 & 0 & 0 \\ -1 & 2 & -1 & 0 \\ 0 & -1 & 2 & -1 \\ 0 & 0 & -1 & 1 \end{bmatrix}, D = d \begin{bmatrix} 1 & -1 & 0 & 0 \\ -1 & 2 & -1 & 0 \\ 0 & -1 & 2 & -1 \\ 0 & 0 & -1 & 1 \end{bmatrix}, \tag{6.5}$$

$m = k = 1$, and a low damping value of $d = 0.01$ is used. The inertia of disk 1 (m_1) is considered to be uncertain in Part 1 of this problem. However, the inertia parameter enters the system dynamics through its inverse. Consequently, we will consider an uncertainty $\tilde{m}$ in the inverse of the inertia, which can be represented as

$$1/m_1 = 1/m_{\text{nom}} + \tilde{m}, \quad m_{\text{nom}} = 0.5. \tag{6.6}$$

Then, as m_1 varies from 1 to 0.25, $\tilde{m}$ varies from -1 to 2. The uncertainty in the dynamics matrix A can then be represented as $\Delta A = -\tilde{m} B_0 C_0$, where

$$B_0^T = -\begin{bmatrix} 0 & 0 & 0 & 0 & 1 & 0 & 0 & 0 \end{bmatrix}, \; C_0 = \begin{bmatrix} -k & k & 0 & 0 & -d & d & 0 & 0 \end{bmatrix}. \tag{6.7}$$

Part 2 of this design considers uncertainties in the stiffness values of the springs k_1 and k_3. Several characteristics make this problem important in the design of controllers for lightly damped structures. As shown in Fig. 6.9, the performance is dominated by the rigid body and first flexible modes, which are essentially unchanged

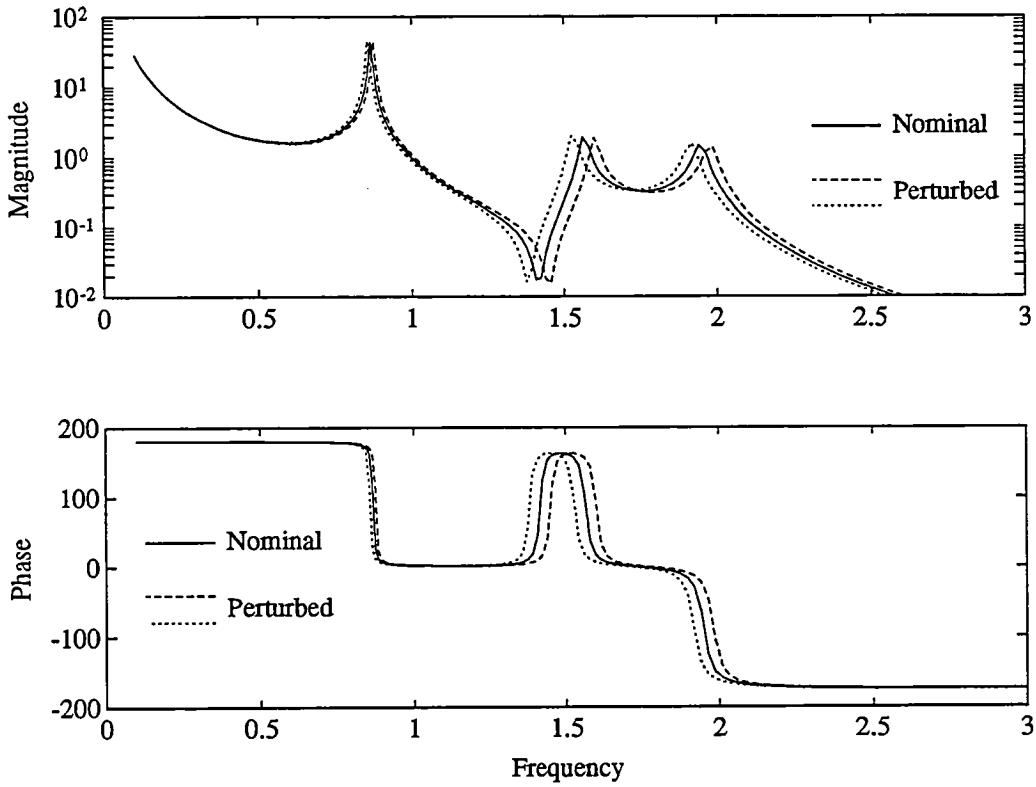

Figure 6.9: Influence of stiffness uncertainty on the transfer function for the four disk problem. The two uncertainties are assumed equal in the analysis. For a lightly damped system, 5% uncertainty in both stiffness values can result in plant phase variations of $\pm 100°$.

by the model uncertainty. Furthermore, the two higher frequency modes and the zero at 1.4 rad/sec are highly uncertain, resulting in large phase uncertainties in the system with only 5% variations in the two stiffness values. The uncertainty in the dynamics matrix A can be represented as $\triangle A = -B_0 \triangle K C_0$, where

$$B_0^T = -\begin{bmatrix} 0 & 0 & 0 & 0 & -2 & 1 & 0 & 0 \\ 0 & 0 & 0 & 0 & 0 & 0 & -1 & 1 \end{bmatrix}, \; C_0 = \begin{bmatrix} 1 & -1 & 0 & 0 & 0 & 0 & 0 & 0 \\ 0 & 0 & 1 & -1 & 0 & 0 & 0 & 0 \end{bmatrix}, \tag{6.8}$$

and $\triangle K = \text{diag}(\Delta k_1, \Delta k_2)$. To complete the noise and performance specifications for the $\mathcal{H}_2$ synthesis, we define $R_{xx} = C_1^T C_1$, $V_2 = R_{uu} = \rho$, and $V_1 = D_1 D_1^T$, where $\rho = 0.005$ and $C_1 = [0\ 0\ 0\ 1\ 0\ 0\ 0\ 0.1]$.

The results for Part 1 are given in Fig. 6.10 and Table 6.3 . The synthesis sequence was terminated at guaranteed bounds of ± 0.16, but the achieved stability limits are actually $-0.22 < \tilde{m} < 0.34$. These actual limits correspond to inertia values in the

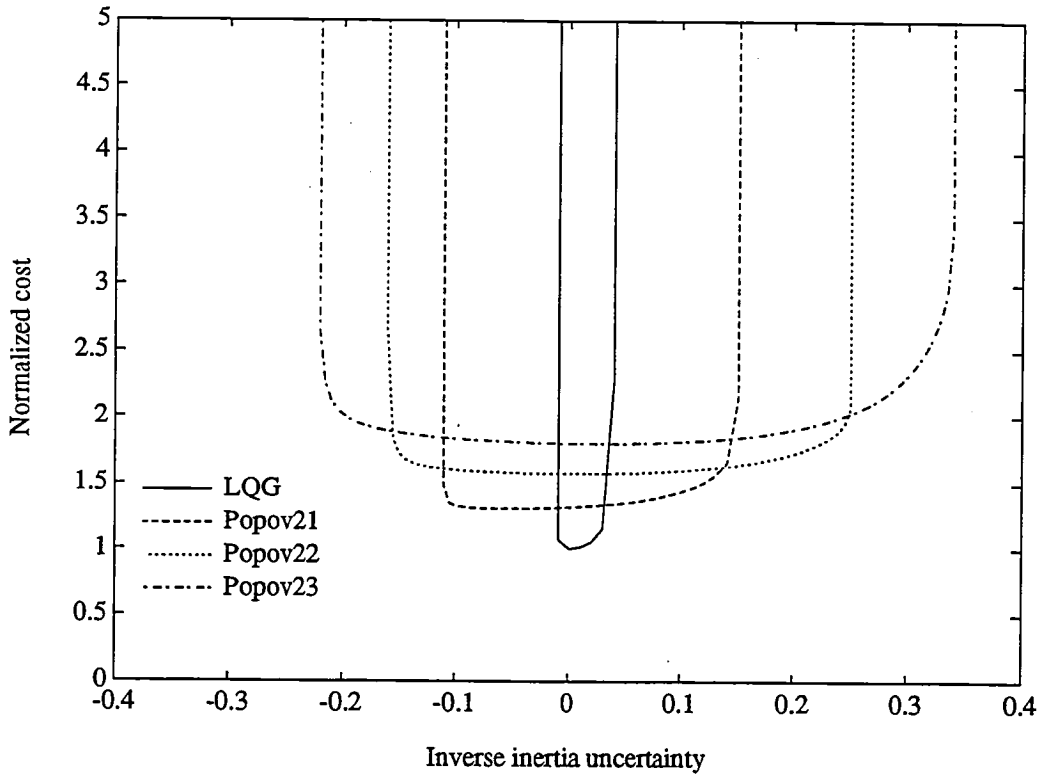

Figure 6.10: Closed-loop robust stability and performance with inertia uncertainty in disk 1. See Table 6.3 for stability bounds.

Table 6.3: Closed-loop robust performance with inertia uncertainty in disk 1.

Fig. 6.10 Label	J_{norm}	Lower stability bound achieved	Lower stability bound guaranteed	Upper stability bound guaranteed	Upper stability bound achieved
LQG	1.00	-0.009	0	0	0.041
Popov21	1.32	-0.110	-0.089	0.021	0.151
Popov22	1.58	-0.160	-0.115	0.115	0.250
Popov23	1.80	-0.220	-0.159	0.159	0.340

range $0.43 < m_1 < 0.56$. This range represents a significant fraction of the variation ($m_1 \approx 0.38$) at which the poles and zeroes change order in Fig. 6.3, and a substantial improvement over the LQG result. The penalty in terms of performance degradation is evident from the J_{norm} values in Table 6.3.

The robust control synthesis procedure for Part 2 assumes that the two stiffness uncertainties are uncorrelated. For simplicity in the analysis, the case with

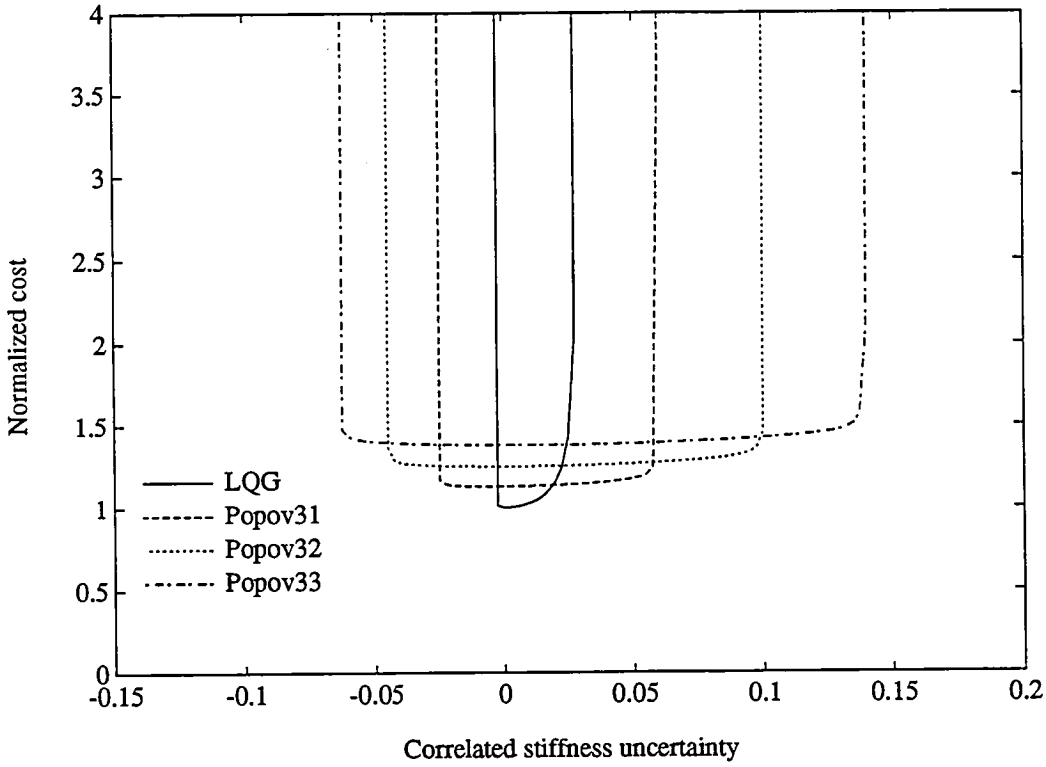

Figure 6.11: Closed-loop robust stability and performance with two stiffness uncertainties. It was assumed that $\Delta k_1 = \Delta k_2$ for the analysis. See Table 6.4 for stability bounds.

$\Delta k_1 = \Delta k_2$ is considered here. The robust stability and performance results are presented in Fig. 6.11 and Table 6.4. The Popov33 compensator guarantees stability for 5% independent variations in the stiffness values, which represents a significant improvement over the values that the LQG design actually achieves. For this lightly damped system, these perturbations correspond to approximately $\pm 100°$ phase variations in the plant.

In these synthesis problems, there typically is a "stiff" uncertainty direction that is more difficult than the other directions. The negative uncertainty values are more difficult to achieve in this example, as can be seen by the closeness of the guaranteed and achieved lower bounds in Table 6.4. While the discrepancy in the guaranteed and achieved upper bounds is, to some extent, a measure of the conservatism in the technique, it is also a reflection of the relative ease of robustifying the system to this

Table 6.4: Robust stability and performance for the closed-loop system with two stiffness uncertainties. It was assumed that $\Delta k_1 = \Delta k_2$ for the analysis.

Fig. 6.11 Label	J_{norm}	Lower stability bound achieved	Lower stability bound guaranteed	Upper stability bound guaranteed	Upper stability bound achieved
LQG	1.00	-0.003	0	0	0.028
Popov31	1.12	-0.025	-0.019	0.019	0.060
Popov32	1.25	-0.045	-0.035	0.035	0.100
Popov33	1.38	-0.063	-0.051	0.051	0.140

particular direction of the uncertainty.

The transfer functions of the optimal LQG and Popov33 compensators are compared in Fig. 6.12. The uncertainty in the zero-pole combination at approximately 1.4 rad/sec is reflected in the Popov compensator by lower compensator gains and much smoother phase. The optimal multiplier for Popov33 is $W_{\text{opt}}(s) = \text{diag}(1 + 0.16s, 2.9(1 + 0.27s))$.

Further comparisons of the LQG and Popov designs are given in Figs. 6.13 and 6.14. In each figure, the lower plot magnifies the region of the complex plane about the Imaginary-axis. The figures show the open-loop and closed-loop pole locations of the system as a function of the uncertainty $\Delta k = \Delta k_1 = \Delta k_2$ for $-0.2 \leq \Delta k \leq 0.2$. The LQG and Popov33 designs from Table 6.4 are compared in these figures. The two sets of closed-loop poles are plotted for the same values of Δk. The graphs also indicate the nominal pole locations. If applicable, the pole locations at the guaranteed stability limits are also identified.

With the LQG compensator in Fig. 6.13, there are nominally two closed-loop poles at approximately 1.4 rad/sec, the frequency of the plant zero. Further analysis of Fig. 6.13 indicates that the more lightly damped of these two pole pairs is extremely sensitive to changes in the stiffness values. This rapid destabilization is expected, given the large system changes in this frequency range shown in Fig. 6.9.

A similar examination of the closed-loop poles with the Popov compensator in Fig. 6.14 indicates that several key changes have occurred. While the three lowest frequency poles are more heavily damped, the highest frequency one is essentially un-

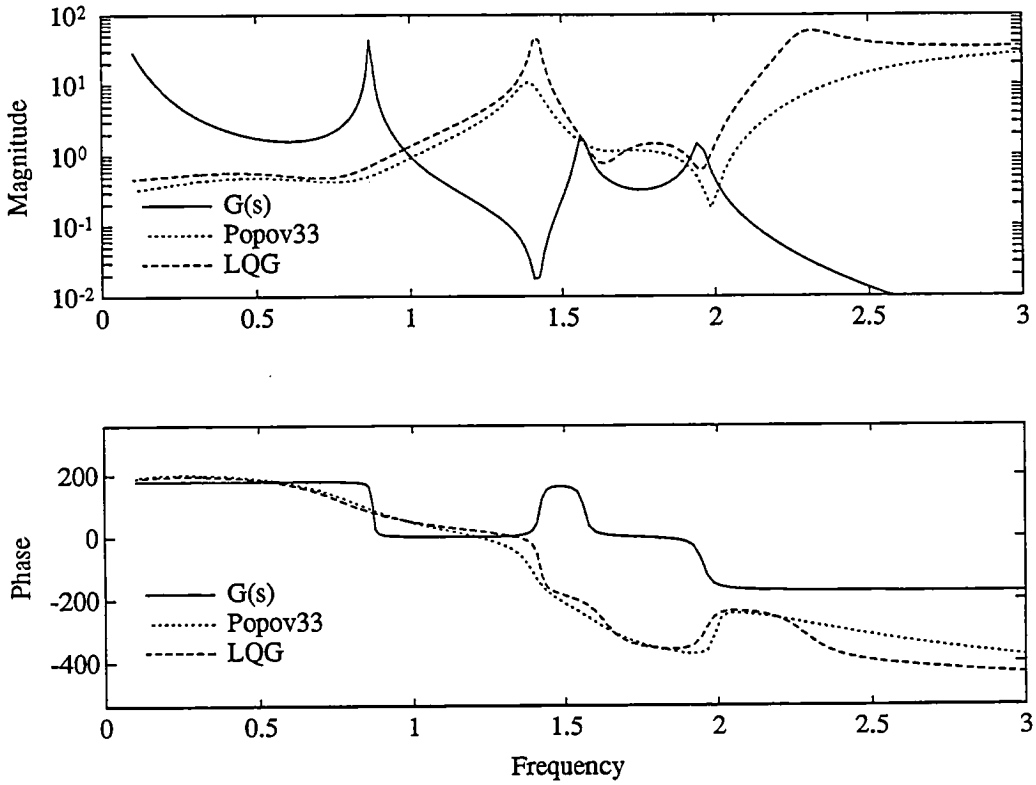

Figure 6.12: Optimal LQG and Popov33 compensator comparison for the system $G(s)$ with two stiffness uncertainties.

changed. The additional robustness of the closed-loop system to stiffness uncertainty is clearly evident from the traces in Fig. 6.14.

To demonstrate the changes that have occurred to the robust controllers, the compensator poles and zeroes are plotted in Fig. 6.15 as a function of the desired stability bounds. Although complicated, the figures illustrate that, in this case, the Popov compensator poles and nonminimum phase zeroes are more heavily damped than their LQG counter part. This conclusion is consistent with the observation that the compensator phase is much smoother than the LQG design. Also evident is the fact that the real minimum phase zeroes of the Popov compensators are at lower frequencies. Furthermore, note that the compensator pole at approximately 1.4 rad/sec is shifted away from the plant zero in the Popov designs, which means that they avoid pole-zero cancellations in the closed-loop systems.

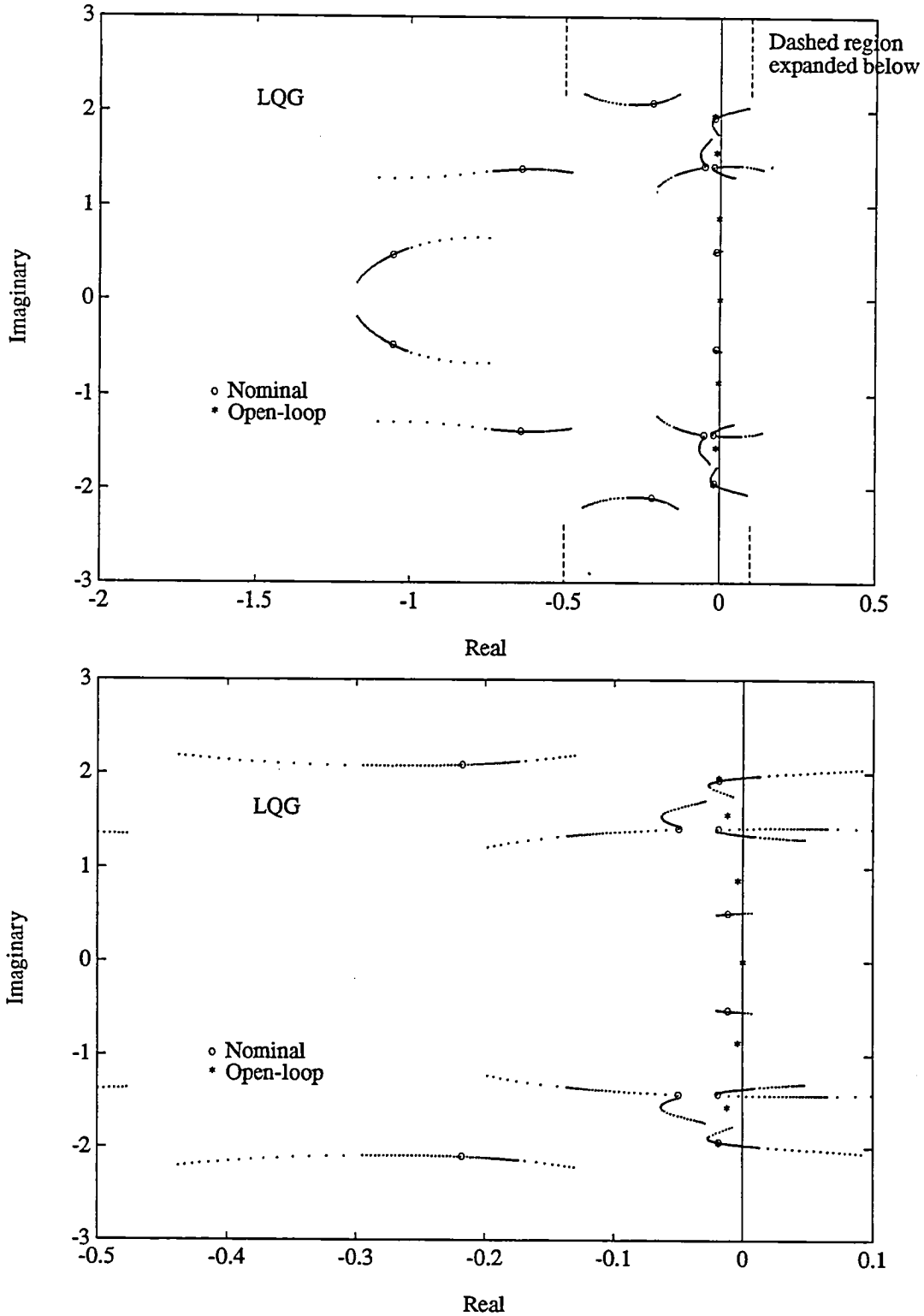

Figure 6.13: Closed-loop pole locations with the LQG compensator for $\Delta k = \Delta k_1 = \Delta k_2$ and $-0.2 \leq \Delta k \leq 0.2$.

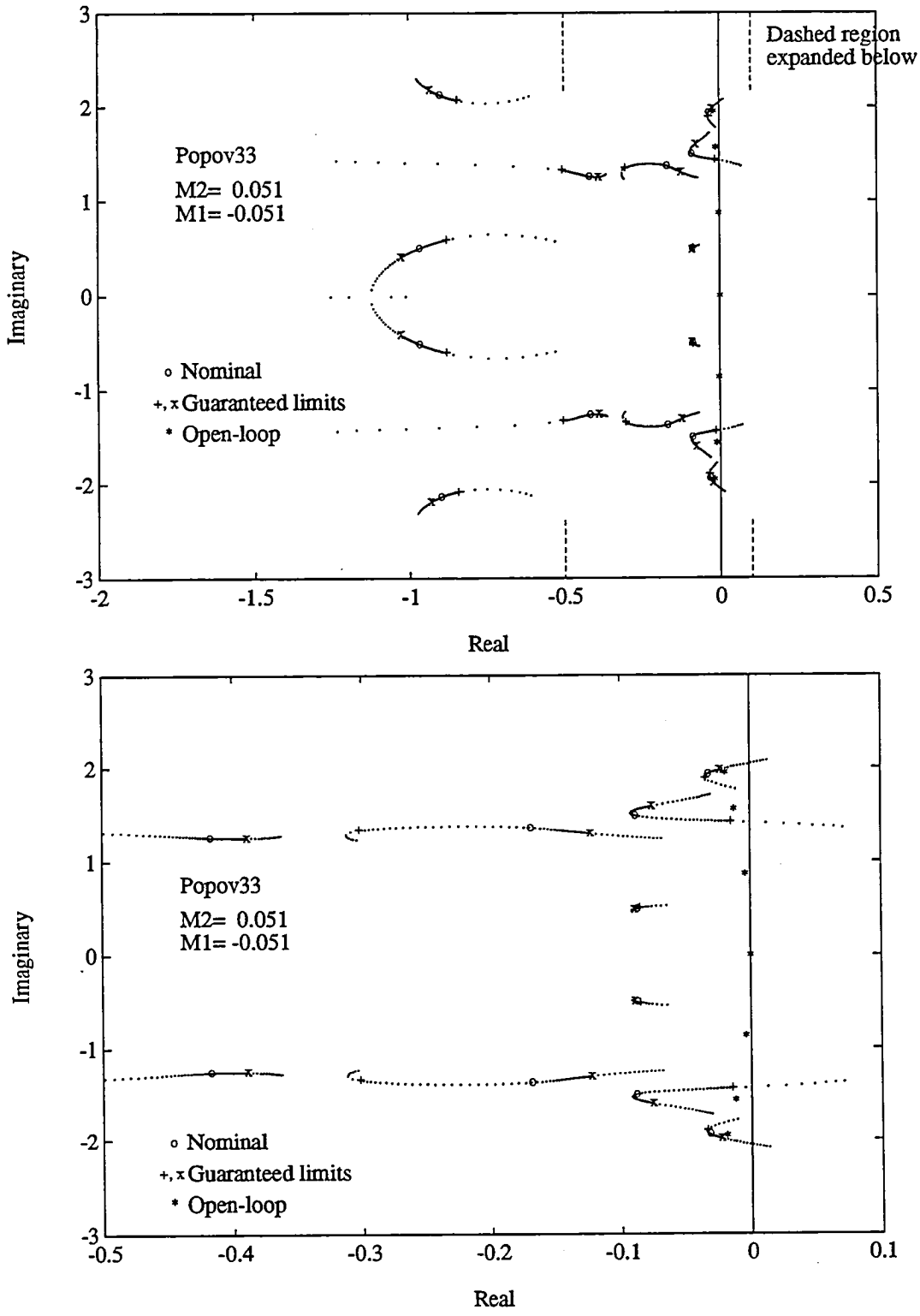

Figure 6.14: Closed-loop pole locations with the Popov33 compensator for $\Delta k = \Delta k_1 = \Delta k_2$ and $-0.2 \leq \Delta k \leq 0.2$.

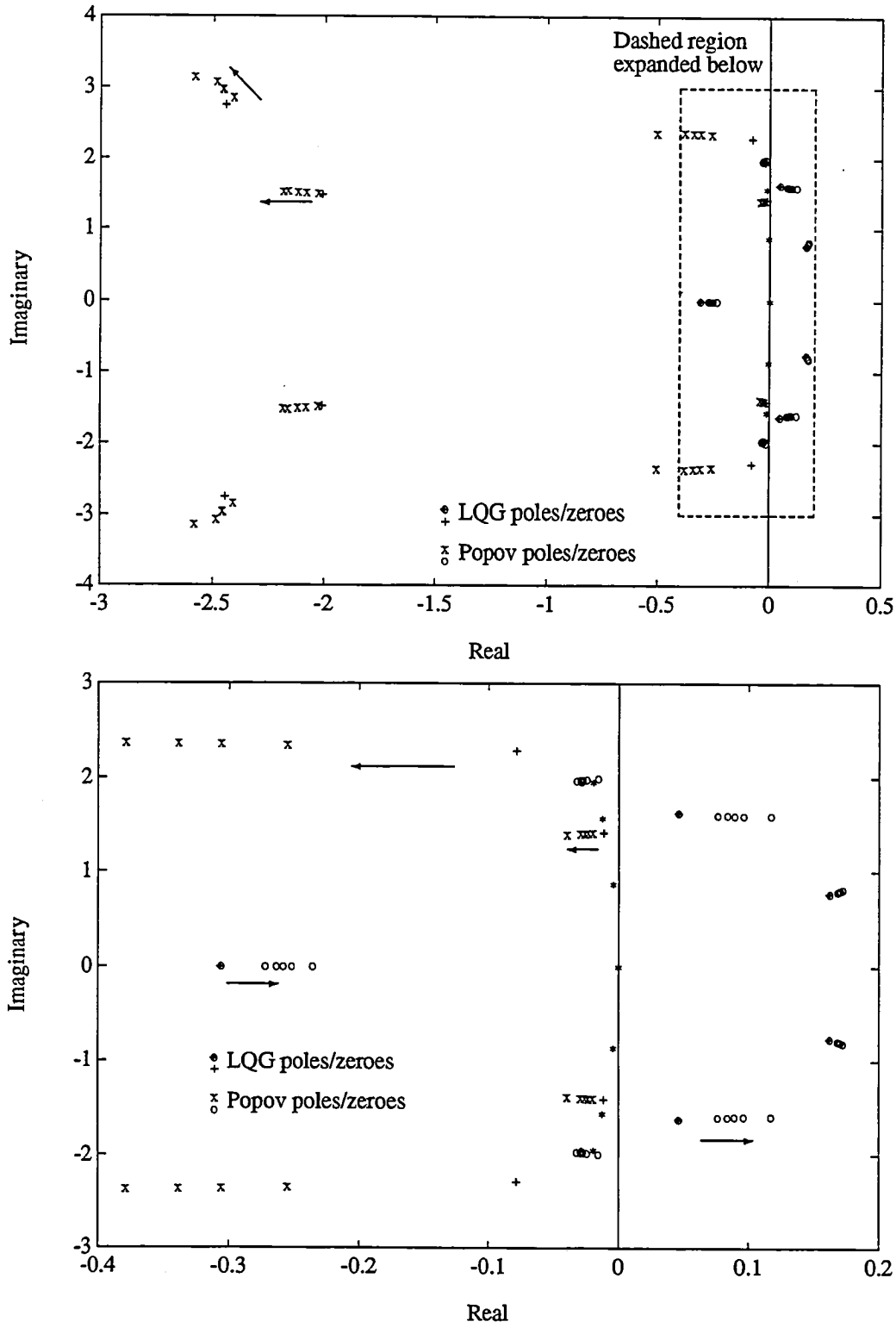

Figure 6.15: Compensator pole and zero locations for increasing guaranteed stability bounds. The arrows indicate the trends with increasing M_2.

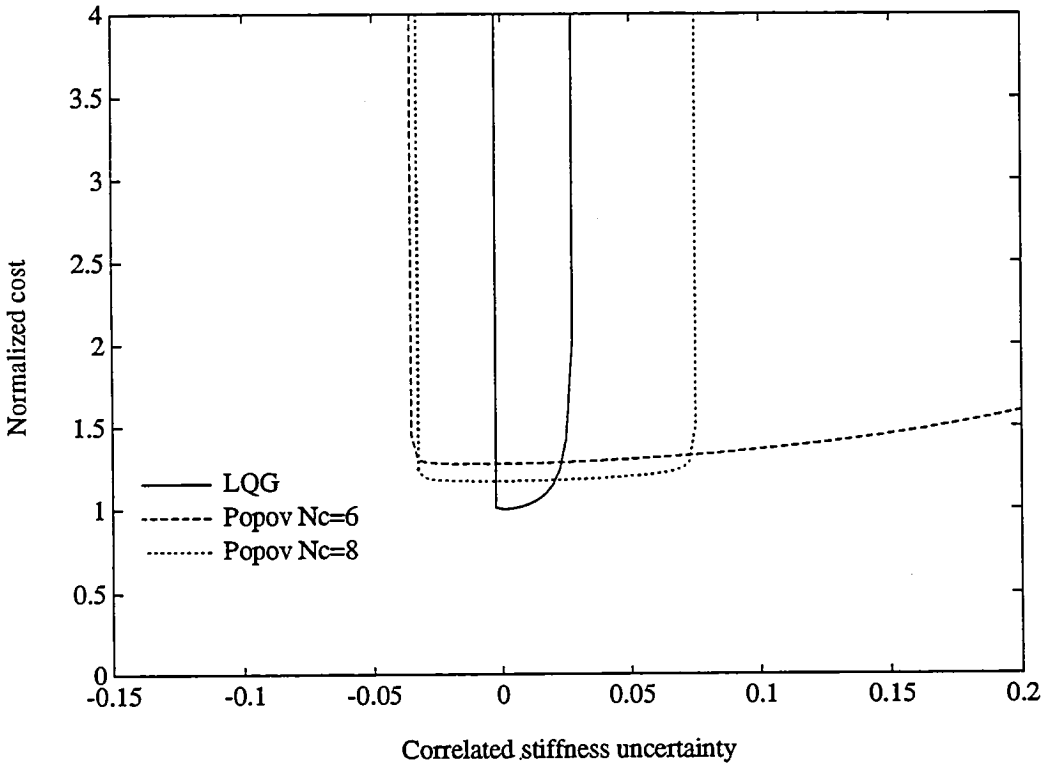

Figure 6.16: Closed-loop robust stability and performance with two stiffness uncertainties. Comparison of full ($n_c = 8$) and reduced-order ($n_c = 6$) designs. It was assumed that $\Delta k_1 = \Delta k_2$ for the analysis. See Table 6.5 for the corresponding stability bounds.

Table 6.5: Closed-loop robust stability and performance with two stiffness uncertainties. Comparison of full ($n_c = 8$) and reduced-order ($n_c = 6$) designs. It was assumed that $\Delta k_1 = \Delta k_2$ for the analysis.

Fig. 6.16 Label	J_{norm}	Lower stability bound achieved	Lower stability bound guaranteed	Upper stability bound guaranteed	Upper stability bound achieved
LQG	1.00	-0.003	0	0	0.028
Popov $n_c = 8$	1.17	-0.033	-0.024	0.024	0.075
Popov $n_c = 6$	1.27	-0.035	-0.025	0.025	0.200

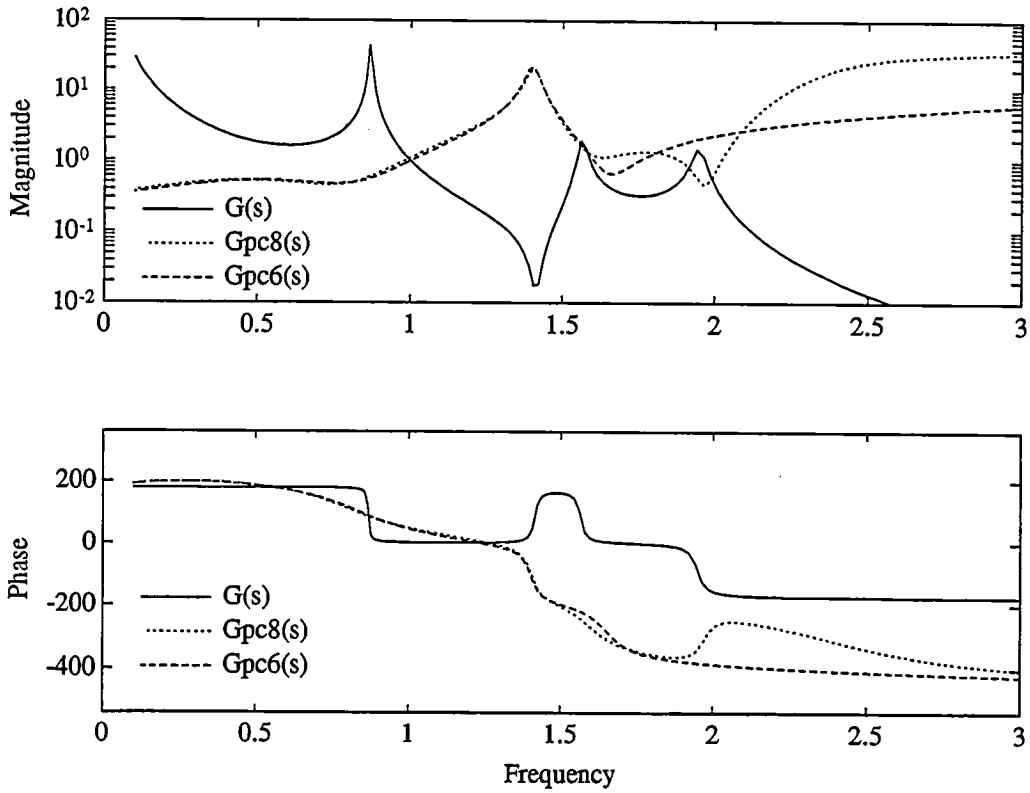

Figure 6.17: Full (Gpc8) and reduced-order (Gpc6) Popov compensators for the system with two stiffness uncertainties. See Tables 6.5 and 6.6.

Table 6.6: Comparison of a full (Gpc8) and reduced-order (Gpc6) Popov compensator for the system with two stiffness uncertainties. Stability boundaries are provided in Table 6.5.

Compensator	Gain	Poles	Zeroes
Popov $n_c = 8$ Gpc8	-0.36	$-0.02 \pm 1.40j$ $-0.31 \pm 2.35j$ $-2.18 \pm 1.51j$ $-2.41 \pm 2.85j$	-0.26 $0.17 \pm 0.80j$ $0.08 \pm 1.60j$ $-0.03 \pm 1.97j$
Popov $n_c = 6$ Gpc6	-0.34	$-0.02 \pm 1.40j$ $-0.85 \pm 0.98j$ $-2.03 \pm 7.15j$	-0.27 $0.17 \pm 0.83j$ $0.06 \pm 1.65j$

To complete the discussion of this problem, a reduced-order Popov controller ($n_c = 6$) is given for Part 2. The stability robustness and performance values are given in Fig. 6.16 and Table 6.5. Since the optimal compensator order is $n_c = n = 8$, the nominal performance of this suboptimal design ($n_c = 6 < n$) is expected to be worse than both the LQG and full-order Popov designs. This is clearly evident in the table by the larger value of J_{norm}. Although Fig. 6.16 apparently indicates that the reduced-order design is more robust to increases in the stiffness values, this conclusion may not be valid for other combinations of Δk_1 and Δk_2.

The poles and zeroes of the full and reduced-order controllers are compared in Table 6.6, and the two compensator transfer functions are given in Fig. 6.17. Both sets of results indicate that the controllers are quite similar up to approximately 1.5 rad/sec. However, the two designs differ at higher frequencies due to the reduced number of compensator poles and zeroes. The reduced-order design loses a pole in the 2.5-3.5 rad/sec range and the zero at 2 rad/sec. The loss of the phase recovery associated with this zero is accounted for in the reduced-order design by moving the highest frequency pole pair to approximately 7 rad/sec.

6.4 Summary

The results from these three examples illustrate the capabilities of Popov controller synthesis for robust control design with constant real parameter uncertainty. Furthermore, the curves in Figs. 6.4, 6.10, and 6.11 illustrate the tradeoffs between robust stability and performance. From the relative flatness of the cost curves, it is clear that similar performance levels are achieved for all parameter variations in the range of guaranteed stability, as demonstrated by the impulse responses in Fig. 6.6.

The last example is considered to be the most important of the three. This lightly damped benchmark problem captures many of the difficulties in the control of structures. The importance of these benchmark problems is that they clearly illustrate how the robustness is achieved. By considering a more complicated system, the results of the next chapter demonstrate that the approach is also effective for realistic systems.

Chapter 7

Experimental Implementation

7.1 Introduction

This chapter considers the design and implementation of robust controllers for the Middeck Active Control Experiment (MACE). The goals of these experiments are to demonstrate the feasibility of Popov controller synthesis for higher order systems and to illustrate the capabilities of the design approach for complex systems with multiple uncertainties. In particular, a robustness problem with the experimental implementation of Linear Quadratic Gaussian (LQG) controllers is identified. It is then demonstrated how this problem can be solved using the more robust Popov controller synthesis technique described in Chapter 5.

The discussion in this chapter focuses on the modifications to the compensators that are required to achieve this additional robustness. In particular, the controllers developed using Popov synthesis are directly compared with the optimal LQG designs. The tools from Chapter 6 are used to demonstrate the stability and performance levels that are achieved on MACE. The effectiveness of the Popov controllers is also demonstrated experimentally by intentionally changing the mass of the structure.

Several design and implementation issues were encountered during these experiments. In particular, at high levels of control authority, the optimal compensators were found to be unstable. Unstable compensators result in conditionally stable closed-loop systems and thus require safeguards to be implemented reliably. This implementation issue is the subject of current research in the MACE program, so

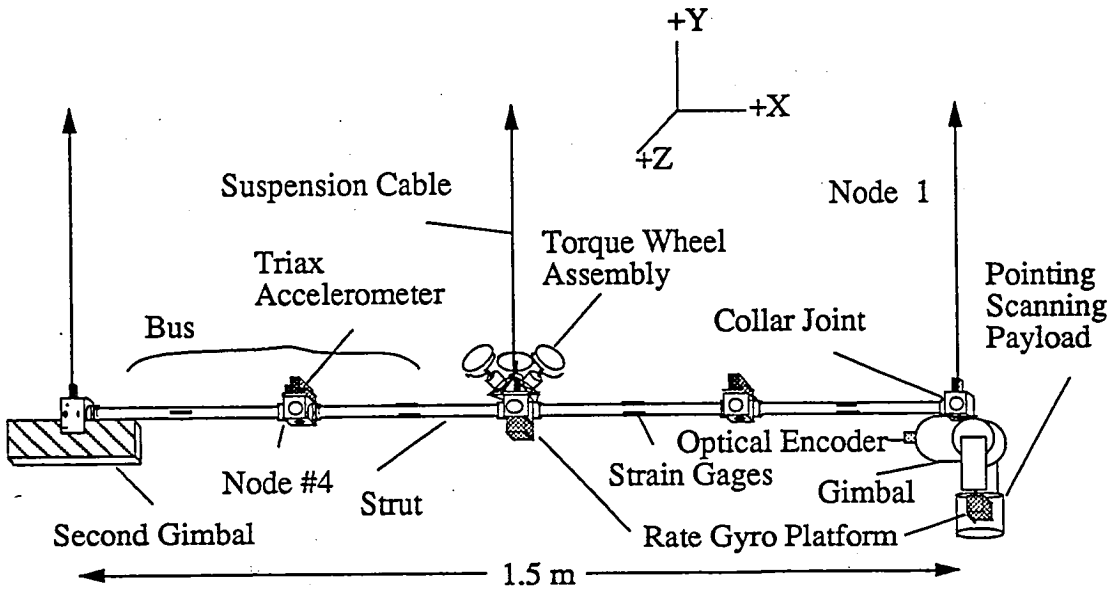

Figure 7.1: Middeck Active Control Experiment (MACE) test article suspended in 1-g.

only stable compensators were designed in this work. Recent experience indicates that noncollocated control problems result in unstable compensators at much lower levels of control authority. Consequently, the experiments in this chapter are of the "1-block" type [104]. In this case, the performance and sensed variables are the same, as are the control and disturbance inputs. Moreover, the system inputs and outputs are collocated. The discussion in this chapter concentrates primarily on the SISO experiment because of the insight that it provides to the robustification process.

7.2 MACE Hardware Configuration

The Middeck Active Control Experiment (MACE) is a Shuttle middeck experiment that is tentatively scheduled for flight in the summer of 1994 [111]. As illustrated in Fig. 7.1, the test article simulates a flexible spacecraft with several independently pointing payloads. The objective of the program is to investigate the extent to which closed-loop behavior in zero gravity (0–g) can be predicted through analysis and ground testing. Sensor noise, unmodelled high frequency dynamics, and the anticipated parameter changes due to gravity will all be major factors in the design of

Table 7.1: Properties of the MACE bus structure from [110].

Property	Value
Length (L)	1.5 m
Cross-sectional Area (A)	2.25×10^{-4} m^2
Geometric inertia (I)	1.4×10^{-8} m^4
Mass per unit Length (ρ_l)	0.27 kg/m
Young's Modulus (E)	2.3×10^9 Pa

controllers for MACE [43]. Previous flight experiments indicate that, in orbit, there will be large changes in the structural dynamics due to the absence of gravity [12]. Even with current prediction techniques, it is anticipated that these changes will result in large parameter uncertainties in the system model [134].

The first bending mode of the bus structure is at approximately 1.8 Hz, which is within the bandwidth of most payload pointing controllers [41]. If these compensators are designed with incomplete or inaccurate knowledge of the structural dynamics of the system, there is potential for an unstable interaction between the controllers and the bus structure. This phenomenon, known as Control-Structures Interaction (CSI), has been the subject of much recent research [57, 92]. In particular, the Controlled Structure Technology (CST) approach has been developed at the M.I.T. Space Engineering Research Center (SERC) [42] to address this phenomenon. A conclusion from this CST research is that, to achieve the stringent overall performance objectives on a test article such as MACE, the compensators must be designed to control the dynamics of the structure. The following is a brief description of MACE and the sensors and actuators that are required to control the device.

The final configuration of the MACE hardware will consist of two articulating payloads mounted at either end of a 1.5 m long bus that is constructed from four Lexan tubes connected by aluminum nodes. The properties of the bus structure are given in Table 7.1. The orientation of each payload is controlled by a two-axis gimbal system, while the bus attitude is controlled by three torque wheels. Several sensors, including rate gyros, accelerometers, strain gauges, and angle encoders, are available

for performance evaluation and control feedback. The properties of these sensors and actuators are discussed in detail in Ref. [139]. Note that the three torque wheels must be combined to generate a torque about each axis in the figure [111]. The appropriate transformations for these torques were calculated from the design geometry.

The experiments in this chapter use the torque wheel actuators and rate gyro sensors. The sensors are Bendix Cheshire 3-axis DC/AC rate sensors. Full sensor range is 75 degrees/sec, with a sensitivity of 0.04 V/(degree/sec). The natural frequency of the sensor is nominally at 48 Hz, with approximately 30% (of critical) damping. The noise specification for the device is 4 mV (rms) between 0–20 Hz. Several of the 1 kg rate gyro packages are attached to the structure. The experiments in this chapter use the package that is located on the middle node below the bus structure. The rate gyro electronics package includes a single pole low-pass filter with a 3 dB break frequency at about 80 Hz. The torque wheel actuators are connected by a base that is clamped to the top of the middle node. Each torque wheel weighs approximately 1 kg. The combination of the base structure and the three wheels and motors weighs about 7.3 kg. The Aerotech DS8020 servo amplifiers and permanent magnet motors are rated at 0.029 Nm/Amp. The amplifiers have been modified so that they are current limited at ± 10 Amps, with a peak output voltage of ± 50 Volts.

To facilitate ground testing of the hardware, the 27.8 kg test article is supported in 1–g by a three point active pneumatic/electric suspension system. The resulting system dynamics then include two dominant suspension modes at approximately 0.4 Hz and 0.8 Hz and several higher frequency "violin" modes that start at about 6 Hz [138]. The hardware configuration in Fig. 7.1 is called the MACE Development Model (DM). The second payload in this configuration is a 7.1 kg dummy mass. A 40 mode finite element model of the DM test article was developed by Rey and Glase [135]. Table 7.2 gives the frequency, damping ratio, and mode type for each mode below 60 Hz. The damping was measured experimentally for all modes up to 50 Hz, and assigned a nominal 1% value for higher frequency modes.

The real-time computer for MACE is an AC100 with 16 digital, 16 analog, and 8 encoder inputs and 16 digital, 8 analog, and 2 fast analog outputs [139]. The device

Table 7.2: Frequency, damping ratio, and mode type for each mode in the finite element model of the MACE Development Model in the 0–60 Hz frequency range [135].

Frequency (Hz)	Damping ratio	Mode type
0	1	Torque wheel #1
0	1	Torque wheel #2
0	1	Torque wheel #3
0.20	0.15	Suspension – bounce
0.22	0.15	Suspension – X–axis pendulum
0.23	0.15	Suspension – Y–axis pendulum
0.23	0.15	Suspension – Z–axis pendulum
0.33	0.08	Suspension – tilt
0.20	0.15	Suspension – 1^{st} twist
1.21	0.15	Outer gimbal pendulum
1.29	0.05	Inner gimbal pendulum
1.86	0.04	1^{st} X–Y bending
3.13	0.04	1^{st} X–Z bending
6.72	0.02	2^{nd} X–Y bending
6.87	0.01	2^{nd} X–Z bending
8.85	0.02	Suspension – 2^{nd} twist
9.40	0.008	3^{rd} X–Y bending
13.29	0.007	3^{rd} X–Z bending
14.00	0.007	4^{th} X–Y bending
14.25	0.007	Suspension – 3^{rd} twist
17.40	0.006	4^{th} X–Z bending
36.00	0.011	Suspension – 4^{th} twist
39.10	0.02	Suspension – 5^{th} twist
42.50	0.015	5^{th} X–Y bending
64.12	0.01	5^{th} X–Z bending

includes two 80386 processors and one Weitek 3167 co-processor, which all operate at 20 MHz. With one processor and co-processor, the computer can run a 24 state SISO compensator at 1 KHz, and a 59 state 3-input/3-output compensator at 500 Hz.

The first step in designing controllers for this structure is to develop a model of the system. The controllers discussed in this chapter were designed using a state space model of the structure obtained from measured transfer functions. For the MIMO problem, the transfer functions for each of three disturbance inputs were identified separately and then combined using a reduction approach described by Gilpin [56]. Formal identification techniques are available to provide estimates of both the system parameters and their uncertainty [160].

As outlined by the component functional flow chart in Ref. [139], there are several connections required to measure a transfer function on MACE. The data for the model are obtained by applying band limited white noise (0–50 Hz) from a Tektronix Fourier Analyzer to an A/D input of the real-time computer. The signal is then transformed to produce a net disturbance torque about a particular axis. These three signals are then taken from the D/A (channels 1–3) and applied to the torque wheel motors through the amplifiers (1–3). The measurements from the rate gyro signal amplifiers (gain of 6) are passed through 8-pole anti-aliasing analog Bessel filters (3 dB break frequency at 150 Hz), and the output is then sent to the AC100. The AC100 input signals are then converted into estimates of the bus angle by 0.03 Hz second order (0.71 damping) stabilized integrators [111]. Finally, the signals are multiplied by a factor of 50 to reduce the quantization error in the fixed resolution D/A conversion (12 bits for 20 Volts). The AC100 analog output is then measured by the Tektronix Fourier Analyzer.

To obtain a disturbance torque about a particular bus axis, the output from the Tektronix Analyzer is sent to the AC100 before it is applied to the system. Since the control torques are generated in the AC100, there is an extra time delay in the measured data that is not present in the loop to be closed. Consequently, the state space model must be designed to match the measured data that have been corrected to account for this extra delay. With a state space model of the structure, the design

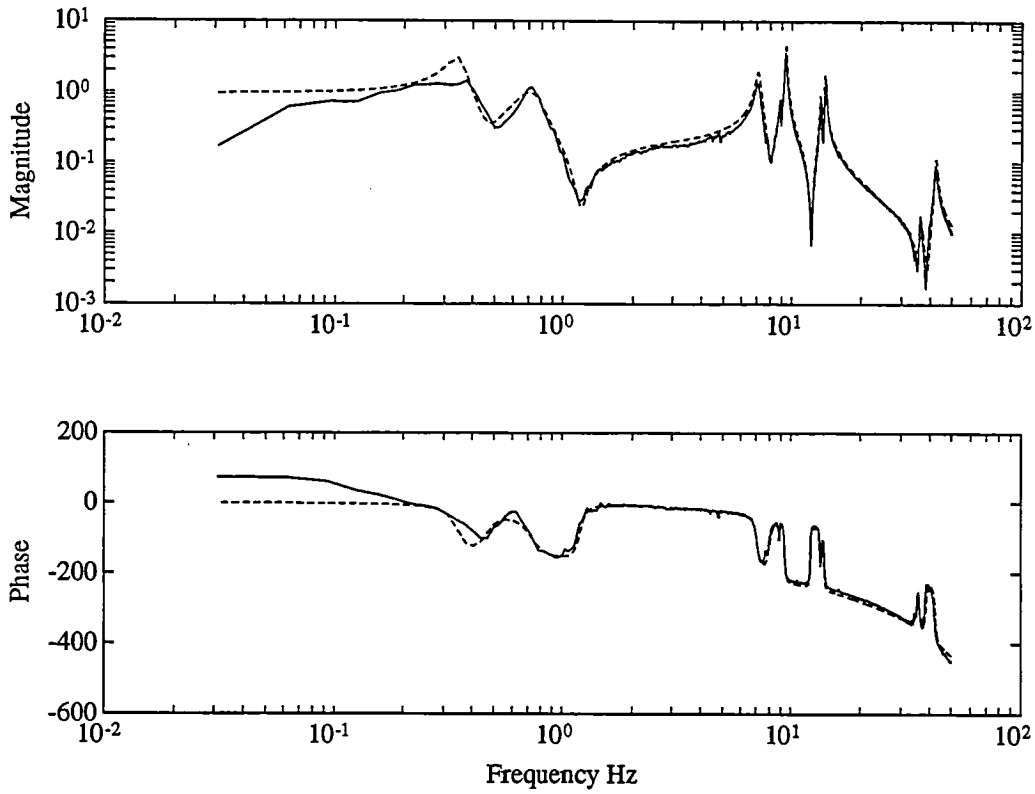

Figure 7.2: Comparison of the 24 state model and measured data for the z-axis torque wheel to bus rate gyro loop.

of SISO and MIMO robust controllers can now be presented.

7.3 SISO Control Design and Implementation

This section presents the results of the design and implementation of a robust SISO controller for the current MACE configuration, which is called the Development Model. As discussed, the SISO loop is between the z-axis bus rate gyro sensor and a combination of the three torque wheels as an actuator. The disturbance and control inputs are applied to the torque wheels through the transformation $T_z = [-0.817, 0.408, 0.408]$ to generate a net torque about the z-axis. Therefore, the loop is essentially between a collocated and dual sensor/actuator pair. The bus z-axis inertial angle is the performance variable, and the disturbances are added directly to the control signals in the AC100 real-time computer.

Fig. 7.2 illustrates the accuracy of a 24 state model of this SISO system. The rate

gyro sensor dynamics, which consist of a highly damped pole pair at approximately 48 Hz and a single pole at 80 Hz, are not explicitly modelled in this system. However, the curve-fit procedure resulted in two heavily damped poles at approximately 150 Hz. Since these sensor dynamics are well above the bandwidth of interest (about 20–30 Hz), this approximation is sufficiently accurate for these controllers, but higher bandwidth designs will need to model these sensor dynamics more completely.

A 4-pole Pade approximation is included in the model to account for the computational time delay of 12.2 msec. Two suspension and seven flexible modes are observable in this transfer function up to a frequency of about 45 Hz. Five of the flexible modes are clumped around 10 Hz, and the other two are at 36 Hz and 42 Hz. The damping in these modes varies between 0.5% and 2.0%. Using the notation of Chapter 5, the 24 state model of the system can be written as

$$\dot{x} = Ax + Bu + [B\ 0]w \tag{7.1}$$

$$y = Cx + [0\ 1]w. \tag{7.2}$$

The weighting matrices for the $\mathcal{H}_2$ performance problem are $R_{xx} = C^T C$, $R_{uu} = \rho = 5V_2$, and $V_1 = BB^T$. The transfer function in Fig. 7.2 is quite clean, which indicates that the rate gyro sensor noise is small. Consequently, V_2 in the performance problem was chosen to obtain a desired level of closed-loop performance, rather than to reflect an anticipated noise level in the system.

Several optimal LQG controllers were designed for this system using a range of values for $\rho = (10^{-2},\ 10^{-3},\ 6 \times 10^{-4})$. In the following, designs with lower values of ρ are referred to as having a higher control authority because it is expected that the control gains and bandwidth will be larger. An investigation of the loop transfer function for the three LQG controllers indicates that the gain and phase margins of the two higher authority designs are quite small. In fact, they were both found to be unstable when implemented on the actual system.

The controller ($\rho = 6 \times 10^{-4}$) shown in Fig. 7.3 illustrates several key characteristics of the LQG compensators that led to an instability near 12 Hz. At this level of control authority, the system is essentially inverted in the compensator in the 5–

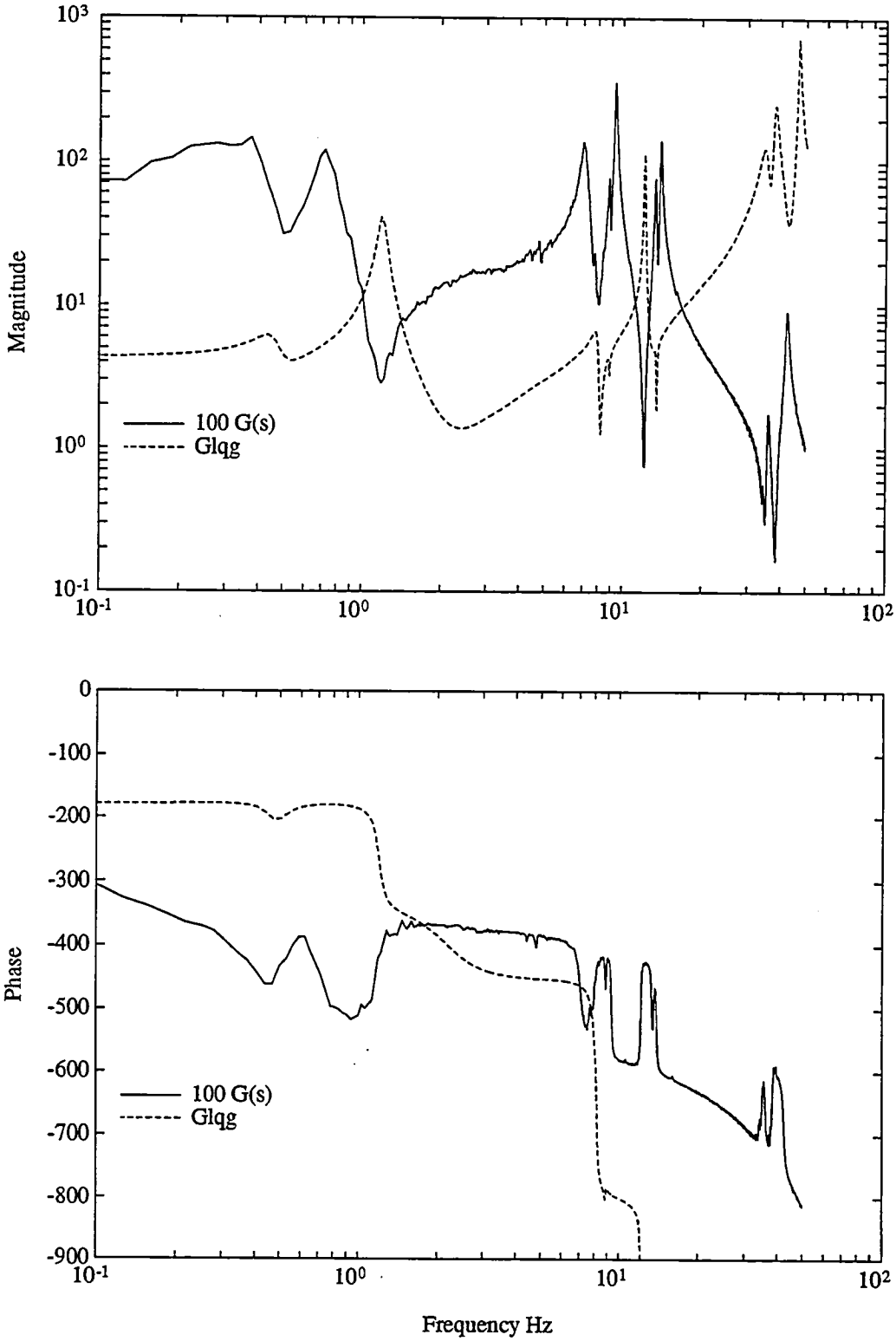

Figure 7.3: LQG (Glqg) controller for the SISO system with $\rho = 6 \times 10^{-4}$.

15 Hz frequency range. A similar result is seen in many LQG/LTR controllers [152]. The lightly damped compensator pole pairs at the frequencies of the plant zeroes (8 and 12 Hz) are two examples of this plant inversion. The sensitivity of a closed-loop system to small changes in the plant parameters when the compensator uses these plant inversion techniques was discussed in Chapter 6.

The loop transfer function with the LQG compensator ($\rho = 6 \times 10^{-4}$) is plotted in Fig. 7.4. The low phase and gain margins at 12 Hz are an indication of the sensitivity of this system to plant perturbations. The actual sensitivity is illustrated in Fig. 7.4 by implementing the compensator on two perturbed models of the system. These two modified models of the system were obtained by changing the frequencies of the four modes near the zero at 12 Hz by $\pm 1\%$ of their nominal values. The transfer functions with the two perturbed systems demonstrate that small parameter changes can result in large changes to the loop magnitude and phase (which now indicate instability). It is clear that some knowledge of the uncertainty in the plant poles and zeroes in this frequency region must be incorporated into the control design to avoid the sensitivity of this so-called plant inversion.

An approach to modelling the parameter uncertainty in a state space model is given in Section 2.2. The section also discusses the difficulties in directly treating the frequency uncertainty of a system zero. However, as shown by the intentional perturbations in Fig. 7.4, changing the frequencies of the plant poles also has a large affect on the system zeroes. Consequently, a good approximation of the problem with uncertainty in both the poles and the zeroes is just to consider the uncertainty in the system poles. Analysis of several experimental transfer functions indicates that the frequencies of the poles and zeroes near 12 Hz are certain to within $\pm 1\%$ of their nominal values. The four modes at 8.8 Hz, 9.4 Hz, 13.3 Hz, and 13.9 Hz will be treated as uncertain in these designs. The goal is to obtain the best possible closed-loop performance with a compensator that guarantees stability of the closed-loop system for these uncertainties.

For the design of the robust controllers, the system A matrix in Eq. 7.1 was written

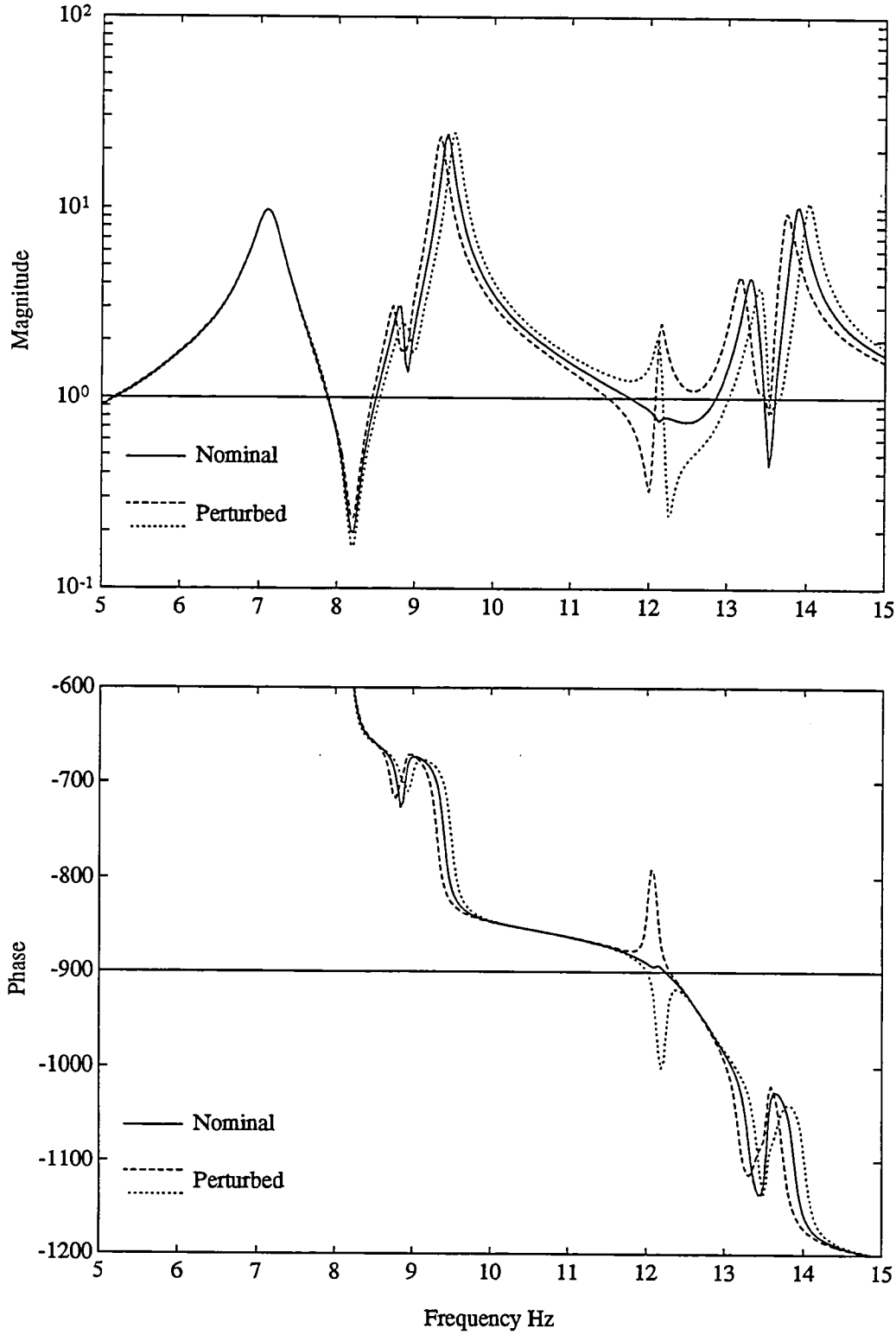

Figure 7.4: Loop transfer function with the LQG controller on the nominal and intentionally perturbed plant models.

in second order canonical form $A = \text{blockdiag}(A_i)$, $i = 1, \ldots, m$, where

$$A_i = \begin{bmatrix} 0 & 1 \\ -\omega_i^2 & -2\zeta_i\omega_i \end{bmatrix}. \tag{7.3}$$

As discussed in Section 2.2, the uncertainty in the modal frequency is then approximated as an uncertainty in ω_i^2. The actual dynamics can then be written as $\hat{A}_i = A_i + \Delta A_i$, where

$$\Delta A_i = \delta_i B_{0i} C_{0i}, \; B_{0i} = \begin{bmatrix} 0 \\ -\omega_i \end{bmatrix}, \text{ and } C_{0i} = [\, \omega_i \;\; 0 \,], \; i = 1, \ldots, m. \tag{7.4}$$

The B_0 and C_0 matrices for the full system can be constructed from these two sets. In this case, as with many of the examples in Chapter 6, $C_{0i}B_{0i} = 0$ with this uncertainty structure. This observation simplifies R_0 in Eq. 5.4 and $\partial\mathcal{L}/\partial N_0$ in Eq. 5.48.

Several robust controllers were designed for this system, with varying bounds on the uncertainty. Since the uncertainty is in ω_i^2, the final values in the homotopy must be set to $(M_{2f})_{ii} = -(M_{1f})_{ii} = 0.02$. Robust compensators were designed for the same three values of ρ. The BFGS optimization/stability bound homotopy solution algorithm discussed in Chapter 5 was used to solve for the optimal compensators. Iterative solutions of Eqs. 5.39–5.41 provided initial conditions for the optimization. Low authority compensators were typically used to provide initial guesses for the higher authority designs.

The optimal LQG and Popov compensators are compared in Figs. 7.5a and 7.5b. The two Popov controllers were designed with different guaranteed stability bounds that are presented in Table 7.4. The compensator Gpc2 (Gpc4) guarantees stability for 0.5% (1.0%) independent variations in ω_i. Fig. 7.5a demonstrates that the three controllers are quite similar in magnitude for frequencies above and below the region of uncertainty (5–15 Hz). In the Popov designs, the LQG poles at 0.45 Hz have been replaced with two real poles at approximately 1 Hz and 2.5 Hz. Fig. 7.5b concentrates on the uncertain region (5–15 Hz), providing a clear illustration of the differences between the Popov and LQG designs. The lightly damped LQG compensator poles at about 12 Hz are more heavily damped in the Gpc2 design, a trend that continues in the Gpc4 controller. A similar effect can be seen at the plant zero at 8 Hz which is also

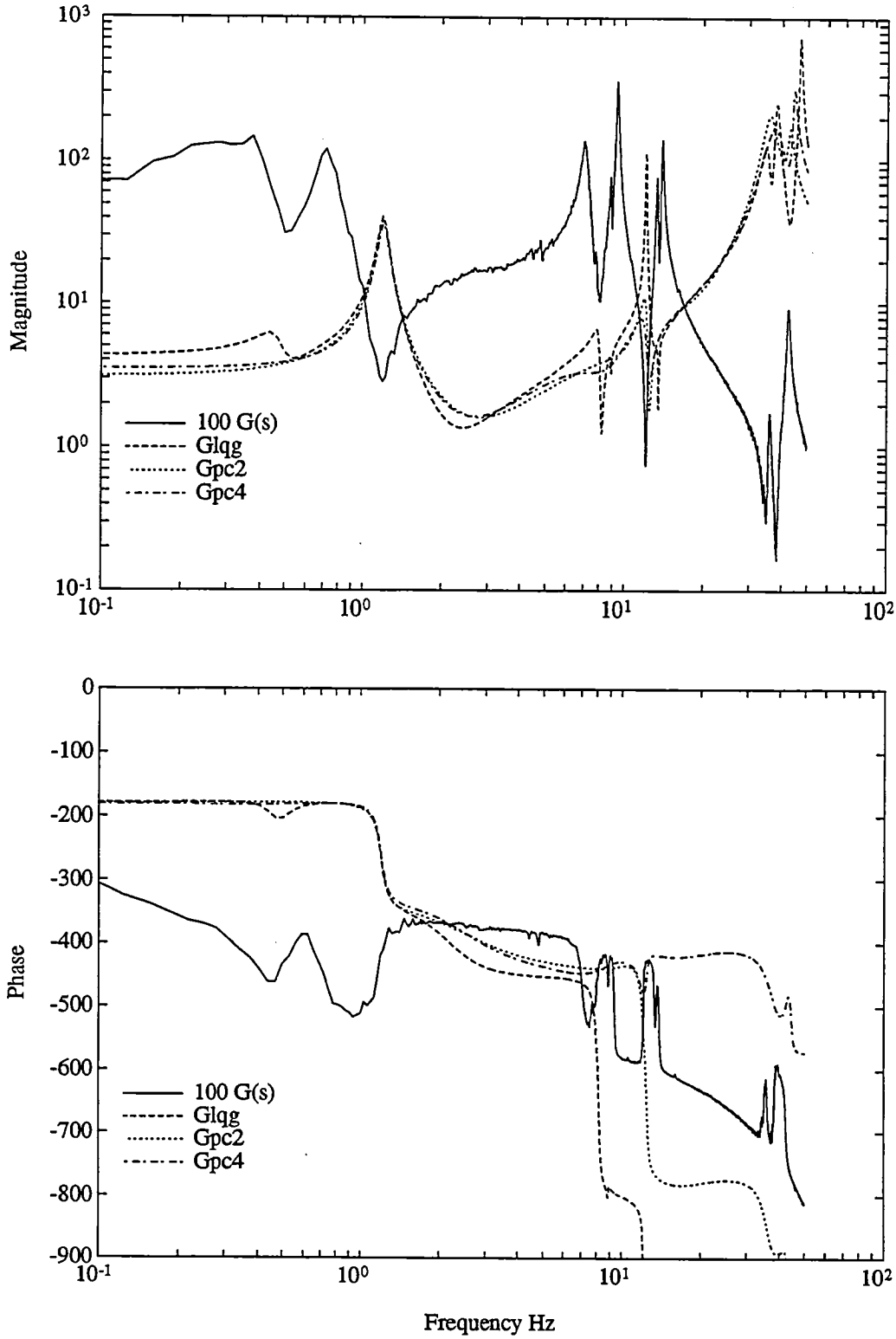

Figure 7.5a: Comparison of LQG (Glqg) and Popov (Gpc2 and Gpc4) controllers.

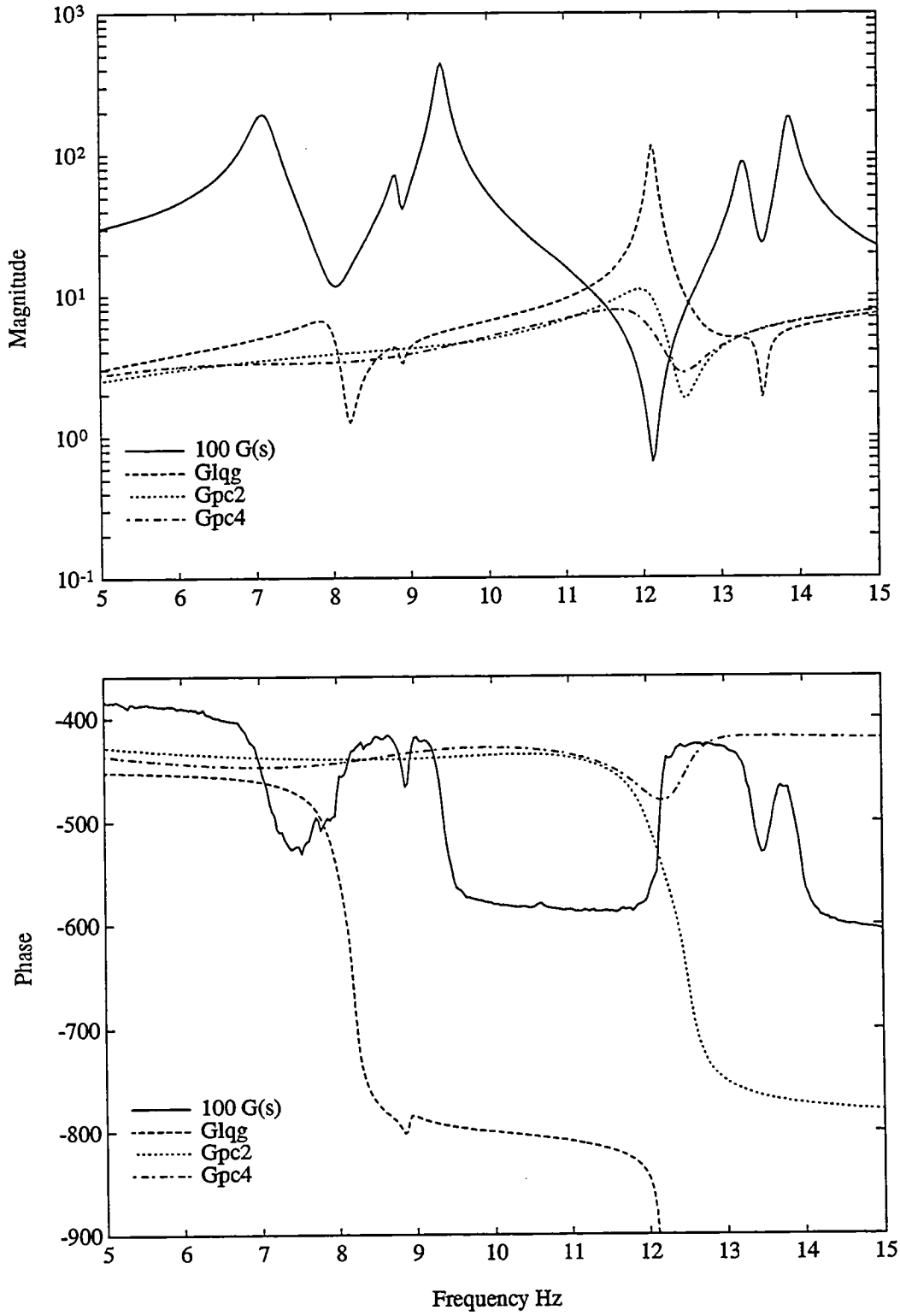

Figure 7.5b: Comparison of LQG (Glqg) and Popov (Gpc2 and Gpc4) controllers. Focuses on the region of uncertainty.

influenced by these changes in the poles frequencies. The results show that the robust compensators are significantly different from the LQG design in the frequency range of the uncertainties. Furthermore, they demonstrate that the robustness specification does not have many adverse effects on the compensators in other frequency ranges.

There are several important features of these robust controllers that can be studied in more detail. Both the LQG and Gpc2 compensators have a nonminimum phase zero at approximately 12.5 Hz. Combined with the pole at about 12 Hz, the result is a 300° change in the compensator phase. The corresponding zero is minimum phase in the Gpc4 design, resulting in the characteristic "phase blip" in Fig. 7.5b of closely spaced minimum phase poles and zeroes. The zero for an intermediate design, Gpc3, is also minimum phase, but more lightly damped than the Gpc4 design. The location of the compensator zero is important because it indicates a fundamental change in the robustification technique. These differences are clearly seen by comparing Figs. 7.4, 7.6, and 7.7. As discussed before, each graph compares the loop transfer functions for the nominal and two perturbed systems. The LQG design gain stabilizes the nominal system in the 12 Hz range. Fig. 7.6 illustrates that the Gpc2 controller, which has a nonminimum phase zero, also gain stabilizes the loop in this frequency range. However, the Gpc4 controller, which was designed for larger guaranteed stability bounds, both gain and phase stabilizes the system in this range.

A comparison of the three figures shows the dramatic difference between the loop transfer functions with these compensators. The increase in the gain and phase margins for the nominal plant is an indication of a decrease in the sensitivity of the compensator. Furthermore, the loop transfer functions indicate that the Gpc4 controller will not only stabilize the two perturbed system models, but should also achieve good closed-loop performance.

The actual sensitivity of the controllers to plant variations can be obtained from the performance robustness curves described in Chapter 6. The closed-loop cost is evaluated for several perturbed models of the system. The cost curves, commonly called "buckets", are then obtained by plotting J_{norm}, the cost normalized by the open-loop value, versus the system perturbations. As with previous examples, the

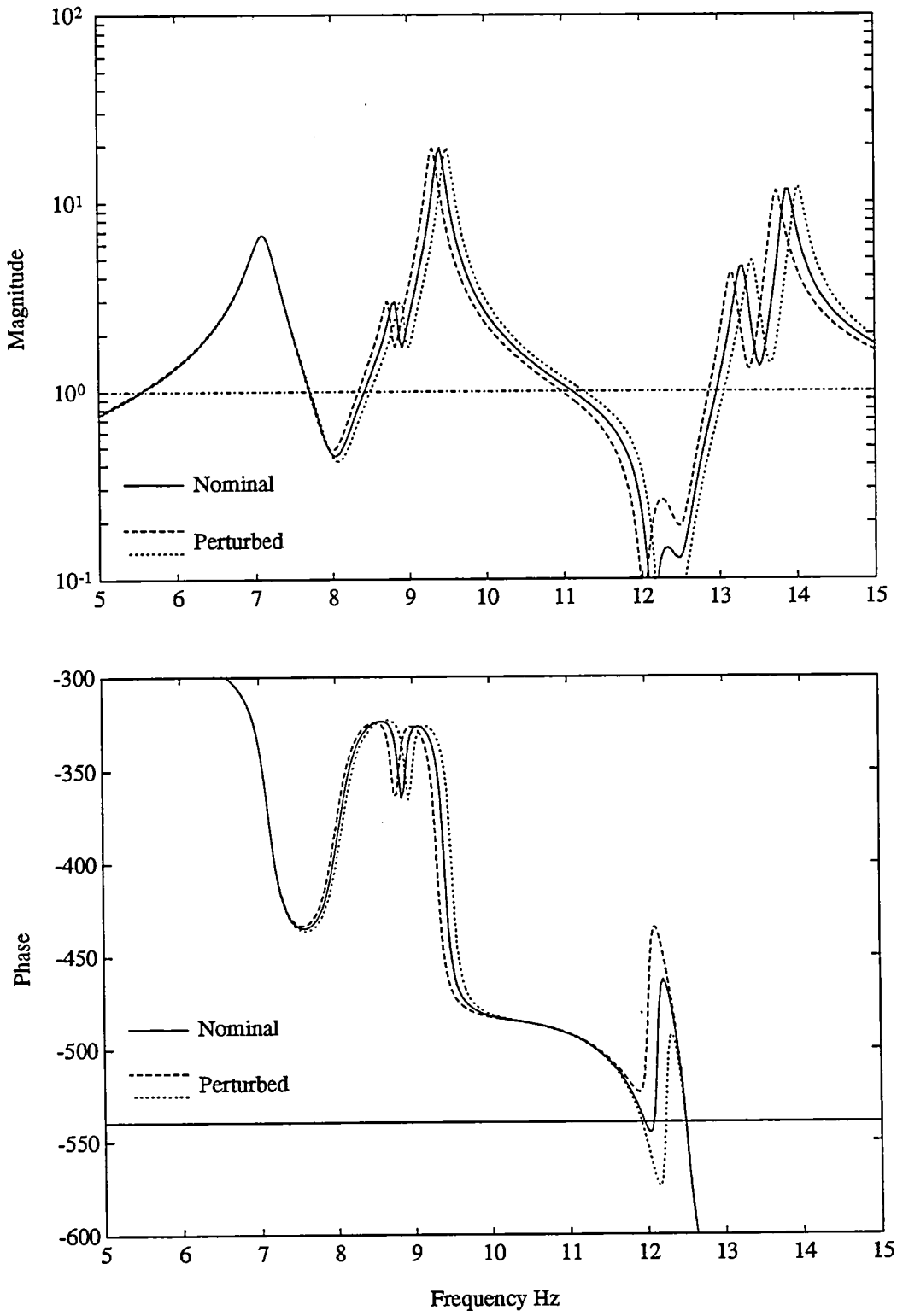

Figure 7.6: Loop transfer function with a Popov (Gpc2) controller on the nominal and intentionally perturbed plant models.

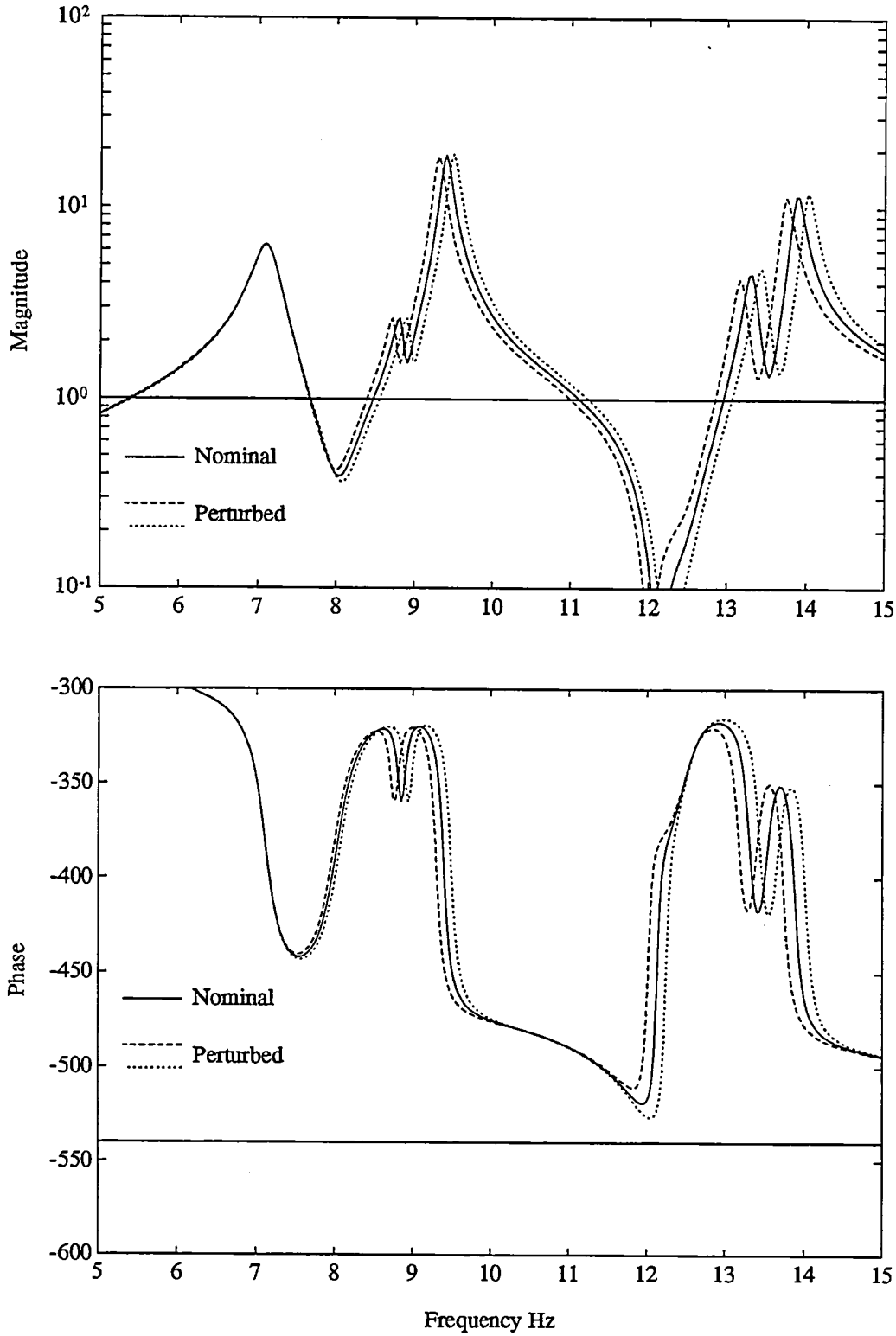

Figure 7.7: Loop transfer function with a Popov (Gpc4) controller on the nominal and intentionally perturbed plant models.

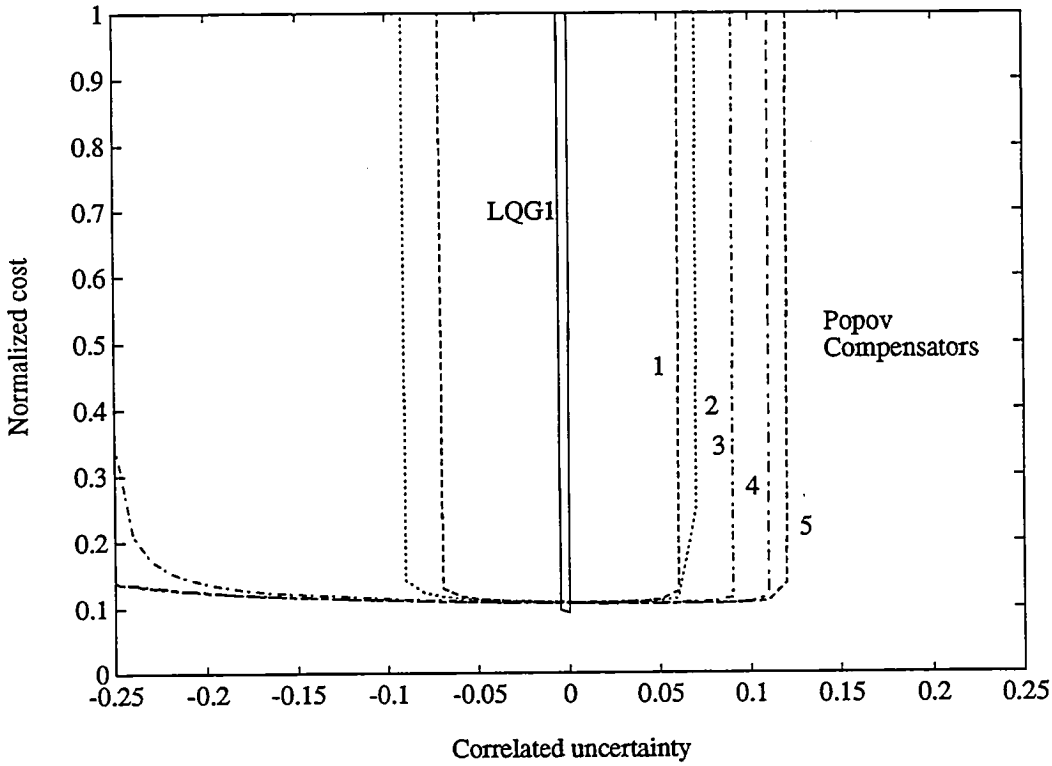

Figure 7.8: Robust stability and performance curves for two LQG and five Popov controllers. The stability bounds are presented in Table 7.3.

four uncertain frequencies are correlated for this analysis.

Three robust performance figures are presented. Fig. 7.8 shows the performance and robustness of one LQG and five Popov controllers for this uncertain system. Notice that the "stiff" uncertainty direction in these designs now corresponds to positive changes in the modal frequencies. Only symmetric sectors were considered here, but this knowledge of a difficult direction could be used to refine the stability bounds and accentuate the robustness for positive changes. The corresponding stability values are given in Table 7.3. Each row of the table corresponds to a curve in Fig. 7.8. The nominal performance (zero uncertainty) values are normalized with respect to the open-loop cost. The other four values in each row correspond to the stability limits. The two middle values are the guaranteed bounds which are always between the achieved values. The flatness of these buckets and the small increase in the nom-

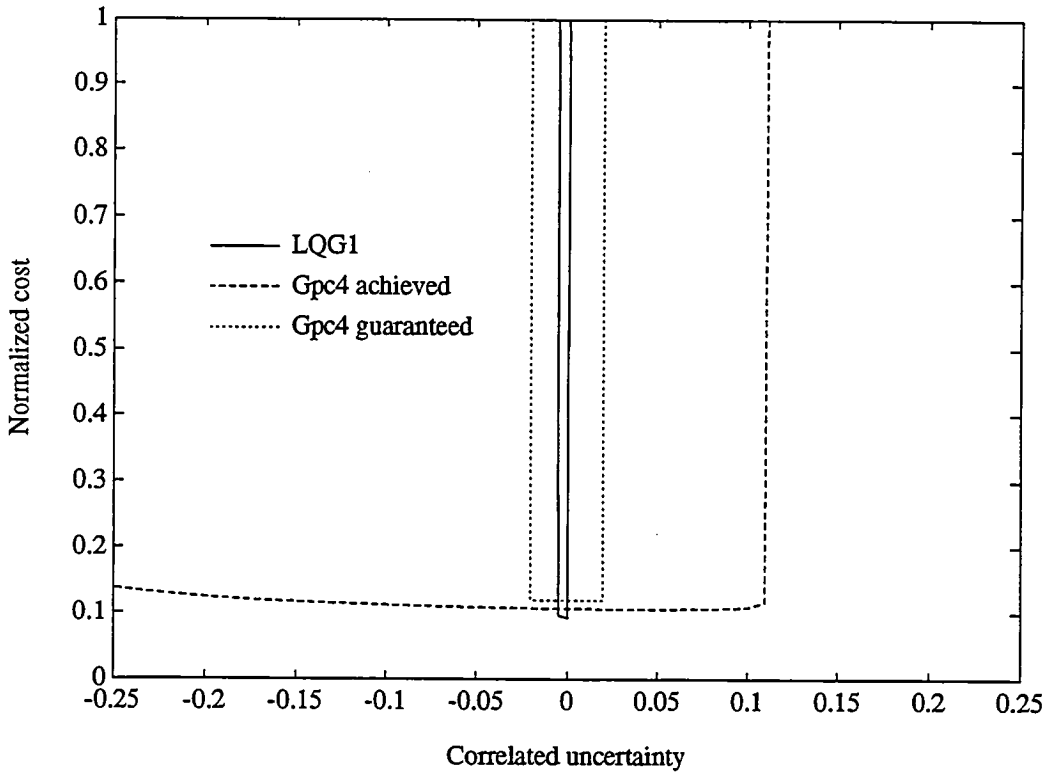

Figure 7.9: Comparison of LQG1 robust stability and performance to the guaranteed and achieved Popov results (Gpc4).

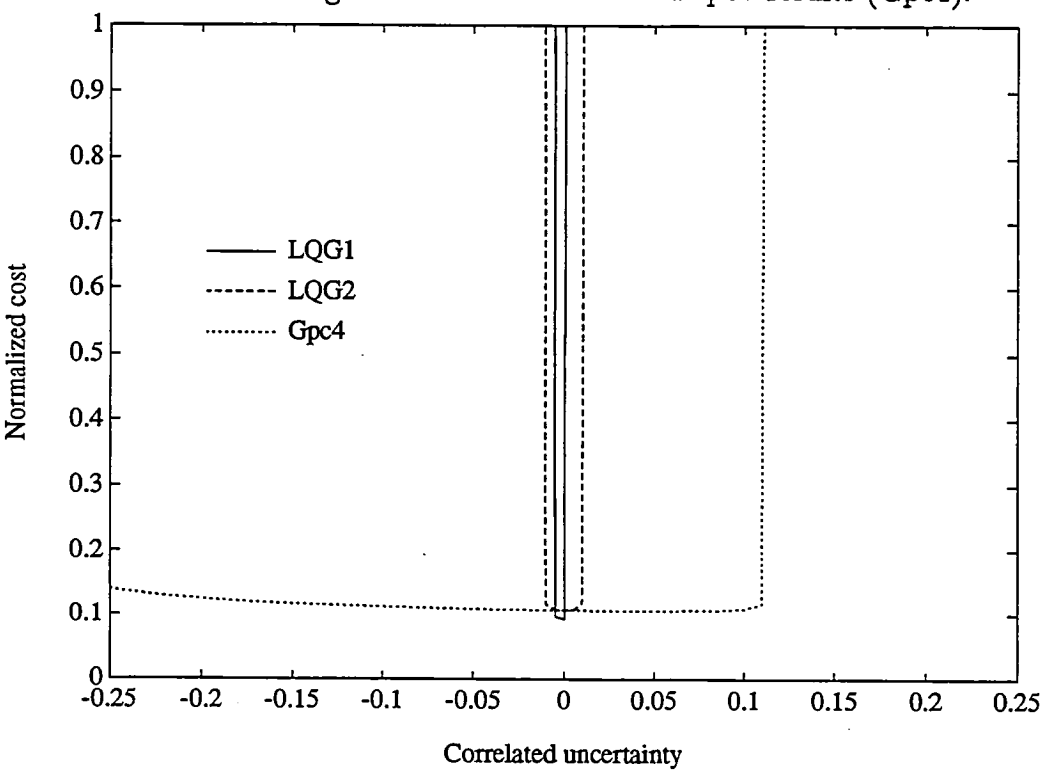

Figure 7.10: Robust stability and performance curves for two LQG controllers and a Popov compensator (Gpc4).

Table 7.3: Robust performance for the closed-loop system with uncertainty in four modes. Frequency uncertainty assumed correlated for the analysis.

Fig. 7.8 Label	J_{norm}	Lower stability bounds achieved	Lower stability bounds guaranteed	Upper stability bounds guaranteed	Upper stability bounds achieved
LQG1	0.09	-0.005	0	0	0.000
LQG2	0.11	-0.010	0	0	0.010
Gpc1	0.11	-0.070	-0.008	0.008	0.060
Gpc2	0.11	-0.090	-0.010	0.010	0.070
Gpc3	0.11	-0.250	-0.016	0.016	0.090
Gpc4	0.11	-0.250	-0.020	0.020	0.110
Gpc5	0.11	-0.250	-0.022	0.022	0.120

inal performance values are quite striking, indicating that guaranteed performance robustness can be achieved with only a small increase in the cost. The curves in Fig. 7.8 clearly illustrate the increase in the bucket width as the guaranteed range is increased.

An indication of the tightness of the overbounds in the optimization process is given in Fig. 7.9. The wider curve corresponds to the achieved performance and stability limits with the Gpc4 compensator. The result with the LQG1 controller is given for comparison. The third curve corresponds to the guaranteed bounds used in the optimization of Gpc4. The two vertical asymptotes at ± 0.02 correspond to the values of M_1 and M_2. The depth of the curve is given by the optimal value of the cost overbound (0.12). As expected, the Popov controller achieves a nominal cost that lies between the optimal LQG value and the overbounding cost. These results show that the cost function of the auxiliary minimization problem in Chapter 5 is a relatively tight upper bound. While the discrepancy in the guaranteed and achieved bounds is, to some extent, a measure of the conservatism in the robustification technique, it is also a reflection of the relative ease of robustifying the system to this type of uncertainty.

Table 7.3 provides the cost and stability values for two LQG designs. The first design refers to the optimal controller for the problem as specified earlier. The second is a suboptimal LQG design developed using R_{uu} and V_2 values that are increased by

Table 7.4: Optimal diagonal multipliers for four Popov controllers with $\rho = 6 \times 10^{-4}$.

Uncertain Mode	Gpc2		Gpc3		Gpc4		Gpc5	
	H_0	N_0	H_0	N_0	H_0	N_0	H_0	N_0
8.83 Hz	17.79	0.027	14.18	0.053	4.66	0.050	4.58	0.057
9.40 Hz	9.82	0.045	8.10	0.043	8.39	0.043	8.33	0.045
13.30 Hz	17.83	0.025	13.23	0.025	11.83	0.026	11.71	0.028
13.88 Hz	1.00	0.081	1.00	0.080	1.00	0.082	1.00	0.083

a factor of 3. This controller achieves a nominal performance value that is comparable to those achieved by the five Popov designs. However, the results in Fig. 7.10 demonstrate that simply reducing the control authority and designing a suboptimal compensator does not produce a significantly more robust design.

Table 7.4 compares the optimal multiplier values for the last four Popov designs. In each case, the last diagonal element of H_0 was set to 1 and the other numbers were optimized relative to this value. The initial values were set at $H_0 = [30\ 20\ 10\ 1]$ and $N_0 = 0.02\mathrm{I}_4$. The results indicate that large changes in H_0 and N_0 occur as M_2 is increased. These changes in turn demonstrate the importance of allowing the multipliers to vary in the synthesis of the robust controllers.

The next step is to compare the predicted closed-loop performance for the LQG1 and Gpc4 controllers. The results, shown in Fig. 7.11, illustrate that the robust Popov controller exerts a significant influence on the flexible modes of the structure, even in the region of uncertainty. Recall that this LQG controller actually destabilizes the experimental system. With $\rho = 6 \times 10^{-4}$, the predicted performance improvement with the LQG controller is 11.23 dB. The Popov design is predicted to achieve a 10.36 dB reduction; a ratio that agrees with the results in Table 7.3. The changes required in the compensator to achieve greater robustness are clearly evident in the closed-loop curves.

The continuous time controllers were discretized and implemented on the AC100 at 1 KHz. The experimental results are presented in Fig. 7.12 with $\rho = 10^{-3}$ and in Fig. 7.13 with $\rho = 6 \times 10^{-4}$. The graphs compare the open and closed-loop

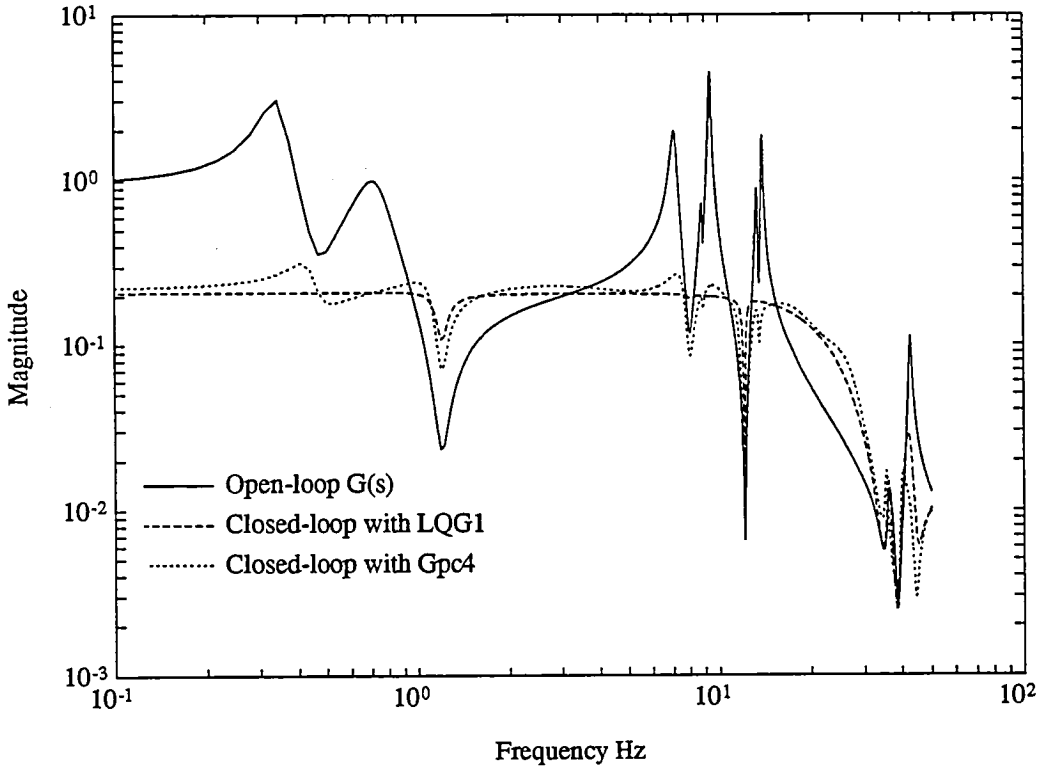

Figure 7.11: Predicted closed-loop performance with the LQG and Popov (Gpc4) controllers on the 24 state model.

results with two robust controllers. In each plot, the closed-loop results with the last LQG design that stabilized the experimental system ($\rho = 10^{-2}$) are shown for comparison. This lower authority design corresponds to an 8.97 dB improvement in the performance. By comparison, the Popov controller in Fig. 7.12 yields a 10.78 dB performance improvement. The one in Fig. 7.13 achieves an 11.38 dB improvement, which is within 1 dB of the predicted result.

A comparison of the curves in Figs. 7.11, 7.12, and 7.13 shows that the predicted and experimental results agree very well. However, there are some differences. The zero at 1.2 Hz is much stronger in the experimental curves than in the predicted results. As shown in Fig. 7.5a, both the LQG and Popov designs have compensator poles at this frequency. The predicted closed-loop results show that these compensator poles essential cancel a plant zero. However, this cancellation is not as exact in the experimental results, which indicates that the frequencies of the compensator pole and

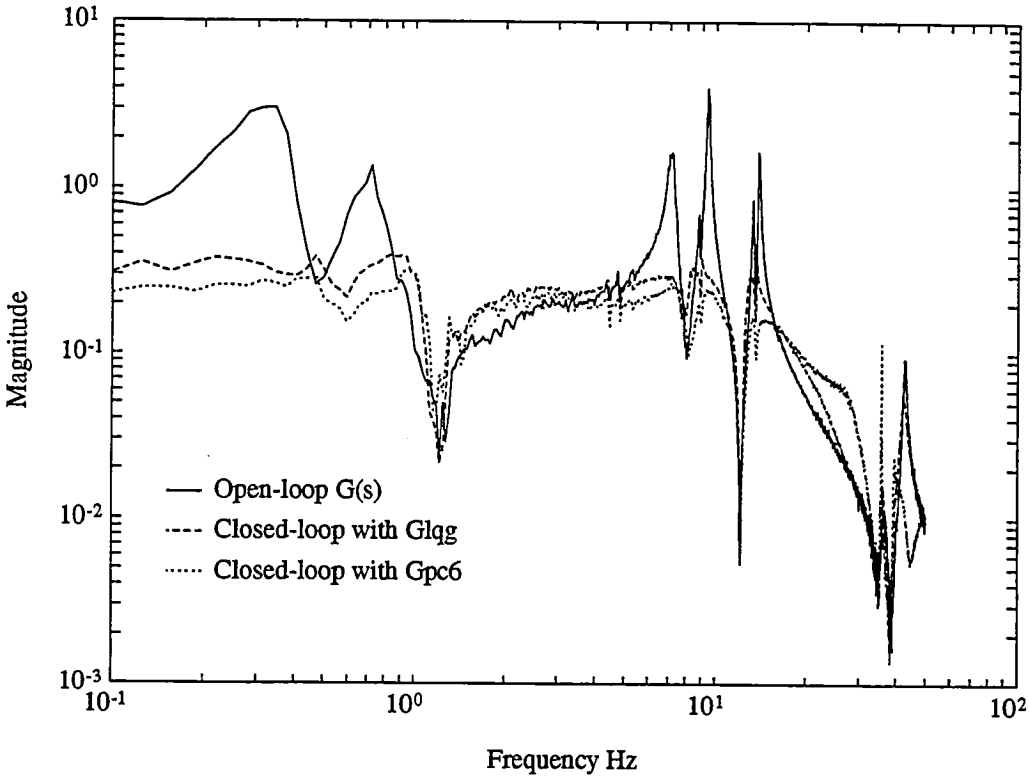

Figure 7.12: Performance comparison between open-loop, the last stable LQG controller ($\rho = 10^{-2}$), and a Popov design Gpc6 ($\rho = 10^{-3}$).

the plant zero do not match as well as they do in the model. This slight mismatch in the frequencies is an example of the type of problem that led to an instability at 12 Hz with the LQG controllers.

There is also a problem in the closed-loop results at 32–33 Hz. The peak in the transfer function is an indication that a mode has been adversely affected by the controller. Similar results were obtained from several experiments on the z-axis using a variety of design approaches. The source of this problem is unknown, but is probably related to the poor modelling of a plant zero in the 32–35 Hz frequency range. An attempt to improve the performance in this region by treating the two plant modes at 36 Hz and 42 Hz as highly uncertain lowered the response at this frequency by a factor of 2.

The Popov controllers for this SISO experiment can be compared with several others that have been developed using the sensitivity weighted LQG (SWLQG), multiple

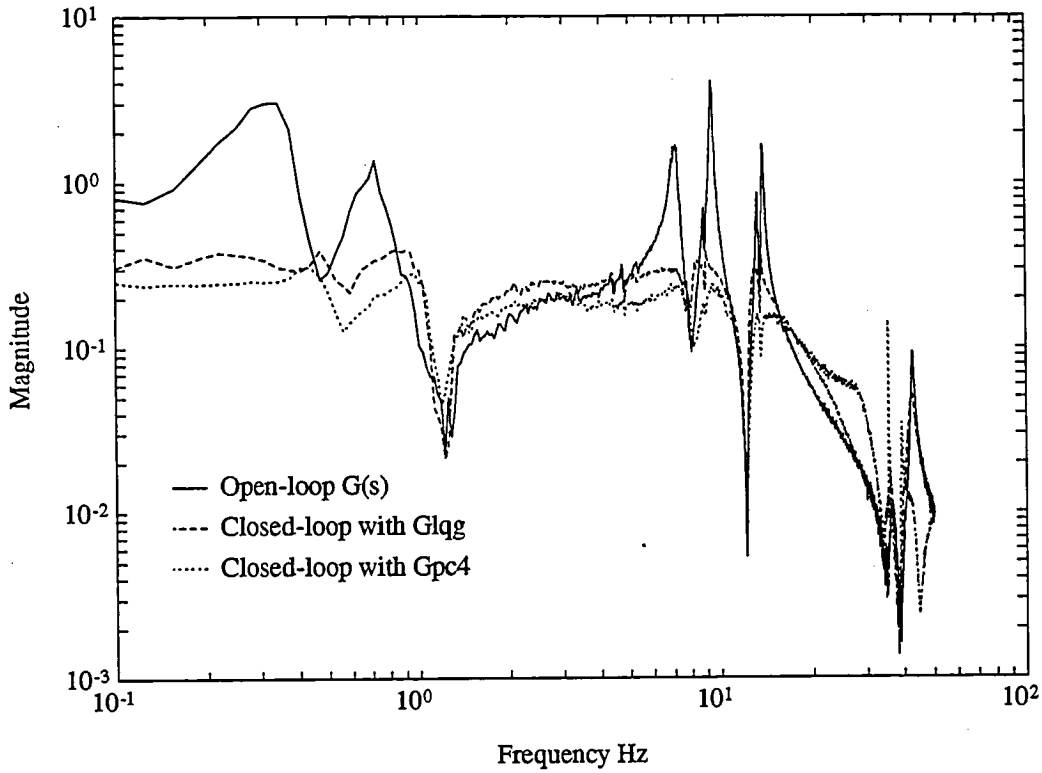

Figure 7.13: Performance comparison between open-loop, the last stable LQG controller ($\rho = 10^{-2}$), and a Popov design Gpc4 ($\rho = 6 \times 10^{-4}$).

model (MM), and Maximum Entropy (ME) techniques discussed in the Introduction. The SWLQG and MM designs in Refs. [58,59] are similar to the Popov design (Gpc2) because, in all three cases, the system robustness is increased by gain stabilization. An ME controller that both gain and phase stabilizes the system in the 11-13 Hz frequency range was developed by increasing the parameter in the stochastic model of the uncertainty. The resulting compensator can then be compared to the Gpc4 Popov design.

However, it is difficult to accurately compare these controllers because of the trade-offs between stability robustness and nominal/robust performance. For the compensators considered here, the MM and Popov robustification techniques did not degrade performance as much as the SWLQG approach. The ME designs achieved slightly better nominal performance than the other three approaches. Of course, a key difference between these four techniques is the robustness guarantees that they

provide. As discussed in the Introduction, the SWLQG approach is *ad hoc* and does not offer any guarantees of robust stability. The MM controllers only provide guarantees for a small number of system models, which represent specific combinations of the parameter uncertainties. The compensator can still exhibit sensitivity, and even instability, for other combinations of the uncertainties. Finally, with the ME technique, it is often difficult to correlate the uncertainty added in the stochastic model of the system to the robustness levels achieved by the controller.

In contrast to these three approaches, the Popov compensators guarantee robust stability for independent variations of each uncertainty. Furthermore, the results in Table 7.3 show that good closed-loop performance can be achieved with guaranteed stability bounds that exceed $\pm 1\%$ in the nominal frequencies. For this lightly damped system, these frequency shifts correspond to $60° - 100°$ changes in the frequency response of the system. A robustness technique that provides such large stability guarantees has many advantages for an experimental system, such as MACE, with potentially large parameter uncertainties. Section 7.5 discusses a control design technique that combines the various numerical/robustness advantages of these sensitivity weighted, multiple model, and Popov design techniques.

7.4 Demonstration of Robust Performance

This section describes the results of an experiment that was designed to demonstrate the robust performance that can be achieved by the Popov compensators. The robustness of the controllers was shown by intentionally modifying the MACE hardware to change the frequencies of the poles and zeroes. In this experiment, the mass of the second payload was changed by adding several aluminum plates. A total of 1.6 kg was added to the existing 7 kg mass. The results, shown in Figs. 7.14a and 7.14b, demonstrate that only the modes in the 5–15 Hz range are significantly modified by this perturbation to MACE. The curves also clearly show that both the poles and zeroes are affected by the extra mass. The changes in the two low frequency suspension modes reflect the fact that the suspension system had to be reset after each mass addition.

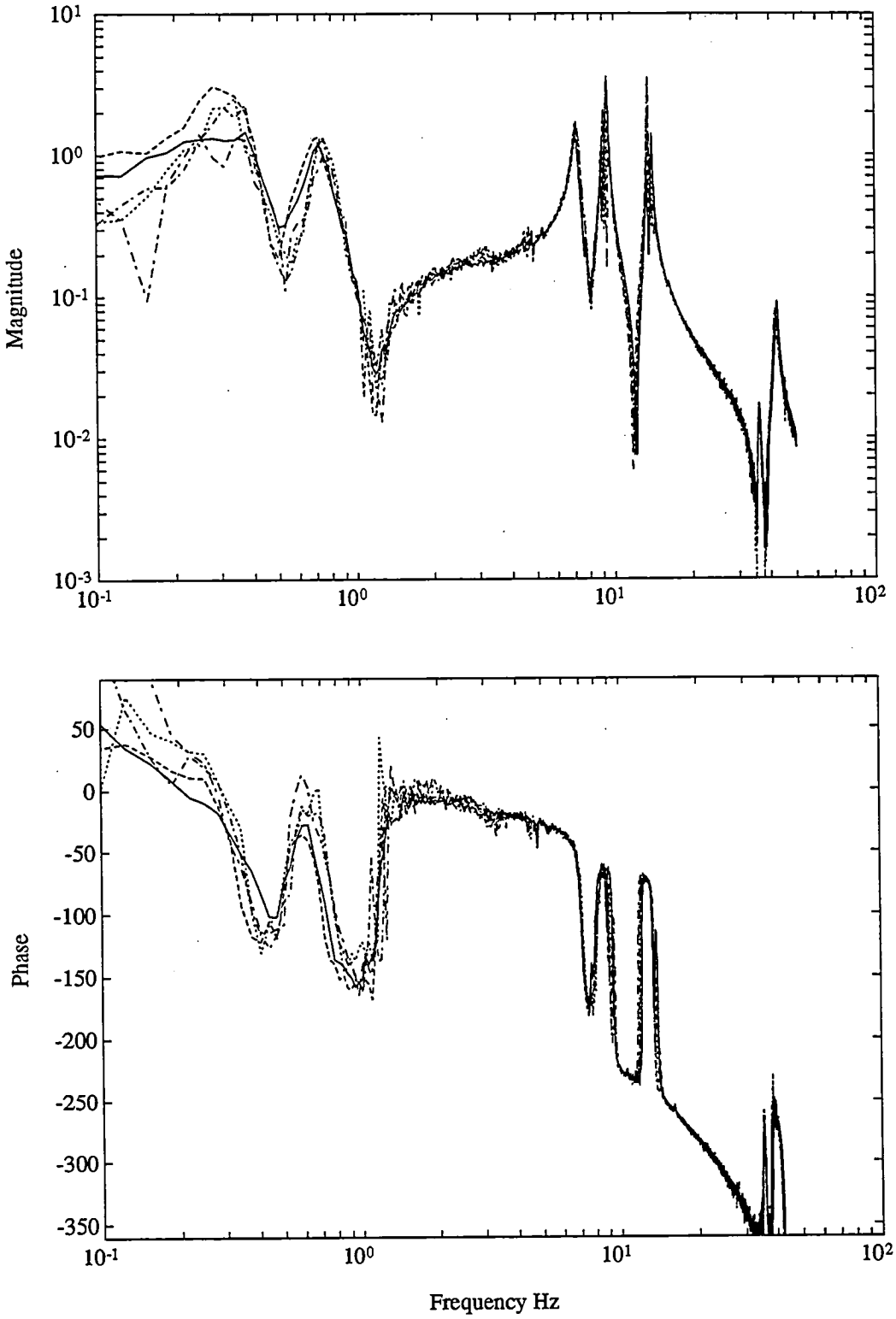

Figure 7.14a: Open-loop transfer functions with variations in the mass of the second payload. Mass perturbations and pole variations are given in Table 7.5.

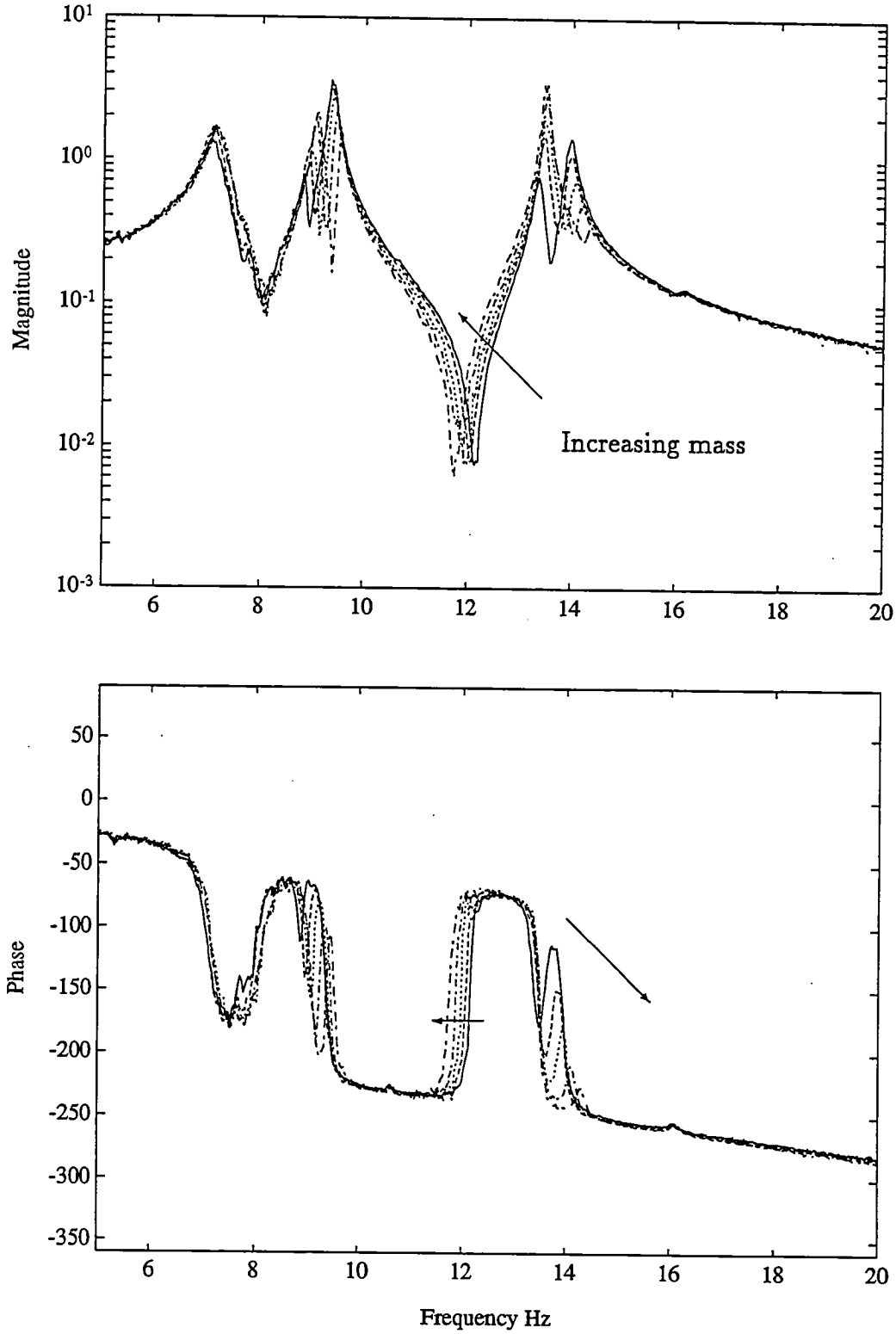

Figure 7.14b: Open-loop transfer function with variations in the mass of the second payload. Mass perturbations and pole variations are given in Table 7.5.

Table 7.5: Effect of changes in the mass of the second payload on the open-loop poles.

Nominal	$\Delta M = 3\%$	$\Delta M = 5\%$	$\Delta M = 12\%$	$\Delta M = 22\%$
$-0.15 \pm 7.13j$	$-0.16 \pm 7.09j$	$-0.17 \pm 7.18j$	$-0.17 \pm 7.16j$	$-0.18 \pm 7.02j$
	-0.6%	0.7%	0.4%	-1.5%
$-0.06 \pm 8.85j$	$-0.06 \pm 8.96j$	$-0.08 \pm 9.02j$	$-0.08 \pm 9.08j$	$-0.08 \pm 9.05j$
	1.2%	1.9%	2.6%	2.3%
$-0.07 \pm 9.41j$	$-0.08 \pm 9.36j$	$-0.07 \pm 9.39j$	$-0.06 \pm 9.53j$	$-0.06 \pm 9.83j$
	-0.5%	-0.2%	1.3%	4.5%
$-0.09 \pm 13.31j$	$-0.08 \pm 13.45j$	$-0.07 \pm 13.49j$	$-0.06 \pm 13.46j$	$-0.06 \pm 13.39j$
	1.1%	1.4%	1.1%	0.6%
$-0.09 \pm 13.88j$	$-0.10 \pm 13.95j$	$-0.10 \pm 14.00j$	$-0.12 \pm 14.29j$	$-0.14 \pm 14.82j$
	0.5%	0.9%	3.0%	6.8%

Fig. 7.14b concentrates on the 5–20 Hz frequency range to show the changes that occur in the plant poles and zeroes. The open-loop poles and the percentage change from their nominal frequencies are given in Table 7.5. For a 20% variation in the payload mass, the modal frequencies vary by as much as 6.5%. Each of the modes is affected differently by the mass perturbation, so the robustness results are not exactly equivalent to those considered previously in Fig. 7.8.

The robust controllers in the previous section were not designed for this mass uncertainty. However, it is clear from these figures that uncertainty in this payload mass is primarily reflected as uncertainties in the poles and zeroes in the 5–15 Hz frequency range. Consequently, intentionally changing the mass of the second payload should be an effective means of demonstrating the robust performance of the controllers.

A Popov compensator (Gpc6) with $\rho = 10^{-3}$ and $M_2 = -M_1 = 0.022\mathrm{I}_4$ was implemented on each of the open-loop systems in Fig. 7.14a. The experimental closed-loop results with $\Delta M = 0.05$ and $\Delta M = 0.12$ are shown in Figs. 7.15a and 7.15b. Two plots are used for each compensator to show the overall effect and the performance in the region of uncertainty. Recall that at this level of control authority, the LQG design destabilizes the actual system even without any intentional perturbations. The graphs compare the open and closed-loop transfer functions on the system with no perturbations to the closed-loop results on the perturbed plant. The figures show that the closed-loop performance is essentially unchanged from the nominal result for both perturbations to the payload mass. These results clearly demonstrate the good

robust stability and performance that are guaranteed for this system.

For comparison with the results in Table 7.4, the optimal multipliers for the Gpc6 compensator are $H_0 = \text{diag}(5.13, 8.98, 12.84, 1.00)$ and $N_0 = \text{diag}(0.064, 0.052, 0.032, 0.092)$. These results further illustrate the need to treat the multiplier values as free parameters in the compensator design.

7.5 MIMO Control Design

The previous sections presented a detailed analysis of a single-axis controller for MACE. However, to achieve the desired levels of performance on the fully noncollocated MACE system, it is anticipated that MIMO controllers will have to be developed. Thus, the goal of this section is to extend the SISO results and discuss the design and implementation of a 3-input/3-output robust controller.

The development of the design model for this case is similar to the process for the SISO system. Of course, because more modes are observable in the transfer functions, the process is much more difficult. To obtain the nine transfer functions, a disturbance was applied about each of the X, Y, and Z bus axes using different combinations of the torque wheels. The transfer functions between each input and the three rate gyro sensors were measured. The identification was performed on each of the three single-input three-output systems. The result was three subsystem models which were combined using the approach discussed by Gilpin [56]. A potential problem exists with these subsystem models if a mode is identified differently in the subsystems. Ref. [6] provides an example of the scatter in the data that can be expected in the identification of six sets of transfer functions for a complex system. The duplicated modes must either be repeated or approximated in the model. In this MIMO example, the three subsystems were combined to form a single 50 state model. The MIMO compensators were implemented on the AC-100 at 500 Hz, so a 3 pole Pade approximation of the 15.2 msec time delay was included in each output channel, for a total of 59 states.

Grocott *et al.* [59] suggest a technique based on the multivariable Nyquist and Nichols criteria to determine the frequency ranges in which the system uncertainty

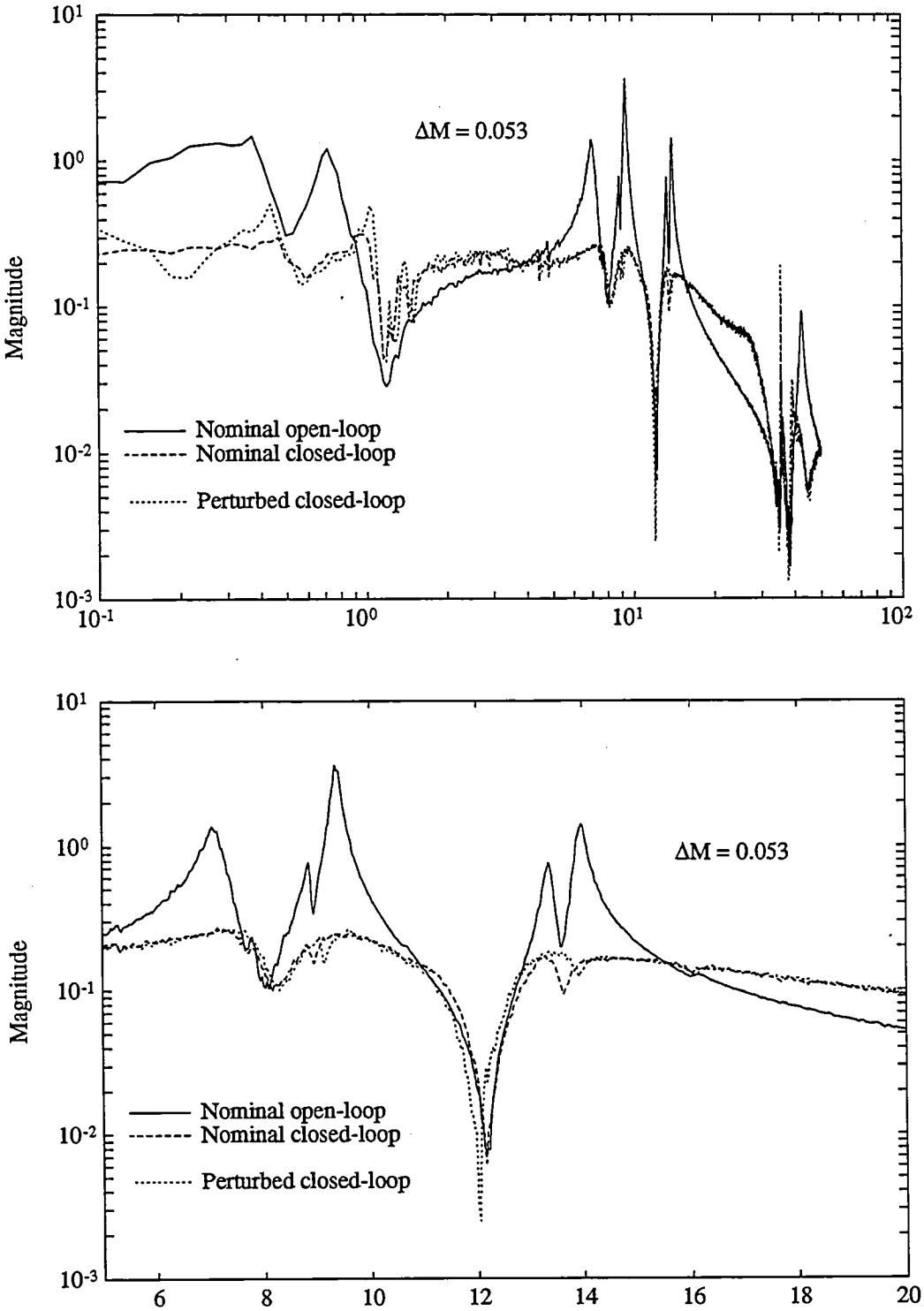

Figure 7.15a: Experimental demonstration of robust performance with the Popov controller (Gpc6) on the hardware with a 5% variation in the mass of the second payload.

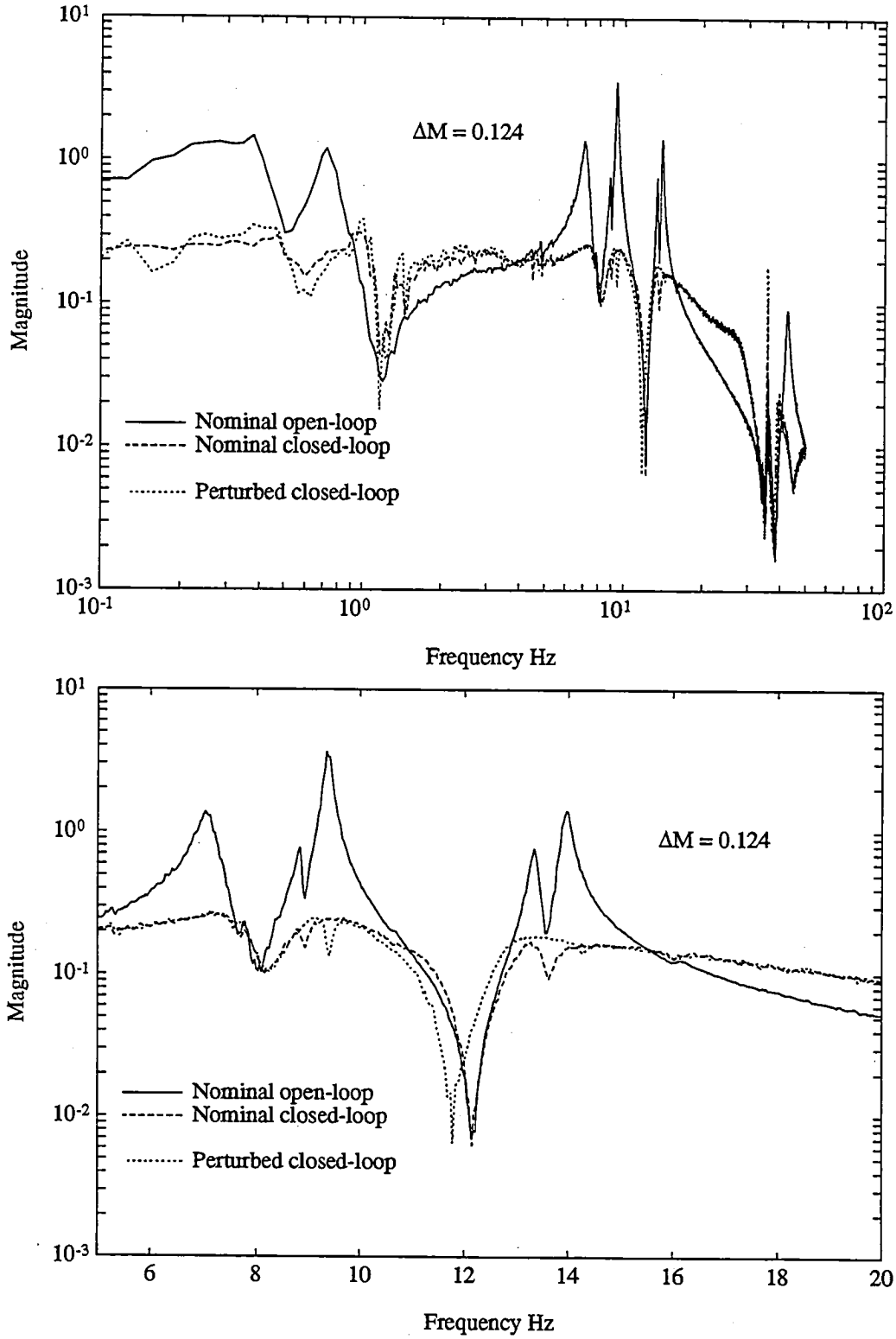

Figure 7.15b: Experimental demonstration of robust performance with the Popov controller (Gpc6) on the hardware with a 12% variation in the mass of the second payload.

is most important. The process is particularly effective if the loop transfer function is based on the measured open-loop data. Note that in this case, the multivariable zeroes must be considered for this system, and these are not necessarily related to the zeroes of the individual transfer functions. The open-loop data indicate that there is a sufficient level of coupling in the system to require a full MIMO control design.

For this system, eleven out of twenty five modes were identified as requiring some level of robustification. The scale of this problem compared to the SISO design discussed in the previous sections (59 states instead of 24 and 11 uncertainties instead of 4) required that a much better initial guess be obtained for the optimization process. The approach adopted here was to build on the results in Grocott *et al.* [59]. These authors develop robust controllers using a multiple model approach with initial guesses based on sensitivity weighted LQG designs. In this thesis, these optimal multiple model controllers were combined with estimates of the guaranteed stability bounds and the multipliers to form an initial condition for the Popov optimization. Recent results indicate that Maximum Entropy controllers would also provide good initial guesses.

These other designs are currently easier to solve numerically, but they offer no guarantees of robustness. However, with these as an initial guess, the Popov controllers can be found more quickly. Using these initial guesses results in an approach that significantly reduces the overall computational effort. As discussed in Chapter 5, the final design is a controller that guarantees robust stability and performance for independent variations in the uncertainties. The design sequence then leads to a unified approach to robust control design, with each step providing further guarantees in the robustness of the closed-loop system.

The MIMO design uses three rate gyro signals as sensors and performance variables and torques about the three bus axes as the disturbance and control inputs. The state cost for the $\mathcal{H}_2$ problem is defined as

$$J_{xx} = 0.2\sigma_x^2 + \sigma_y^2 + \sigma_z^2, \tag{7.5}$$

where σ_i^2 is the variance of the inertial angular motion for each bus axis. X-axis motion

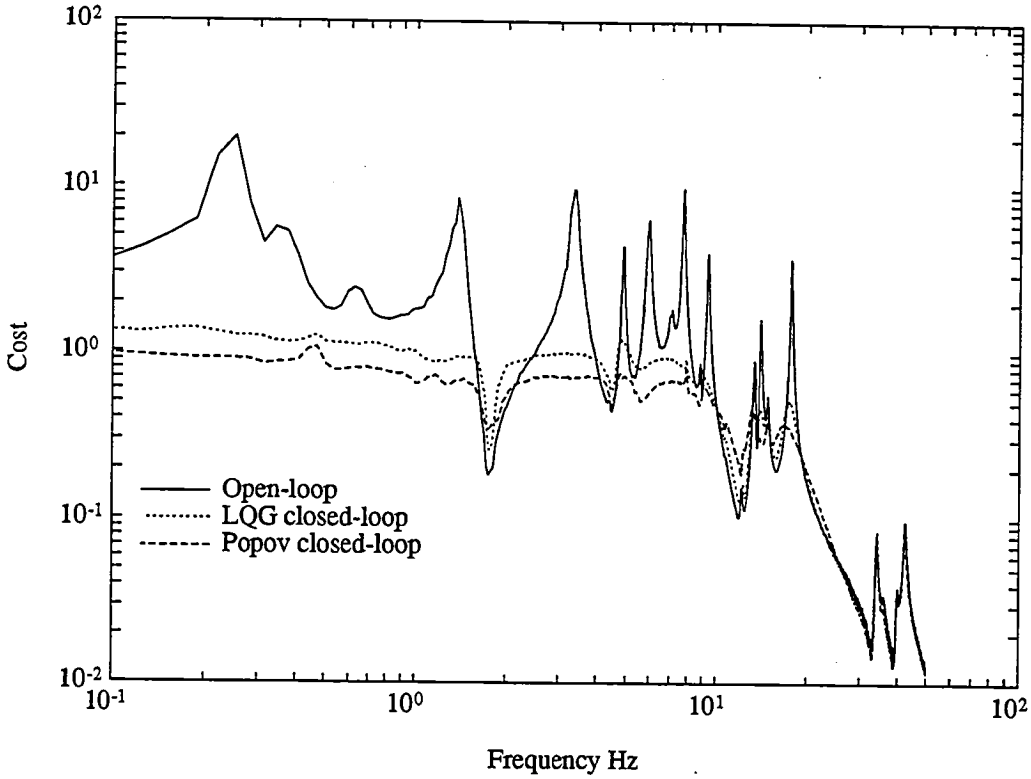

Figure 7.16: MIMO closed-loop performance comparison showing the results with the best stable LQG design and the robust Popov controller.

is weighted less heavily because rotation about this axis has a smaller influence on the payload pointing angle, which is the overall objective of the MACE project.

A single MIMO robust controller with $R_{uu} = 2 \times 10^{-2} \mathrm{I}_3 = 10V_2$ was designed for this system. The uncertain modes, the guaranteed upper and lower stability limits, and the optimal multiplier for these bounds are presented in Table 7.6. Recall that typically one element of H_0 is fixed in the optimization. Several attempts were made to develop initial guesses of the multiplier matrices by fixing the first element of H_0 to unity. However, in these cases, the optimization would result in negative values of H_0. A technique for restricting the positive definiteness of H_0 and N_0 was discussed in Section 5.3. A second approach is to fix different elements of the H_0 matrix. Based on the experience from the SISO designs, the last H_0 value was fixed at 20. In this case, as shown in the table, the resulting optimal values are positive. The relatively

Table 7.6: Optimal multiplier and stability bounds for a MIMO Popov controller.

Mode Hz	$M_2 = -M_1$	H_0	N_0
1.40	0.067	2.29	0.059
3.35	0.022	4.83	0.125
4.88	0.028	6.79	0.152
5.92	0.058	10.00	0.153
8.76	0.028	11.00	0.152
8.91	0.022	18.95	0.205
9.42	0.022	14.92	0.190
13.31	0.022	16.92	0.183
13.90	0.028	12.97	0.177
14.80	0.022	20.91	0.171
33.78	0.022	20.00	0.063

large M_2 values for the 1.4 Hz and 5.9 Hz modes reflect a high uncertainty in the zeroes in these frequency ranges.

To compare the experimental performance of the best stable LQG design and the Popov controller, we can write the state cost as

$$J = \int_{-\infty}^{+\infty} \text{tr } G_{cl}^*(\jmath\omega) Q G_{cl}(\jmath\omega)\, d\omega, \tag{7.6}$$

where

$$Q = \begin{bmatrix} 0.2 & 0 & 0 \\ 0 & 1 & 0 \\ 0 & 0 & 1 \end{bmatrix}, \tag{7.7}$$

and $G_{cl}(s)$ is a frequency domain representation of the closed-loop system. The square root of the integrand of this cost is plotted in Fig. 7.16. With uncorrelated disturbances of equal intensity, this plot is analogous to the transfer function from the disturbance source to the performance metric in the SISO case [59]. The LQG result in the figure corresponds to the best performance that could be achieved using this approach without destabilizing the testbed.

The solid line in this figure corresponds to the open-loop system. Notice that significantly more modes are observable in this transfer function than in the equivalent SISO plots. The next line is the best performance that could be achieved using LQG controllers. The lowest line corresponds to the Popov design. The performance

improvements are 10.2 dB for LQG and 12.4 dB for Popov. The multiple model design used as an initial guess for the optimization achieved a 12.6 dB performance improvement, but this is obtained with fewer guarantees of stability for the eleven uncertain modes.

The additional robustness constraints can result in a degradation in the closed-loop performance on the system model. However, because the sensitivity of the controllers to changes in pole and zero frequencies is guaranteed to decrease, it is possible to achieve much better performance on the experimental hardware.

7.6 Summary

Several robust controllers were designed and implemented on the development model of the Middeck Active Control Experiment (MACE). The results demonstrate the feasibility of Popov controller synthesis for large order systems and illustrate the capabilities of the design approach for complex systems with multiple constant real uncertainties. The controllers were developed to reduce the sensitivity of the LQG designs that destabilized the system for high levels of control authority. The robustness curves show that the overbounding cost functions in Chapters 4 and 5 are not overly conservative for the problem with constant real parameter uncertainty. Good robust performance with a Popov controller was demonstrated experimentally by intentionally changing the mass of the second payload on MACE.

Chapter 8

Conclusions and Recommendations

8.1 Summary

This thesis investigates an alternative approach to robust control design for systems with real parameter uncertainties. The approach directly considers nonlinear parameter uncertainties and treats linear uncertainties as a special case of this much broader class. The analysis and synthesis problems are investigated for several classes of nonlinear uncertainties. The supply rate and storage function concepts of Willems [165, 166] were demonstrated to significantly simplify the derivation of the state space stability criteria. The recent work by Haddad and Bernstein on sector-bounded nonlinearities [66, 69] was reformulated and extended in this thesis using the wealth of literature on absolute stability theory [2, 123, 131, 172]. The storage functions were combined to form parameter-dependent Lyapunov functions that restrict both the allowable time-variation and the class of the nonlinear uncertainties. The stability analysis was developed for time-invariant real nonlinear uncertainties, but can also be used to represent constant linear real uncertainties.

As discussed in Chapter 3, graphical frequency domain tests played a crucial role in the original developments of absolute stability theory. Frequency domain analysis tests also played a crucial role in this thesis. Most importantly of all, these tests provide a direct connection between this approach based on nonlinear stability theory

from the 1960's and current work on mixed μ and K_m synthesis [141,170]. This connection has largely been ignored in many of the recent developments in robust control, but unifies these two diverse bodies of research. Furthermore, the observation indicates that the stability multipliers are a parameterization of the μ scaling functions and that μ theory is just a generalization of the results from absolute stability theory. A geometric interpretation in terms of frequency dependent off-axis circles clarifies the important role of the multiplier phase in these stability criteria. This interpretation provides a qualitative indication of the conservatism in a particular selection of the multipliers (scaling functions), which is not provided by μ theory. Finally, the interpretation shows that both the magnitude and phase of the uncertainty are considered in the robustness tests.

The state space criteria that guarantee stability are included in an $\mathcal{H}_2$ performance objective to provide a powerful tool for the design of robust controllers. Robustness and performance are combined using the Ω-bound fixed structure framework developed by Bernstein and Haddad [23]. It is demonstrated that conservatism can be further reduced in this approach by optimizing the cost functional with respect to the free parameters in the stability multiplier. The result is a numerical synthesis algorithm in which the fixed-order controller and multiplier matrices are optimized simultaneously. The approach avoids the explicit D–K iteration required by the μ and K_m synthesis techniques. Architecture constraints on the controller, which are essential for most realistic systems, can also be included in the state space optimization.

Finally, several controllers were designed using the analysis test based on the Popov stability multiplier. Both low-order benchmark problems and more complicated experiments were considered. The low-order examples demonstrate the modifications to the compensator that are required to achieve guaranteed robust stability. The more complicated experiments demonstrate that the approach is feasible for more realistic systems. Several SISO and MIMO controllers were implemented on the Middeck Active Control Experiment (MACE). The experimental results indicate that guaranteed stability robustness can be achieved for complex systems with mul-

tiple uncertainties. Moreover, these guarantees can be achieved without significant sacrifices in the performance. In fact, extremely good robust performance was experimentally demonstrated on MACE by intentionally changing the structure with additional mass at one payload.

8.2 Conclusions and Contributions

1: The results in this thesis show the many connections between mixed μ and absolute stability theory. In particular, it is shown that the upper bounds for mixed μ are just a generalization of the results obtained from absolute stability theory. This important observation has largely been ignored in many recent developments in robust control theory, but unifies these two diverse bodies of research. Similar connections are developed between the approach in this thesis and concurrent work on K_m synthesis by Safonov *et al.* [34, 142]. The results in this thesis are considered to be an extension of μ theory, because both linear and nonlinear real parameter uncertainties are analyzed.

2: Both state space and frequency domain criteria are developed for several nonlinearities and stability multipliers using the wealth of literature on absolute stability theory. In the process, it is demonstrated that the concepts of supply rates and storage functions from Ref. [165] provide a powerful framework for developing stability criteria. By considering the monotonic and odd monotonic classes of nonlinear functions, the state space criteria in this thesis extend recent work by Haddad and Bernstein on sector-bounded nonlinearities [66]. The stability criteria are written in terms of Riccati equations and parameter-dependent Lyapunov functions. Based on the connections discussed previously, it can also be concluded that these results provide parameter-dependent Lyapunov functions to support the mixed μ results of Doyle *et al.* [53].

3: An interpretation of the equivalent frequency domain criteria in terms of off-axis circles clarifies several features of the robustness tests. The frequency dependent location of the circle centers illustrates the important role of the multiplier phase. These conditions also demonstrate that both the magnitude and phase of the

uncertainty are considered, which, as discussed in the Introduction, is essential for problems with real parameter uncertainties. This geometric interpretation indicates that the more general multipliers associated with the monotonic and odd monotonic nonlinearities provide even less conservative robustness tests, because there is more freedom to control the location of the circle centers.

4: The robust controller synthesis problem is addressed using the Ω-bound framework of Haddad and Bernstein [23]. The performance objective for the control design is specified in terms of an $\mathcal{H}_2$ cost functional. The state space stability criteria are used to develop an auxiliary minimization problem with an overbound of this cost. Both static and dynamic feedback controllers are presented in the thesis. The optimal reduced-order designs are written in terms of the solutions of coupled Riccati and Lyapunov equations. A quasi-Newton optimization with a homotopy on the stability bounds was developed to solve the robustness problem based on the Popov stability multiplier. A key advantage of this combined $\mathcal{H}_2$/real μ synthesis technique is that it avoids the explicit D–K iteration of μ synthesis by optimizing the controller and multiplier values simultaneously. Furthermore, order and architecture constraints on the compensator can easily be included in the optimization [109]. These constraints are essential for most realistic systems, but cannot be incorporated into the $\mathcal{H}_\infty$ design approach. Several compensators were designed using this Popov controller synthesis approach. The results are typically presented as a family of controllers to illustrate the trade-offs between performance and guaranteed robustness.

5: The numerical examples on the benchmark problems and the laboratory experiments on MACE serve to illustrate that this approach is a very powerful alternative for robust controller synthesis. The low-order numerical examples clearly illustrate the mechanisms by which the robustness is achieved. The more complicated experiments demonstrate that the design technique is feasible on more realistic systems. Furthermore, the experiments on a lightly damped structure

with uncertain pole and zero frequencies show that Popov controller synthesis results in good performance with relatively large robust stability guarantees.

8.3 Recommendations

1: The complete synthesis approach is given in Chapter 4 using the stability criteria with the extended multipliers. Synthesis with the Popov stability multiplier was used to illustrate that the conservatism can be reduced even further by optimizing an overbounding cost functional with respect to the multipliers. This approach can also be applied to the case with the extended multipliers, but there are several difficulties. First of all, the derivation of the optimality conditions for the multipliers is complicated by the fact that the multiplier coefficients appear in the A_a matrix. A second problem is that the constraints on the multiplier coefficients in Eq. 4.9 will require that the controllers be designed using a constrained optimization algorithm.

2: As mentioned in Remark 3.6, the results in this thesis can be extended by including more general parameterizations of the multipliers for the odd monotonic nonlinearities. A more fundamental extension is the possibility of developing a parameter-dependent Lyapunov function for the Nyquist criterion using the LC class of multipliers [63, 118, 157]. These new multipliers have poles and zeroes on the imaginary axis and thus provide even more general functions of the multiplier phase.

3: Collins *et al.* [38] have recently developed a numerically robust technique for designing full-order Maximum Entropy controllers, and it is believed that many of the ideas in this new algorithm can be applied to the Popov synthesis problem [36]. Unfortunately, the numerical difficulties with reduced-order designs still exist, although Collins *et al.* [37, 38] present some major extensions of the approach by Mercadal [109].

4: One problem with research on space structures is that measurement based models cannot be developed for many systems. In these cases, we must rely on finite

element models (FEM) to design controllers. As might be expected, the errors in these FEM's tend to be much larger than those in measured models. An important extension of the work in this thesis would be to develop a controller that is robust the errors in a FEM of the system. In this case, performance could be achieved without the extensive effort necessary to develop measured models or upgrade the FEM. This problem is particularly important for the MACE project because gravity effects have been shown to have such a large effect on structures [12, 43]. Even with current prediction techniques based on the FEM, these changes will result in large parameter uncertainties in the model [134].

References

[1] Ackerman, J., "Parameter Space Design of Robust Control Systems," *IEEE Trans. on Auto. Control*, Vol. AC–25, No. 5, 1980, pp. 1058–1072.

[2] Aizerman, M. A. and F. R. Gantmacher, *Absolute Stability of Regulator Systems*, Holden-Day, Inc., San Francisco, 1964.

[3] Anderson, B. D. O., "A System Theory Criterion for Positive Real Matrices," *SIAM J. of Control and Opt.*, Vol. 5, 1967, pp. 171–182.

[4] Anderson, B. D. O., "The Small-gain Theorem, the Passivity Theorem, and their Equivalence," *J. Franklin Inst.*, Vol. 293, 1972, pp. 105–115.

[5] Anderson, B. D. O. and S. Vongpanitlerd, *Network Analysis and Synthesis: A Modern Systems Theory Approach*, Prentice-Hall, Englewood Cliffs, NJ, 1973.

[6] Anderson, E. H., G. H. Blackwood, and J. P. How, "Passive Damping in the M.I.T. SERC Controlled Structures Testbed," *Proceedings, International Symposium on Active Materials and Adaptive Structures*, Alexandria, VA, Nov. 1991.

[7] Anderson, E. H. and J. P. How, "Implementation Issues in the Control of a Flexible Mirror Testbed," *Proceedings, SPIE Conference on Active and Adaptive Optical Components*, San Diego, CA, July 1991.

[8] Ashkenazi, A. and A. E. Bryson Jr., "Control Logic for Parameter Insensitivity and Disturbance Attenuation," *AIAA J. of Guid., Control, and Dyn.*, Vol. 5, No. 4, July 1982, pp. 383–388.

[9] Athans, M., "The Matrix Minimum Principle," *Information and Control*, Vol. 11, 1968, pp. 592–606.

[10] Balakrishnan, V., E. Feron, and S. P. Boyd, "Computing Bounds for the Structured Singular Value Via Interior Point Algorithm," *Proceedings, American Control Conference*, Chicago, IL, June 1992, pp. 2195–2196.

[11] Balas, G. J., P. M. Young, and J. C. Doyle, "μ-Based Control Design as Applied to Large Space Structure: Control Design for the Minimast Facility," Tech. Rep., NASA CSI/GI Final Report, August 1992.

[12] Barlow, M., *Modelling and Ground Modal Identification of Space Structures*, Master's thesis, Massachusetts Institute of Technology, 1992. M.I.T. SERC #1-92.

[13] Barmish, R. B., "New Tools for Robustness Analysis," *Proceedings, IEEE Conference on Decision and Control*, Austin Texas, Dec. 1988, pp. 1–6.

[14] Barmish, R. B., P. P. Khargonekar, Z. C. Shi, and R. Tempo, "Robustness Margin need not be a Continuous Function of the Problem Data," *Systems and Control Letters*, Vol. 15, 1990, pp. 91–98.

[15] Bartlet, A. C., C. V. Hollot, and H. Lin, "Root Locations of an Entire Polytope of Polynomials: It Suffices to Check the Edges," *Mathematics of Control, Signals and Systems*, Vol. 1, 1987, pp. 61–71.

[16] Bergen, A. R. and M. A. Sapiro, "The Parabola Test for Absolute Stability," *IEEE Trans. on Auto. Control*, June 1967, pp. 312–314.

[17] Bernstein, D. S. and W. M. Haddad, "The Optimal Projection Equations with Petersen-Hollot Bounds: Robust Stability and Performance via Fixed-order Dynamic Compensation for Systems with Structured Real-valued Parameter Uncertainty," *IEEE Trans. on Auto. Control*, Vol. AC-33, 1988, pp. 578–582.

[18] Bernstein, D. S. and W. M. Haddad, "LQG Control with an $\mathcal{H}_\infty$ Performance Bound: A Riccati Equation Approach," *IEEE Trans. on Auto. Control*, Vol. AC–34, No. 3, Mar. 1989, pp. 293–305.

[19] Bernstein, D. S. and W. M. Haddad, "Robust Stability and Performance via Fixed-order Dynamic Compensation with Guaranteed Cost Bounds," *Math. Contr. Sig. Sys.*, Vol. 3, 1990, pp. 139–163.

[20] Bernstein, D. S., W. M. Haddad, and D. C. Hyland, "Small Gain Versus Positive Real Modeling of Real Parametric Uncertainty," *AIAA J. of Guid., Control, and Dyn.*, Vol. 15, No. 2, March 1992, pp. 538–540.

[21] Bernstein, D. S., W. M. Haddad, D. C. Hyland, and F. Tyan, "Maximum Entropy-type Lyapunov Functions for Robust Stability and Performance Analysis," *Proceedings, American Control Conference*, June 1992.

[22] Bernstein, D. S. and D. C. Hyland, "Optimal Projection Equations for Reduced-Order Modelling, Estimation, and Control of Linear Systems with Multiplicative White Noise," *J. of Opt. Theory and Applications*, Vol. 58, No. 3, Sept. 1988, pp. 387–409.

[23] Bernstein, D. S. and D. C. Hyland, "Optimal Projection for Uncertain Systems (OPUS): A Unified Theory of Reduced Order, Robust Control Design," in *Large Space Structures: Dynamics and Control* (Atluri, S. N. and A. K. Amos, eds.), pp. 263–302, Springer-Verlag, New York, 1988.

[24] Bernstein, D. S. and D. C. Hyland, "The Optimal Projection Approach to Robust, Fixed-Structure Control Design," in *Mechanics and Control of Space Structures* (Junkins, J. L., ed.), pp. 237–293, AIAA, Washington, D. C., 1990.

[25] Bhattacharyya, S. P., *Robust Stabilization Against Structured Perturbations*, Springer-Verlag, New York, 1987.

[26] Blelloch, P. A. and D. L. Mingori, "Robust Linear Quadratic Gaussian Control for Flexible Structures," *AIAA J. of Guid., Control, and Dyn.*, Vol. 13, No. 1, Jan.–Feb. 1990, pp. 66–72.

[27] Boyd, S. and Q. Yang, "Structured and Simultaneous Lyapunov Functions for System Stability Problems," *Int. J. of Control*, Vol. 94, No. 6, 1989, pp. 2215–2240.

[28] Brockett, R. W. and J. L. Willems, "Frequency Domain Stability Criteria – Part I," *IEEE Trans. on Auto. Control*, Vol. AC–10, No. 3, July 1965, pp. 255–261.

[29] Brockett, R. W. and J. L. Willems, "Frequency Domain Stability Criteria – Part II," *IEEE Trans. on Auto. Control*, Vol. AC–10, No. 4, October 1965, pp. 407–412.

[30] Calise, A. J. and E. V. Byrns, "Parameter Sensitivity Reduction in Fixed-order Dynamic Compensation," *AIAA J. of Guid., Control, and Dyn.*, Vol. 15, No. 2, March–April 1992, pp. 440–447.

[31] Cannon, R. H. and D. E. Rosenthal, "Experiments in Control of Flexible Structures with Noncolocated Sensors and Actuators," *AIAA J. of Guid., Control, and Dyn.*, Vol. 7, No. 5, Sept.-Oct. 1984, pp. 546–553.

[32] Cavallo, A., G. De Maria, and L. Verde, "Robust Flight Control Systems: A Parameter Space Design," *AIAA J. of Guid., Control, and Dyn.*, Vol. 15, No. 5, Sept.–Oct. 1992, pp. 1207–1215.

[33] Cheung, M.-F. and S. Yurkovich, "On the Robustness of MEOP Designs Versus Asymptotic LQG Synthesis," *IEEE Trans. on Auto. Control*, Vol. AC–33, No. 11, Nov. 1988.

[34] Chiang, R. Y. and M. G. Safonov, "Real K_m-Synthesis via Generalized Popov Multipliers," *Proceedings, American Control Conference*, Chicago, IL, June 1992.

[35] Cho, Y.-S. and K. S. Narendra, "An Off-Axis Circle Criterion for the Stability of Feedback Systems with a Monotonic Nonlinearity," *IEEE Trans. on Auto. Control*, Aug. 1968, pp. 413–416.

[36] Collins, Jr., E. G., Personal Communication, 1992.

[37] Collins, Jr., E. G., L. D. Davis, and S. Richter, "Design of Reduced-Order, $\mathcal{H}_2$ Optimal Controllers using a Homotopy Algorithm," submitted to *1993 American Control Conference*, Aug. 1992.

[38] Collins, Jr., E. G., L. D. Davis, and S. Richter, "Homotopy Algorithms for $\mathcal{H}_2$ Optimal Reduced Order Dynamic Compensation and Maximum Entropy Control," Tech. Rep. 54-7609, Harris Corporation, Government Systems Division, August 1992.

[39] Collins, Jr., E. G., W. M. Haddad, and L. D. Davis, "Riccati Equation Approaches for Robust Stability and Performance Analysis Using the Small Gain, Positivity, and Popov Theorems," submitted to *AIAA J. Guidance, Control, and Dynamics*, 1992.

[40] Collins, Jr., E., J. King, and D. Bernstein, "Application of Maximum Entropy/Optimal Projection Design Synthesis to a Benchmark Problem," *AIAA J. of Guid., Control, and Dyn.*, Vol. 15, No. 5, Sept.-Oct. 1992, pp. 1094–1102.

[41] Crawley, E. F., J. de Luis, and D. W. Miller, "Middeck Active Control Experiment (MACE) Phase A Final Report," Tech. Rep. SERC #16-90-R, Space Engineering Research Center, Massachusetts Institute of Technology, June 1989.

[42] Crawley, E. F. and S. R. Hall, "The Dynamics of Controlled Structures," Tech. Rep. SERC #10-91-I, M.I.T. Space Engineering Research Center, July 1991.

[43] Crawley, E., M. Barlow, M. van Schoor, and A. Bicos, "Variation in the Modal Parameters of Space Structures," *Proceedings, Proceedings of the* 33^{rd} *AIAA/ASME/ASCE/AHS Structures, Structural Dynamics, and Materials Conference*, (Dallas, TX), Apr. 1992.

[44] Desoer, C. A. and M. Vidyasagar, *Feedback Systems: Input-Output Properties*, Academic Press, New York, 1975.

[45] Douglas, J., *Linear Quadratic Control for Systems with Structured Uncertainty*, Master's thesis, Massachusetts Institute of Technology, 1991. M.I.T. SERC report #12-91.

[46] Doyle, J. C., "Guaranteed Margins for LQG Regulators," *IEEE Trans. on Auto. Control*, Vol. 23, No. 4, August 1978, pp. 756–757.

[47] Doyle, J. C., "Analysis of Feedback Systems with Structured Uncertainties," *IEE Proceedings*, Vol. 129, Part D, No. 6, Nov. 1982, pp. 242–250.

[48] Doyle, J. C., "Structured Uncertainty in Control System Design," *Proceedings, IEEE Conference on Decision and Control*, Ft. Lauderdale, FL, 1985, pp. 260–265.

[49] Doyle, J. C., B. A. Francis, and A. R. Tannenbaum, *Feedback Control Theory*, Macmillan Publishing Company, New York, 1992.

[50] Doyle, J. C., K. Glover, P. P. Khargonekar, and B. A. Francis, "State-Space Solutions to Standard $\mathcal{H}_2$ and $\mathcal{H}_\infty$ Control Problems," *IEEE Trans. on Auto. Control*, Vol. AC–34, No. 8, Aug. 1989, pp. 831–847.

[51] Doyle, J. C., K. Zhou, and B. Bodenheimer, "Optimal Control with Mixed $\mathcal{H}_2$ and $\mathcal{H}_\infty$ Performance Objectives," *Proceedings, American Control Conference*, Pittsburgh, PA, 1989, pp. 2065–2070.

[52] Fan, M. K. H. and A. L. Tits, "On the Generalized Numerical Range," *Linear and Multilinear Algebra*, Vol. 21, 1987, pp. 313–320.

[53] Fan, M. K. H., A. L. Tits, and J. C. Doyle, "Robustness in the Presence of Mixed Parametric Uncertainty and Unmodelled Dynamics," *IEEE Trans. on Auto. Control*, Vol. AC–36, No. 1, Jan. 1991, pp. 25–38.

[54] Francis, B. A., *A Course in $\mathcal{H}_\infty$ Control Theory*, Springer-Verlag, New York, 1987.

[55] Ganesh, C. and J. Pearson, "$\mathcal{H}_2$-Optimization with Stable Controllers," *Automatica*, Vol. 25, No. 4, 1989, pp. 629–634.

[56] Gilpin, K., *Identification of a Lightly Damped Structure for Control/Structure Interaction*, Master's thesis, Massachusetts Institute of Technology, Aug. 1991. SERC report #11-91.

[57] Grantham, W. and R. Laskin, "NASA CSI Technology Program Focus Mission and Benefit Studies," in *Proceedings of the Fourth NASA/DOD Controls/Structures Interaction Technology Conference*, Nov. 1990.

[58] Grocott, S., *Multivariable Robust Control for MACE*, Master's thesis, Massachusetts Institute of Technology, manuscript in preparation 1993.

[59] Grocott, S. C. O., D. G. MacMartin, and D. W. Miller, "Experimental Implementation of a Multiple Model Technique for Robust Control of the MACE Test Article," to appear in the *Third International Conference on Adaptive Structures*, Nov. 1992.

[60] Grujić, L. T., A. A. Martynyuk, and M. Ribbens-Pavella, *Large-scale Systems Stability under Structural and Singular Perturbations*, Springer, New York, 1987.

[61] Guillemin, E. A., *Synthesis of Passive Networks*, Chapman and Hall Ltd., New York, 1957.

[62] Gupta, N., "Frequency–Shaped Cost Functionals: Extension of Linear Quadratic Gaussian Methods," *AIAA J. of Guid., Control, and Dyn.*, Vol. 3, No. 6, Nov.–Dec. 1980, pp. 529–535.

[63] Haddad, W. M., Personal Communication, 1992.

[64] Haddad, W. M. and D. S. Bernstein, "Parameterized Lyapunov functions, Real Parameter Uncertainty, and Phase Information in Robust Fixed Structure Control," submitted to the 1992 *IEEE CDC.*

[65] Haddad, W. M. and D. S. Bernstein, "Generalized Riccati Equations for the Full- and Reduced-order Mixed-norm $\mathcal{H}_2/\mathcal{H}_\infty$Standard Problem," *Systems and Control Letters*, Vol. 14, 1990, pp. 185–197.

[66] Haddad, W. M. and D. S. Bernstein, "Parameter-Dependent Lyapunov Functions, Constant Real Parameter Uncertainty, and the Popov Criterion in Robust Analysis and Synthesis, Parts I and II," *Proceedings, IEEE Conf. on Decision and Control*, Dec. 1991, pp. 2274–2279, 2632–2633. Submitted to *IEEE Trans. on Auto. Control.*

[67] Haddad, W. M. and D. S. Bernstein, "Robust Stabilization with Positive Real Uncertainty: Beyond the Small Gain Theorem," *Systems and Control Letters*, Vol. 17, 1991, pp. 191–208.

[68] Haddad, W. M. and D. S. Bernstein, "Controller Design with Regional Pole Constraints," *IEEE Transactions on Automatic Control*, Vol. 37, No. 1, 1992, pp. 54–69.

[69] Haddad, W. M. and D. S. Bernstein, "Explicit Construction of Quadratic Lyapunov Functions for the Small Gain, Positivity, Circle, and Popov Theorems and their Application to Robust Stability Part I and II:," *Int. J. Robust and Nonlinear Control, to appear*, 1992.

[70] Haddad, W. M. and D. S. Bernstein, "The Multivariable Parabola Criterion for Robust Controller Synthesis: A Riccati Equation Approach," submitted to *Sys. Contr. Lett.*, 1992.

[71] Haddad, W. M. and D. S. Bernstein, "New Absolute Stability Criteria for Robust Stability and Performance with locally Slope-Restricted Monotonic Nonlinearities," *Proceedings, Preprint, submitted to the 1993 ACC*, Sept. 1992.

[72] Haddad, W. M., J. P. How, S. R. Hall, and D. S. Bernstein, "Extensions of Mixed-μ Bounds to Monotonic and Odd Monotonic Nonlinearities Using Absolute Stability Theory," *Proceedings, IEEE Conference on Decision and Control*, Tucson, AZ, December 1992, pp. 2713–2819, 2820–2823. Submitted to *International Journal of Control.*

[73] Hagander, P. and B. Bernhardsson, "On the Notion of Strong Stabilizability," Tech. Rep., Lund Institute of Technology, Department of Automatic Control, Sept. 1989.

[74] Hagood, N. W., *Cost Averaging Techniques for Robust Control of Parametrically Uncertain Systems*, Ph.D. thesis, Department of Aeronautics and Astronautics, M.I.T., Cambridge, MA, June 1991.

[75] Hagood, N. W., "Cost Averaging Techniques for Robust Control of Parametrically Uncertain Systems," Presented at *AIAA Guidance, Navigation and Control Conference*, Aug. 1991. AIAA Paper 91-2605.

[76] Halevi, Y., D. S. Bernstein, and W. M. Haddad, "On Stable Full-order and Reduced-order LQG Controllers," *Optimal Control Applications and Methods*, Vol. 12, 1991, pp. 163–172.

[77] Hall, S. R., D. G. MacMartin, and D. S. Bernstein, "Incoherence, Equipartition, and Covariance Averaging in the Analysis of Uncertain Systems," to appear *IEEE Transactions on Automatic Control*, 1992.

[78] Hill, D. J., "Dissipativeness, Stability Theory and some Remaining Problems," in *Analysis and Control of Nonlinear Systems* (Byrnes, C. I., C. F. Martin, and R. E. Saeks, eds.), North Holland, Amsterdam, 1988.

[79] Hill, D. J. and P. J. Moylan, "The Stability of Nonlinear Dissipative Systems," *IEEE Trans. on Auto. Control*, Vol. AC–21, 1976, pp. 708–711.

[80] Hill, D. J. and P. J. Moylan, "Dissipative Dynamical Systems: Basic Input-output and State Properties," *Journal of the Franklin Institute*, Vol. 309, 1980, pp. 327–357.

[81] How, J. P., W. M. Haddad, and S. R. Hall, "Application of Popov Controller Synthesis to Benchmark Problems with Real Parameter Uncertainty," submitted to *AIAA Journal of Guidance, Control, and Dynamics*, Oct. 1992.

[82] How, J. P., W. M. Haddad, and S. R. Hall, "Robust Control Synthesis Examples with Real Parameter Uncertainty using the Popov Criterion," submitted to *1993 American Control Conference*, Sept. 1992.

[83] How, J. P. and S. R. Hall, "Connections between the Popov Stability Criterion and Bounds for Real Parameter Uncertainty," submitted to *IEEE Trans. on Auto. Control*, May 1992. M.I.T. SERC Report #9-92-J.

[84] How, J. P. and S. R. Hall, "Connections between the Popov Stability Criterion and Bounds for Real Parameter Uncertainty," submitted to the *1993 American Control Conference*, Sept. 1992. M.I.T. SERC Report #9-92-J.

[85] How, J. P. and S. R. Hall, "Robust Controllers for the Middeck Active Control Experiment using Popov Controller Synthesis," submitted to *1993 AIAA Guidance, Navigation, and Control Conference*, Jan. 1993.

[86] Hsu, J. C. and A. U. Meyer, *Modern Control Principles and Applications*, McGraw-Hill Book Company, New York, 1968.

[87] Hyland, D. C., "Maximum Entropy Stochastic Approach to Controller Design for Uncertain Structural Systems," *Proceedings, American Control Conference*, Arlington, VA, June 1982, pp. 680–688.

[88] Hyland, D. C. and D. S. Bernstein, "The Optimal Projection Equations for Fixed-Order Dynamic Compensation," *IEEE Trans. on Auto. Control*, Vol. AC–29, No. 11, Nov. 1985, pp. 1034–1037.

[89] Hyland, D. C. and D. S. Bernstein, "The Majorant Lyapunov Equation: A Nonnegative Matrix Equation for Guaranteed Robust Stability and Performance of Large Scale Systems," *IEEE Trans. on Auto. Control*, Vol. AC–32, 1987.

[90] Hyland, D., "Optimal Regulation of Structural Systems With Uncertain Parameters," Tech. Rep. TR-551, M.I.T., February 1981. DDC#ADA-099111/7.

[91] Hyland, D., "Minimum Information Stochastic Modeling of Linear Systems with a Class of Parameter Uncertainties," *Proceedings, AIAA J. of Guid., Control, and Dyn.*, (Arlington, VA), June 1982, pp. 620–627.

[92] Junkins, J. L., *Mechanics and Control of Space Structures*, AIAA, Washington, D. C., 1990.

[93] Khargonekar, P. P., A. M. Pascoal, and R. Ravi, "Strong, Simultaneous, and Reliable Stabilization of Finite-Dimensional Linear Time-Varying Plants," *IEEE Trans. on Auto. Control*, Vol. AC–33, No. 12, Dec. 1988, pp. 1158–1161.

[94] Khargonekar, P. P., I. R. Petersen, and K. Zhou, "Robust Stabilization of Uncertain Linear Systems: Quadratic Stabilizability and $\mathcal{H}_\infty$ Control Theory," *IEEE Trans. on Auto. Control*, Vol. AC–35, 1990, pp. 356–361.

[95] Khargonekar, P. P. and M. A. Rotea, "Multiple Objective Optimal Control of Linear Systems: The Quadratic Norm Case," *IEEE Trans. on Auto. Control*, Vol. AC–36, No. 1, Jan. 1991, pp. 14–24.

[96] Kharitonov, V. L., "Asymptotic Stability of an Equilibrium Position of a Family of Systems of Linear Differential Equations," *Differencial'nye Uravenija*, Vol. 14, No. 11, 1978, pp. 2086–2088.

[97] LaSalle, J. P., "Some Extensions of Liapunov's Second Method," *IRE Trans. Cir. Theory*, 1960, pp. 520–527.

[98] Leal, M. A. and J. S. Gibson, "A First Order Lyapunov Robustness Method for Linear Systems with Uncertain Parameters," *IEEE Trans. on Auto. Control*, Vol. AC–35, No. 9, Sept. 1990, pp. 1068–1070.

[99] Lee, L. and A. L. Tits, "On Continuity/Discontinuity in Robustness Indicators," *Proceedings, IEEE Conference on Decision and Control*, Brighton, England, Dec. 1991, pp. 547–548.

[100] Lefschetz, S., *Stability of Nonlinear Control Systems*, Academic Press, New York, 1965.

[101] Leitmann, G., "Guaranteed Asymptotic Stability for some Linear Systems with Bounded Uncertainties," *Trans. of the ASME*, Vol. 101, Sept. 1979, pp. 212–216.

[102] Lozano-Leal, R. and S. Joshi, "Strictly Positive Real Transfer Functions Revisited," *IEEE Trans. on Auto. Control*, Vol. AC–35, 1990, pp. 1243–1245.

[103] Ly, U.-L., "A Design Algorithm for Robust Low-Order Controllers," Tech. Rep. SUDAAR 536, Stanford University, Nov. 1982.

[104] Maciejowski, J., *Multivariable Feedback Design*, Addison–Wesley Publishing Company, Wokingham, England, 1989.

[105] MacMartin, D. G., *A Stochastic Approach to Broadband Control of Parametrically Uncertain Structures*, Ph.D. thesis, Department of Aeronautics and Astronautics, M.I.T., Cambridge, MA, June 1992.

[106] MacMartin, D. G., S. R. Hall, and D. S. Bernstein, "Fixed Order Multi-Model Estimation and Control," *Proceedings, American Control Conference*, Boston, MA, June 1991, pp. 2113–2118.

[107] Makila, P. M., "Multiple Models, Multiplicative Noise and Linear Quadratic Control-algorithm Aspects," 1991. Preprint.

[108] Malyshev, V. V. and P. V. Pakshin, "Applied Stochastic Stability and Optimal Stationary Control Theory," *Soviet Journal of Computer and System Sciences*, Vol. 28, No. Part I, 2, Part II, 6, 1990, pp. 78–101,86–108.

[109] Mercadal, M., *$\mathcal{H}_2$ Fixed Architecture, Control Design for Large Scale Systems*, Ph.D. thesis, Department of Aeronautics and Astronautics, M.I.T., Cambridge, MA, June 1990.

[110] Mercadal, M., "Analysis of the First Middeck Active Control Experiment (MACE) Sample Problem," Tech. Rep. SERC #7-91-R, Space Engineering Research Center, Massachusetts Institute of Technology, June 1991.

[111] Miller, D., E. Saarmaa, and R. Jacques, "Preliminary Structural Control Results From the Middeck Active Control Experiment (MACE)," in *AIAA Dynamics Specialist Conference*, (Dallas, TX), April 1992, pp. 566–576. Paper AIAA-92-2138-CP.

[112] Miyazawa, Y., "Robust Flight Control System Design with Multiple Model Approach," *Proceedings, AIAA Guidance, Navigation, and Control Conference*, Portland, OR, Aug. 1990, pp. 874–882.

[113] Morton, B. G. and R. M. McAfoos, "A Mu-Test for Robustness Analysis of Real Parameter Variation Problem," *Proceedings, American Control Conference*, May 1985, pp. 135–138.

[114] Mukhopadhyay, V., "Stability Robustness Improvement Using Constrained Optimization Techniques," *AIAA J. of Guid., Control, and Dyn.*, Vol. 10, No. 2, March–April 1987, pp. 172–177.

[115] Mukhopadhyay, V., "Digital Robust Control Law Synthesis Using Constrained Optimization Techniques," *AIAA J. of Guid., Control, and Dyn.*, Vol. 12, No. 2, March–April 1989, pp. 175–181.

[116] Mustafa, D., "Relations Between Maximum-entropy/$\mathcal{H}_\infty$ Control and Combined $\mathcal{H}_\infty$/LQG Control," *Systems and Control Letters*, Vol. 12, 1989, pp. 193–203.

[117] MuSyn Inc., *μ-Analysis and Synthesis Toolbox: User's Guide*, The Math Works, Inc., Natick, MA, 1991.

[118] Narendra, K. S., "Author's reply to Stability of Linear Time-Invariant Systems," *IEEE Trans. on Auto. Control*, Vol. AC–12, 1967, pp. 336–337.

[119] Narendra, K. S., "Stability of Nonlinear Systems," in *Nonlinear System Analysis and Synthesis: Volume 1 - Fundamental Principles* (Hedrick, K. and H. Paynter, eds.), pp. 35–71, The Dynamic Systems and Controls Division, ASME, New York, 1976.

[120] Narendra, K. S. and Y.-S. Cho, "Stability of Feedback Systems Containing a Single Odd Monotonic Nonlinearity," *IEEE Trans. on Auto. Control*, Aug. 1967, pp. 448–450.

[121] Narendra, K. S. and C. P. Neuman, "On the Absolute Stability of Continuous Time Dynamical Systems with m-feedback Nonlinearities," Vol. CT–1, 1965.

[122] Narendra, K. S. and C. P. Neuman, "Stability of a Class of Differential Equations with a Single Monotone Nonlinearity," *SIAM J. of Control*, Vol. 4, 1966, pp. 295–308.

[123] Narendra, K. S. and J. H. Taylor, *Frequency Domain Criteria for Absolute Stability*, Academic Press, New York, 1973.

[124] Obradovic, D. and L. Valavani, "Stability and Performance Analysis in the Presence of Magnitude Bounded Real Uncertainty," Tech. Rep., Massachusetts Institute of Technology, Laboratory for Information and Decision Systems, Nov. 1991.

[125] Ogata, K., *Modern Control Engineering*, Prentice–Hall, Inc., Englewood Cliffs, NJ, 1970.

[126] Okada, K. and R. E. Skelton, "Sensitivity Controller for Uncertain Systems," *AIAA J. of Guid., Control, and Dyn.*, Vol. 13, No. 2, 1990, pp. 321–329.

[127] Packard, A., "Continuity Properties of Real/Complex μ," *Proceedings, IEEE Conference on Decision and Control*, Brighton, England, Dec. 1991, pp. 1159–1160.

[128] Packard, A. and J. C. Doyle, "Quadratic Stability with Real and Complex Perturbations," *IEEE Trans. on Auto. Control*, Vol. AC–35, 1990, pp. 198–201.

[129] Petersen, I. R. and C. V. Hollot, "A Riccati Equation Approach to the Stabilization of Uncertain Systems," *Systems and Control Letters*, Vol. 8, 1987, pp. 351–357.

[130] Pinzoni, S. and J. C. Willems, "The Dissipation Inequality for Systems Described by High-order Differential Equations," *Proceedings, IEEE Conference on Decision and Control*, Dec. 1992, pp. 1439–1440.

[131] Popov, V. M., "On Absolute stability of Non-linear Automatic Control Systems," *Avtomatika I Telemekhanika*, Vol. 22, No. 8, 1961, pp. 961–979.

[132] Popov, V. M., *Hyperstability of Control Systems*, Springer, New York, 1973.

[133] Rekasius, Z. V. and J. E. Gibson, "Stability Analysis of Nonlinear Control Systems by the Second Method of Liapunov," *IRE Transactions on Automatic Control*, January 1962, pp. 3–15.

[134] Rey, D., *Gravity and Suspension Effects on Controlled Flexible Spacecraft*, Master's thesis, Massachusetts Institute of Technology, 1993.

[135] Rey, D. and R. Glase, "Finite Element Model of the Middeck Active Control Experiment," 1993. Preprint, submitted to the *1993 AIAA Structures, Structural Dynamics, and Materials Conference.*

[136] Richter, S., "Reduced Order Control Design via the Optimal Projection Equations: A Homotopy Algorithm for Global Optimality," *Proceedings,* 6^{th} VPI&SU/AIAA *Symposium on Dynamics and Control of Large Structures*, Blacksburg, VA, 1987.

[137] Rotea, M. A. and P. P. Khargonekar, "Mixed $\mathcal{H}_2/\mathcal{H}_\infty$ Control via Convex Programming," *Proceedings, American Control Conference*, Boston, MA, June 1991, pp. 1149–1154.

[138] Saarmaa, E., "Middeck Active Control Experiment (MACE) Development Model (DM) Dynamic Testing and Modelling," Tech. Rep. MACE Document 1-170, Massachusetts Institute of Technology, October 1991.

[139] Saarmaa, E., "Sensor/Actuator Specifications Document," Tech. Rep. MACE Document 1-370, Massachuesetts Institute of Technology, October 1991.

[140] Safonov, M. G., *Stability and Robustness of Multivariable Feedback Systems*, M.I.T. Press, Cambridge, MA, 1980.

[141] Safonov, M. G. and R. Y. Chiang, "Real/Complex K_m-Synthesis without Curve Fitting," in *Control and Dynamic Systems*, Academic Press, New York, 1993.

[142] Safonov, M. G. and P. H. Lee, "A Multiplier Method for Computing Real Multivariable Stability Margin," *Proceedings,* submitted to *the IFAC World Congress*, Sydney, Australia, July 1993.

[143] Safonov, M. G. and G. Wyetizner, "Computer-aided Stability Analysis Renders Popov Criterion Obsolete," *IEEE Trans. on Auto. Control*, Vol. AC–32, 1987, pp. 1128–1131.

[144] Scales, L. E., *Introduction to Non-Linear Optimization*, Springer-Verlag, New York, 1985.

[145] Sesak, J. R. and D. D. Likins, "Model Error Sensitivity Suppression: Quasi-static Optimal Control for Flexible Structures," *Proceedings, IEEE Conference on Decision and Control*, Ft. Lauderdale, FL, Dec. 1988.

[146] Shaked, U. and E. Soroka, "On the Stability of the Continuous Time LQG Optimal Control," *IEEE Trans. on Auto. Control*, Vol. AC–30, Oct. 1985.

[147] Shanno, D. F. and K. H. Phua, "Numerical Comparison of Several Variable-metric Algorithms," *J. of Optimization Theory and Applications*, Vol. 25, 1978, pp. 507–518.

[148] Shanno, D. F. and K. H. Phua, "Minimization of Unconstrained Multivariable Functions," *ACM Trans. Math. Appl.*, Vol. 6, 1980, pp. 618–622.

[149] Siljak, D. D., *Large Scale Dynamic Systems: Stability and Structure*, North–Holland, Amsterdam, the Netherlands, 1978.

[150] Siljak, D. D., "Parameter Space Methods for Robust Control Design: A Guided Tour," *IEEE Trans. on Auto. Control*, Vol. AC–34, No. 7, July 1989, pp. 674–688.

[151] Smith, M. C. and K. P. Sondergeld, "On the Order of Stable Compensators," *Automatica*, Vol. 22, No. 1, 1986, pp. 127–129.

[152] Stein, G. and M. Athans, "The LQG/LTR Procedures for Multivariable Feedback Control Design," Tech. Rep., M.I.T., 1984.

[153] Tahk, M. and J. Speyer, "Modeling of Parameter Variations and Asymptotic LQG Synthesis," *IEEE Trans. on Auto. Control*, No. 9, Sept. 1987, pp. 793–801.

[154] Tahk, M. and J. Speyer, "Parameter Robust Linear–Quadratic Gaussian Design Synthesis with Flexible Structure Control Applications," *AIAA J. of Guid., Control, and Dyn.*, No. 4, 1988, pp. 460–468.

[155] Tekawy, J. A., M. G. Safonov, and R. Y. Chiang, "Convexity Property of the One-sided Multivariable Stability Margin," *IEEE Trans. on Auto. Control*, Vol. AC–37, 1992, pp. 496–498.

[156] Thathachar, M. A. L. and M. D. Srinath, "Some Aspects of the Lur'e Problem," *IEEE Trans. on Auto. Control*, Vol. AC–12, No. 4, Aug. 1967, pp. 451–453.

[157] Thathachar, M. A. L. and M. D. Srinath, "Stability of Linear Time-Invariant Systems," *IEEE Trans. on Auto. Control*, Vol. AC–12, 1967, pp. 335–336.

[158] Thathachar, M. A. L., M. D. Srinath, and H. K. Ramapriyan, "On a Modified Lur'e Problem," *IEEE Trans. on Auto. Control*, Vol. AC–12, No. 6, Dec. 1967, pp. 731–739.

[159] Trentelman, H. L. and J. C. Willems, "The Dissipation Inequality and the Algebraic Riccati Equation," in *The Riccati Equation* (Bittanti, Laub, and Willems, eds.), pp. 197–242, Springer-Verlag, New York, 1991.

[160] Valery, V. I., D. W. Miller, W. Vander Velde, and E. F. Crawley, "Identification of Model Parameters and Associated Uncertainties as a Basis for Robust Control," Preprint, 1992.

[161] Wagie, D. A. and R. E. Skelton, "Sensitivity Controller for Uncertain Systems," *Automatica*, Vol. 22, 1986, pp. 295–308.

[162] Weinmann, A., *Uncertain Models and Robust Control*, Springer-Verlag, New York, 1991.

[163] Wen, J. T., "Time Domain and Frequency Domain Conditions for Strict Positive Realness," *IEEE Trans. on Auto. Control*, Vol. AC–33, 1988, pp. 988–992.

[164] Wie, B. and D. S. Bernstein, "Benchmark Problems for Robust Control Design," *AIAA J. of Guid., Control, and Dyn.*, Vol. 15, No. 5, Sept.–Oct. 1992, pp. 1057–1059.

[165] Willems, J. C., "Dissipative Dynamical Systems Part I: General Theory," *Archive Rational Mechanics Analysis*, Vol. 45, 1972, pp. 321–351.

[166] Willems, J. C., "Dissipative Dynamical Systems Part II: Linear Systems with Quadratic Supply Rates," *Archive Rational Mechanics Analysis*, Vol. 45, 1972, pp. 352–393.

[167] Yedavalli, R. K. and R. E. Skelton, "Controller Design for Parameter Sensitivity Reduction in Linear Regulators," Optimal Control Applications and Methods, Vol. 3, No. 3, 1982, pp. 221–240.

[168] Yeh, H.-H. and S. S. Banda, "Necessary and Sufficient Conditions for Mixed $\mathcal{H}_2$ and $\mathcal{H}_\infty$ Optimal Control," *Proceedings, IEEE Conference on Decision and Control*, Honolulu, HI, Dec. 1990.

[169] Young, P. M. and J. C. Doyle, "Computation of μ with Real and Complex Uncertainties," *Proceedings, IEEE Conference on Decision and Control*, Honolulu, Hawaii, Dec. 1990, pp. 1230–1235.

[170] Young, P. M. and J. C. Doyle, "Properties of the Mixed-μ Problem and its Bounds," Preprint, submitted to *IEEE Transactions on Automatic Control*, Oct. 1992.

[171] Young, P. M., M. P. Newlin, and J. C. Doyle, "μ Analysis with Real Parametric Uncertainty," *Proceedings, IEEE Conference on Decision and Control*, Brighton, England, Dec. 1991, pp. 1251–1256.

[172] Zames, G., "On the Input-Output Stability of Time-Varying Nonlinear Feedback Systems Part I: Conditions Derived Using Concepts of Loop Gain, Conicity, and Positivity," *IEEE Trans. on Auto. Control*, Vol. AC–11, No. 2, April 1966, pp. 228–238.

[173] Zames, G., "On the Input-Output Stability of Time-Varying Nonlinear Feedback Systems Part II: Conditions Involving Circles in the Frequency Domain and Sector Nonlinearities," *IEEE Trans. on Auto. Control*, Vol. AC–11, No. 3, July 1966, pp. 465–476.

[174] Zames, G. and P. Falb, "Stability Conditions for Systems with Monotone and Slope-restricted Nonlinearities," *SIAM J. of Control*, Vol. 6, No. 1, Jan. 1968, pp. 89–108.

[175] Zhou, K., J. C. Doyle, K. Glover, and B. Bodenheimer, "Mixed $\mathcal{H}_2$ and $\mathcal{H}_\infty$ Control," *Proceedings, American Control Conference*, San Diego, CA, May 1990, pp. 2502–2507.

End date Nov 16, 1994.